Multi-Omics Characterisation of Drug-Induced Liver Injury in Human-Derived Hepatocyte Models

Thomas Petar Kralj

Bachelor of Pharmaceutical Science (Honours)

A thesis submitted for the degree of

Doctor of Philosophy

at

Monash University

Drug Delivery, Disposition and Dynamics

Monash Institute of Pharmaceutical Sciences

Monash University

Melbourne, Victoria, Australia

Copyright notice

Table of Contents

THESIS ABSTRACT ..... **VII**

DECLARATION ..... **X**

ACKNOWLEDGEMENTS ..... **XI**

PUBLICATIONS ..... **XII**

COMMUNICATIONS ..... **XII**

LIST OF ABBREVIATIONS ..... **XIII**

CHAPTER 1: INTRODUCTION **1**

Abstract **2**

Drug-Induced Liver Injury **3**

Prevalence of Drug-Induced Liver Injury in Pharmaceuticals 5

Severity and Clinical Impact of Drug-Induced Liver Injury 8

Pathology and Biochemical Pathways of Drug-Induced Liver Injury 10

Models for Drug-Induced Liver Injury 20

Analytical Techniques for Investigation of Drug-Induced Liver Injury 30

Application of Omics to Investigate Drug-Induced Liver Injury 35

Thesis Aims **46**

References **50**

CHAPTER 2: COMPARISON OF THE PRIMARY HUMAN HEPATOCYTE AND HEPARG PROTEOME AND MULTI-OMICS CHARACTERISATION OF DRUG-INDUCED METABOLIC PERTURBATIONS **70**

Abstract **71**

Introduction **71**

Methods **75**
Materials 75
Cell Culture 75
Treatment with drugs associated with drug-induced liver injury and metabolomics extraction 76
Liquid chromatography-mass spectrometry metabolomic analysis 77
Proteomic data-independent analysis 78
Multivariate and statistical analysis 80

Results **81**
Multivariate analysis of differences in primary human hepatocyte and HepaRG proteomes 81
Comparison of proteins from major metabolic pathways in primary human hepatocytes and HepaRG cells 86
Multivariate analysis of metabolome changes in response to DILI-associated drugs 89
Perturbation of metabolites and protein abundance in major metabolic pathways 94

Discussion **107**

References **115**

CHAPTER 3: MULTI-OMICS ANALYSIS OF IN VITRO PRIMARY HUMAN HEPATOCYTES AFTER TREATMENT WITH CHOLESTATIC DRUGS **122**

Abstract **123**

Introduction **123**

Material and methods **128**
Materials 128
Cell Culture 129
C-DILI™ hepatotoxicity assay 130
B-CLEAR® transport assay 132
Drug treatment with drugs associated with DILI and metabolomics extraction 133
24-hour time course drug treatment 134
Liquid chromatography-mass spectrometry metabolomic analysis 135
Proteomic data-independent analysis 137
Statistical analysis 139

Results **140**
Cholestatic potential of DILI-associated drugs 140
Effect of drug treatment on bile acid transport in HuH-7 cells 142
Liquid chromatography-mass spectrometry analysis of cellular bile acids after drug treatment of PHH 144

Time course of bile acid abundance in HepaRG™ cells after drug treatment 146
Drug-induced changes in drug metabolism and the bile acid-associated proteome in PHH 147

Discussion 152

References 161

CHAPTER 4: LIPIDOMICS CHARACTERISATION OF STEATOSIS-INDUCED CHANGES TO LIPID PROFILES IN HUMAN HEPATOCYTES 166

Abstract 167

Introduction 167

Materials and methods 171
Materials 171
Cell Culture 171
Fluorescent imaging of steatosis and phospholipidosis 172
DILI drug treatment and lipid extraction 174
Lipid extraction of clinical and in vitro-induced steatotic PHH samples 175
Liquid chromatography-mass spectrometry lipidomics analysis 175
Statistical analysis 176

Results 177
Comparative analysis of lipid profiles in hepatocytes from patients with NASH and IVIS PHH 177
Multivariate analysis of NASH-related lipids 180
BODIPY plate assay of DILI drug panel for identification of in vitro steatotic-DILI 183
Identification of intracellular lipids predictive of steatotic-based liver injury 185

Discussion 193

References 198

CHAPTER 5: CONCLUSION AND FUTURE DIRECTIONS 202

Research Summary 203
Characterisation and application of alternative in vitro liver models 203
Multi-omics analysis of metabolic perturbations induced by DILI 206
Identification of liver injury-associated lipids 208

Concluding Remarks 209

References 213

APPENDIX 217
Appendix 1 218
Appendix 2 251
Appendix 3 252
Appendix 4 255
Appendix 5 257
Appendix 6 259

Thesis Abstract

Drug-induced liver injury (DILI) is a significant clinical burden that can affect up to 2 million people annually with a mortality rate of up to 10%. It is prevalent across nearly all drug classes including antimicrobial, neurological, anti-neoplastic, and non-steroidal anti-inflammatory drugs. An analysis of 1,036 Food and Drug Administration (FDA)-approved drugs revealed that 45% demonstrated some degree of DILI concern. The burden of DILI is further complicated because it can occur as one or a combination of 12 different liver injury phenotypes, with cholestasis and steatosis being two of the most common. Understanding the mechanism(s) responsible for DILI is imperative in order to improve the clinical management of this condition, and to minimize the occurrence of this major safety concern during the development of new drugs. *In vitro* liver models, including primary human hepatocytes (PHH), HuH-7, and HepaRG™ cells, offer an accessible platform through which various plate-based assays and omics techniques can be applied to achieve a deeper and broader understanding of the mechanism(s) of DILI. The primary aim of this thesis is to use such *in vitro* models to investigate the biological perturbations induced in the proteome, metabolome, and lipidome of liver cells treated with DILI-associated drugs.

PHH are the gold-standard for *in vitro* liver models, although HepaRG™ cells offer a potential cost-efficient, human-derived, hepatic-like alternative. Proteomics analysis of PHH and HepaRG™ cells demonstrated that there was a degree of similarity in the proteomes of the two cell types. However, while the whole cell proteomes had Pearson's *r* coefficients of up to 0.86, comparison of the major metabolic pathway proteomes showed poorer correlation, with *r* values ranging from 0.75 to 0.78. Furthermore, multi-omics analysis of metabolically competent PHH *in*

vitro models treated with DILI-associated drugs identified drug-induced biological perturbations to proteins and metabolites from the TCA cycle, and from glucose, nicotinamide, phase I, glucuronidation, and glutathione metabolism. These changes indicated that impairment of mitochondrial respiration had occurred, and that there was increased activity of pathways that are protective against oxidative stress. This analysis gave insight into the potential mechanism(s) through which drug-induced hepatoxicity could occur by identifying perturbations to vital metabolic pathways.

The impact of DILI-associated drugs on bile acid homeostasis is critical to assess because such biological perturbations may be mechanistically linked to cholestatic DILI. Cell viability assays indicated that diclofenac, ethinyl estradiol, ritonavir, and troglitazone had significant potential to induce cholestatic hepatoxicity, with ethinyl estradiol, ritonavir, and troglitazone also capable of significantly impairing biliary transport. PHH and HepaRG™ cells were treated with diclofenac, ethinyl estradiol, ritonavir, and troglitazone as well as pioglitazone which, while it did not appear to induce cholestatic hepatoxicity, significantly impaired biliary transport. The drug-treated cells underwent metabolomic and proteomic analysis, which showed significant decreases in the cellular abundance of taurocholate, glycocholate, and glycochenodeoxycholate for PHH and HepaRG™ cells. Additionally, while proteomics analysis did not reveal significant changes in the abundance of bile acid transporters, there was a significant increase in the abundance of various CYP enzymes and cytochrome P450 oxidoreductase, which may have resulted in increased phase I metabolism of bile acids leading to reduced cellular abundance of bile acids.

Steatotic liver injury, which can result from a variety of stimuli, can cause severe liver damage and even liver failure. In patients experiencing steatotic liver injury from non-alcoholic steatohepatitis (NASH), lipidomics analysis demonstrated that there was

a unique increase in total phospholipid abundance in NASH PHH, in addition to an anticipated accumulation of neutral lipids. Lipidomic analysis of the hepatocellular lipid profiles of *in vitro* PHH treated with drugs associated with steatotic DILI was performed. The analysis of these lipid profiles revealed that phospholipids were significantly altered under steatotic conditions and, using receiver operating characteristic (ROC) curve analysis, lipids, such as linoleic acid or phosphoserine (32:1), could act as predictive biomarkers for steatotic DILI.

The research presented in this thesis demonstrates the value of multi-omics and metabolically competent *in vitro* liver models in expanding the current understanding of the biological effects and mechanisms of DILI. This thesis demonstrated the utility of multi-omics in toxicology to elucidate potential mechanism(s) of DILI that involve impairment of major metabolic pathways or the induction of specific liver injury phenotypes such as cholestasis. Furthermore, data generated demonstrate the translational potential of multi-omics studies, which can be used to assess the metabolic competency of liver models to allow for the selection of the most metabolically relevant *in vitro* model or the identification of predictive biomarkers of liver injury.

Declaration

This thesis contains no material which has been accepted for the award of any other degree or diploma at any university or equivalent institution and that, to the best of my knowledge and belief, this thesis contains no material previously published or written by another person, except where due reference is made in the text of the thesis.

Thomas Petar Kralj

Date: 28/07/21

Acknowledgements

I wish to offer my deepest thanks to Assoc. Prof. Darren Creek and Assoc. Dean Kim Brouwer. Without the immense support and decades of collective knowledge from both Darren and Kim, I am sure the completion of this thesis would have been all but impossible.

I would also like to thank the members of the Creek lab, especially Amanda De Paoli, Dr. Carlo Giannangelo, and Dr. Ghizal Siddiqui, who offered their time and knowledge in helping me learn new techniques and develop new skills. I would like to also give special thanks to Dr. Dovile Anderson for running a nearly unending number of LC-MS samples for me and developing new methods for my study of bile acids.

The assistance and helpfulness of the Brouwer Lab must not go unappreciated. The Brouwer Lab warmly welcomed me onto their team during my 6-month placement and showed me the ropes in a new lab and field. For her never-ending assistance with both the B-CLEAR assays and the ever temperamental HuH-7 cells, I would sincerely like to thank Dr. Chitra Saran for sharing her knowledge and time with me.

I must acknowledge both Monash University and the University of North Carolina at Chapel Hill for the opportunities they have afforded me during my doctoral candidature and through the PharmAlliance. I have a profound amount of gratitude to BioIVT and their Vice President, Dr. Kenneth Brouwer, for their support in culturing of hepatocytes and generating valuable samples. Furthermore, I am deeply grateful for the wealth of knowledge Dr. Ken Brouwer generously shared with me about DILI and hepatocytes; this was invaluable.

Finally, I would like to thank my family and friends for the opportunities, love, and support that they have given me throughout this long journey which has helped me reach where I am today. Thanks to my Mum and Dad, for their support and every opportunity they have willingly and happily worked hard to give me, and to my brother, whose admiration for what I was trying to achieve was forever encouraging and inspiring. Thanks to Maria Valentic and Hayden Truelson, who may have always been confused about what exactly I did but were always willing to let me lament every challenging day I had and helped brighten those days as well as every other.

Publications

During my doctoral candidature, the following manuscript was accepted for publication:

Thomas Kralj, Kim L R Brouwer, Darren J Creek, Analytical and Omics-based Advances in the Study of Drug-Induced Liver Injury, *Toxicol Sci*, 2021; kfab069, https://doi.org/10.1093/toxsci/kfab069

Communications

The results of this thesis were presented at the following scientific conferences:

1. **Kralj T**, Anderson D, De Paoli A, Srivastava A, Creek DJ. Mechanistic Investigation of Anti-Retroviral Related Liver Injury through the Use of Metabolomics and Lipidomics Techniques. IUTOX 15th International Congress of Toxicology, Honolulu, Hawaii. 2019
2. **Kralj T**, Creek DJ. Using Metabolomics to Investigate Drug Toxicity. APSA Annual Conference, Monash University, Melbourne, Australia. 2019. Presented by Creek DJ.
3. **Kralj T**, Saran C, Brouwer KLR, Creek DJ. Characterisation of cholestatic drug-induced liver injury using *in vitro* models. PharmAlliance E-Conference. 2020
4. **Kralj T**, Brouwer KLR, Creek DJ. Characterisation of drug-induced liver injury using proteomic and metabolomic techniques. DILISym. Dec 2020.

List of Abbreviations

ACN	Acetonitrile
ADR	Adverse drug reactions
ALDH	Aldehyde dehydrogenase
ALP	Alkaline phosphatase
ALT	Alanine aminotransferase
ANPEP	Aminopeptidase N
APAP	Acetaminophen
AST	Aspartate aminotransferase
ATP	Adenosine triphosphate
BAAT	Bile acid-CoA:amino acid N-acyltransferase
BCA	Bicinchoninic acid assay
BEI	Biliary excretion index (%)
BODIPY	4,4-difluoro-4-bora-3a,4a-diaza-*s*-indacene
BSEP	Bile salt export pump
CA	Cholate
CAD	Cationic amphiphilic drugs
CDCA	Chenodeoxycholic acid
cGMP	Cyclic guanosine monophosphate
CNS	Central nervous system
CO_2	Carbon dioxide
cPKC	Classical protein kinase C
CYP	Cytochrome P450
CysA	Cyclosporin A
DAG	Diacylglycerides

ddH_2O	Double distilled water
DILI	Drug-induced liver injury
DMSO	Dimethyl sulfoxide
DNA	Deoxynucleic acid
DON	Deoxynivalenol
DTT	Dithiothreitol
EDTA	Ethylenediaminetetraacetic acid
EMA	European Medicines Agency
FAO	Fatty acid oxidation
FDA	Food and Drug Administration
FXR	Farnesoid X receptor
g	Gram
g	Gravitational force equivalent
GAPDH	Glyceraldehyde-3-phosphate dehydrogenase
GCA	Glycocholate
GCDCA	Glycochenodeoxycholic acid
GCK	Glucokinase
GGCT	Gamma-glutamylcyclotransferase
GGT	Gamma-glutamyl transpeptidase
GLUT	Glucose uptake transporter
GOT1	Glutamic-oxaloacetic transaminase 1
GPI	Glucose-6-phosphate isomerase
GPX	Glutathione peroxidase
GSS	Glutathione synthase
GST	Glutathione S-transferase
HBSS	Hanks' Balanced Salt Solution

HCl	Hydrochloric acid
HDS	Herbal and Dietary Supplements
HEPES	4-(2-hydroxyethyl)-1-piperazineethanesulfonic acid
HESI	Heated electrospray ionisation
HILIC	Hydrophilic interaction liquid chromatography
HIV	Human immunodeficiency virus
HLA	Human interleukin antigen
IDH	Isocitrate dehydrogenase
IL	Interleukin
IVIS	*In vitro*-induced steatosis
LCA	Lithocholic acid
LCMS	Liquid chromatography and mass spectroscopy
LDH	Lactate dehydrogenase
MAG	Monoacylglycerides
MDB	Mallory-Denk bodies
MDR	Multidrug resistance protein
mg	Milligram
mL	Millilitre
mM	Millimolar
mRNA	Messenger ribonucleic acid
MRP	Multidrug resistance-associated protein
mtDNA	Mitochondrial DNA
MTTP	Microsomal triglyceride transfer protein
NAFLD	Non-alcoholic fatty liver disease
NAMPT	Nicotinamide phosphoribosyltransferase
NAPQI	N-acetyl-p-benzoquinone

NAT2	N-acetyltransferase 2
NASH	Non-alcoholic steatohepatitis
nm	Nanometre
NSAID	Non-steroidal anti-inflammatory
NTCP	Na^+-taurocholate transporting polypeptide
NVP	Nevirapine
OAT	Organic anion transporter
OATP	Organic anion transporting polypeptide
OCT	Organic cation transporter
OSTα/β	Organic solute transporter α/β
PA	Phosphatidic acid
PC	Phosphatidylcholine
PC1	Principal component 1
PC2	Principal component 2
PCA	Principal component analysis
PCK1	Phosphoenolpyruvate carboxykinase 1
PE	Phosphatidylethanolamine
PEPCK	Phosphoenolpyruvate carboxykinase
PG	Phosphatidylglycerol
Pg-P	P-glycoprotein
PHH	Primary human hepatocytes
PI	Phosphatidylinositol
PI3K	Phosphoinositide 3-kinase
PLS-DA	Partial least-squares discriminant analysis
POR	Cytochrome P450 oxidoreductase
PPARα	Peroxisome proliferator-activated receptor alpha

PRH	Primary rat human
PS	Phosphatidylserine
PSC	Primary sclerosing cholangitis
RBKS	Ribokinase
RNA	Ribonucleic acid
rpm	Revolutions per minute
ROC	Receiver operating characteristic
ROS	Reactive oxygen species
SCX	Strong cation exchange
SDC	Sodium deoxycholate
SDH	Succinate dehydrogenase
SDS	Sodium dodecyl sulfate
SIRT	NAD-dependent deacetylase sirtuin
SNP	Single nucleotide polymorph
sPLS-DA	Sparse partial least-squares discriminant analysis
SUCLG2	Succinate-CoA ligase subunit beta
TAG	Triacylglycerides
TCA	Tricarboxylic acid
TCDCA	Taurochenodeoxycholate
TCDD	2,3,7,8-tetrachlorodibenzo-p-dioxin
TCEP	Tris(2-carboxyethyl) phosphine hydrochloride
TDO	Tryptophan 2,3-dioxygenase
TEAB	Tetraethylammonium bromide
TGA	Therapeutic Goods Administration
Tris	Trisaminomethane
TUDCA	Tauroursodexycholate

ULN	Upper limit of normal
UDP	Uridine diphosphate
UGT	Uridine 5'-diphospho-glucuronosyltransferase
US	United States
VBDS	Vanishing bile duct syndrome
ZEA	Zearalenone
% v/v	mL liquid volume/100mL solution volume
% w/v	g solute weight/100mL solution volume
°C	Degrees Celsius
µg	Microgram
µL	Microlitre
µM	Micromolar

Chapter 1

Introduction[1]

[1] Please note approximately 50% of this chapter has being accepted for publication (Appendix 1)

Abstract

Drug-induced liver injury (DILI) is a significant clinical issue, affecting 1-1.5 million patients annually, and remains a major challenge during drug development, with toxicity and safety concerns being the second highest reason for drug candidate failure. By developing a greater understanding of the biological mechanisms behind DILI, its future prevalence can be minimised. However, representative models and analytical techniques are needed to study DILI. *In vitro*, *ex vivo*, and *in vivo* models using hepatocytes and hepatic-like cells offer accessible systems capable of effectively reproducing various characteristic features of liver cells suitable for investigating DILI. In addition to an appropriate model, accurate and analytical techniques are also vital to characterising DILI. *In vitro* assays are capable of characterising specific aspects of a drug's hepatotoxic nature; however, many of these techniques are restricted in the breadth of information that they can offer. Multiplexed assays are capable of characterising and scoring a drug's association with DILI. A holistic approach to provide global insight into the mechanisms of DILI can be achieved using omics-based analytical techniques: genomics, transcriptomics, proteomics, and metabolomics. These omics analytical techniques can offer qualitative and quantitative insight into genetic susceptibilities to DILI, the impact that a drug treatment may have on gene expression, and the effect it may have on proteins and metabolite abundance. This review will discuss the various *in vitro* liver models and analytical techniques that can be applied to characterise the biological mechanisms of DILI.

Drug-Induced Liver Injury

Drug-induced liver injury (DILI) is a form of adverse drug reaction (ADR) that refers to a variety of related conditions that have resulted from exposure to hepatotoxic pharmaceuticals. DILI is a globally prevalent issue and various population studies have identified DILI occurring at rates of 3 to 24 cases per 100,000 people annually (1-5). DILI is also a significant issue in drug development, with a large portion of drug attrition being due to toxicity and safety concerns (6). However, it is likely that rates of DILI occurring during clinical development are higher as a result of under-reporting, since identification of DILI as the primary cause of liver injury is often complicated by other factors such as co-morbidity and co-infections, including hepatic infections and fatty liver disease arising from lifestyle factors.

DILI is a prevalent medical issue affecting a significant number of patients who receive prescription medications with some of these DILI cases leading to organ failure and/or death. A study of a Finnish cohort found that 1.4% of all medical in-patients will experience DILI (7). While relatively low, this incidence is still concerning as up to 10.1% of cases may be fatal or require a liver transplant (3, 8-11). A study of 1,089 DILI cases, where recovery outcomes were assessed, found that 9.8% of patients died or underwent a liver transplant (12). Of these severe cases, DILI was reported as the primary cause of death or liver transplant in 64% of patients and contributed to an additional 14% of deaths or liver transplants.

DILI is not just a condition of clinical concern but is also a prevalent problem faced during drug development, with toxicity and safety concerns being the second highest reason for drug failure (6). Hepatotoxicity issues with drug safety should ideally be

detected during the preclinical stages of testing using *in vitro* methods and animal models. In the preclinical phase of drug development, the attrition rate of drug candidates due to safety concerns is 40% (6). Furthermore, toxicity issues are still detected during phase I, II, and III clinical trials, and even during post market surveillance. There is a failure rate due to safety and toxicological concerns of 38% for phase I, the trial phase that is intended to address safety concerns in humans. However, it is clear that this phase does not comprehensively identify all safety and toxicity issues, as phase II and phase III clinical trials have a 33% and 17% failure rate, respectively, due to safety and toxicological concerns (6, 13). The proportion of these toxicity concerns that are specifically related to hepatotoxicity is not always clear. Incidents such as the 1994 fialuridine trials, that resulted in 5 fatalities, and the 2018 phase IIb/III atabecestat trials, which were discontinued due to indications of liver injury, provide additional evidence that issues with drug hepatotoxicity are occurring in later stages of clinical trials and can be life threatening (14, 15).

DILI is problematic for clinicians and other medical professionals for several reasons; probably the most notable is a lack of active medical intervention options to treat DILI upon diagnosis. This is largely because treatment options are very limited and primarily involve discontinuing the medication followed by observation by a medical professional (16). Treatment is mainly supportive unless liver failure occurs, in which case a liver transplant is the only possible option to prevent death (17). Exceptions to this are injury caused by paracetamol (acetaminophen; APAP) and poisoning as a result of ingesting mushrooms from the *Amanita* family. Prevention of hepatotoxicity due to APAP overdose is treated by an intravenous infusion of N-acetyl cysteine within 24 hours of

ingestion. This prevents depletion of glutathione (GSH) reserves in the liver and allows the toxic APAP metabolite, N-acetyl-p-benzoquinone (NAPQI), to be safely quenched by glutathione instead of forming protein and nucleic acid conjugates that can result in liver damage (18). *Amanita* mushroom poisoning results from interactions of amatoxins with RNA polymerase II, thus impairing protein synthesis and leading to centrilobular liver necrosis. While not strictly characterised as DILI, two treatment options are available: activated charcoal, to prevent reabsorption of toxins by enterohepatic circulation, and silibinin, which competes with amatoxins for hepatic uptake (19). With limited options available for treating DILI, an emphasis is placed on reducing DILI prevalence and improving the monitoring of DILI-associated drugs by: (1) reducing the number of new DILI-associated drugs being released, and (2) improving pharmacovigilance for DILI-associated drugs already on the market to prevent future occurrences of severe and potentially lethal cases of DILI.

Prevalence of Drug-Induced Liver Injury in Pharmaceuticals

DILI is not restricted to a limited number of drug classes, rather, it can be found ubiquitously across a wide range of drug classes, and even in herbal and dietary supplements (HDS). Drug classes affected by DILI include antimicrobials (antibiotics, antifungals, antivirals, and antiparasitic drugs), HDS, cardiovascular drugs, central nervous system (CNS) drugs, anti-neoplastic drugs, analgesics [particularly non-steroidal anti-inflammatory drugs (NSAIDs)], and immunomodulatory and endocrine drugs (8, 20-22). A study of 899 DILI cases across the United States (US) found that antimicrobials were responsible for the greatest number of DILI cases (45%), with amoxicillin-clavulanate solely responsible for the highest number of individual cases (10%). Nine of

the top ten DILI-inducing drugs were antibiotics while other classes responsible for a significant number of DILI cases were HDS (16%), cardiovascular agents (10%), and CNS drugs (9%) (20). These DILI cases are not resulting from a small pool of prescription drugs; 189 different prescription drugs were identified as the primary agents in 84% of the identified DILI cases. These findings were supported by another US DILI study conducted between 2003 to 2007, which also found that antimicrobials and CNS drugs were the two most represented drug classes responsible for the greatest number of cases (46% and 15%, respectively) (8). This study also highlighted the importance of considering an individual drug's hepatotoxic nature, as most (73%) cases were a result of the use of a single prescription drug and not the cumulative effect of several prescription drugs. Similar to the previous two studies, an assessment of 461 Spanish DILI cases recorded between 1994 and 2004 also reported antimicrobials as the leading cause of DILI cases (37%), followed by CNS drugs and NSAIDs (17% of cases each) (21).

An analysis of 1,036 Food and Drug Administration (FDA)-approved drugs found that 192 drugs (19%) have strong DILI concerns and only 62 (6%) of these drugs were discontinued. For the remaining drugs assessed, 278 (27%) have minor DILI concerns, 254 (25%) have ambiguous DILI concerns, and 312 (30%) have no DILI concerns (22). An additional assessment of 671 currently marketed drugs found only 318 (47%) had no DILI implications, while 220 (32%) had more than 3 published reports of DILI incidents, with 48 (7%) having been reported in more than 50 DILI incidents (23). While these data show that there is already a significant presence of DILI-associated drugs on the market, the true prevalence of DILI cases and their severity is likely to be much higher due to underreporting by clinicians and complications contributed by other diseases.

Pharmacovigilance is vital to identifying a drug's capacity to cause DILI after it has reached the market. This involves the identification and assessment of ADRs by market surveillance and adverse event reporting by health professionals. With proper pharmacovigilance, on-market drugs that possess undetected hepatotoxic properties can be identified as hazardous and appropriate action can be taken to prevent further harm. Effective pharmacovigilance requires a collaborative effort between health professionals, patients, and regulatory bodies such as the FDA, Therapeutic Goods Administration (TGA), or European Medicines Agency (EMA).

As alluded to previously, underreporting contributes largely to underestimated case rates of DILI diagnosis in the clinical setting. Indeed, studies have highlighted significant underreporting of ADRs, with reporting occurring as low as one in every 1144 cases (24). Similarly, several European studies have found that the median clinical underreporting rate for serious cases of ADRs is 94%, with a range of 47-95% (24-28). While this does cover all forms of ADR and not specifically DILI, one particular study that separated ADRs into different injury categories found that liver dysfunction due to ADRs was underreported at a rate of 94% (29). Furthermore, underreporting may not be the only reason for inaccurate estimations of DILI occurrence, as DILI and other ADRs, are not always properly identified by clinicians. For hospital in-patients, 20 to 24% of ADRs were not identified either upon admission or during the patient's stay (30, 31). It should also be noted that it is not predominantly mild cases of ADR that are overlooked; 16.5% of severe or fatal reactions, and 23.2% of mild or moderate reactions, were not recognised (30). Clinically, ADRs, including DILI, are a prevalent issue that may be occurring at higher rates than currently estimated.

Severity and Clinical Impact of Drug-Induced Liver Injury

One of the most significant examples of drug failure due to DILI is the 1993 fialuridine clinical trial (14). During a phase II clinical trial of patients with chronic hepatitis B infections, 7 of the 15 participants who received fialuridine experienced severe DILI-associated liver failure that resulted in two participants requiring a liver transplant and five fatalities. Testing in rats, dogs, and monkeys with doses ranging from 3 to 510 mg/kg/day over a range of 30 to 90 days indicated a high tolerance to fialuridine; however, a dose of 0.25 mg/kg/day for 2 months in humans resulted in hepatic failure in seven participants (32). Suspected differences in fialuridine tolerance have been attributed to the presence of the human equilibrative nucleoside transporter 1 found in the mitochondria of human cells. This transporter is involved in increased uptake of fialuridine into the hepatocyte mitochondria that results in toxicity (33). The fialuridine tragedy nevertheless illustrates the limitations of translating drug safety profiles between preclinical animal models and testing in humans.

Fialuridine is not the only example of a hepatotoxic drug that has progressed through preclinical safety assessment into human patients. Several hepatotoxic drugs have reached the market and caused severe liver damage and, in some cases, fatalities (20, 21, 34). Troglitazone was released to the market in March 1997 for treatment of type 2 diabetes and was one of the most prominent DILI-associated drugs to have reached the market. However, by 1998 several reports of liver failure induced by troglitazone had been filed (35-41). After 83 cases of troglitazone-associated liver failure, this drug was removed from the market in March 2000. Troglitazone was found to cause liver failure in patients at a rate of 2.7 to 8.3 per 100,000 person-years, which is between 3- and 9.5-

fold greater than the baseline liver failure rate of patients with type 2 diabetes (0.88 per 100,000 person-years) (42, 43). Furthermore, as alluded to previously, this number is likely to be a misrepresentation, and cases are likely to be greatly underestimated as reporting of adverse events by physicians occurred in only 3% to 13% of cases (44, 45). Similarly, the drugs lumiracoxib, sitaxentan, alatrofloxacin, and trovafloxacin have all been withdrawn from the market in certain countries or worldwide since 2000 due to concerns about their hepatotoxicity and fatal incidences of DILI (46-49). Trovafloxacin and alatrofloxacin were associated with 14 cases of acute liver failure in the US with 6 of the cases resulting in death; although trovafloxacin was released in 1998, it was not until 2006 that the two drugs were withdrawn from the market (50). Lumiracoxib was responsible for eight reports of serious liver damage in Australia, resulting in 2 patients requiring liver transplants and 2 deaths during its use from 2003 to 2007. Furthermore, lumiracoxib has been withdrawn from markets in Australia and other countries including New Zealand, Canada, Germany, Austria, Belgium, Cyprus, and Brazil, and was refused approval by the FDA due to DILI concerns (51). In 2010, sitaxentan was withdrawn from the market in the European Union, Australia, and Canada due to association with two cases of fatal liver failure (47).

While several drugs have been removed from the market due to their ability to cause DILI, there are still numerous commonly prescribed drugs on the market that are associated with high rates of DILI. Amoxicillin/clavulanate, a commonly prescribed antibiotic combination, induced DILI in 43 patients per 100,000; diclofenac, an over-the-counter NSAID induced DILI in 11 patients per 100,000; nitrofurantoin, an antibiotic used to treat urinary tract infections, induced DILI in 73 patients per 100,000; and azathioprine,

an immunosuppressant, induced DILI in 752 patients per 100,000 (1, 52). With the inherent potential for many drugs to cause DILI, it is important to strongly monitor and regulate drugs that pose a significant risk of DILI-associated mortality, with current overall estimates as high as 11.7%. In some specific cases, such as halothanes, mortality rates are as high as 40% if DILI occurs (1-3, 7, 10, 20, 21, 34). Additionally, larger drug dosages correlate with a greater risk of developing DILI. Dosages >50 mg were found to cause 72-77% of DILI cases. Severe cases, which are those that result in a fatal outcome or require a liver transplant, were found to increase with dosage; for dosages of <10 mg, 11-49 mg and >50mg, severe DILI occurred at a rate of 2%, 9.4%, and 13.2%, respectively (53, 54).

Overall, DILI is a pervasive issue affecting 1 to 1.5 million people annually, with approximately 10,000 to 16,000 cases resulting in death or the need for a liver transplant. There is also a risk of DILI progressing undetected through clinical trials of new drugs to clinical treatment of patients. Analysis of 1,036 FDA-approved drugs on the market identified that 45% are associated with DILI concerns, with the remaining 55% of drugs having ambiguous or no DILI interactions (22). DILI remains a complicated issue with no specific, non-invasive diagnostics, minimal understanding of the exact mechanisms responsible for hepatotoxic behaviour, and limited ability to predict the DILI liability of new drugs in development.

Pathology and Biochemical Pathways of Drug-Induced Liver Injury

Effectively identifying DILI as the primary cause of a patient's liver disease remains a challenge due to a lack of uniform pathological features and delayed onset across various DILI phenotypes, in addition to a lack of specific diagnostic tests. Currently, DILI is diagnosed by excluding other reasonable disease states, or environmental and lifestyle

factors that may have led to a patient's symptoms. Diagnosis is achieved using detailed medical histories, blood tests, hepatobiliary imaging, and liver biopsy (55-57). DILI can occur as one or more combinations of 12 phenotypic disease states:

- Acute hepatic necrosis (58-61)
- Acute hepatitis (62, 63)
- Cholestatic hepatitis (64-67)
- Mixed hepatocellular-cholestatic hepatitis (68-70)
- Enzyme elevations without jaundice (69, 71, 72)
- Bland cholestasis (73-76)
- Hepatic steatosis with lactic acidosis (77-81)
- Non-alcoholic fatty liver (82, 83)
- Chronic hepatitis (84)
- Sinusoidal obstruction syndrome (85, 86)
- Nodular regenerative hyperplasia (73, 87)
- Hepatic tumours (88-90)

Each phenotype possesses different latencies to onset, symptoms, serum enzyme elevation patterns, and causative drugs (55). Across all DILI phenotypes, there is a large variation in latency to onset, ranging from 1 day to 7 years following drug administration. However, it is more common for the latency to onset to be in the range of 4 weeks to 6 months (60, 67, 68, 74, 78-80, 89). This leads to DILI being a diverse and variable condition that is difficult to diagnose.

In a clinical setting, DILI has been simplified into three general classes (hepatocellular, mixed, and cholestatic liver injury), which are defined in a clinical setting by serum enzyme ratios based on the upper limit of normal (ULN) (Table 1).

Table 1: Aetiology and Clinical Characterisation of DILI (91-94).

Clinical Classification	**R*-Value Range**	**Prevalence Range**
Hepatocellular	R ≥ 5	52 – 59%
Mixed	2 < R < 5	6 – 23%
Cholestatic	R ≤ 2	18 – 29%

*$R = \frac{ALT}{ULN_{ALT}} \div \frac{ALP}{ULN_{ALP}}$, ALT = Alanine aminotransferase, ALP = Alkaline phosphatase

While this classification system allows clinicians to categorise a patient's liver injury based on a less invasive blood test (compared to a liver biopsy for histological assessment), it oversimplifies the different phenotypes of DILI and can even lead to misclassification of a patient's DILI phenotype. A histological evaluation of 249 DILI patient liver biopsies revealed that while R values were somewhat effective in identifying hepatocellular injury, it showed a much poorer capacity to distinguish cholestatic liver injury from mixed liver injury (93). Furthermore, hepatocellular liver injury is quite a general class of liver injury, occurring in 52 – 59% of cases (91-94). Hepatocellular liver injury acts as a catch-all class containing any form of DILI that is not cholestatic in nature, including acute hepatic necrosis, acute hepatitis, chronic hepatitis, hepatic steatosis with lactic acidosis, and non-alcoholic fatty liver disease (NAFLD) (58, 62, 77, 82, 84, 95). These classes all possess different histological presentations and mechanisms of cellular dysfunction.

Cholestatic Drug-Induced Liver Injury

Cholestatic liver injury is the other common classification for DILI and is a much more uniform classification than its hepatocellular counterpart. Cholestatic liver injury results from the reduction or impairment of bile acid transport, occurring as hepatocellular or canalicular bile stasis, or significant duct loss, which then leads to cholestasis (95). Cholestatic liver injury occurs in up to 52% of cases as either the sole DILI phenotype or as a comorbidity with hepatocellular DILI phenotypes (91-93). Such DILI phenotypes are classified as either acute or chronic cholestatic liver injury, and the specific form of cholestasis is determined by the alkaline phosphatase (ALP), aspartate aminotransferase (AST), and alanine aminotransferase (ALT) levels. Acute cholestatic liver injury can present as cholestasis with hepatitis, cholestasis without hepatitis, and cholestasis with bile duct injury. Acute cholestatic liver injury with hepatitis may present with inflammation and hepatocellular necrosis. Additionally, the biochemical features of cholestasis with hepatitis as a comorbidity is hyperbilirubinemia with a <3-fold ALP elevation and a 1- to 8-fold increase of the AST/ALT ratio. When cholestatic liver injury presents without hepatitis, there is minimal or no inflammation or necrosis. However, the liver histology may show dilated canaliculi filled with bile. Cholestasis without hepatitis also features hyperbilirubinemia and has a 2- to 10-fold increase in the AST/ALT ratio, with a >3-fold increase of ALP. Acute hepatic cholestasis can also present as cholestasis with bile duct injury where biliary ductules are filled with numerous bile aggregates and vesicular lipid accumulation within hepatocytes but with little to no inflammation or necrosis. The biochemical features of acute hepatic cholestasis are similar to that of cholestasis without hepatitis but with the addition of elevated γ-glutamyl transpeptidase (GGT) (96, 97).

Chronic cholestatic liver injury may occur as mild, non-specific bile duct injury, vanishing bile duct syndrome (VBDS), or primary sclerosing cholangitis-like liver injury. Mild non-specific bile duct injury is an asymptomatic form of chronic cholestatic DILI that presents with minimal bile duct epithelial disarray and occasional inflammation with mild elevation of ALP or GGT. VBDS involves the loss of more than 50% of bile ducts. VBDS has the same biochemical features as acute cholestasis with bile duct injury, but with the addition of hypercholesterolemia and an absence of antimitochondrial antibodies (96, 98). Primary sclerosing cholangitis-like cholestatic liver injury presents with a pathology similar to that of primary sclerosing cholangitis (PSC) with bile duct destruction and hepatocellular necrosis showing biochemical features similar to that of acute cholestasis without hepatitis with the addition of hypercholesterolemia (96).

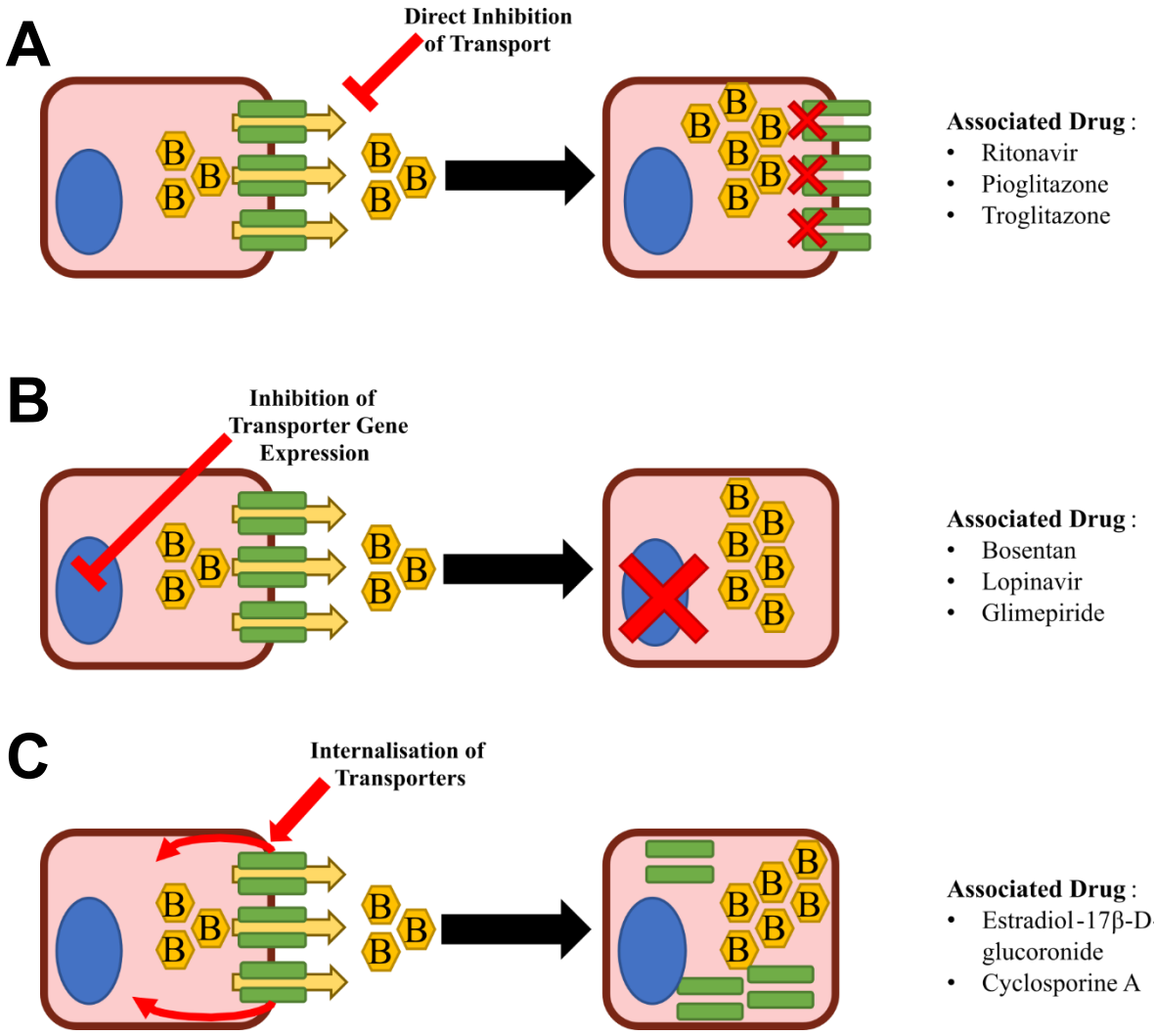

Figure 1: Common mechanisms by which a cholestatic drug may cause impaired bile acid transport. A) direct inhibition of the transporter, B) inhibition of transporter gene expression, and C) internalisation of transporters. Transporters are depicted in green, the nucleus in blue, and bile acids (B) in yellow.

The causative drugs for cholestasis are diverse and include antimicrobials, anti-cancer drugs, antidepressants, antipsychotics, immune suppressants, antiepileptic drugs, contraceptive drugs, anabolic steroids, diabetes medication, opioid analgesics, and non-steroidal anti-inflammatory drugs (NSAID) (57, 96-99). While specific mechanistic and causal links of drug-induced cholestasis remain poorly characterised for many of these

drugs, it has been shown that impact on the bile acid transporters is the primary cause (15, 100-103). Cholestasis-associated drugs have been shown to directly inhibit bile acid transporters, alter gene expression, and the localisation of bile acid transporters (Fig. 1). The bile salt export pump (BSEP) is the primary bile acid exporter and is directly inhibited by a wide variety of cholestasis-associated drugs including ethinyl estradiol, pioglitazone, ritonavir, rosiglitazone, and troglitazone (100). Additionally, many of the compounds that inhibit BSEP also inhibit other bile acid exporters, such as multidrug resistance-associated proteins 2, 3, and 4 (MRP2, MRP3 and MRP4, respectively), although commonly with reduced potency (101). Furthermore, some cholestasis-associated drugs may affect gene expression of bile acid transporters. In an investigation of 30 drugs, 15 caused downregulation of BSEP messenger RNA (mRNA) and decreased BSEP protein levels (15). Bosentan, ethinyl estradiol, ritonavir, and troglitazone were among the 15 drugs that decreased BSEP expression and are all known to be cholestasis-associated drugs (76, 104-106). Finally, while not as common as direct inhibition of bile acid transporters or downregulation of bile acid transporter expression, cholestasis also may be induced by a drug causing internalisation and intracellular retention of bile acid transporters. Estradiol-17β-D-glucuronide, a glucuronide metabolite of estradiol that occurs endogenously and that is also generated from drugs such as ethinyl estradiol, has been found to prevent the canalicular localisation of BSEP and MRP2 in *in vivo* rat studies at 15 μmol/kg (102, 103). This internalisation and intracellular retention is due to activation of classical protein kinase C (cPKC) and phosphoinositide 3-kinase (PI3K) pathways (107). Similarly, cyclosporine A causes internalisation and intracellular retention of BSEP in rat hepatocytes, which may be due to its capacity to activate cPKC

and PI3K pathways (108-110). Cholestasis, while occurring through several mechanisms, is primarily caused by drugs interfering with the normal function of bile acid transporters in hepatocytes leading the accumulation of bile acids within the liver.

Steatotic Drug-Induced Liver Injury

Steatosis, the accumulation of lipids within hepatocytes, is another commonly occurring DILI phenotype, especially as a comorbidity, which has been reported to occur in 64% of DILI cases (93). Drug-induced steatosis is a form of NAFLD caused by drugs such as amiodarone, methotrexate, NSAIDs, and tetracycline (111-114). Steatosis is a concerning occurrence as a DILI phenotype because it has been reported that 73% of patients who required a liver transplant or had a fatal outcome exhibited steatosis as a histological feature (93). Steatosis has a histological presentation that occurs as microvesicular, macrovesicular, or mixed steatosis, which presents with both microvesicular and macrovesicular histologies (115). Microvesicular steatosis is characterised by lipid accumulation within hepatocytes that occurs as clusters of minute lipid vacuoles within hepatocytes that gives the cells a foamy appearance, but does not displace the cell's nucleus (116). In contrast, the histology of macrovesicular steatosis occurs as large vacuoles of lipids, classically a single large droplet, but also may occur as clusters of small or medium droplets that displace the nucleus. Both forms of steatosis may occur with or without lobular inflammation, however liver injury severity often correlates with the degree of inflammation (117). Clinically, macrovesicular steatosis is the more common of the two forms, occurring in 72% of cases solely, or 14% of cases as mixed steatosis (93). A more severe form of steatotic liver injury is steatohepatitis, distinguished from steatosis by the occurrence of hepatocyte "ballooning". Hepatocyte

ballooning presents as a 1.5 to 2 times enlargement of hepatocytes with rarefied cytoplasm and injury to the cytoskeleton including (1) loss of intact cytokeratin 8 and 18, (2) increased presence of Mallory-Denk bodies, and (3) increased presence of cytokeratin 18 fragments (118-120). Steatohepatitis is a concerning occurrence with DILI as compared to other NAFLD injury phenotypes that have a liver-related mortality rate of 1.7% while non-alcoholic steatohepatitis (NASH) has a liver-related mortality rate of 11% (121). The damage to hepatocytes related to the cellular ballooning results in more severe hepatocellular damage compared to lipid accumulation or steatosis-induced inflammation. Phospholipidosis involves the lysosomal accumulation of phospholipids. Clinically, it is not usually well distinguished from glycerolipids-based steatosis as its main feature is lamellar bodies that requires techniques such as electron microscopy to identify (122-124). Drug-induced hepatic phospholipidosis is characterised by the accumulation of phospholipids within hepatocytes and lamellar inclusions, both commonly of lysosomal origin (125).

Drugs induce hepatic lipid accumulation by multiple, diverse mechanisms (Fig. 2). Microvesicular steatosis is associated with drugs such as amiodarone, tetracycline, and valproic acid (126-129), and is likely to result primarily from impairment in the capacity of mitochondria to perform fatty acid oxidation (FAO). The non-esterified fatty acids are not significantly oxidized by the mitochondria and, therefore, undergo esterification into glycerolipids that accumulate in microvesicles in the liver (130). Macrovesicular steatosis is associated with drugs such as amiodarone, diclofenac, and estrogens (131-133). While macrovesicular steatosis also may be induced by impairment of FAO, it also can be caused by impaired microsomal triglyceride transfer proteins (MTTP), a drug-induced

increase in uptake of fatty acids, and/or direct stimulation of lipid synthesis within the liver through activation of lipogenic transcription factors (134-137). Phospholipidosis is strongly associated with cationic amphiphilic drugs (CAD) such as amiodarone and perhexiline (131, 138). There are two predominant hypotheses for the mechanism of drug-induced phospholipidosis: 1) drugs directly bind to the phospholipids producing drug-phospholipid complexes that accumulate within lysosomes and cannot be digested by phospholipases, and 2) direct or indirect inhibition of phospholipases by the phospholipid-associated drugs (125, 139).

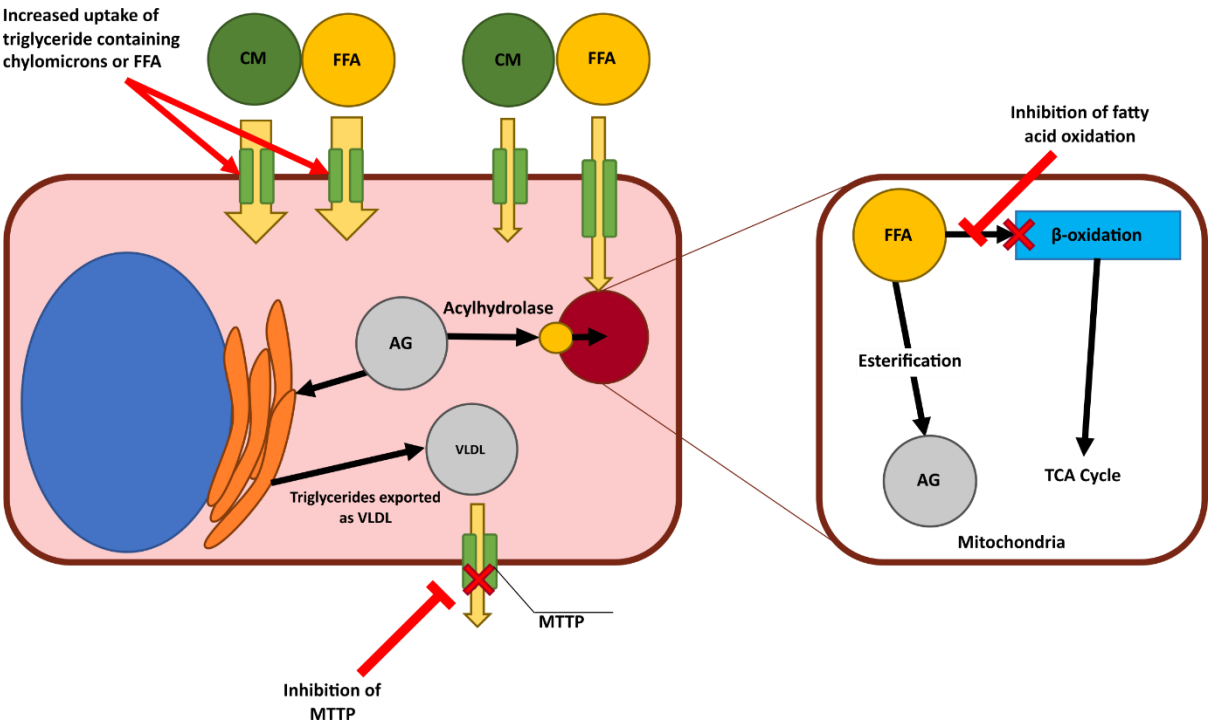

Figure 2: Mechanisms by which drugs may disrupt lipid transport and metabolism leading to steatosis in hepatocytes. Drug-induced steatosis may result from increased uptake of free fatty acids (FFA) and chylomicrons (CM), impaired fatty acid oxidation (β-oxidation) and resulting esterification of excess FFA to glycerolipids (AG), and impaired exported of very low-density lipoproteins (VLDL) by inhibition of microsomal triglyceride transfer proteins (MTTP).

Models for Drug-Induced Liver Injury

One of the most effective methods to combat DILI is to identify causative agents before they are released to market, and to understand the mechanisms that cause the hepatotoxicity of current DILI-associated compounds. To achieve these objectives, effective and translatable liver models are needed. A number of *in vitro*, *in vivo* and *ex vivo* liver models have demonstrated utility for experimental studies of DILI. The greatest strength of *in vivo* and *ex vivo* models is that they offer a holistic view that can account for the interactions of various cell types and tissue structures, more complex transport and biosynthesis pathways, more robust cellular protection mechanisms, and, for *in vivo* models, interorgan interactions (140-142). While *in vivo* and *ex vivo* animal models might seem ideal for studying DILI, they are usually more costly, less accessible and require significant ethical considerations to prevent any unnecessary suffering of animal subjects, especially considering the toxicological nature of DILI research. Most importantly, hepatotoxicity data generated in animal models may not translate to humans due to species-specific differences in DILI mechanisms. Alternatively, *in vitro* models using human hepatocytes and hepatic-like cells are more practical for many researchers to investigate DILI. The *in vitro* liver models include the use of various cell types such as primary hepatocytes, which offer the most similar genomic expression to liver tissue, and immortalised hepatic-like cells that are capable of proliferation and, therefore, offer an affordable and practical means to generate a large volume of hepatic-like cells for experimental studies (143). Additionally, immortalised hepatic-like cells have the added benefit that genetic modifications can be applied, such as knocking out specific

transporters; these cell lines offer an affordable alternative to primary hepatocytes with similar genomic and proteomic profiles (143-145).

In vitro primary human hepatocytes (PHH) are the ideal choice of cells to achieve the greatest similarity in genomic expression to human liver tissue (143). Furthermore, PHH offer a metabolically competent and physiologically relevant *in vitro* model for translation to human liver tissue (146). A study comparing the genomic expression profiles of human liver tissue to PHH obtained a Pearson product-moment correlation coefficient (*r*) of 0.920, indicating a strong correlation in expression profiles. However, 22% of genes had a greater than 2-fold differential expression when comparing human liver tissue to PHH. This was attributed to the fact that human liver tissue is comprised of 70-80% hepatocytes with the remainder consisting of epithelial cells, cholangiocytes, stellate macrophages, and other hepatic cell types that possess different gene expression profiles (143). While there are options to utilise primary hepatocytes from other species, such as rats or dogs, this can introduce unwanted variability due to species-based differences; the fialuridine trial is a prime example of this. A significant issue in the use of primary hepatocytes from other species as an *in vitro* model for the human liver is the difference in protein abundance and function. While there are many conserved proteins, such as the cytochrome P450 (CYP) enzymes or transporters, these occur in different abundances and isoforms between species that alter their behaviour, which is especially problematic when investigating drug interactions with these proteins (147-151). Although the use of PHHs may provide the closest representation to human liver in response to drug exposure, the same experiment performed using hepatocytes from another species may give vastly different results. Variations between primary human and non-human

hepatocytes have been observed in numerous studies. A significant limitation to using animal models in place of humans, especially in the context of investigating DILI where a bile acid dependence may be present, is the species-based variation in bile acid composition. The variations in plasma bile acid composition and abundance are substantial between humans and other animals (Fig. 3). For example, Sprague-Dawley rats have 3-times higher concentrations of total plasma bile acids compared to humans (12 μM vs 3.9 μM, respectively) with cholic acid comprising 30% of the rat's total plasma bile acid pool but only 11% of human's total plasma bile acid pool (152).

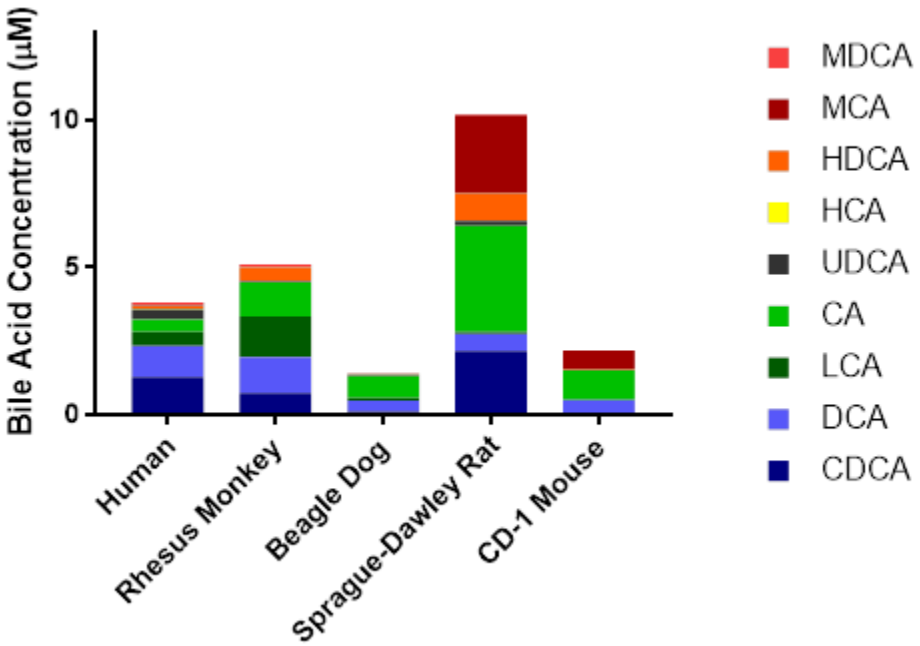

Figure 3: Concentrations of plasma bile acids in different mammalian species. Murideoxycholic acid (MDCA), muricholic acid (MCA), hyodeoxycholic acid (HDCA), hyocholic acid (HCA), murideoxycholic acid (MDCA), ursodeoxycholic acid (UDCA), cholic acid (CA), lithocholic acid (LCA), deoxycholic acid (DCA) and chenodeoxycholic acid (CDCA) were quantified among a variety of different mammalian species (152).

Furthermore, drug treatment of primary hepatocytes with rifampicin, a potent CYP3A4 inducer in humans, had no effect on CYP3A4 induction in primary rat

hepatocytes (PRH) (126). Rates of drug metabolism can also vary among species. For instance, diazepam metabolism occurs 3.6 times faster in primary pig hepatocytes and 1.5 times slower in PRH compared to PHH (153). There are examples in which the experimental outcome was completely different between human and animal-derived primary hepatocytes. This was evident in the treatment of PHH and PRH with chenodeoxycholic acid CDCA, which caused an increase in intracellular abundance of CDCA, taurochenodeoxycholic acid (TCDCA), and glycochenodeoxycholic acid (GCDCA) in PRH over a 24-hour treatment while PHH showed a depletion of these compounds (154). Additionally, treatment with lithocholic acid (LCA) showed significantly different degrees of toxicity and a vast difference in the abundance of intracellular lithocholic acid conjugates between PRH and PHH (154). Another facet of inter-species variation that is vital to recognise is the variation in hepatic transporters, both in abundance and isoforms. The variation in transporter expression between species is vast, with the relative abundance of transporters such as BSEP, Na^+-taurocholate co-transporting polypeptide (NTCP), MRP2, and organic-anion-transporting polypeptides (OATP) varying markedly (Table 2) (151, 155).

Table 2: Relative Abundance (%) of Quantifiable Transporters in Liver Tissue of Humans, Monkeys, Rats, and Dogs (151)

Relative Abundance (%)					
Origin of Liver Tissue	***BSEP***	***NTCP***	***OATP***	***MRP2***	***OCT1***
Human	13%	13%	29%	9%	27%
Monkey	7.5%	3%	46.5%	9%	32%
Sprague-Dawley Rat	6%	22%	43%	20%	6%
Wistar Rat	5%	18%	48%	20%	6%
Dog	8%	N/A	69%	9%	2%

Such discrepancies in transporter abundance and species-related isoforms can lead to variations that may impair the ability of an animal-derived hepatocyte to sufficiently model human liver function. Species-related isoforms may cause certain transporters to exhibit different K_m and V_{max} values, resulting in different transport capacity of certain substrates. Accurate modelling of BSEP transporter function is vital when studying DILI because it is linked to several mechanisms for cholestasis (15, 76, 104-106). Using non-human Bsep proteins can be problematic. For example, even though rat BSEP (rBSEP) or dog BSEP (dBSEP) transporters share 82% and 89.4% of their amino acid sequence with human BSEP (hBSEP), respectively, variations are still present (150, 156). The transport of taurocholate by BSEP is known to differ between species: dBSEP (K_m: 33.7 µM, V_{max}: 219 pmol/min/mg protein), rBSEP (K_m: 22.2 µM, V_{max}: 237 pmol/min/mg protein), and hBSEP (K_m: 19.9 µM, V_{max}: 98.5 pmol/min/mg protein) (150). Furthermore, proteins from different species respond with difference sensitivities to drug treatment, with Bsep inhibition by drug treatment varying up to 25-fold when comparing rBSEP to hBSEP

(150). It is critical to take these species differences into consideration when selecting a model to study human diseases, such as DILI, since using a model with different drug sensitivities, affinities, protein abundance, and other variations in metabolic behaviour, can reduce the ability for the results to translate from the non-clinical to the clinical setting. Although PHH offer an *in vitro* gold standard in recreating *in vivo* metabolic activity in humans, there are still a significant number of conserved metabolic characteristics between species that do allow for animal-derived primary hepatocytes to be applicable for research when selected appropriately (143, 148).

A common alternative to PHHs is immortalised hepatic-like cells such as HepaRG, HepG2, and HuH-7 cell lines. Immortalised hepatic-like cells derived from patients with liver carcinomas are capable of indefinite proliferation and possess various hepatocyte-specific characteristics (157-159). By far the most commonly used immortalised hepatocyte cell line is the HepG2 cell line, which was established in 1979 from a liver tumour biopsy of a 15-year-old Caucasian male with hepatocellular carcinomas (157). The prevalence of HepG2 as a model for human hepatocytes can be attributed to the fact that it is a highly accessible and affordable cell line with some metabolic similarity to PHHs (143-145, 160, 161). HepG2 cells, as with many carcinoma-derived cell lines, rapidly proliferate with a doubling time of 48 hours and require only a simple culture media of Modified Eagle Media, fetal bovine serum, and glutamine (157). While this allows ready access to HepG2 cells for many researchers, the similarity of HepG2 cells to PHHs and human liver tissue is limited. When assessing its genomic expression profile, the similarity to liver tissue gene expression was only moderate (r= 0.791) (143). While a moderate correlation may still be adequate for some studies, it was less than PHH (r=0.920) (143).

There are a large number of differentially expressed genes in the HepG2 cell line when compared to PHH (37%) and liver tissue (39%) (143). While this indicates some overlap in metabolic behaviour between HepG2 cells, PHH and liver tissue, there are limitations in the ability of HepG2 cells to act as a holistic model for *in vivo* hepatocyte behaviour. This is further illustrated when comparing the protein expression from major metabolic pathways between HepG2 cells and PHH such as fatty acid β-oxidation (8.4% of PHH), the TCA cycle (9.5% of PHH), and bile acid biosynthesis (5.1% of PHH). Expression of phase I and phase II enzymes is substantially decreased, as low as 0.6% and 0.7% of PHH, respectively, with major enzymes such as CYP3A4 expressed at 0.5 to 1.5% of PHH (144, 145). Transport proteins, which are vital to hepatocyte behaviour, are also significantly altered with all major transporters showing decreased expression, including BSEP, NTCP, and OATPs with the exception of multidrug resistance protein 1 (MDR1) (221% of PHH), MRP2 (114% of PHH), and OCT3 (186% of PHH) (Table 3) (144). However, while HepG2 cells may show some limitations, they are capable of forming bile canalicular structures and sufficiently express MDR1, MRP2, OCT3, and several phase I and II enzymes (144, 145, 162). For studies focussing on these well-expressed proteins, HepG2 cells offer a sufficient model that is accessible and affordable.

Table 3: Relative Abundance (%) of Various Hepatic Excretion and Uptake Transporters in HepG2 Cells Compared to PHH (144)

HepG2 vs PHH (%)			
Excretion Transporters		***Uptake Transporters***	
BSEP	1%	*OAT2/7*	1.3%
MDR1	221%	*OAT7*	1%
MRP2	114%	*OCT1*	0.6%
MRP3	11%	*OCT3*	186%
MRP6	5%	*OATP1B1*	0.6%
MATE1	405%	*OATP1B3*	0.5%
		NTCP	4%

A recent alternative to HepG2 cells is differentiable HepaRG cells. HepaRG cells were established from the liver tumour of a female patient with an Edmondson grade I differentiated liver tumour associated with chronic hepatitis C (158). HepaRG cells are capable of proliferation, allowing for large cell volumes to be generated from an initial stock. In addition, they also can be differentiated by the inclusion of DMSO in the media, producing a culture with closer similarities to PHH (143, 145, 160). The similarity of genomic expression in HepaRG cells to human liver tissue was better than HepG2 cells (r=0.881 vs 0.791, respectively), but still less than PHH (r=0.920). Additionally, only 26% of genes were differentially expressed in HepaRG cells compared to human liver tissue, and 28% when compared to PHH (143). HepaRG cells demonstrate metabolic competency in relation to PHH by having comparable levels of protein expression in major metabolic pathways such as the TCA cycle (59% of PHH), bile acid synthesis (42% of

PHH), and fatty acid β-oxidation (34% of PHH). Although these values are lower, they are still within the same order of magnitude of PHH expression levels, unlike HepG2 cells (145). The value of HepaRG cells as an alternative model for PHH is further illustrated when assessing the activity and abundance of CYP enzymes. The predominant phase I liver enzyme, CYP3A4, is highly expressed in HepaRG cells within an order of magnitude of PHH (236% of PHH) and shows similar levels of activity, especially when compared to HepG2 cells (Table 4) (145, 163).

Table 4: Comparison of Metabolic Rates of CYP3A4 from PHH, HepaRG, and HepG2 Cells Using Midazolam as a Probe Substrate (163)

Cell Type	***CYP3A4 Activity (pmol/h/50,000 cells)***
2D-cultured PHH	27.4 ± 1.5
2D-cultured HepaRG	85.6 ± 4.5
2D-cultured HepG2	0.64 ± 0.04

Expression of other Phase I and II enzymes in HepaRG cells is comparable to PHH, including CYP3A5, CYP4FB, CYP20A, glutathione S-transferase A1, glutathione S-transferase K1, glutathione S-transferase T1, UDP-glucuronosyltransferase 1A9, and UDP-glucuronosyltransferase 2A3 (145). However, there are still a number of enzymes that have significantly decreased expression in HepaRG cells, such as UDP-glucuronosyltransferase 2B7 (1.5% of PHH), UDP-glucuronosyltransferase 2B10 (2% of PHH), CYP1A2 (2.4% of PHH), and CYP2D6 (1.6% of PHH) (145). HepaRG cells also offer a suitable surrogate to PHH across a variety of important liver transporters including MRP2, MRP3, NTCP, OAT2, OCT3, and OATPs; although BSEP is present at only 8%

of expression in PHH, this still represents an 8-fold increase over HepG2 cells (Table 5)(145, 164). In addition to improved expression of important liver enzymes, HepaRG cells can form distinct and well-polarised biliary canaliculi (165). While HepaRG cells may still show some differential gene expression and metabolic behaviour when compared to PHH, they offer an accessible alternative to PHH. Their ability to proliferate allows for generation of a large number of cells that can be differentiated into non-proliferating hepatic-like cells with improved metabolic competency compared to HepG2 cells.

Table 5: Relative Abundance (%) of Various Hepatic Excretion and Uptake Transporters in HepaRG Cells Compared to PHH (145, 164)

HepaRG vs PHH (%)			
Excretion Transporters		***Uptake Transporters***	
BSEP	8%	*OAT2*	44%
MDR1	174%	*OCT3*	60%
MRP2	78%	*OATP1B1*	22-38%
MRP3	167%	*OATP1B3*	2-15%
MRP6	32%	*NTCP*	191-247%

Another hepatocyte cell line of note are HuH-7 cells, which were established in 1982 and derived from a surgically removed hepatoma tissue of a 57-year-old Japanese male (159). While this cell line possesses similar metabolic and genomic expression to HepG2 cells, it has been shown to be a useful surrogate to PHH for specific transport studies (166-168). HuH-7 cells, when cultured for 4 weeks with dexamethasone, form distinct canalicular structures with BSEP, MDR1, and MRP2 expressed and localised to the canalicular membrane. This expression of bile acid transporters and formation of

biliary canaliculi led to the use of HuH-7 cells for hepatocyte transporter studies (167). Furthermore, HuH-7 cells express OATPs and OSTα/β transporters on the basolateral membrane, offering a useful alternative to PHH for studies related to these transporters (168). With such a wide variety of different hepatocyte and hepatic-like options for use as *in vitro* models to study DILI, it is important that selection of a hepatocyte model is made carefully to best represent the desired *in vivo* conditions.

Analytical Techniques for Investigation of Drug-Induced Liver Injury

Identifying the potential for drugs to cause DILI and the mechanisms by which this occurs is possible using *in vitro* models. These studies can range from simple plate-based methods such as the B-CLEAR® transporter assay, or microscope imaging-based assays, to more complex studies analysing variations in biomolecules such as genomics, transcriptomics, proteomics, and metabolomics. These studies offer a wide variety of different outputs that can help describe the capacity for a drug to cause DILI and potential mechanisms by which toxicity occurs (Table 6).

Table 6: Non-omics Based Analytical Techniques Applicable for DILI Studies

Assay	Method	Outcome	Advantages/Limitations
Cell viability assay	A spectroscopic change is made to a chemical indicator based on the function of a cell's mitochondria. Viability is commonly measured by the cellular ATP content or the presence of viable mitochondrial enzymes	Quantifies the relative number of functional mitochondria present in a culture	Accessible measurement of cytotoxicity that can be conducted in a high-throughput manner . Measurements are non-specific and are based on biomarkers of viability which may be impacted without permanent cell death
C-DILI™ assay	Comparison of viability of drug-treated control hepatocytes and cholestatic-sensitised hepatocytes	Determines a drug's potential to cause bile acid-mediated hepatotoxicity and its risk of causing cholestatic DILI	Specific assay for high-throughput determination of cholestatic potential of chemicals. Requires use of Transporter Certified primary human hepatocytes
Membrane integrity assay	A spectroscopic change is made to a chemical indicator based on the amount of lactate dehydrogenase (LDH) released from cells due to the loss of cell membrane integrity	Quantifies the amount of LDH released from cells due to loss of cell membrane integrity. In many cases, it is assumed that the loss of integrity is due to cell death	Accessible measurement of cytotoxicity that can be conducted in a high-throughput manner. Measurements are non-specific and rely on the presence of LDH, which has a 6- to 8-hour half-life potentially leading to inaccurate results
Apoptosis assay	A spectroscopic change is made to a chemical indicator based on the caspase-3 and/or -7 abundance within a cell culture	Gives an indication of the relative amount of apoptosis that a cell population is experiencing	Accessible measurement of apoptosis that can be conducted in a high-throughput manner . Cell death occurring through non-apoptotic pathways may be poorly assessed
Western blot	Gel electrophoresis followed by attachment of a primary antibody to a target protein followed by the attachment of a secondary antibody	Determines if a specific protein is present in a biological protein extract, and provides a semi-quantitative indication of relative abundance	Antibodies are specific and sensitive to target proteins; data are only semi-quantitative. Primary antibodies are expensive and may not be available for all target proteins
B-CLEAR® assay	Comparison of cellular accumulation vs cellular and biliary accumulation of transporter substrates by comparing cells with and without sealed tight	Quantifies functional changes in hepatocyte basolateral (uptake) and canalicular (biliary excretion) transporters	Offers quantitative measurement of changes in transport and cellular concentrations of bile acids and/or xenobiotics. Requires use of Transporter Certified

	junctions forming bile canaliculi		primary human hepatocytes for greatest accuracy
Transporter localisation	Immunofluorescence microscopy of target transport proteins via the use of primary and fluorescent-labelled secondary antibodies	Assesses the localisation of hepatic transporters	Offers semi-quantitative spatial information about transporter location within cells; cannot be applied to live cells and antibodies
Neutral lipid staining	Staining of hepatocytes with lipophilic dyes (e.g., BODIPY, Oil Red O) for fluorescence microscopy	Identifies the intracellular accumulation of neutral lipids caused by drug treatment resulting in steatosis	Allows for the accessible and potentially high-throughput visualisation of neutral lipid accumulation. Degree of accumulation can only be assessed semi-quantitatively and does not stain phospholipids
Lysosomal staining	Staining of acidic lysosomal environment with dyes (e.g., NBD-PE, HCS LipidTOX™, LysoTracker™) for fluorescence microscopy	Determines whether lysosomes have increased in size or abundance and may be used to identify phospholipidosis	Allows for the accessible and potentially high-throughput visualisation of changes in lysosomes. Lysosomal changes are semi-quantitative

The B-CLEAR® transport assay is a plate-based assay that can be used to quantify the impairment of hepatic transporters (169, 170). Functional transporters are an important factor for hepatocyte homeostasis and the prevention of toxic accumulation of xenobiotics or endogenous molecules, and dysfunction of transporters commonly leads to cholestasis or other harmful forms of liver injury (15, 66, 100-104). By assessing changes in the biliary excretion index (BEI) of hepatocytes or hepatic-like cells, the B-CLEAR® assay can provide insights regarding the drug accumulation in hepatocytes and the impact that cholestatic-associated compounds, such as bosentan or troglitazone, can have on biliary transport (170, 171). Troglitazone and bosentan, well-known cholestasis-associated drugs, were shown by the B-CLEAR® assay to decrease uptake of taurocholate, an NTCP substrate, by 3- and 12-fold, respectively. Uptake of estradiol-

17β-D-glucuronide, an OATP substrate, was reduced by 4-fold in response to troglitazone treatment and 7-fold by bosentan treatment. Furthermore, troglitazone and bosentan decreased the biliary excretion index of taurocholate from 55% to 27% and 10%, respectively (170). Thus, the B-CLEAR® assay can: 1) assess the capacity of a drug to impact hepatic transporters and, therefore, its potential to disrupt hepatocyte homeostasis, and 2) identify possible mechanisms that may lead to the onset of DILI.

The capacity of a compound to inhibit the hBSEP transporter is not sufficient to determine a drug's cholestatic-inducing potential due to the involvement of other transporters and compensatory mechanisms in hepatocytes (101, 172). Therefore, the C-DILI™ plate-based assay was developed to assess more accurately the potential for a drug to specifically induce cholestasis. Using this system, free fatty acids (FFA) and exogenous bile acids are added to appropriately challenge hepatocytes so that any drugs capable of inducing cholestasis will have a distinct hepatotoxic impact under these conditions. This was illustrated in a C-DILI™ study comparing cyclosporin A (CysA) and troglitazone, both potent BSEP inhibitors (CysA, IC_{50}=0.5 µM; troglitazone, IC_{50}=3 µM) (101, 173). While both drugs are capable of inhibiting BSEP, there is a much greater potential for fatal cholestatic liver injury caused by troglitazone compared to CysA observed in the C-DILI™ assay, which has been reflected in clinical studies (35-41, 173-178).

Image-based assays can provide information about the effects of drugs on transporter localisation or their potential for inducing the liver injury phenotypes associated with steatosis and phospholipidosis. A common and powerful imaging tool for assessing transporter localisation and abundance are immunofluorescence microscopy

assays (IFAs). IFAs utilise affinity-based biology (antibodies) coupled with fluorescent reporters and can be performed in two ways: direct, where the fluorophore is conjugated directly to the antibody targeting a specific transporter; or indirect, which involves a secondary antibody/fluorophore conjugate that targets the anti-transporter immunoglobulin class (such as anti-IgG) (103, 108, 167, 168). The added benefit of these techniques is the variety of fluorophores available for multiplexing assays, allowing the investigation of multiple transporters in a single assay. IFAs have been used to assess and optimise the expression and localisation of organic anion transporters as well as MDR1 and BSEP in HuH-7 cells under different *in vitro* conditions (167, 168). Additionally, IFAs have been used to demonstrate the capacity for estradiol 17β-D-glucuronide and CysA to cause the internalisation of the BSEP transporter in PRH (103, 108). Lipid staining dyes, such as the green, fluorescent dye, BODIPY, or the red colourimetric dye, Oil Red O, are commonly used to assess the accumulation of neutral lipid droplets and can be used to detect drug-induced steatosis (179-182). Identifying the ability of a drug to increase the presence of neutral lipids as droplet accumulations *in vitro* can be used to assess the potential for causing drug-induced steatosis *in vivo*. Clinical data for steatogenic drugs correlate well with their ability to cause *in vitro* steatosis; drugs such as amiodarone, methotrexate, tamoxifen, and tetracycline have steatogenic properties both in clinical and *in vitro* studies (22, 183). However, these lipid dyes mentioned above primarily detect glycerolipids-based lipid accumulation but poorly identify phospholipidosis and, therefore, modified dyes or techniques are needed to detect accumulation of multiple lipid species (124). The detection of phospholipidosis is performed most commonly by using electron microscopy to identify lamellar inclusions in

hepatocytes; however, this is a tedious technique that does not allow for high-throughput screening and requires expert training. Phospholipidosis may be identified with lysosomal dyes including 2-(4,4-difluoro-5-methyl-4-bora-3a,4a-diaza-*s*-indacene-3-dodecanoyl)-1-hexadecanoyl-*sn*-glycero-3-phosphocholine (β-BODIPY C_{12}-HPC), N-(7-nitrobenz-2-oxa-1,3-diazol-4-yl)-dipalmitoylphosphati-dylethanolamine (NBD-PE), HCS LipidTOX™, or LysoTracker™, which would be used to detect an increased volume and abundance of lysosomal vesicles, the accumulation site of phospholipids when phospholipidosis is induced (124, 184). The use of image-based detection assays for glycerolipids and phospholipids allows for high-throughput screening of drugs to identify their potential to cause steatosis or phospholipidosis (184, 185).

Recently, high-content plate-based assays were developed in which various assays using fluorescent probes, antibodies, and reactive dyes were combined to characterise the nature of a drug's hepatotoxicity behaviour across several parameters (186). These parameters can assess the production of reactive oxygen species and changes in glutathione abundance, changes to membrane permeability, formation of biliary canaliculi, lipid accumulation, bile-acid dependant toxicity, and impairment of mitochondrial membrane potential and mitochondrial toxicity (186, 187). Furthermore, using receiver operating characteristic analysis can allow for the outcomes of these assays to grade the hepatotoxic potential of the drugs tested (186).

Application of Omics to Investigate Drug-Induced Liver Injury

Omics is a broad term that encompasses the four fields of genomics, transcriptomics, proteomics, and metabolomics. Each of these fields offers powerful tools that can be used to investigate and dissect DILI from susceptibilities and changes

in gene expression after drug treatment to biological perturbations of proteins and metabolites, which may offer mechanistic insight into the causes of DILI.

Genomics

Genomics was one of the first omics fields to be developed. Genomics is the science of characterising an organism's genetic code, focussing on evolutionary relationships, genome structure and correlating gene sequences with biological functions of the organism (188). Genomics is a powerful tool in the DILI field; research has concentrated on identifying single nucleotide polymorphisms (SNPs) – gene variants that may lead to increased susceptibility to DILI (189). A common cause of susceptibility comes from SNPs within immune-related genes, such as the human leukocyte antigen (HLA) gene or genes related to cytokines (190-195). Amoxicillin-clavulanate, lapatinib, and lumiracoxib have all been associated with specific HLA gene variants that have resulted in a greater susceptibility of patients to DILI. Amoxicillin-clavulanate was associated with three haplotypes for susceptibility to DILI; HLA class II *DRB1*15:01-DQB1*06:02*, which is known to indicate susceptibility to other drugs as well, and HLA class I *A*02:01* (191, 196). Lapatinib and lumiracoxib also were found to increase susceptibility to DILI in patients with the *HLA-DQA1*02:01* and *HLA-DQA1*01:02* genotypes, respectively. These variants were associated with a significantly increased occurrence of DILI versus control populations after treatment with lapatinib (71% vs 21%) and lumiracoxib (77% vs 46%) (194, 195). Furthermore, gene variants related to cytokines such as interleukin (IL)-4, IL-10, and Tumour Necrosis Factor (TNF)-α are associated with increased incidence of idiosyncratic DILI. IL-4 and IL-10 phenotypic susceptibilities were identified after treatment with diclofenac. The SNPs responsible for

these susceptibilities, IL-10-A627C (Odds ratio (OR): 2.84), and IL-4-T590C (OR: 2.6), demonstrated a significant association with diclofenac-induced liver injury, with the greatest effect occurring when both SNPs were present (OR: 5.3) (190). A similar trend also was observed with a gene variant of TNF-α, in which the TNF-α-G308A variant was identified to correlate as a risk factor for hepatitis induced by anti-tuberculosis drugs including isoniazid, rifampicin, and pyrazinamide (197). Genetic variants of phase II liver enzymes also introduce susceptibility to DILI, primarily because many of these gene variants exhibit reduced activity. N-acetyltransferase 2 (NAT2) is a phase II N-acetylation enzyme known to have several alleles in the human population. Patients with the *NAT2*5*, *NAT2*6*, and *NAT2*7* alleles are referred to as “slow acetylators”, in which the rate at which these alleles acetylate their substrates is reduced in comparison to other NAT2 alleles (198). These slow acetylation variants increase susceptibility to isoniazid and rifampicin-induced liver injury from 4- to 28-fold in Japanese patients (199). Additionally, for a population of 24 Singaporean patients treated with isoniazid, there was a significant correlation between DILI and slow *NAT2* variants (OR: 13.9) (200). Isoniazid and rifampicin are both substrates of NAT2, and the DILI observed among those with the slow acetylation variant is likely due to prolonged exposure to higher plasma concentrations of the anti-tuberculosis drug (201, 202). Furthermore, double null genotypes of the glutathione S-transferase genes *(GSTT1-GSTM1*) have been identified as risk factors for DILI induced by tacrine, troglitazone, NSAIDs, and amoxicillin-clavulanate (OR: 3.7, 2.8, 5.61, and 2.8, respectively) (203-205).

Transcriptomics

Transcriptomics is the next layer down from genomics and, instead of assessing variations in gene sequences and their association with DILI susceptibilities, it can be used to identify changes to genetic expression profiles that occur in response to treatment with DILI-associated drugs. Transcriptomics involves the use of microarrays or, more recently, RNA sequencing (RNA-seq), which allows for the characterisation of a biological system's transcriptome and changes to this transcriptome in response to stimuli. RNA-seq is commonly used in the pharmaceutical industry to investigate the potential for DILI. Recent animal studies showed that the larger dynamic range of RNA-seq can capture a greater number of differentially expressed genes with improved coverage of pathways that are relevant to hepatotoxicity compared to microarrays (206).

There is significant application of transcriptomics in drug development through the use of toxicogenomics for safety screening of new chemical entities (207). It is important to understand how the transcriptome of hepatocytes changes with exposure to a drug with DILI potential because this information can provide predictive and mechanistic insight into DILI. Transcriptomics has been used to generate predictive *in vitro* models for detecting DILI, with a predictive accuracy of 73% when comparing drugs strongly associated with severe and no incidence of DILI (208, 209). These models primarily focus on analysing variations in the expression of genes related to general cell injury such as apoptosis, necrosis, and inflammation (208, 210).

Transcriptomics also has been used to identify mechanistic perturbations that may result in hepatotoxicity associated with a specific drug. For example, several DILI-associated drugs, including ethinyl estradiol and ritonavir, impair BSEP gene expression

in an farnesoid X receptor (FXR)-dependant manner, which may be mechanistically linked to their cholestatic liver injury phenotype (15). In another example, CysA down-regulates OATP1B1, NTCP, Cytochrome P450 (CYP)3A4, and bile acid-CoA:amino acid N-acyltransferase (BAAT) (211). Valproic acid suppresses the expression of several ATP-synthases, fatty acid transporters, and other mitochondrial genes leading to mitochondrial dysfunction, steatosis and hepatotoxicity (212). Transcriptomics can be applied to determine the hepatocellular responses that may protect from fatal hepatotoxicity and allow for recovery from DILI. In a study of mouse models using APAP to induce both non-lethal DILI and DILI resulting in fatal liver failure, the non-lethal dose increased expression of *Myc*, *Bag3*, and *Btc,* which did not occur at a lethal dose. These genes are related to cell survival, as well as protective, repair, and stress responses; *Bag3* has anti-apoptotic activities and *Btc* induces cell survival and may explain how fatal liver failure is mitigated at lower doses (213). Additionally, betacellulin, the protein encoded by *Btc*, is present in serum and could potentially be used as a biomarker to predict a patient's likelihood of recovery from DILI.

A recent development in transcriptomics is single cell RNA-seq, which allows for individual cells to be sequenced. This can be invaluable when there is heterogeneity between cells, a known characteristic of hepatocytes (214, 215). The impact this heterogeneity could have on a hepatocyte's response to injury was shown in cholestatic mice in which several heterogenous groups of cholestatic hepatocytes were identified and shown to differentially regulate genes that affected their lipid metabolism and localisation, cholesterol esterification, and inflammatory-related gene expression (216). Single cell

RNA-seq is, therefore, a vital tool for investigating and characterising how cell heterogeneity can affect and alter a biological system's response to toxic stimuli.

Proteomics

It could be said that proteomics has long been used for detecting DILI in patients because the primary clinical assay for identification of DILI is detection of elevated AST and ALT liver enzymes in the blood. This concept of using serum proteins to detect liver injury has been further developed, improving the accuracy and sensitivity for detecting DILI. The accuracy that can be achieved by detecting elevations of apolipoprotein E (89%) is a notable improvement on the current clinical standard method of detecting changes in AST, ALT, and bilirubin (81%); however, further improvement to the detection accuracy for DILI is achieved when detecting changes in apolipoprotein E, inter-alpha-trypsin inhibitor, gelsolin, complement component C7, and serum amyloid P-component proteins (95%) in mice (217). Furthermore, detection assays for a specific DILI-associated drug have been proposed. APAP-induced liver injury is detectable by quantification of urinary levels of calmodulin in humans, which correlate with plasma APAP concentrations (r= 0.97) and were detectable before any ALT elevations in blood occurred (217). An assay for the detection of diclofenac-induced liver injury was developed *in vitro* and validated in patients with diclofenac-mediated DILI. A patient would be considered positive for diclofenac-mediated DILI if the serum expression levels of integrin beta 3 (ITGB3)-positive cells decreased below 60%, a decrease not observed in other DILI patients or other forms of liver injury not associated with a drug treatment (218). These new proteomic-based detection methods could prove to be important tools in reducing the large number of DILI cases that are not clinically identified, and potentially allow for

clinicians to intervene earlier before severe DILI occurs (30, 31). An even greater strength of proteomics is its ability to investigate biological perturbations of hepatotoxic compounds to identify mechanisms of toxicity. For example, HepaRG cells dosed with the mycotoxins deoxynivalenol (DON) and zearalenone (ZEA) exhibited a change in the abundance of up to 96 proteins, depending on dosing format and duration of exposure. The proteins that were significantly altered by DON and ZEA exposure included proteins related to cellular metabolic processes, stress response pathways, and cellular development and proliferation (219). Most notable was the significant decrease in abundance of DNA topoisomerase 1 and DNA topoisomerase 2-alpha, both shown previously to be affected as part of the broader mycotoxin mechanism of toxicity (219-221). Nevirapine (NVP), a non-nucleoside reverse-transcriptase inhibitor, has been associated with a high rate of DILI; with 5-12% of treated patients experiencing NVP-associated liver injury (222, 223). Dosing of HepG2 cells with NVP led to mitochondrial dysfunction, as indicated by altered abundance of 13 mitochondrial proteins (224). Important mitochondrial enzymes such as glyceraldehyde-3-phosphate dehydrogenase (GAPDH) and phosphoenolpyruvate carboxykinase (PEPCK) showed a 2.2- and 12.2-fold decrease in abundance following exposure to NVP, resulting in inhibition of DNA polymerase gamma leading to mitochondrial dysfunction and mitochondrial-mediated apoptosis (224-226).

Metabolomics

The final omics technique, metabolomics, is capable of characterising and determining changes to the metabolome of a biological system, which allows for identification of small molecular biomarkers and mechanistic insight into DILI. There has

been a variety of studies performed using metabolomics to identify serum biomarkers of DILI for use in pathology, and for discovery of *in vitro* biomarkers that predict DILI, as well as for characterisation of the injury phenotype. Several serum biomarkers have been identified and proposed for use in DILI diagnosis based on metabolites from primary and secondary bile acid biosynthesis, α-linolenic acid metabolism, and glycerophospholipid metabolism (227, 228). A significant increase in serum levels of palmitic acid, TCDCA, glycocholate (GCA), and tauroursodexycholate (TUDCA), in addition to a significant decrease in serum lysophosphatidylethanolamine levels was observed in DILI patients vs healthy controls. Additionally, the severity of DILI corresponded with increased serum levels of glycine and taurine conjugates [GCA, taurocholate, TUDCA, GCDCA, and taurodeoxycholate (TDCA)], with decreased serum levels of CDCA, deoxycholic acid (DCA), and LCA also corresponding to more severe DILI pathology (227, 228). The serum bile acids that increased in response to DILI were sensitive and specific differentiators of DILI compared to healthy controls, while the decreased serum bile acids were poor serum biomarkers of DILI (227). One limitation of the serum biomarkers is that their capacity to differentiate between DILI and other forms of liver injury is yet to been shown. MetaMap®-Tox is an excellent example of the application of metabolomics to identify the toxicological mode of action of compounds. MetaMap®-Tox is a database of serum metabolites from Wistar rats treated with compounds that have known toxicological modes of action; these metabolites are analysed and categorised to produce a database of biomarkers that can be used to determine a novel compound's toxicological mode of action (229-231). This toxicological biomarker database has been applied to identify the potential toxicological mode of action of drugs such as phenytoin, lamivudine, zidovudine, and phenobarbital

(232, 233). *In vitro* metabolomic studies can be used to classify the DILI-associated drugs into general classes of hepatotoxic mechanisms through the combined use of metabolomics analysis and Principal Component Analysis (PCA)-based clustering (234, 235). PCA comparisons of metabolomic data can be used to identify metabolite biomarkers of the DILI phenotypes such as oxidative stress, steatosis, and phospholipidosis. Metabolite biomarkers can be used to predict the likely general mechanism of hepatotoxicity based on metabolite fingerprints generated from DILI-associated drugs with known mechanisms of hepatotoxicity (235). A notable example of this was the use of lipidomics, a form of metabolomics that focuses on the analysis of hydrophobic metabolites commonly known as lipids, for the classification of steatogenic drugs by the increase in total triglycerides, diglycerides and phospholipids, and a metabolite profile indicating oxidative stress distinguishing between well-known mechanisms involving impaired β-oxidation and mitochondrial dysfunction (235-238). Additionally, lipidomic analysis of drug-treated 3D human microtissues allowed for a lipid fingerprint to be generated that showed that alterations to triacylglycerides and lysophosphatidylcholines abundance was indicative of a higher DILI risk. The lipidomics profile of the drugs tested in this study correlated with the DILIrank classification for their potential to cause DILI with drugs of higher risk showing similar changes to their lipid profiles (239). APAP is a drug that has been repeatedly studied for toxicity- and mechanism-related biomarkers. From mouse hepatic extracts, metabolomic studies have shown that APAP treatment results in glutathione depletion. The depletion of glutathione can lead to depletion of glutathione precursor metabolites such as hypotaurine and methionine, reflecting a cellular response to protect against APAP-induced oxidative

stress. In addition, mitochondrial dysfunction was observed due to impaired ATP synthesis and up-regulation of energy-related pathways indicated by the depletion of glucose and glycogen and the elevation of D-3-hydroxybutyrate (240). Urinary biomarkers for APAP toxicity assessed in rats revealed that the urine concentration of S-adenosylmethionine, a glutathione precursor, inversely correlated with APAP metabolites. Furthermore, urinary creatine, a general toxin-induced biomarker of oxidative stress, strongly correlated with APAP metabolites (241-243). Both of these metabolomic studies identified potential urinary biomarkers that are metabolically linked to APAP-induced oxidative stress. While the use of metabolomics to identify the mechanisms of specific DILI-associated drugs is limited, it has already been applied for toxicological examination of other compounds. The toxicological mechanisms of a variety of traditional Chinese medicines have been studied (244-248). Triptolide, an active constituent of *Tripterygium wilfordii* used to treat auto-immune disease, exhibited a mechanism of hepatotoxicity that involved perturbations to several pathways including glutathione metabolism, purine metabolism, taurine and hypotaurine metabolism, glycerophospholipid metabolism, and pyrimidine metabolism. These alterations to hepatocyte homeostasis resulted in increased reactive oxygen species (ROS), and subsequent oxidative stress to hepatocytes, dysfunction of the TCA cycle, and a decrease in anti-apoptosis metabolites such as cyclic guanosine monophosphate (cGMP) and taurine (244, 245). Metabolomics also has been applied to *in vitro* models studying the mechanisms of known toxins. For example, 2,3,7,8-tetrachlorodibenzo-p-dioxin (TCDD) is a well-known hepatotoxic carcinogen with anti-proliferative effects that causes a decrease in nucleotide and polyamine levels associated with TCDD's inhibition of DNA

synthesis and down regulation of ornithine decarboxylase, the main enzyme of polyamine biosynthesis. Furthermore, TCDD treatment of HepG2 cells decreased amino acids and metabolites in the fatty acid, sterol and energy metabolism pathways resulting from TCDD down-regulation or inhibition of important enzymes (249, 250). These perturbations are consistent with previous documentation of TCDD's toxic effects (251, 252). Previous investigations utilizing metabolomics, and omics techniques in general, have demonstrated how these powerful analytical tools could be applied to investigate DILI.

DILI is an important safety concern for numerous drugs prescribed to patients as well as for drugs in development. For decades, animal models and in vitro plate-based assays have served as the primary tools to detect potentially toxic drugs prior to first-in-human trials. With advancing technologies including sophisticated, human-relevant *in vitro* models, *in silico* tools, and even artificial intelligence (AI), there is an abundance of new approaches that can identify safety concerns earlier in drug development. However, for these models to achieve the greatest benefit, they need to be coupled with powerful analytical techniques that offer both a profound breadth and depth of information about biochemical changes due to toxic stimuli. Genomics, transcriptomics, proteomics, and metabolomics provide the technology to allow this to be achieved. For sophisticated, human-relevant models, the greatest benefit in using these models is achieved when an equally sophisticated analytical technique can determine the mechanism responsible for DILI for each drug. Furthermore, for the development of accurate *in silico* or AI models, which could predict DILI based on a chemical structure, extensive information will be required about DILI-associated mechanisms of existing compounds. This "big data" can be obtained through robust omics analysis. Previous investigations using omics

techniques have shown that these are immensely powerful analytical tools that can provide highly relevant mechanistic and predictive insight into DILI. It is imperative that an interdisciplinary and intersectoral approach is taken toward expanding the implementation of omics in pharmacology and toxicology to achieve the incredible potential that this analytical approach offers to revolutionize drug safety.

Thesis Aims

The core hypothesis of this thesis is that multi-omics, utilising proteomics, metabolomics, and lipidomics, can achieve broad and in-depth characterisation of *in vitro* models and biochemical perturbations that occur as a result of DILI. DILI is fundamentally the result of drugs having “off target” effects which cause changes to metabolic pathways leading to harmful perturbations to hepatocellular homeostasis and function. These changes can impact the proteome, metabolome, and lipidome of hepatocytes resulting in oxidative stress, mitochondrial dysfunction, and liver injury phenotypes such as cholestasis and steatosis (237, 253, 254). Additionally, for multi-omics to achieve the greatest insight into the toxicological perturbations to a biological system, the selection of metabolically competent *in vitro* models is paramount. The need for metabolically competent *in vitro* models is especially important when studying cholestasis and steatosis, liver injury phenotypes strongly associated with significant metabolic perturbations. It is vital to gain a better understanding of DILI as it is potentially fatal, with insidious onset and it often goes undiagnosed until severe liver damage has occurred (4, 24-28).

The first aim of this thesis was to utilise proteomics and metabolomics to characterise the differences between *in vitro* liver models and changes to an *in vitro* liver

model after treatment with DILI-associated drugs. Proteomics characterisation of the proteome of PHH and comparison with the proteome of HepaRG™ cells, an alternative *in vitro* liver model, was performed using multivariate analysis to determine if HepaRG™ cells would offer a similar level of metabolic competency as PHH. HepaRG™ cells are known to have a similar gene expression profile as that of human liver tissue and also form well-polarised biliary canaliculi (143, 165). However, it is imperative to assess whether the similarity in gene expression profiles translates to a proteome that is comparable to that of PHH. Furthermore, metabolomics and proteomics have a substantial capacity to characterise changes to metabolic behaviour. There would be immense value in applying a multi-omics approach, which utilises proteomics and metabolomics, to analyse the metabolic perturbations that are a result of exposure to DILI-associated drugs. Drugs such as ritonavir and troglitazone have a wide variety of detrimental effects on several important metabolic pathways, including glucose metabolism and mitochondrial respiration (255-257). Proteomics and metabolomics can be applied to characterise the proteome of an *in vitro* model, to assess its metabolic competency, and offer analytical and mechanistic insight into the perturbations of metabolites and proteins from vital metabolic pathways induced by treatment with a DILI-associated drug (Chapter 2).

The second aim of this thesis was to investigate the impact that cholestasis-associated drugs can have on bile acid-associated metabolites and proteins by applying a multi-faceted approach using relevant *in vitro* liver models. Drugs including troglitazone and estradiol have been shown to induce cholestasis, and it is imperative to understand the biochemical mechanisms through which these drugs can induce cholestatic liver injury

(104, 258). Cholestasis occurs due to the dysregulation of bile acid homeostasis and is known to be induced through at least one of three mechanisms; impairment of hepatocellular transport of bile acids, disruption of hepatocellular structure, and altered bile canalicular dynamics (254). A holistic multi-faceted approach towards characterising the cholestatic potential of DILI-associated drugs can be achieved by the application of functional plate-based assays, to determine bile acid-dependent hepatotoxicity and impairment of biliary transport, in combination with targeted bile acid metabolomics and proteomics, to determine alterations to the abundance of bile acid associated metabolites and proteins in response to drug treatment. Developing a greater understanding of the mechanism(s) of cholestatic DILI and the techniques through which it can be identified will allow for greater accessibility to the knowledge and tools required to prevent future cholestatic drugs from reaching the market (Chapter 3).

The final aim of this thesis was to utilise lipidomics to identify characteristic lipid changes that are specific to NASH and drug-induced steatotic liver injury. A wide variety of lipids are altered in patients experiencing NASH and steatotic DILI, with a number of changes to the serum lipid profile known to occur (259-261). The change in extracellular lipid profiles should be associated with similar changes in the intracellular lipid profiles of hepatocytes, which should be characteristic to NASH or drug-induced steatotic liver injury. Lipidomics and multivariate analysis would, therefore, be capable of characterising the changes in the lipid profiles and determining which changes are characteristic of NASH or drug-induced steatotic liver injury. Identifying characteristic lipid profiles for NASH and steatotic DILI would present an invaluable addition to toxicological screenings

during drug development for determining the steatogenic potential of a drug or identifying potential serum biomarkers (Chapter 4).

The research presented in this thesis was focused on using multi-omics to gain a greater depth of knowledge of the metabolic nature of *in vitro* liver models and the biochemical perturbations through which drugs can cause DILI. Understanding the pathways and mechanisms by which a drug may cause liver injury in metabolically competent liver models allows for a greater breadth and depth of knowledge in the field of DILI and liver toxicology, which can lead to the development of safer drugs and more powerful diagnostic techniques for liver injury. While the impact of DILI may be relatively small compared to other medical challenges, the insidious nature of DILI, the presence of DILI in nearly all drug classes, and the additional layer of risk that DILI adds to many pharmaceutical interventions clearly demonstrates the critical need to advance knowledge regarding the diagnosis and prevention of DILI.

References

1. Bjornsson ES, Bergmann OM, Bjornsson HK, Kvaran RB, Olafsson S. Incidence, presentation, and outcomes in patients with drug-induced liver injury in the general population of Iceland. *Gastroenterology*. 2013;144(7):1419-25.
2. Sgro C, Clinard F, Ouazir K, Chanay H, Allard C, Guilleminet C, et al. Incidence of drug-induced hepatic injuries: a French population-based study. *Hepatology*. 2002;36(2):451-55.
3. Suk KT, Kim DJ, Kim CH, Park SH, Yoon JH, Kim YS, et al. A prospective nationwide study of drug-induced liver injury in Korea. *Am J Gastroenterol*. 2012;107(9):1380-7.
4. Shen T, Liu Y, Shang J, Xie Q, Li J, Yan M, et al. Incidence and etiology of drug-induced liver injury in mainland China. *Gastroenterology*. 2019;156(8):2230-41.e11.
5. Goldberg DS, Forde KA, Carbonari DM, Lewis JD, Leidl KBF, Reddy KR, et al. Population-representative incidence of drug-induced acute liver failure based on an analysis of an integrated health care system. *Gastroenterology*. 2015;148(7):1353-61.e3.
6. Waring MJ, Arrowsmith J, Leach AR, Leeson PD, Mandrell S, Owen RM, et al. An analysis of the attrition of drug candidates from four major pharmaceutical companies. *Nat Rev Drug Discov*. 2015;14(7):475-86.
7. Meier Y, Cavallaro M, Roos M, Pauli-Magnus C, Folkers G, Meier PJ, et al. Incidence of drug-induced liver injury in medical inpatients. *Eur J Clin Pharmacol*. 2005;61(2):135-43.
8. Chalasani N, Fontana RJ, Bonkovsky HL, Watkins PB, Davern T, Serrano J, et al. Causes, clinical features, and outcomes from a prospective study of drug-induced liver injury in the United States. *Gastroenterology*. 2008;135(6):1924-34.
9. Friis H, Andreasen PB. Drug-induced hepatic injury: an analysis of 1100 cases reported to the Danish committee on adverse drug reactions between 1978 and 1987. *J Intern Med*. 1992;232(2):133-8.
10. Bjornsson E, Olsson R. Suspected drug-induced liver fatalities reported to the WHO database. *Dig Liver Dis*. 2006;38(1):33-8.
11. Idilman R, Bektas M, Cinar K, Toruner M, Cerit ET, Doganay B, et al. The characteristics and clinical outcome of drug-induced liver injury: a single-center experience. *J Clin Gastroenterol*. 2010;44(6):e128-32.
12. Hayashi PH, Rockey DC, Fontana RJ, Tillmann HL, Kaplowitz N, Barnhart HX, et al. Death and liver transplantation within 2 years of onset of drug-induced liver injury. *Hepatology*. 2017;66(4):1275-85.

13. Hwang TJ, Carpenter D, Lauffenburger JC, Wang B, Franklin JM, Kesselheim AS. Failure of investigational drugs in late-stage clinical development and publication of trial results. *JAMA Intern Med*. 2016;176(12):1826-33.

14. Manning F, Swartz M. Review of the Fialuridine (FIAU) Clinical Trials. 1995;Eli Lilly Trial H3X-MC-PPPC (NIH Protocol 93-DK-0031).

15. Garzel B, Yang H, Zhang L, Huang SM, Polli JE, Wang H. The role of bile salt export pump gene repression in drug-induced cholestatic liver toxicity. *Drug Metab Dispos*. 2014;42(3):318-22.

16. Dienstag JL IK. Toxic and drug-induced hepatitis. Harrison's Principles of Internal Medicine. 22001. p. 1737–41.

17. Giordano C, Rivas J, Zervos X. An update on treatment of drug-induced liver injury. *J Clin Transl Hepatol*. 2014;2(2):74-9.

18. Heard KJ. Acetylcysteine for acetaminophen poisoning. *N Engl J Med*. 2008;359(3):285-92.

19. Santi L, Maggioli C, Mastroroberto M, Tufoni M, Napoli L, Caraceni P. Acute liver failure caused by Amanita phalloides poisoning. *Int J Hepatol*. 2012;2012:487480.

20. Chalasani N, Bonkovsky HL, Fontana R, Lee W, Stolz A, Talwalkar J, et al. Features and outcomes of 899 patients with drug-induced liver injury: the DILIN prospective study. *Gastroenterology*. 2015;148(7):1340-52.e7.

21. Andrade RJ, Lucena MI, Fernandez MC, Pelaez G, Pachkoria K, Garcia-Ruiz E, et al. Drug-induced liver injury: an analysis of 461 incidences submitted to the Spanish r egistry over a 10-year period. *Gastroenterology*. 2005;129(2):512-21.

22. Chen M, Suzuki A, Thakkar S, Yu K, Hu C, Tong W. DILIrank: the largest reference drug list ranked by the risk for developing drug-induced liver injury in humans. *Drug Discov Today*. 2016;21(4):648-53.

23. Björnsson ES. Hepatotoxicity by drugs: the most common implicated agents. *Int J Mol Sci*. 2016;17(2):224-24.

24. Alvarez-Requejo A, Carvajal A, Begaud B, Moride Y, Vega T, Arias LH. Under-reporting of adverse drug reactions. Estimate based on a spontaneous reporting scheme and a sentinel system. *Eur J Clin Pharmacol*. 1998;54(6):483-8.

25. Montastruc P, Damase-Michel C, Lapeyre-Mestre M, Puget C, Damase L, Hurstel JF, et al. A prospective intensive study of adverse drug reactions in urban general practice. *Clin Drug Investig*. 1995;10(2):117-22.

26. Moride Y, Haramburu F, Requejo AA, Begaud B. Under-reporting of adverse drug reactions in general practice. *Brit J Clin Pharmacol*. 1997;43(2):177-81.

27. Heeley E, Riley J, Layton D, Wilton LV, Shakir SA. Prescription-event monitoring and reporting of adverse drug reactions. *Lancet*. 2001;358(9296):1872-3.

28. Lewis MA, Kühl-Habich D, Rosen J. Drug use and adverse event monitoring in German children. *Int J Clin Pharmacol Ther*. 2001;39:507-12.

29. Torello Iserte J, Castillo Ferrando JR, Lainez MM, Garcia Morillas M, Arias Gonzalez A. Adverse reactions to drugs reported by the primary care physicians of Andalusia. Analysis of underreporting. *Aten Primaria*. 1994;13(6):307-11.

30. Klopotowska JE, Wierenga PC, Smorenburg SM, Stuijt CCM, Arisz L, Kuks PFM, et al. Recognition of adverse drug events in older hospitalized medical patients. *Eur J Clin Pharmacol*. 2013;69(1):75-85.

31. Nebeker JR, Hoffman JM, Weir CR, Bennett CL, Hurdle JF. High rates of adverse drug events in a highly computerized hospital. *Ann Intern Med*. 2005;165(10):1111-16.

32. Medicine Io. Review of the fialuridine (FIAU) Clinical Trials. Manning FJ, Swartz M, editors. Washington, DC: The National Academies Press; 1995. 280 p.

33. Lai Y, Tse CM, Unadkat JD. Mitochondrial expression of the human equilibrative nucleoside transporter 1 (hENT1) results in enhanced mitochondrial toxicity of antiviral drugs. *J Biol Chem*. 2004;279(6):4490-97.

34. Bjornsson E, Olsson R. Outcome and prognostic markers in severe drug-induced liver disease. *Hepatology*. 2005;42(2):481-9.

35. Gitlin N, Julie NL, Spurr CL, Lim KN, Juarbe HM. Two cases of severe clinical and histologic hepatotoxicity associated with troglitazone. *Ann Intern Med*. 1998;129(1):36-38.

36. Li H, Heller DS, Leevy CB, Zierer KG, Klein KM. Troglitazone-induced fulminant hepatitis: report of a case with autopsy findings. *J Diabetes Complicat*. 2000;14(3):175-77.

37. Fukano M, Amano S, Sato J, Yamamoto K, Adachi H, Okabe H, et al. Subacute hepatic failure associated with a new antidiabetic agent, troglitazone: a case report with autopsy examination. *Hum Pathol*. 2000;31(2):250-53.

38. Herrine SK, Choudhary C. Severe hepatotoxicity associated with troglitazone. *Ann Intern Med*. 1999;130(2):163-64.

39. Jagannath S, Rai R. Rapid-onset subfulminant liver failure associated with troglitazone. *Ann Intern Med*. 2000;132(8):677-77.

40. Vella A, de Groen PC, Dinneen SF. Fatal hepatotoxicity associated with troglitazone. *Ann Intern Med*. 1998;129(12):1080.

41. Shibuya A, Watanabe M, Fujita Y, Saigenji K, Kuwao S, Takahashi H, et al. An autopsy case of troglitazone-induced fulminant hepatitis. *Diabetes Care*. 1998;21(12):2140-43.

42. Jick SS, Stender M, Myers MW. Frequency of liver disease in type 2 diabetic patients treated with oral antidiabetic agents. *Diabetes Care*. 1999;22(12):2067-71.

43. Graham DJ, Drinkard CR, Shatin D. Incidence of idiopathic acute liver failure and hospitalized liver injury in patients treated with troglitazone. *Am J Gastroenterol*. 2003;98(1):175-9.

44. Rogers AS, Israel E, Smith CR, Levine D, McBean AM, Valente C, et al. Physician knowledge, attitudes, and behavior related to reporting adverse drug events. *Ann Intern Med*. 1988;148(7):1596-600.

45. Scott HD, Rosenbaum SE, Waters WJ, Colt AM, Andrews LG, Juergens JP, et al. Rhode Island physicians' recognition and reporting of adverse drug reactions. *R I Med J*. 1987;70(7):311-6.

46. Therapuetic Goods Adminstration. Lumiracoxib (Prexige). 2007. [cited: 2019 November 8] Available from: https://www.tga.gov.au/product-recall/lumiracoxib-prexige

47. Therapuetic Goods Adminstration. Thelin (sitaxentan): worldwide withdrawal. 2010. [cited: 2019 November 8]. Available from: https://www.tga.gov.au/alert/thelin-sitaxentan-worldwide-withdrawal

48. Keisu M, Andersson TB. Drug-induced liver injury in humans: the case of ximelagatran. *Handb Exp Pharmacol*. 2010(196):407-18.

49. Qureshi ZP, Seoane-Vazquez E, Rodriguez-Monguio R, Stevenson KB, Szeinbach SL. Market withdrawal of new molecular entities approved in the United States from 1980 to 2009. *Pharmacoepidemiol Drug Saf*. 2011;20(7):772-77.

50. US FDA: FDA issues public health advisory on liver toxicity associated with the antibiotic trovan: M2 Presswire; 1999. [cited: 2019 November 8]. Available from: https://www.proquest.com/docview/446249097/73CAA751DF5449B2PQ/1

51. Therapuetic Goods Adminstration. Lumiracoxib (Prexige): Urgent advice regarding management of patients. 2007. [cited: 2019 November 8]. Available from: https://www.tga.gov.au/alert/lumiracoxib-prexige-urgent-advice-regarding-management-patients

52. Fontana RJ. Pathogenesis of idiosyncratic drug-induced liver injury and clinical perspectives. *Gastroenterology*. 2014;146(4):914-28.

53. Lammert C, Einarsson S, Saha C, Niklasson A, Bjornsson E, Chalasani N. Relationship between daily dose of oral medications and idiosyncratic drug-induced liver injury: search for signals. *Hepatology*. 2008;47(6):2003-9.

54. Lucena MI, Andrade RJ, Kaplowitz N, García-Cortes M, Fernández MC, Romero-Gomez M, et al. Phenotypic characterization of idiosyncratic drug-induced liver injury: the influence of age and sex. *Hepatology*. 2009;49(6):2001-09.

55. Chalasani NP, Hayashi PH, Bonkovsky HL, Navarro VJ, Lee WM, Fontana RJ, et al. ACG clinical guideline: the diagnosis and management of idiosyncratic drug-induced liver injury. *Am J Gastroenterol*. 2014;109(7):950-66.

56. Teschke R, Danan G. Diagnosis and management of drug-induced liver injury (DILI) in patients with pre-existing liver disease. *Drug Saf*. 2016;39(8):729-44.

57. Fisher K, Vuppalanchi R, Saxena R. Drug-induced liver injury. *Arch Pathol Lab Med*. 2015;139(7):876-87.

58. Acute hepatic necrosis. Bethesda (MD): National Institute of Diabetes and Digestive and Kidney Diseases. 2012. [cited: 2019 November 8]. Available from: https://www.ncbi.nlm.nih.gov/books/NBK548560/.

59. Pye M, Northcote RJ, Cobbe SM. Acute hepatitis after parenteral amiodarone administration. *Brit Heart J*. 1988;59(6):690-91.

60. Hinson JA, Roberts DW, James LP. Mechanisms of acetaminophen-induced liver necrosis. *Handb Exp Pharmacol*. 2010(196):369-405.

61. Patterson DJ, Dew EW, Gyorkey F, Graham DY. Niacin hepatitis. *South Med J*. 1983;76(2):239-41.

62. Acute hepatitis. Bethesda (MD): National Institute of Diabetes and Digestive and Kidney Diseases. 2012. [cited: 2019 November 8]. Available from: https://www.ncbi.nlm.nih.gov/books/NBK548606/.

63. Rigal J, Furet Y, Autret E, Breteau M. Severe mixed hepatitis caused by fenofibrate? A review of the literature apropos of a case. *Rev Med Interne*. 1989;10(1):65-7.

64. Werther JL, Korelitz BI. Chlorpromazine jaundice; analysis of twenty-two cases. *Am J Med*. 1957;22(3):351-66.

65. Cholestatic hepatitis. Bethesda (MD): National Institute of Diabetes and Digestive and Kidney Diseases. 2012. [cited: 2019 November 8]. Available from: https://www.ncbi.nlm.nih.gov/books/NBK548914/.

66. Kleinman MS, Presberg JE. Cholestatic hepatitis after dicloxacillin-sodium therapy. *J Clin Gastroenterol*. 1986;8(1):77-8.

67. Mikhail NE. Methimazole-induced cholestatic jaundice. *South Med J*. 2004;97(2):178-82.

68. Gloria L, Serejo F, Cruz E, Freitas J, Costa A, Ramalho F, et al. Diphenylhydantoin-induced hepatitis: a case report. *Hepatogastroenterology*. 1998;45(20):411-4.

69. Mixed hepatitis. Bethesda (MD): National Institute of Diabetes and Digestive and Kidney Diseases. 2012. [cited: 2019 November 8]. Available from: https://www.ncbi.nlm.nih.gov/books/NBK547938/.

70. May LD, Lefkowitch JH, Kram MT, Rubin DE. Mixed hepatocellular-cholestatic liver injury after pioglitazone therapy. *Ann Intern Med*. 2002;136(6):449-52.

71. Mitchell JR, Long MW, Thorgeirsson UP, Jollow DJ. Acetylation rates and monthly liver function tests during one year of isoniazid preventive therapy. *Chest*. 1975;68(2):181-90.

72. Watkins PB, Kaplowitz N, Slattery JT, Colonese CR, Colucci SV, Stewart PW, et al. Aminotransferase elevations in healthy adults receiving 4 grams of acetaminophen daily: a randomized controlled trial. *JAMA*. 2006;296(1):87-93.

73. Bland cholestasis. Bethesda (MD): National Institute of Diabetes and Digestive and Kidney Diseases. 2012. [cited: 2019 November 8]. Available from: https://www.ncbi.nlm.nih.gov/books/NBK548511/.

74. Singh C, Bishop P, Willson R. Extreme hyperbilirubinemia associated with the use of anabolic steroids, health/nutritional supplements, and ethanol: response to ursodeoxycholic acid treatment. *Am J Gastroenterol*. 1996;91(4):783-5.

75. Boake WC, Schade SG, Morrissey JF, Schaffner F. Intrahepatic cholestatic jaundice of pregnancy followed by Enovid-induced cholestatic jaundice. *Ann Intern Med*. 1965;63:302-8.

76. Lieberman DA, Keeffe EB, Stenzel P. Severe and prolonged oral contraceptive jaundice. *J Clin Gastroenterol*. 1984;6(2):145-8.

77. Acute fatty liver with lactic acidosis and hepatic dysfunction. Bethesda (MD): National Institute of Diabetes and Digestive and Kidney Diseases. 2012. [cited: 2019 November 8]. Available from: https://www.ncbi.nlm.nih.gov/books/NBK547917/.

78. Norman MG, Lowden JA, Hill DE, Bannatyne RM. Encephalopathy and fatty degeneration of the viscera in childhood: II. Report of a case with isolation of influenza B virus. *Can Med Assoc J*. 1968;99(11):549-54.

79. Bleeker-Rovers CP, Kadir SW, van Leusen R, Richter C. Hepatic steatosis and lactic acidosis caused by stavudine in an HIV-infected patient. *Neth J Med*. 2000;57(5):190-3.

80. Cornejo-Juarez P, Sierra-Madero J, Volkow-Fernandez P. Metabolic acidosis and hepatic steatosis in two HIV-infected patients on stavudine (d4T) treatment. *Arch Med Res*. 2003;34(1):64-9.

81. Robinson MJ, Rywlin AM. Tetracycline-associated fatty liver in the male. Report of an autopsied case. *Am J Gastroenterol*. 1970;15(9):857-62.

82. Nonalcoholic fatty liver. Bethesda (MD): National Institute of Diabetes and Digestive and Kidney Diseases. 2012. [cited: 2019 November 8]. Available from: https://www.ncbi.nlm.nih.gov/books/NBK547860/.

83. Itoh S, Igarashi M, Tsukada Y, Ichinoe A. Nonalcoholic fatty liver with alcoholic hyalin after long-term glucocorticoid therapy. *Gastroenterol Hepatol*. 1977;24(6):415-8.

84. Chronic hepatitis. Bethesda (MD): National Institute of Diabetes and Digestive and Kidney Diseases. 2012. [cited: 2019 November 8]. Available from: https://www.ncbi.nlm.nih.gov/books/NBK547983/.

85. Ceci G, Bella M, Melissari M, Gabrielli M, Bocchi P, Cocconi G. Fatal hepatic vascular toxicity of DTIC. Is it really a rare event? *Cancer*. 1988;61(10):1988-91.

86. Enzyme elevations without jaundice. Bethesda (MD): National Institute of Diabetes and Digestive and Kidney Diseases. [cited: 2019 November 8]. 2012. Available from: https://www.ncbi.nlm.nih.gov/books/NBK548558/.

87. Daniel F, Cadranel JF, Seksik P, Cazier A, Duong Van Huyen JP, Ziol M, et al. Azathioprine induced nodular regenerative hyperplasia in IBD patients. *Gastroenterol Clin Biol*. 2005;29(5):600-3.

88. Steinbrecher UP, Lisbona R, Huang SN, Mishkin S. Complete regression of hepatocellular adenoma after withdrawal of oral contraceptives. *Dig Dis Sci*. 1981;26(11):1045-50.

89. Haring MPD, Gouw ASH, de Haas RJ, Cuperus FJC, de Jong KP, de Meijer VE. The effect of oral contraceptive pill cessation on hepatocellular adenoma diameter: a retrospective cohort study. *Liver Int*. 2019;39(5):905-13.

90. Liver tumors. Bethesda (MD): National Institute of Diabetes and Digestive and Kidney Diseases. 2012. [cited: 2019 November 8]. Available from: https://www.ncbi.nlm.nih.gov/books/NBK548322/.

91. Licata A, Minissale MG, Calvaruso V, Craxi A. A focus on epidemiology of drug-induced liver injury: analysis of a prospective cohort. *Eur Rev Med Pharmacol Sci*. 2017;21(1 Suppl):112-21.

92. Fontana RJ, Seeff LB, Andrade RJ, Björnsson E, Day CP, Serrano J, et al. Standardization of nomenclature and causality assessment in drug-induced liver injury: summary of a clinical research workshop. *Hepatology*. 2010;52(2):730-42.

93. Kleiner DE, Chalasani NP, Lee WM, Fontana RJ, Bonkovsky HL, Watkins PB, et al. Hepatic histological findings in suspected drug-induced liver injury: systematic evaluation and clinical associations. *Hepatology*. 2014;59(2):661-70.

94. Lu RJ, Zhang Y, Tang FL, Zheng ZW, Fan ZD, Zhu SM, et al. Clinical characteristics of drug-induced liver injury and related risk factors. *Exp Ther Med*. 2016;12(4):2606-16.

95. Kleiner DE. The Pathology of Drug-Induced Liver Injury. *Semin Liver Dis*. 2009;29(04):364-72.

96. Padda MS, Sanchez M, Akhtar AJ, Boyer JL. Drug-induced cholestasis. *Hepatology*. 2011;53(4):1377-87.

97. Erlinger S. Drug-induced cholestasis. *J Hepatol*. 1997;26:1-4.

98. Sundaram V, Björnsson ES. Drug-induced cholestasis. *Hepatol Commun*. 2017;1(8):726-35.

99. Andrade RJ, Aithal GP, Björnsson ES, Kaplowitz N, Kullak-Ublick GA, Larrey D, et al. EASL clinical practice guidelines: drug-induced liver injury. *J Hepatol*. 2019;70(6):1222-61.

100. Morgan RE, Trauner M, van Staden CJ, Lee PH, Ramachandran B, Eschenberg M, et al. Interference with bile salt export pump function is a susceptibility factor for human liver injury in drug development. *Toxicol Sci*. 2010;118(2):485-500.

101. Morgan RE, van Staden CJ, Chen Y, Kalyanaraman N, Kalanzi J, Dunn RT, II, et al. A multifactorial approach to hepatobiliary transporter assessment enables improved therapeutic compound development. *Toxicol Sci*. 2013;136(1):216-41.

102. Mottino AD, Cao J, Veggi LM, Crocenzi F, Roma MG, Vore M. Altered localization and activity of canalicular Mrp2 in estradiol-17β-D-glucuronide–induced cholestasis. *Hepatology*. 2002;35(6):1409-19.

103. Crocenzi FA, Mottino AD, Cao J, Veggi LM, Pozzi EJS, Vore M, et al. Estradiol-17β-D-glucuronide induces endocytic internalization of Bsep in rats. *Am J Physiol Gastrointest Liver Physiol*. 2003;285(2):G449-G59.

104. Funk C, Pantze M, Jehle L, Ponelle C, Scheuermann G, Lazendic M, et al. Troglitazone-induced intrahepatic cholestasis by an interference with the hepatobiliary export of bile acids in male and female rats. Correlation with the gender difference in troglitazone sulfate formation and the inhibition of the canalicular bile salt export pump (Bsep) by troglitazone and troglitazone sulfate. *Toxicology*. 2001;167(1):83-98.

105. Neuman MG, Schneider M, Nanau RM, Parry C. HIV-antiretroviral therapy induced liver, gastrointestinal, and pancreatic injury. *Int J Hepatol*. 2012;2012:760706.

106. Eriksson C, Gustavsson A, Kronvall T, Tysk C. Hepatotoxicity by bosentan in a patient with portopulmonary hypertension: a case-report and review of the literature. *J Gastrointestin Liver Dis*. 2011;20(1):77-80.

107. Boaglio AC, Zucchetti AE, Sánchez Pozzi EJ, Pellegrino JM, Ochoa JE, Mottino AD, et al. Phosphoinositide 3-kinase/protein kinase B signaling pathway is involved in estradiol 17β-d-glucuronide–induced cholestasis: complementarity with classical protein kinase c. *Hepatology*. 2010;52(4):1465-76.

108. Román ID, Fernández-Moreno MD, Fueyo JA, Roma MG, Coleman R. Cyclosporin A induced internalization of the bile salt export pump in isolated rat hepatocyte couplets. *Toxicol Sci*. 2003;71(2):276-81.

109. sarró E, Tornavaca O, Plana M, Meseguer A, Itarte E. Phosphoinositide 3-kinase inhibitors protect mouse kidney PCT3 cells from cyclosporine- induced cell death. *Kidney Int*. 2008;73:77-85.

110. Chen C, Johnston TD, Jeon H, Gedaly R, McHugh P, Ranjan D. Cyclosporin A up-regulates and activates protein kinase C-zeta in EBV-infected and EBV-transformed human B-cells. *J Surg Res*. 2009;153(1):156-61.

111. Vitins AP, Kienhuis AS, Speksnijder EN, Roodbergen M, Luijten M, van der Ven LT. Mechanisms of amiodarone and valproic acid induced liver steatosis in mouse in vivo act as a template for other hepatotoxicity models. *Arch Toxicol*. 2014;88(8):1573-88.

112. Antherieu S, Rogue A, Fromenty B, Guillouzo A, Robin MA. Induction of vesicular steatosis by amiodarone and tetracycline is associated with up-regulation of lipogenic genes in HepaRG cells. *Hepatology*. 2011;53(6):1895-905.

113. Dalaklioglu S, Genc GE, Aksoy NH, Akcit F, Gumuslu S. Resveratrol ameliorates methotrexate-induced hepatotoxicity in rats via inhibition of lipid peroxidation. *Hum Exp Toxicol*. 2013;32(6):662-71.

114. Freneaux E, Fromenty B, Berson A, Labbe G, Degott C, Letteron P, et al. Stereoselective and nonstereoselective effects of ibuprofen enantiomers on mitochondrial beta-oxidation of fatty acids. *J Pharmacol Exp Ther*. 1990;255(2):529-35.

115. Yeh MM, Brunt EM. Pathological features of fatty liver disease. *Gastroenterology*. 2014;147(4):754-64.

116. Brown GT, Kleiner DE. Histopathology of nonalcoholic fatty liver disease and nonalcoholic steatohepatitis. *Metabolism*. 2016;65(8):1080-86.

117. Yeh MM, Brunt EM. Pathological Features of Fatty Liver Disease. *Gastroenterology*. 2014;147(4):754-64.

118. Gramlich T, Kleiner DE, McCullough AJ, Matteoni CA, Boparai N, Younossi ZM. Pathologic features associated with fibrosis in nonalcoholic fatty liver disease. *Hum Pathol*. 2004;35(2):196-9.

119. Younossi ZM, Gramlich T, Liu YC, Matteoni C, Petrelli M, Goldblum J, et al. Nonalcoholic fatty liver disease: assessment of variability in pathologic interpretations. *Mod Pathol*. 1998;11(6):560-5.

120. Zatloukal K, French SW, Stumptner C, Strnad P, Harada M, Toivola DM, et al. From mallory to mallory-denk bodies: what, how and why? *Exp Cell Res*. 2007;313(10):2033-49.

121. Rafiq N, Bai C, Fang Y, Srishord M, McCullough A, Gramlich T, et al. Long-term follow-up of patients with nonalcoholic fatty liver. *Clin Gastroenterol Hepatol*. 2009;7(2):234-38.

122. Shahane SA, Huang R, Gerhold D, Baxa U, Austin CP, Xia M. Detection of phospholipidosis induction: a cell-based assay in high-throughput and high-content format. *J Biomol Screen*. 2014;19(1):66-76.

123. Pospischil A, Walther P, Dingemanse J. Phospholipidosis in healthy subjects participating in clinical studies: ultrastructural findings in white blood cells. *Exp Toxicol Pathol*. 2010;62(5):567-71.

124. Schurdak ME, Vernetti LA, Abel SJ, Thiffault C. Adaptation of an in vitro phospholipidosis assay to an automated image analysis system. *Toxicol Mech Methods*. 2007;17(2):77-86.

125. Reasor MJ, Hastings KL, Ulrich RG. Drug-induced phospholipidosis: issues and future directions. *Expert Opin Drug Saf*. 2006;5(4):567-83.

126. Brien JF, Jimmo S, Brennan FJ, Ford SE, Armstrong PW. Distribution of amiodarone and its metabolite, desethylamiodarone, in human tissues. *Can J Physiol Pharmacol*. 1987;65(3):360-4.

127. Rotmensch HH, Belhassen B, Swanson BN, Shoshani D, Spielman SR, Greenspon AJ, et al. Steady-state serum amiodarone concentrations: relationships with antiarrhythmic efficacy and toxicity. *Ann Intern Med*. 1984;101(4):462-9.

128. Freneaux E, Labbe G, Letteron P, The Le D, Degott C, Geneve J, et al. Inhibition of the mitochondrial oxidation of fatty acids by tetracycline in mice and in man: possible role in microvesicular steatosis induced by this antibiotic. *Hepatology*. 1988;8(5):1056-62.

129. Scott DA, Gholson CF, Netchvolodoff CV, Ray M, Gonzalez E, Bacon BR. Incidental microvesicular steatosis due to valproic acid anticonvulsant therapy. *Am J Gastroenterol*. 1991;86(4):500-2.

130. Fromenty B, Pessayre D. Inhibition of mitochondrial beta-oxidation as a mechanism of hepatotoxicity. *Pharmacol Ther*. 1995;67(1):101-54.

131. Anthérieu S, Rogue A, Fromenty B, Guillouzo A, Robin MA. Induction of vesicular steatosis by amiodarone and tetracycline is associated with up-regulation of lipogenic genes in HepaRG cells. *Hepatology*. 2011;53(6):1895-905.

132. Selvaraj S, Oh JH, Spanel R, Länger F, Han HY, Lee EH, et al. The pathogenesis of diclofenac induced immunoallergic hepatitis in a canine model of liver injury. *Oncotarget*. 2017;8(64):107763-824.

133. Grimbert S, Fisch C, Deschamps D, Berson A, Fromenty B, Feldmann G, et al. Effects of female sex hormones on mitochondria: possible role in acute fatty liver of pregnancy. *Am J Physiol Gastrointest Liver Physiol*. 1995;268(1):G107-G15.

134. Serviddio G, Bellanti F, Vendemiale G, Altomare E. Mitochondrial dysfunction in nonalcoholic steatohepatitis. *Expert Rev Gastroenterol Hepatol*. 2011;5(2):233-44.

135. Lettéron P, Sutton A, Mansouri A, Fromenty B, Pessayre D. Inhibition of microsomal triglyceride transfer protein: another mechanism for drug-induced steatosis in mice. *Hepatology*. 2003;38(1):133-40.

136. Blas-García A, Apostolova N, Ballesteros D, Monleón D, Morales JM, Rocha M, et al. Inhibition of mitochondrial function by efavirenz increases lipid content in hepatic cells. *Hepatology*. 2010;52(1):115-25.

137. Schadinger SE, Bucher NLR, Schreiber BM, Farmer SR. PPARγ2 regulates lipogenesis and lipid accumulation in steatotic hepatocytes. *Am J Physiol Endocrinol Metab*. 2005;288(6):E1195-E205.

138. Halliwell WH. Cationic amphiphilic drug-induced phospholipidosis. *Toxicol Pathol*. 1997;25(1):53-60.

139. Sawada H, Takami K, Asahi S. A toxicogenomic approach to drug-induced phospholipidosis: analysis of its induction mechanism and establishment of a novel in vitro screening system. *Toxicol Sci*. 2004;83(2):282-92.

140. Fröhlich E. Comparison of conventional and advanced in vitro models in the toxicity testing of nanoparticles. *Artif Cells Nanomed Biotechnol*. 2018;46(Supplementary 2):1091-107.

141. Dusinska M, Rundén-Pran E, Schnekenburger J, Kanno J. Chapter 3 - Toxicity tests: in vitro and in vivo. In: Fadeel B, Pietroiusti A, Shvedova AA, editors. Adverse Effects of Engineered Nanomaterials 2nd ed: Academic Press; 2017. p. 51-82.

142. Wang X, Wu Q, Liu A, Anadón A, Rodríguez JL, Martínez-Larrañaga MR, et al. Paracetamol: overdose-induced oxidative stress toxicity, metabolism, and protective effects of various compounds in vivo and in vitro. *Drug Metab Rev*. 2017;49(4):395-437.

143. Hart SN, Li Y, Nakamoto K, Subileau EA, Steen D, Zhong XB. A comparison of whole genome gene expression profiles of HepaRG cells and HepG2 cells to primary human hepatocytes and human liver tissues. *Drug Metab Dispos*. 2010;38(6):988-94.

144. Wiśniewski JR, Vildhede A, Norén A, Artursson P. In-depth quantitative analysis and comparison of the human hepatocyte and hepatoma cell line HepG2 proteomes. *J Proteomics*. 2016;136:234-47.

145. Sison-Young RLC, Mitsa D, Jenkins RE, Mottram D, Alexandre E, Richert L, et al. Comparative proteomic characterization of 4 human liver-derived single cell culture models reveals significant variation in the capacity for drug disposition, bioactivation, and detoxication. *Toxicol Sci*. 2015;147(2):412-24.

146. Godoy P, Hewitt NJ, Albrecht U, Andersen ME, Ansari N, Bhattacharya S, et al. Recent advances in 2D and 3D in vitro systems using primary hepatocytes, alternative hepatocyte sources and non-parenchymal liver cells and their use in investigating mechanisms of hepatotoxicity, cell signaling and ADME. *Arch Toxicol*. 2013;87(8):1315-530.

147. Guengerich FP. Comparisons of catalytic selectivity of cytochrome P450 subfamily enzymes from different species. *Chem Biol Interact*. 1997;106(3):161-82.

148. Martignoni M, Groothuis GMM, de Kanter R. Species differences between mouse, rat, dog, monkey and human CYP-mediated drug metabolism, inhibition and induction. *Expert Opin Drug Metab Toxicol*. 2006;2(6):875-94.

149. Smith DA. Species differences in metabolism and pharmacokinetics: are we close to an understanding? *Drug Metab Rev*. 1991;23(3-4):355-73.

150. Yabuuchi H, Tanaka K, Maeda M, Takemura M, Oka M, Ohashi R, et al. Cloning of the dog bile salt export pump (BSEP; ABCB11) and functional comparison with the human and rat proteins. *Biopharm Drug Dispos*. 2008;29(8):441-48.

151. Wang L, Prasad B, Salphati L, Chu X, Gupta A, Hop CECA, et al. Interspecies variability in expression of hepatobiliary transporters across human, dog, monkey, and rat as determined by quantitative proteomics. *Drug Metab Dispos*. 2015;43(3):367-74.

152. Thakare R, Alamoudi JA, Gautam N, Rodrigues AD, Alnouti Y. Species differences in bile acids I. Plasma and urine bile acid composition. *J Appl Toxicol*. 2018;38(10):1323-35.

153. Vilei MT, Granato A, Ferraresso C, Neri D, Carraro P, Gerunda G, et al. Comparison of pig, human and rat hepatocytes as a source of liver specific metabolic functions in culture systems--implications for use in bioartificial liver devices. *Int J Artif Organs*. 2001;24(6):392-6.

154. Yang K, Guo C, Woodhead JL, St Claire RL, 3rd, Watkins PB, Siler SQ, et al. Sandwich-cultured hepatocytes as a tool to study drug disposition and drug-induced liver injury. *J Pharm Sci*. 2016;105(2):443-59.

155. Li N, Bi YA, Duignan DB, Lai Y. Quantitative expression profile of hepatobiliary transporters in sandwich cultured rat and human hepatocytes. *Mol Pharm*. 2009;6(4):1180-89.

156. Strautnieks SS, Bull LN, Knisely AS, Kocoshis SA, Dahl N, Arnell H, et al. A gene encoding a liver-specific ABC transporter is mutated in progressive familial intrahepatic cholestasis. *Nat Genet*. 1998;20(3):233-38.

157. Aden DP, Fogel A, Plotkin S, Damjanov I, Knowles BB. Controlled synthesis of HBsAg in a differentiated human liver carcinoma-derived cell line. *Nature*. 1979;282(5739):615-6.

158. Parent R, Marion MJ, Furio L, Trépo C, Petit MA. Origin and characterization of a human bipotent liver progenitor cell line. *Gastroenterology*. 2004;126(4):1147-56.

159. Nakabayashi H, Taketa K, Miyano K, Yamane T, Sato J. Growth of human hepatoma cell lines with differentiated functions in chemically defined medium. *Cancer Res*. 1982;42(9):3858-63.

160. Gerets HHJ, Tilmant K, Gerin B, Chanteux H, Depelchin BO, Dhalluin S, et al. Characterization of primary human hepatocytes, HepG2 cells, and HepaRG cells at the mRNA level and CYP activity in response to inducers and their predictivity for the detection of human hepatotoxins. *Cell Biol Toxicol*. 2012;28(2):69-87.

161. Hurrell T, Segeritz CP, Vallier L, Lilley KS, Cromarty AD. Proteomic comparison of various hepatic cell cultures for preclinical safety pharmacology. *Toxicol Sci*. 2018;164(1):229-39.

162. Sormunen R, Eskelinen S, Lehto VP. Bile canaliculus formation in cultured HEPG2 cells. *Lab Invest*. 1993;68(6):652-62.

163. Berger B, Donzelli M, Maseneni S, Boess F, Roth A, Krähenbühl S, et al. Comparison of liver cell models using the basel phenotyping cocktail. *Front Pharmacol*. 2016;7(443).

164. Kotani N, Maeda K, Debori Y, Camus S, Li R, Chesne C, et al. Expression and transport function of drug uptake transporters in differentiated HepaRG cells. *Mol Pharm*. 2012;9(12):3434-41.

165. Mayati A, Moreau A, Le Vée M, Bruyère A, Jouan E, Denizot C, et al. Functional polarization of human hepatoma HepaRG cells in response to forskolin. *Sci Rep*. 2018;8(1):16115.

166. Shi J, Wang X, Lyu L, Jiang H, Zhu HJ. Comparison of protein expression between human livers and the hepatic cell lines HepG2, Hep3B, and Huh7 using SWATH and MRM-HR proteomics: focusing on drug-metabolizing enzymes. *Drug Metab Pharmacokinet*. 2018;33(2):133-40.

167. Kang HE, Malinen MM, Saran C, Honkakoski P, Brouwer KLR. Optimization of canalicular ABC transporter function in HuH-7 cells by modification of culture conditions. *Drug Metab Dispos*. 2019;47(10):1222-30.

168. Malinen MM, Ito K, Kang HE, Honkakoski P, Brouwer KLR. Protein expression and function of organic anion transporters in short-term and long-term cultures of Huh7 human hepatoma cells. *Eur J Pharm Sci*. 2019;130:186-95.

169. Liu X, Chism JP, LeCluyse EL, Brouwer KR, Brouwer KLR. Correlation of biliary excretion in sandwich-cultured rat hepatocytes and in vivo in rats. *Drug Metab Dispos*. 1999;27(6):637-44.

170. Kemp DC, Zamek-Gliszczynski MJ, Brouwer KLR. Xenobiotics inhibit hepatic uptake and biliary excretion of taurocholate in rat hepatocytes. *Toxicol Sci*. 2005;83(2):207-14.

171. Abe K, Bridges AS, Brouwer KLR. Use of sandwich-cultured human hepatocytes to predict biliary clearance of angiotensin II receptor blockers and HMG-CoA reductase inhibitors. *Drug Metab Dispos*. 2009;37(3):447-52.

172. Chan R, Benet LZ. Measures of BSEP inhibition in vitro are not useful predictors of DILI. *Toxicol Sci*. 2017;162(2):499-508.

173. Jonathan P. Jackson KMF, Robert L. St. ClaireIII, Chris B. Black, Kenneth R. Brouwer. Cholestatic drug induced liver injury: a function of bile salt export pump inhibition and farnesoid x receptor antagonism. *Appl In Vitro Toxicol*. 2018;4(3):265-79.

174. Cyclosporin in cadaveric renal transplantation: one-year follow-up of a multicentre trial. *Lancet*. 1983;2(8357):986-9.

175. Group CMTS. A randomized clinical trial of cyclosporine in cadaveric renal transplantation. *N Engl J Med*. 1983;309(14):809-15.

176. Ferguson RM, Rynasiewicz JJ, Sutherland DE, Simmons RL, Najarian JS. Cyclosporin A in renal transplantation: a prospective randomized trial. *Surgery*. 1982;92(2):175-82.

177. Ganschow R, Albani J, Grabhorn E, Richter A, Burdelski M. Tacrolimus-induced cholestatic syndrome following pediatric liver transplantation and steroid-resistant graft rejection. *Pediatr Transplant*. 2006;10(2):220-4.

178. Reuben A, Koch DG, Lee WM. Drug-induced acute liver failure: results of a U.S. multicenter, prospective study. *Hepatology*. 2010;52(6):2065-76.

179. Jiang L, Gu Y, Ye J, Liu F, Zhao Y, Wang C, et al. Resveratrol prevents hepatic steatosis induced by hepatitis C virus core protein. *Biotechnol Lett*. 2012;34(12):2205-12.

180. Liu F, Wang C, Zhang L, Xu Y, Jang L, Gu Y, et al. Metformin prevents hepatic steatosis by regulating the expression of adipose differentiation-related protein. *Int J Mol Med*. 2014;33(1):51-58.

181. Fam TK, Klymchenko AS, Collot M. Recent advances in fluorescent probes for lipid droplets. *Materials*. 2018;11(9):1768.

182. Ohsaki Y, Shinohara Y, Suzuki M, Fujimoto T. A pitfall in using BODIPY dyes to label lipid droplets for fluorescence microscopy. *Histochem Cell Biol*. 2010;133(4):477-80.

183. Donato MT, Martínez-Romero A, Jiménez N, Negro A, Herrera G, Castell JV, et al. Cytometric analysis for drug-induced steatosis in HepG2 cells. *Chem Biol Interact*. 2009;181(3):417-23.

184. Funk RS, Krise JP. Cationic amphiphilic drugs cause a marked expansion of apparent lysosomal volume: implications for an intracellular distribution-based drug interaction. *Mol Pharm*. 2012;9(5):1384-95.

185. Donato MT, Tolosa L, Jiménez N, Castell JV, Gómez-Lechón MJ. High-content imaging technology for the evaluation of drug-induced steatosis using a multiparametric cell-based assay. *J Biomol Screen*. 2012;17(3):394-400.

186. Kawaguchi M, Nukaga T, Sekine S, Takemura A, Susukida T, Oeda S, et al. Mechanism-based integrated assay systems for the prediction of drug-induced liver injury. *Toxicol Appl Pharmacol*. 2020;394:114958.

187. Saito J, Okamura A, Takeuchi K, Hanioka K, Okada A, Ohata T. High content analysis assay for prediction of human hepatotoxicity in HepaRG and HepG2 cells. *Toxicol In Vitro*. 2016;33:63-70.

188. Aronson SJ, Rehm HL. Building the foundation for genomics in precision medicine. *Nature*. 2015;526(7573):336-42.

189. Andrade RJ, Robles M, Ulzurrun E, Lucena MI. Drug-induced liver injury: insights from genetic studies. *Pharmacogenomics*. 2009;10:1467-87.

190. Aithal GP, Ramsay L, Daly AK, Sonchit N, Leathart JB, Alexander G, et al. Hepatic adducts, circulating antibodies, and cytokine polymorphisms in patients with diclofenac hepatotoxicity. *Hepatology*. 2004;39(5):1430-40.

191. Lucena MI, Molokhia M, Shen Y, Urban TJ, Aithal GP, Andrade RJ, et al. Susceptibility to amoxicillin-clavulanate-induced liver injury is influenced by multiple HLA class I and II alleles. *Gastroenterology*. 2011;141(1):338-47.

192. Pachkoria K, Lucena M, Crespo E, Ruiz-Cabello F, Lopez-Ortega S, Fernandez M, et al. Analysis of IL-10, IL-4 and TNF-α polymorphisms in drug-induced liver injury (DILI) and its outcome. *J Hepatol*. 2008;49:107-14.

193. Petros Z, Lee MTM, Takahashi A, Zhang Y, Yimer G, Habtewold A, et al. Genome-wide association and replication study of anti-tuberculosis drugs-induced liver toxicity. *BMC Genom*. 2016;17(1):755.

194. Singer JB, Lewitzky S, Leroy E, Yang F, Zhao X, Klickstein L, et al. A genome-wide study identifies HLA alleles associated with lumiracoxib-related liver injury. *Nat Genet*. 2010;42(8):711-4.

195. Spraggs CF, Budde LR, Briley LP, Bing N, Cox CJ, King KS, et al. HLA-DQA1*02:01 is a major risk factor for lapatinib-induced hepatotoxicity in women with advanced breast cancer. *J Clin Oncol*. 2011;29(6):667-73.

196. Andrade RJ, Lucena MI, Alonso A, García-Corŕes M, García-Ruiz E, Benitez R, et al. HLA class II genotype influences the type of liver injury in drug-induced idiosyncratic liver disease. *Hepatology*. 2004;39(6):1603-12.

197. Kim S-H, Kim S-H, Yoon HJ, Shin DH, Park SS, Kim Y-S, et al. TNF-α genetic polymorphism −308G/A and antituberculosis drug-induced hepatitis. *Liver International*. 2012;32(5):809-14.

198. Agúndez JA, Olivera M, Martínez C, Ladero JM, Benítez J. Identification and prevalence study of 17 allelic variants of the human NAT2 gene in a white population. *Pharmacogenet*. 1996;6(5):423-8.

199. Ohno M, Yamaguchi I, Yamamoto I, Fukuda T, Yokota S, Maekura R, et al. Slow N-acetyltransferase 2 genotype affects the incidence of isoniazid and rifampicin-induced hepatotoxicity. *Int J Tuberc Lung Dis*. 2000;4:256-61.

200. Chan SL, Chua APG, Aminkeng F, Chee CBE, Jin S, Loh M, et al. Association and clinical utility of NAT2 in the prediction of isoniazid-induced liver injury in Singaporean patients. *PLoS One*. 2017;12(10):e0186200.

201. Touré A, Cabral M, Niang A, Diop CAK, Garat A, Humbert L, et al. Prevention of isoniazid toxicity by NAT2 genotyping in Senegalese tuberculosis patients. *Toxicol Rep*. 2016;3:826 - 31.

202. Kumar AH, Ramesh K, Kannan T, Sudha V, Haribabu H, Lavanya J, et al. N-acetyltransferase gene polymorphisms & plasma isoniazid concentrations in patients with tuberculosis. *Indian J Med Res*. 2017;145(1):118.

203. Simon T, Becquemont L, Mary-Krause M, de Waziers I, Beaune P, Funck-Brentano C, et al. Combined glutathione-S-transferase M1 and T1 genetic polymorphism and tacrine hepatotoxicity. *Clin Pharmacol Ther*. 2000;67(4):432-37.

204. Watanabe I, Tomita A, Shimizu M, Sugawara M, Yasumo H, Koishi R, et al. A study to survey susceptible genetic factors responsible for troglitazone-associated hepatotoxicity in Japanese patients with type 2 diabetes mellitus. *Clin Pharmacol Ther*. 2003;73(5):435-55.

205. Lucena MI, Andrade RJ, Martínez C, Ulzurrun E, García-Martín E, Borraz Y, et al. Glutathione S-transferase m1 and t1 null genotypes increase susceptibility to idiosyncratic drug-induced liver injury. *Hepatology*. 2008;48(2):588-96.

206. Rao MS, Van Vleet TR, Ciurlionis R, Buck WR, Mittelstadt SW, Blomme EAG, et al. Comparison of RNA-seq and microarray gene expression platforms for the toxicogenomic evaluation of liver from short-term rat toxicity studies. *Front Genet*. 2019;9(636).

207. Liu Z, Huang R, Roberts R, Tong W. Toxicogenomics: a 2020 vision. *Trends Pharmacol Sci*. 2019;40(2):92-103.

208. Jennen D, Polman J, Bessem M, Coonen M, van Delft J, Kleinjans J. Drug-induced liver injury classification model based on in vitro human transcriptomics and in vivo rat clinical chemistry data. *Syst Biomed (Austin)*. 2014;2(4):63-70.

209. Kohonen P, Parkkinen JA, Willighagen EL, Ceder R, Wennerberg K, Kaski S, et al. A transcriptomics data-driven gene space accurately predicts liver cytopathology and drug-induced liver injury. *Nat Commun*. 2017;8(1):15932.

210. Rodrigues RM, Heymans A, De Boe V, Sachinidis A, Chaudhari U, Govaere O, et al. Toxicogenomics-based prediction of acetaminophen-induced liver injury using human hepatic cell systems. *Toxicol Lett*. 2016;240(1):50-59.

211. Wolters JEJ, van Herwijnen MHM, Theunissen DHJ, Jennen DGJ, Van den Hof WFPM, de Kok TMCM, et al. Integrative "-omics" analysis in primary human hepatocytes unravels persistent mechanisms of cyclosporine a-induced cholestasis. *Chem Res Toxicol*. 2016;29(12):2164-74.

212. Wolters JEJ, van Breda SGJ, Grossmann J, Fortes C, Caiment F, Kleinjans JCS. Integrated 'omics analysis reveals new drug-induced mitochondrial perturbations in human hepatocytes. *Toxicol Lett*. 2018;289:1-13.

213. Li C, Ming Y, Hong W, Tang Y, Lei X, Li X, et al. Comparison of hepatic transcriptome profiling between acute liver injury and acute liver failure induced by acetaminophen in mice. *Toxicol Lett*. 2018;283:69-76.

214. Halpern KB, Shenhav R, Matcovitch-Natan O, Toth B, Lemze D, Golan M, et al. Single-cell spatial reconstruction reveals global division of labour in the mammalian liver. *Nature*. 2017;542(7641):352-56.

215. MacParland SA, Liu JC, Ma XZ, Innes BT, Bartczak AM, Gage BK, et al. Single cell RNA sequencing of human liver reveals distinct intrahepatic macrophage populations. *Nat Commun*. 2018;9(1):4383.

216. Chang N, Tian L, Ji X, Zhou X, Hou L, Zhao X, et al. Single-cell transcriptomes reveal characteristic features of mouse hepatocytes with liver cholestatic injury. *Cells*. 2019;8(9):1069.

217. van Swelm RPL, Laarakkers CMM, van der Kuur EC, Morava-Kozicz E, Wevers RA, Augustijn KD, et al. Identification of novel translational urinary biomarkers for acetaminophen-induced acute liver injury using proteomic profiling in mice. *PLoS One*. 2012;7(11):e49524.

218. Dragoi D, Benesic A, Pichler G, Kulak NA, Bartsch HS, Gerbes AL. Proteomics analysis of monocyte-derived hepatocyte-like cells identifies integrin beta 3 as a specific biomarker for drug-induced liver injury by diclofenac. *Front Pharmacol*. 2018;9:699-99.

219. Smith MC, Timmins-Schiffman E, Coton M, Coton E, Hymery N, Nunn BL, et al. Differential impacts of individual and combined exposures of deoxynivalenol and zearalenone on the HepaRG human hepatic cell proteome. *J Proteomics*. 2018;173:89-98.

220. Cosimi S, Orta L, Mateos S, Cortés F. The mycotoxin ochratoxin A inhibits DNA topoisomerase II and induces polyploidy in cultured CHO cells. *Toxicol In Vitro*. 2009;23(6):1110-15.

221. Ostry V. Alternaria mycotoxins: an overview of chemical characterization, producers, toxicity, analysis and occurrence in foodstuffs. *World Mycotoxin J*. 2008;1(2):175-88.

222. Dieterich DT, Robinson PA, Love J, Stern JO. Drug-induced liver injury associated with the use of nonnucleoside reverse-transcriptase inhibitors. *Clin Infect Dis*. 2004;38 Suppl 2:S80-S89.

223. Martín-Carbonero L, Nunez MJ, González-Lahoz J, Soriano V. Incidence of liver injury after beginning antiretroviral therapy with efavirenz or nevirapine. *HIV Clin Trials*. 2003;4:115-20.

224. Paemanee A, Sornjai W, Kittisenachai S, Sirinonthanawech N, Roytrakul S, Wongtrakul J, et al. Nevirapine induced mitochondrial dysfunction in HepG2 cells. *Sci Rep*. 2017;7:1-11.

225. Martin JL, Brown CE, Matthews-Davis N, Reardon JE. Effects of antiviral nucleoside analogs on human DNA polymerases and mitochondrial DNA synthesis. *Antimicrob Agents Chemother*. 1994;38(12):2743-9.

226. Pilon AA, Lum JJ, Sanchez-Dardon J, Phenix BN, Douglas R, Badley AD. Induction of apoptosis by a nonnucleoside human immunodeficiency virus type 1 reverse transcriptase inhibitor. *Antimicrob Agents Chemother*. 2002;46(8):2687-91.

227. Ma Z, Wang X, Yin P, Wu R, Zhou L, Xu G, et al. Serum metabolome and targeted bile acid profiling reveals potential novel biomarkers for drug-induced liver injury. *Medicine (Baltimore)*. 2019;98(31):e16717-e17.

228. Xie Z, Chen E, Ouyang X, Xu X, Ma S, Ji F, et al. Metabolomics and cytokine analysis for identification of severe drug-induced liver injury. *J Proteome Res*. 2019;18(6):2514-24.

229. van Ravenzwaay B, Cunha GCP, Leibold E, Looser R, Mellert W, Prokoudine A, et al. The use of metabolomics for the discovery of new biomarkers of effect. *Toxicol Lett*. 2007;172(1):21-28.

230. Mattes WB, Kamp HG, Fabian E, Herold M, Krennrich G, Looser R, et al. Prediction of clinically relevant safety signals of nephrotoxicity through plasma metabolite profiling. *BioMed Res Int*. 2013;2013:202497.

231. van Ravenzwaay B, Sperber S, Lemke O, Fabian E, Faulhammer F, Kamp H, et al. Metabolomics as read-across tool: a case study with phenoxy herbicides. *Regul Toxicol Pharmacol*. 2016;81:288-304.

232. Mattes W, Davis K, Fabian E, Greenhaw J, Herold M, Looser R, et al. Detection of hepatotoxicity potential with metabolite profiling (metabolomics) of rat plasma. *Toxicol Lett*. 2014;230(3):467-78.

233. Kamp H, Fabian E, Groeters S, Herold M, Krennrich G, Looser R, et al. Application of in vivo metabolomics to preclinical/toxicological studies: case study on phenytoin-induced systemic toxicity. *Bioanalysis*. 2012;4(18):2291-301.

234. Ramirez T, Strigun A, Verlohner A, Hans-Albrecht H, Peter E, Herold M, et al. Prediction of liver toxicity and mode of action using metabolomics in vitro in HepG2 cells. *Arch Toxicol*. 2018;92(2):893-906.

235. García- Cañaveras JC, Castell JV, Donato MT, Lahoz A. A metabolomics cell-based approach for anticipating and investigating drug-induced liver injury. *Sci Rep*. 2016;6(1):27239.

236. Donato MT, Gómez-Lechón MJ. Drug-induced liver steatosis and phospholipidosis: cell-based assays for early screening of drug candidates. *Curr Drug Metab*. 2012;13(8):1160-73.

237. Cuykx M, Claes L, Rodrigues RM, Vanhaecke T, Covaci A. Metabolomics profiling of steatosis progression in HepaRG® cells using sodium valproate. *Toxicol Lett*. 2018;286:22-30.

238. Masarone M, Rosato V, Dallio M, Gravina AG, Aglitti A, Loguercio C, et al. Role of oxidative stress in pathophysiology of nonalcoholic fatty liver disease. *Oxid Med Cell Longev*. 2018;2018:9547613-13.

239. Goracci L, Valeri A, Sciabola S, Aleo MD, Moritz W, Lichtenberg J, et al. A novel lipidomics-based approach to evaluating the risk of clinical hepatotoxicity potential of drugs in 3D human microtissues. *Chem Res Toxicol*. 2020;33(1):258-70.

240. Kyriakides M, Maitre L, Stamper BD, Mohar I, Kavanagh TJ, Foster J, et al. Comparative metabonomic analysis of hepatotoxicity induced by acetaminophen and its less toxic meta-isomer. *Arch Toxicol*. 2016;90(12):3073.

241. Sun J, Schnackenberg LK, Beger RD. Studies of acetaminophen and metabolites in urine and their correlations with toxicity using metabolomics. *Drug Metab Lett*. 2009;3(3):130-36.

242. Schnackenberg LK, Chen M, Sun J, Holland RD, Dragan Y, Tong W, et al. Evaluations of the trans-sulfuration pathway in multiple liver toxicity studies. *Toxicol Appl Pharmacol*. 2009;235(1):25-32.

243. Clayton TA, Lindon JC, Everett JR, Charuel C, Hanton G, Le Net JL, et al. An hypothesis for a mechanism underlying hepatotoxin-induced hypercreatinuria. *Arch Toxicol*. 2003;77(4):208-17.

244. Wang Z, Qu L, Li M, Zhang J. Identification of hepatotoxic and nephrotoxic potential markers of triptolide in mice with delayed-type hypersensitivity. *J Pharm Biomed Anal*. 2018;160:404-14.

245. Zhao J, Xie C, Mu X, Krausz KW, Patel DP, Shi X, et al. Metabolic alterations in triptolide-induced acute hepatotoxicity. *Biomed Chromatogr*. 2018;32(10):e4299-e99.

246. Zhao DS, Jiang LL, Fan YX, Wang LL, Li ZQ, Shi W, et al. Investigation of Dioscorea bulbifera rhizome-induced hepatotoxicity in rats by a multisample integrated metabolomics approach. *Chem Res Toxicol*. 2017;30(10):1865-73.

247. Liu Y, Huang R, Liu L, Peng J, Xiao B, Yang J, et al. Metabonomics study of urine from Sprague-Dawley rats exposed to Huang-yao-zi using (1)H NMR spectroscopy. *J Pharm Biomed Anal*. 2010;52(1):136-41.

248. Xue LM, Zhang QY, Han P, Jiang YP, Yan RD, Wang Y, et al. Hepatotoxic constituents and toxicological mechanism of Xanthium strumarium L. fruits. *J Ethnopharmacol*. 2014;152(2):272-82.

249. Jennen D, Ruiz-Aracama A, Magkoufopoulou C, Peijnenburg A, Lommen A, van Delft J, et al. Integrating transcriptomics and metabonomics to unravel modes-of-action of 2,3,7,8-tetrachlorodibenzo-p-dioxin (TCDD) in HepG2 cells. *BMC Syst Biol*. 2011;5:139-39.

250. Ruiz-Aracama A, Peijnenburg A, Kleinjans J, Jennen D, van Delft J, Hellfrisch C, et al. An untargeted multi-technique metabolomics approach to studying intracellular metabolites of HepG2 cells exposed to 2,3,7,8-tetrachlorodibenzo-p-dioxin. *BMC Genom*. 2011;12:251-51.

251. Uno S, Dalton TP, Sinclair PR, Gorman N, Wang B, Smith AG, et al. Cyp1a1(-/-) male mice: protection against high-dose TCDD-induced lethality and wasting syndrome, and resistance to intrahepatocyte lipid accumulation and uroporphyria. *Toxicol Appl Pharmacol*. 2004;196(3):410-21.

252. Senft AP, Dalton TP, Nebert DW, Genter MB, Hutchinson RJ, Shertzer HG. Dioxin increases reactive oxygen production in mouse liver mitochondria. *Toxicol Appl Pharmacol*. 2002;178(1):15-21.

253. Narayanan PK, Hart T, Elcock F, Zhang C, Hahn L, McFarland D, et al. Troglitazone-induced intracellular oxidative stress in rat hepatoma cells: a flow cytometric assessment. *Cytometry A*. 2003;52A(1):28-35.

254. Gijbels E, Vilas-Boas V, Deferm N, Devisscher L, Jaeschke H, Annaert P, et al. Mechanisms and in vitro models of drug-induced cholestasis. *Arch Toxicol*. 2019;93(5):1169-86.

255. Noor MA, Flint OP, Maa JF, Parker RA. Effects of atazanavir/ritonavir and lopinavir/ritonavir on glucose uptake and insulin sensitivity: demonstrable differences in vitro and clinically. *AIDS*. 2006;20(14):1813-21.

256. Hresko RC, Hruz PW. HIV protease inhibitors act as competitive inhibitors of the cytoplasmic glucose binding site of GLUTs with differing affinities for GLUT1 and GLUT4. *PLoS One*. 2011;6(9):e25237.

257. Rachek LI, Yuzefovych LV, Ledoux SP, Julie NL, Wilson GL. Troglitazone, but not rosiglitazone, damages mitochondrial DNA and induces mitochondrial dysfunction and cell death in human hepatocytes. *Toxicol Appl Pharmacol*. 2009;240(3):348-54.

258. Simon FR, Fortune J, Iwahashi M, Gartung C, Wolkoff A, Sutherland E. Ethinyl estradiol cholestasis involves alterations in expression of liver sinusoidal transporters. *Am J Pathol*. 1996;271(6 Pt 1):G1043-52.

259. Goda K, Saito K, Muta K, Kobayashi A, Saito Y, Sugai S. Ether-phosphatidylcholine characterized by consolidated plasma and liver lipidomics is a predictive biomarker for valproic acid-induced hepatic steatosis. *J Toxicol Sci*. 2018;43(6):395-405.

260. Xu S, Chen Y, Ma Y, Liu T, Zhao M, Wang Z, et al. Lipidomic profiling reveals disruption of lipid metabolism in valproic acid-induced hepatotoxicity. *Front Pharmacol*. 2019;10(819).

261. Ma DWL, Arendt BM, Hillyer LM, Fung SK, McGilvray I, Guindi M, et al. Plasma phospholipids and fatty acid composition differ between liver biopsy-proven nonalcoholic fatty liver disease and healthy subjects. *Nutr Diabetes*. 2016;6(7):e220-e20.

Chapter 2

Comparison of the Primary Human Hepatocyte and HepaRG Proteome and Multi-Omics Characterisation of Drug-Induced Metabolic Perturbations

Abstract

In vitro liver models offer an invaluable research platform for studying drug-induced liver injury (DILI). Utilising metabolically competent *in vitro* liver models is important for obtaining translational and mechanistic insights into DILI. Data-independent acquisition (DIA) proteomics allowed for the comparison of primary human hepatocytes (PHH) to HepaRG™ cells. This analysis revealed that while there were moderate similarities between the whole cell proteomes of PHH and HepaRG™ cells, these similarities significantly decreased when comparing proteins associated with major metabolic pathways. Therefore, while HepaRG™ cells could act as a surrogate for PHH, there are likely limitations to the translational capacity due to differences in levels of proteins associated with major metabolic pathways. Further omics-based analysis utilising untargeted metabolomics and DIA proteomics to study DILI-associated perturbations to the major metabolic pathways of PHH demonstrated that there were significant perturbations to metabolites associated with the TCA cycle, as well as glucose, nicotinamide, phase I, glucuronidation, and glutathione metabolism. Multi-omics analysis indicated these perturbations may have resulted from drug-induced impairment of mitochondrial respiration via the inhibition of complex I, increases in oxidative stress, and alterations to nucleotide metabolism.

Introduction

The liver is a vital, metabolically active organ that performs a significant number of key metabolic processes including heme degradation, bilirubin synthesis, glycogenesis, fatty acid oxidation, detoxification, and the production of primary bile acids and albumin

(1). In order to maintain biological homeostasis, these critical functions are performed by a number of metabolism and transport proteins within the liver, including cytochrome P450 (CYP) enzymes, phase II transferase enzymes, uptake and efflux transporters, and metabolite synthesis enzymes. These metabolic functions are primarily performed by hepatocytes, which make up 80% of the liver's cell composition, with the remainder consisting of cholangiocytes, Kupffer cells, stellate cells and sinusoidal endothelial cells (2). With its specialised metabolic and transport proteins driving the unique and vital functions of the liver, it is imperative that any liver model possess relevant metabolic and transport properties that are comparable to liver function *in vivo*.

There are a number of different options for modelling *in vivo* liver behaviour, each with their own benefits and limitations. *In vivo* and *in vitro* animal models are widely used to model the human liver as they are more accessible and practical than using human subjects or primary human hepatocytes (PHH). However, animal-derived primary hepatocytes, as an *in vitro* model, may be limited due to species variations that can result in significant differences to overall hepatocellular transport and metabolism (3). The differences in hepatocellular transport and metabolism are due to interspecies differences in the abundance and activities of liver transporters and metabolic enzymes (3-5). For *in vitro* modelling of *in vivo* human liver behaviour, PHH are considered the "gold standard" model. The genomic expression profiles of isolated PHH have shown significant similarities to the gene expression of human liver tissue (r=0.92) (6). The two primary limitations of PHH are their limited availability and interdonor variability. Interdonor variability can result in the differential expression of up to 2099 genes, with those related to metabolism exhibiting the greatest differential expression between donors (7). A

common alternative to PHH is immortalised hepatic-like cell lines that offer an accessible and phenotypically uniform *in vitro* cell model. HepaRG™ cells are a differentiable hepatocyte-derived cell line with an organotypic phenotype similar to that of PHH (8, 9). When compared to PHH, HepaRG™ cells have similar genomic expression profiles (r=0.881) with comparable protein expression for major liver metabolic pathways including bile acid synthesis, and phase I and II metabolism (6, 10).

Using *in vitro* models that possess comparable protein expression and metabolic competence to the liver is imperative for accurately assessing metabolic perturbations that may result in altered hepatocellular homeostasis or hepatocellular injury. Both PHH and HepaRG™ cells are useful as *in vitro* models for investigating changes resulting from drug-induced liver injury (DILI) and other hepatotoxic compounds (11-14). However, a majority of these DILI studies focused on gene expression, which may not be able to characterise biological perturbations as a result of alterations to translational and post-translational modifications, or altered degradation, localisation or function of proteins and metabolites (15). Significant value can be obtained by using a multi-omics approach to assess changes in both the proteome and metabolome as it gives a direct representation of the metabolic and transport behaviour of cells and can identify mechanistic and predictive biomarkers of DILI and other harmful stimuli (12, 16, 17). A multi-omics approach is invaluable for identifying the mechanism(s) of DILI for drugs such as ritonavir and troglitazone, which are known to impact the behaviour of major energy metabolism pathways including glucose metabolism (18, 19) and the tricarboxylic acid (TCA) cycle, and cause significant liver injury (20, 21). Understanding the mechanism(s) of DILI can allow for improved identification of hepatotoxic compounds, reducing the likelihood of

harmful drugs reaching the market in the future. Identifying predictive biomarkers is urgently needed to improve the accuracy of diagnosing DILI, which may go undetected in up to 95% of patients (22-29).

This study aimed to characterise the metabolic capacity of two *in vitro* liver models, PHH and HepaRG™ cells, and elucidate the impact of DILI-associated drugs on major metabolic pathways using a metabolically competent liver model. In order to characterise the metabolic capacity of the *in vitro* liver models, whole cell proteomes were generated for PHH and HepaRG™ cells using data-independent acquisition (DIA) proteomics. This approach identified considerable variation between the proteomes of PHH and HepaRG™ cells, with notable differences for proteins of major metabolic pathways. Furthermore, *in vitro* PHH cultures were treated with drugs associated with DILI and perturbations to biological pathways were investigated using metabolomics and proteomics. Drug treatments resulted in significant alterations to the abundance of metabolites and proteins associated with the TCA cycle, as well as glucose, nicotinamide, phase I, glucuronidation, and glutathione metabolism.

Material and methods

Materials

Undifferentiated HepaRG™ cells were acquired from Biopredic International under a material transfer agreement and HepaRG™ Maintenance/Metabolism Media was purchased from Biopredic International. Cryoplateable human hepatocytes were acquired from BioIVT along with all QualGro™ Media. Hepatocytes from the BXW donor were Transporter Certified™ and acquired from a female aged 73. Hepatocytes from the JHY donor were cryoplateable and acquired from a male aged 51 (Appendix 2). Pioglitazone and ritonavir were acquired from Merck as pharmaceutical secondary standards. Troglitazone was acquired from Cayman Chemicals. Dimethyl sulfoxide (DMSO), HPLC grade chloroform, LC-MS grade methanol (MeOH), sodium dodecyl sulphate (SDS), and trifluoroacetic acid were also purchased from Merck. LC-MS grade acetonitrile (ACN), 0.25% trypsin-EDTA phenol red, Percoll, Dulbecco's phosphate buffer saline (PBS), and chenodeoxycholic acid (CDCA) were purchased from ThermoFisher Scientific. Ammonium carbonate was purchased from Rowe Scientific. Matrigel® was purchased from Bio-Strategy.

Cell Culture

HepaRG™ cells were cultured in a T75 culture flask and differentiated per the supplier's protocol. On day 0, differentiated HepaRG™ cells were passaged using 0.25% w/v trypsin-EDTA. The cells were plated on either 24- or 96-well BioCoat™ Collagen I-coated plates with $4x10^5$ and $0.8x10^5$ cells seeded per well, respectively. Media was changed every 2-3 days with the cells overlaid on day 3 using HepaRG™

Maintenance/Metabolism Media supplemented with 0.25 mg/mL of Matrigel® and used for experimentation on day 7.

Transporter Certified™ cryoplateable human hepatocytes were thawed and transferred to a 50 mL conical centrifuge tube containing 45 mL of QualGro™ Thawing Media that included 30% v/v Percoll®. This was centrifuged at 100 *g* for 8 min. The QualGro™ Thawing Media was aspirated and the cell pellet was resuspended in QUALGRO™ Seeding Media at 0.8 $x10^6$ cells/ml. The human hepatocytes were plated onto either 24- or 96-well collagen I-coated plates with $4x10^5$ and 0.56 $x10^5$ cells seeded per well, respectively. Media was changed daily with hepatocytes overlaid on day 1 using QUALGRO™ Overlay Media supplemented with 0.25 mg/mL of Matrigel®. Sandwich-cultured hepatocytes were used for experimentation on day 4.

Treatment with drugs associated with drug-induced liver injury and metabolomics extraction

HepaRG™ cells and PHH from the BXW donor cultured on a 24-well plate were treated with the following drugs at the specified concentrations: ritonavir (25 µM), pioglitazone (100 µM), or troglitazone (12.5 µM). The drug treatment concentrations used in subsequent studies were the highest concentrations that were determined to be sub-toxic based on an *in vitro* C-DILI™ hepatotoxicity study (Appendix 3). Controls were treated with 0.1% v/v DMSO and all drug treatments contained 0.1% v/v DMSO. Drug concentrations were sub-toxic, as determined by a previous cytotoxicity study (Appendix 3). Following the 24-hour incubation, the media was aspirated and cells were washed three times with 1 mL PBS. The cells were collected from the well by the addition of 350 µL MeOH:ddH_2O (6:1) and scrapping with a pipette tip. The cells were then transferred

to a Safe-Lock microcentrifuge tube (Eppendorf®) containing 100 µL of chloroform to produce a monophasic 2:6:1 chloroform:MeOH:water (C:M:W) extraction mixture. To collect any residual metabolites or cell debris, the wells of the plate were washed with 1 mL of BuOH:MeOH (3:1), transferred to another microcentrifuge tube and dried to completion using a CentriVap Benchtop Centrifugal Vacuum Concentrator (Labconco). The dried BuOH:MeOH extraction was reconstituted using the C:M:W extraction mixture to consolidate the extracted lipids. This pooled extraction mix was centrifuged at 21,600 *g* for 10 min to pellet insoluble components and transferred to LC-MS vials for analysis. Controls were treated with 0.1% v/v DMSO. Extraction of media samples was performed as above; however, the 450 µL C:M:W extraction solution used 50 µL of the culture media from drug-treated cells instead of water.

Liquid chromatography-mass spectrometry metabolomic analysis

Drug-treated samples were analysed using hydrophilic interaction liquid chromatography (HILIC) with high resolution mass spectrometry as described previously (30). The samples were injected using an Ultimate U3000 liquid chromatography (LC) system (Dionex) fitted with a ZIC-pHILIC column (5 µm, 4.6 by 150 mm; Merck®) at ambient temperature with an injection volume of 10 µL. Chromatography was performed using 20 mM aqueous ammonium carbonate (A) and ACN (B) as the mobile phases. A 30-min gradient at a flow rate of 0.300 mL/min was run starting at 80% B decreasing to 5% B over 21 min followed by a 3-min wash at 5% B and an 8-min re-equilibration at 80% B. The samples were detected by a Q-Exactive Orbitrap mass spectrometer (ThermoFisher Scientific) using a heated electrospray ionisation (HESI) source at 3.5 kV operating in both positive and negative ion mode with rapid switching. A mass range of

85 to 1,275 *m/z* was used over the full 32-min run with an additional mass range of 65 to 975 *m/z* from the 13.5-min to the 17-min time point for detection of glycine, with a mass resolution of 35,000 used for both ranges. LC-MS data were processed in an untargeted manner using the IDEOM workflow: (31) The LC-MS raw file conversion was performed using ProteoWizard and XCMS (32, 33). Mzmatch.R was then used for alignment and filtering of peaks with an intensity cut-off of 100,000, relative standard deviation of less than 0.8, and peak shape noise filter set to of greater than 0.8 using a context-oriented directed associations-Durbin-Watson (CoDA-DW) noise filtering approach (34). Metabolites were identified in IDEOM based on accurate mass and retention time (where standards were available), or accurate mass, using a 3-ppm mass window and predicted retention time for other putative metabolites (31). Metabolites were excluded if they were not associated with known metabolic pathways in KEGG or BioCyc, or if they were identified as glycerolipids or phospholipids, as the LC analysis used was not optimised for glycerolipids or phospholipids. LC-MS peak heights were used for downstream semi-quantitative analysis.

Proteomic data-independent analysis

PHH cultured on a 24-well plate were treated with the following drugs at the specified concentrations: ritonavir (25 µM), pioglitazone (100 µM), or troglitazone (12.5 µM). Protein was collected from hepatocytes by addition of 200 µL of 5% w/v SDS and denatured by heating to 95° C for 10 min. Hepatocyte lysates were processed and digested using S-Trap™ mini columns (ProtiFi) following the manufacturer's protocol. The final samples were solubilised in 2% aqueous ACN with 0.1% trifluoroacetic acid.

A pooled lysate from drug-treated samples (Sample A) and a pooled lysate from untreated PHH and 100 µM CDCA (Sample B) were used to generate a treatment-specific (Library A) and OSTα/β up-regulated (Library B) protein spectral library (35). Both sample A and B were digested and processed as described above; however, once the samples had been eluted from the S-Trap™ column, the samples were fractionated. High-pH reversed phase fractionation was performed as described by Batth T.S, *et al* 2014 to generate 12 fractions for sample A and sample B (36).

LC-MS/MS analysis of the pooled library and drug-treated samples was performed as described by Birrell G.W *et al* 2020 (37). The pooled library samples were analysed with a data-dependent acquisition (DDA) method, and the drug-treated samples were analysed with a DIA acquisition method. Analysis was performed using an Ultimate U3000 Nano LC system (Dionex) coupled to a Q-Exactive Orbitrap mass spectrometer. Samples were loaded onto a reversed-phase Acclaim™ PepMap™ trap column (100 µM x 2 cm; Dionex) at a flow rate of 15 µL/min. Analytes were eluted from the trap column into a reversed-phase LC Packings capillary column (75 µM x 50 cm; Dionex). DDA MS/MS analysis was performed in data-dependent mode at a resolution of 70,000 over the *m/z* range of 375-1575 in positive ion mode. Fragmentation was performed for the top 20 most abundant precursors with a normalised collision energy of 27.0 with a 15 ms activation time and dynamic enabled exclusion. DIA MS/MS analysis was performed in data-independent mode using previously mentioned settings for the mass spectrometer with a 25-fixed window setup of 24 *m/z* precursor isolation over a *m/z* range of 375-975.

Sample A and sample B were analysed using MaxQuant version 16.0.5 as previously described (38). The samples were searched against *Homo sapiens*

(UP000005640, release version June 29, 2020) Uniprot FASTA database to generate two proteome libraries, library A and B, respectively. The output from MaxQuant for library A and B were combined in Spectronaut™ 13.0 to generate a single library (PHH spectral library) to be used for DIA analysis. The combined library contained 82,361 peptides, which allowed for 6,944 proteins to be identified.

The LC-MS/MS data from the drug-treated samples were processed with Spectronaut™ 13.0 using the PHH spectral library. Processing of the drug-treated spectra was performed using default Spectronaut™ settings (Manual for Spectronaut™ 13.0, available on Biognosis website). Quantification in Spectronaut used default settings except for minor group quantity set to sum precursor quantity. The data filtering setting was q-value sparse and global normalisation was performed using median values.

Multivariate and statistical analysis

LC-MS metabolomics and proteomics data were analysed by principal component analysis (PCA) using MetaboAnalyst 5.0 (39). Proteomics network maps were generated using g:Profiler assessing only annotated genes with a g:SCS threshold of 0.05 and a data source for GO biological process using Reactome biological pathways (40). Cytoscape 3.8.2 using the EnrichmentMap application was used to convert the g:Profiler output into a network map figure (41, 42). Significance of the change in abundance of metabolites and proteins was determined by one-way analysis of variance (ANOVA) with *post hoc* Dunnett's test with statistical significance at a p-value ≤ 0.05. All one-way ANOVA and correlation studies were performed using GraphPad Prism 7. Metabolite enrichment analysis was performed using MetaboAnalyst 5.0 using SMPDB *Homo sapiens* pathway database (39).

Results

Multivariate analysis of differences in primary human hepatocyte and HepaRG proteomes

Multivariate analysis of the proteomes of PHH and HepaRG™ cells, generated by DIA proteomics, was performed to assess the similarities between the proteomes of the two cell types and to identify which metabolic pathways showed the most significant variations. The DIA proteomics analysis detected 4627 proteins that were detected in both the PHH and HepaRG™ cells. Comparisons of the whole cell proteomes from two PHH donors (BXW and JHY) and HepaRG™ cells showed a significant variation between the proteomes of each cell type. The strong separation between PHH and HepaRG™ cells across principal component 1 (PC1) indicated that there are significant differences in the abundance of proteins in PHH and HepaRG™ cells (Fig. 1A). In contrast, replicate samples from the two PHH donors are grouped closely with one another, showing strong similarities in their proteomes. To further investigate the major metabolic proteins, a list of proteins from major metabolic pathways was generated from the UniProt Knowledgebase to assess differences in protein abundance that may result in altered metabolic behaviour or competence in HepaRG™ cells compared to PHH (43). These pathways included energy metabolism, metabolite and drug transport, phase I/II metabolism, and bile acid and plasma protein synthesis. The PCA scores plot of major metabolic pathways indicated a marked difference between the proteomes for major metabolic pathways of PHH and HepaRG™ cells (Fig. 1B), with clustering similar to that observed for the whole cell proteome. A network map of the whole cell proteome for the top 100 proteins from PC1 showed a significant number of metabolic proteins had

different abundances between PHH and HepaRG™ cells. These proteins were associated with biological oxidation, phase I, amino acid metabolism, and glucose metabolism pathways based on the Reactome database (Fig. 2A). Additionally, a network map of the top 50 proteins of PC1 from major metabolic pathways showed that the variations in the proteomes between PHH and HepaRG™ cells were associated with 28 major metabolic pathways based on the Reactome database (Fig 2B). The proteins with different abundance were associated with major metabolic processes of the liver involved with bile acid synthesis and metabolism, drug metabolism, plasma protein metabolism, nutrient transport, and several energy metabolism pathways.

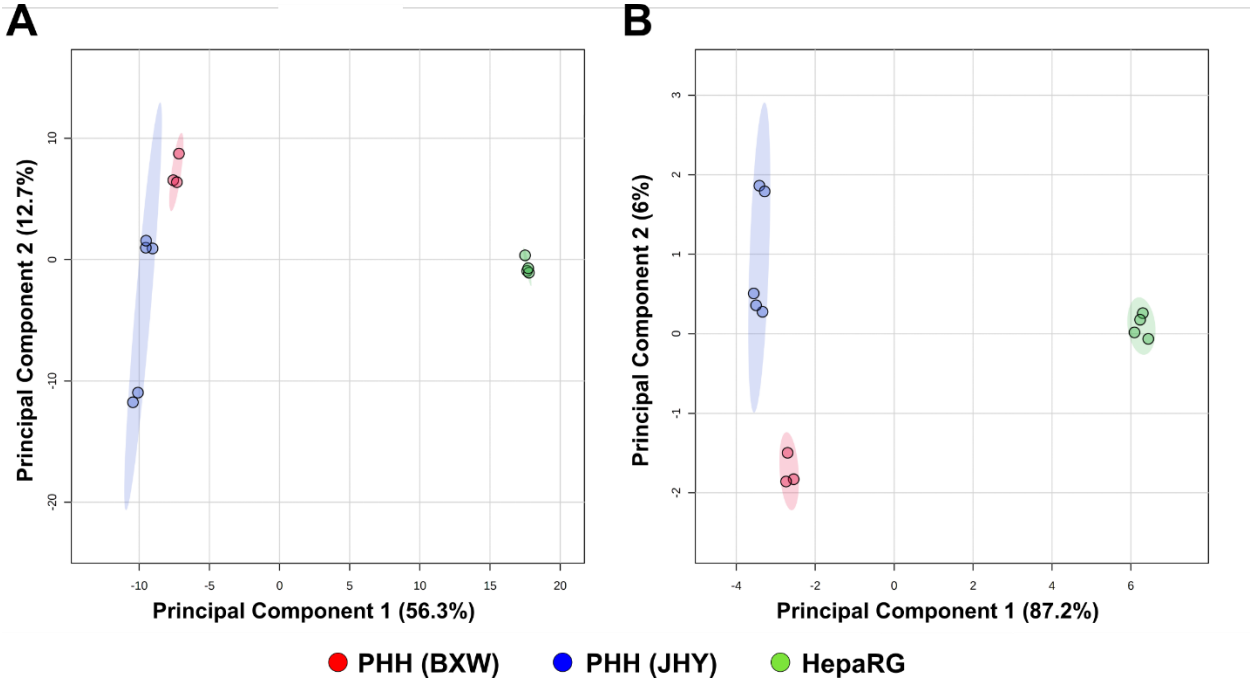

Figure 1: Multivariate analysis of primary human hepatocyte (PHH) and HepaRG whole cell proteome and major metabolic pathways proteome. (A) Principal component analysis (PCA) scores plot of the whole cell proteome of two PHH donors, BXW (red; n=4) and JHY (blue; n=5), and HepaRG cells (green; n=4). (B) Principal component analysis (PCA) scores plot of the major metabolic pathway proteome of two PHH donors and HepaRG cells.

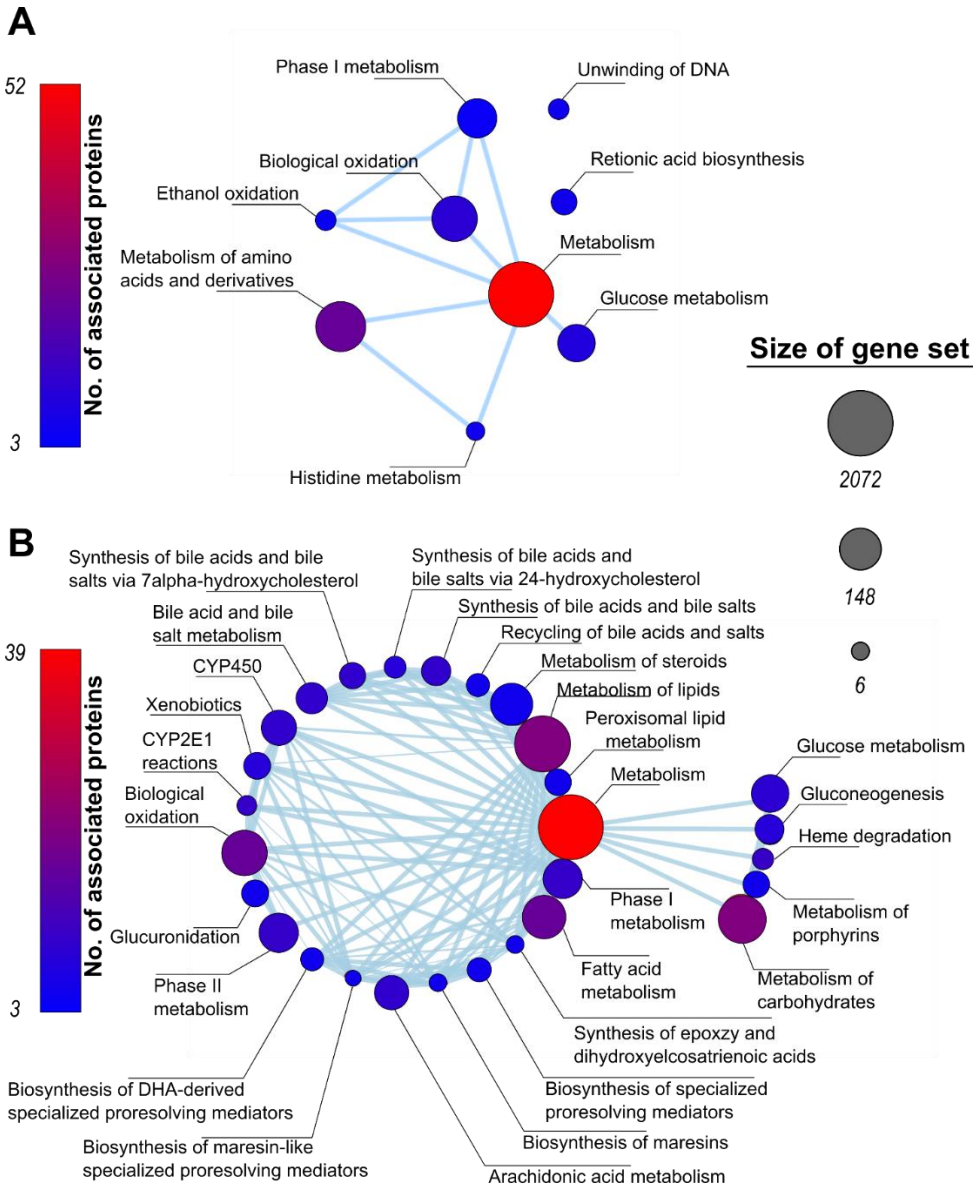

Figure 2: Reactome network map for comparison of primary human hepatocyte (PHH) and HepaRG whole cell proteome and major metabolic pathways proteome. (A) Reactome network map for the top 100 proteins from the whole cell proteome that differed most between PHH and HepaRG cells. (B) Network map for the top 50 proteins from the major metabolic proteome that differed most between PHH and HepaRG cells. Size of circle indicates the number of proteins that are a part of the pathways gene with line showing interconnection between pathways. Red indicates a higher number of proteins are present in different abundance, while blue indicates a lower number of proteins are present in different abundance, between PHH and HepaRG. The top 100 and top 50 proteins for each map were determined from principal component 1 of the PCA.

An analysis of the correlation of protein abundance between HepaRG™ cells and each PHH donor was performed, in addition to a comparison between PHH donors, and correlation plots (Fig. 3). PHH and HepaRG™ cells were compared using the log(total ion current (TIC)) of proteins of the whole cell proteomes (Figs. 3A and B) and for proteins from the major metabolic pathways (Figs. 3C and D). A Pearson product-moment correlation coefficient (*r*) was generated to show the strength of the linear relationship between the abundance of proteins for PHH and HepaRG™ cells and, thus, the similarities between their respective proteomes. For the whole cell proteomes, HepaRG™ cells had an *r* value of 0.8602 and 0.8435 for PHH donors BXW and JHY, respectively (Fig. 3A). The correlation, however, decreased when only assessing the proteins from the major metabolic pathways. For the major metabolic pathways, HepaRG™ cells had an *r* value of to 0.7786 and 0.7476 for PHH donors BXW and JHY, respectively, demonstrating a decrease in correlation (Fig. 3C). In contrast, when the two PHH donors were compared to each other, they had an *r* value of 0.9598 for the whole cell proteome (Fig. 3B) which increased to 0.9739 for the proteins from the major metabolic pathways (Fig. 3D).

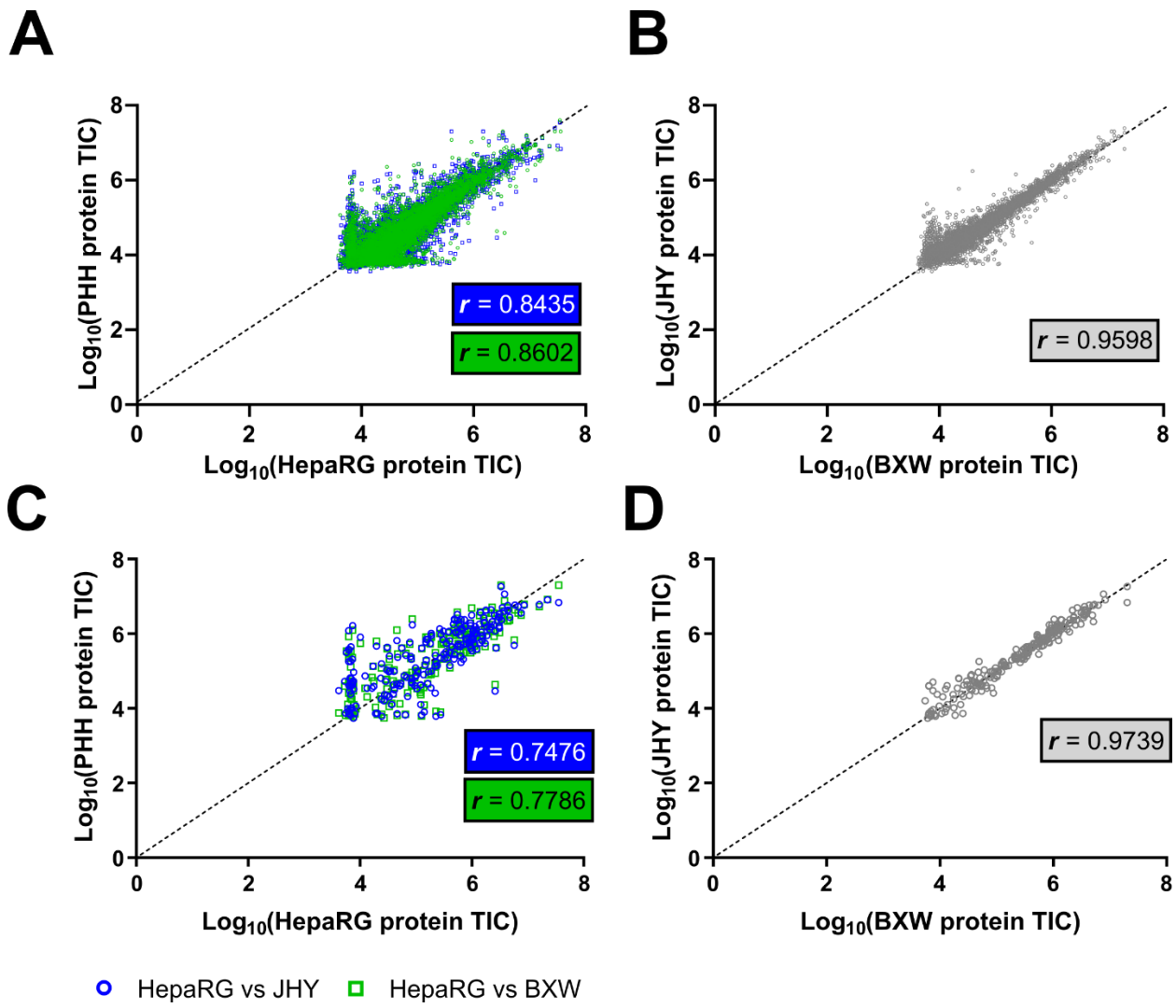

Figure 3: Correlation of protein abundance between HepaRG cells and primary human hepatocytes. Correlation of log_{10}(Protein total ion current (TIC)) between (A) HepaRG (n=4) and PHH donors JHY (blue; n=5) and BXW (green; n=4), and (B) between PHH donors, BXW and JHY (grey) for the whole cell proteome. (C) Correlation between HepaRG and PHH donors JHY (blue) and BXW (green), and (D) between PHH donor BXW and JHY (grey) for major metabolic pathways. Pearson's *r* coefficients were determined for each comparison (n=4).

Comparison of proteins from major metabolic pathways in primary human hepatocytes and HepaRG cells

Further comparison of proteins from major metabolic pathways was performed to characterise the nature of the variation between PHH and HepaRG™ cells. Comparison of PHH donor BXW and HepaRG™ cells revealed that 181 proteins from major metabolic pathways were present at a significantly different abundance, with 99 proteins exhibiting increased abundance (Fig. 4). PHH donor JHY, in comparison to HepaRG™ cells, had 108 proteins that were present in significantly different abundance, with 61 proteins exhibiting increased abundance. A majority of the more abundant proteins in PHH were associated with drug transport and metabolism, and bile acid synthesis. Proteins that were present at lower abundance in PHH compared to HepaRG™ cells were associated with bilirubin synthesis and plasma proteins, in addition to the pentose phosphate pathway, and nutrient and metabolite transport (Fig. 4).

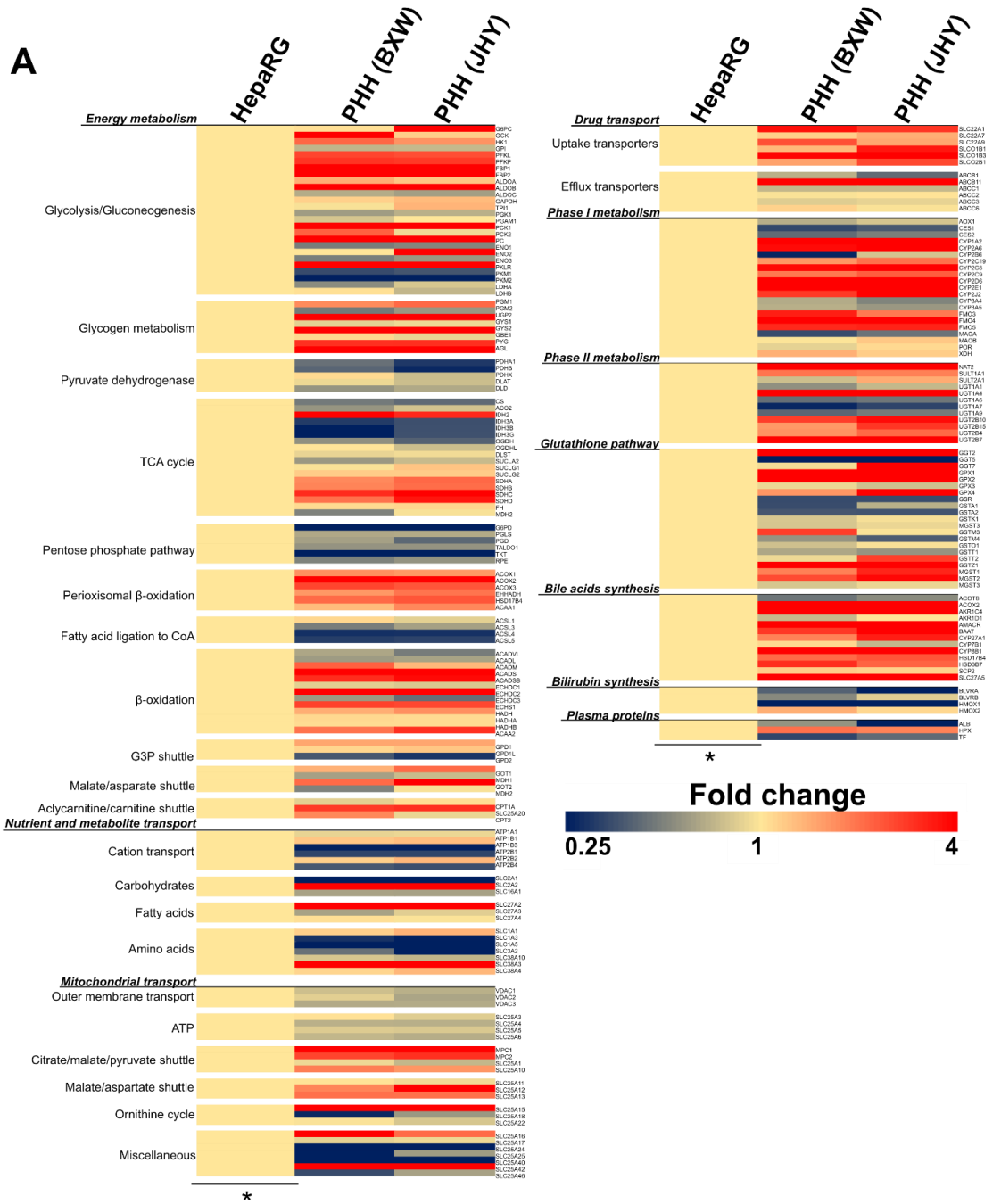

Figure 4: Heatmap of the fold change in protein abundance of major metabolic pathways between HepaRG cells and primary human hepatocytes (PHH). Heatmap shows the fold-difference of PHH, donors BXW (n=4) and JHY (n=5), to HepaRG (n=4) mean protein abundance for each protein. Red, increased abundance; yellow, unchanged abundance; blue, decreased abundance. * fold-difference in protein abundance was normalised with respect to HepaRG protein abundance.

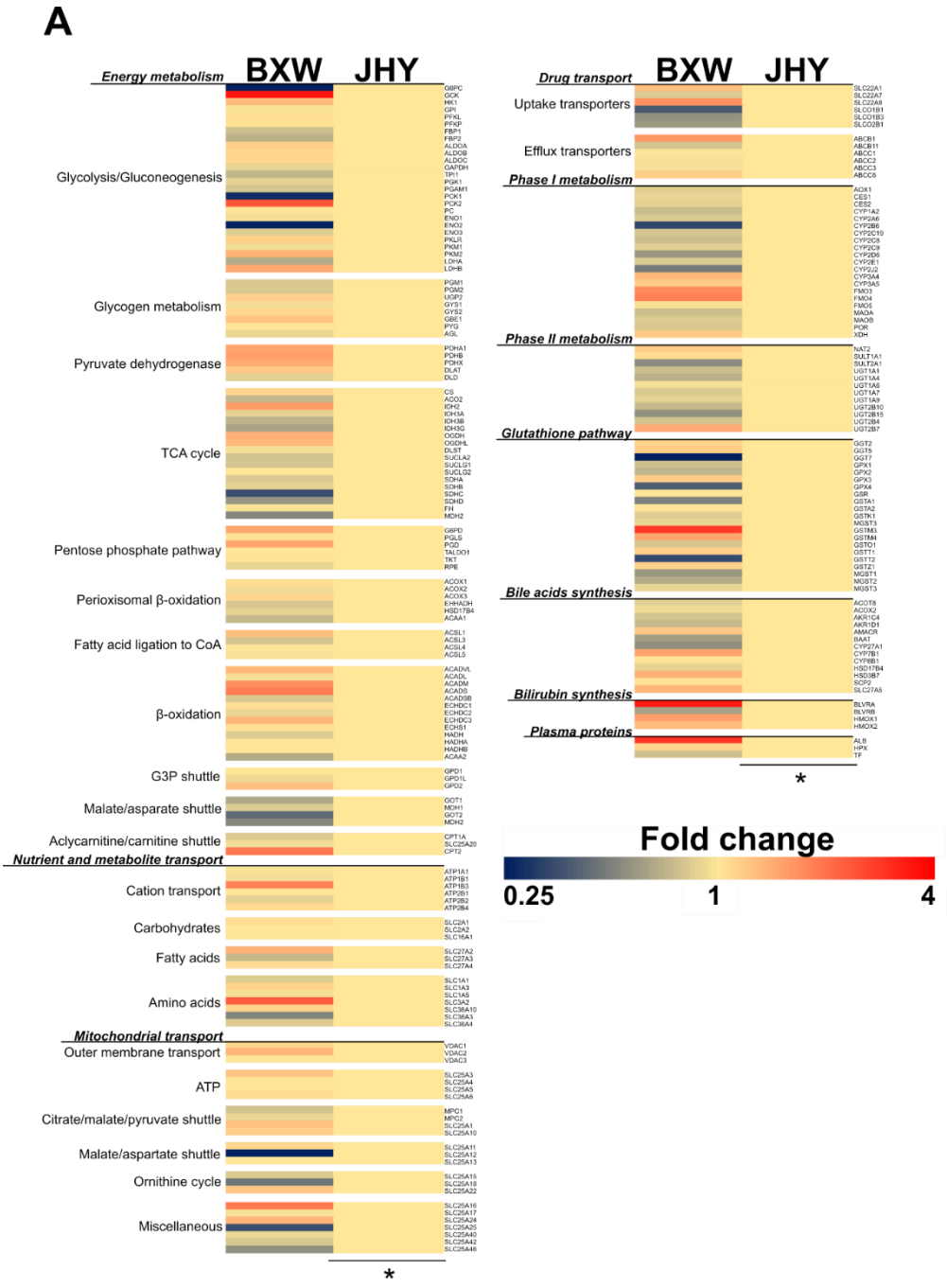

Figure 5: Heatmap of the fold change in protein abundance of major metabolic pathways between primary human hepatocyte (PHH) donors. Heatmap shows the fold-difference of PHH, donors BXW (n=4) and JHY (n=5),) mean protein abundance for each protein. Red, increased abundance; yellow, unchanged abundance; blue, decreased abundance. * fold-difference in protein abundance was normalised with respect to PHH donor JHY protein abundance.

In a comparison between the two PHH donors, there were only 27 proteins that had significantly different abundance between the two donors; 14 of these proteins were associated with energy metabolism, six with drug metabolism, and six with bile acid, bilirubin, and plasma protein synthesis (Fig. 5).

Multivariate analysis of metabolome changes in response to DILI-associated drugs

DILI-associated drugs can have a profound effect on a variety of different metabolic pathways that can result in liver injury. A multi-omics approach utilising metabolomics and proteomics can identify mechanism(s) of DILI by characterising changes in the abundance of metabolites and proteins of important metabolic pathways, such as energy metabolism and detoxification pathways. PHH from the BXW donor were treated with ritonavir (25 µM), pioglitazone (100 µM), and troglitazone (12.5 µM), drugs clinically associated with DILI, for 24 h. After a 24-h drug treatment, metabolite and protein extraction was performed, and extracts were analysed using LC-MS untargeted metabolomic and DIA proteomic analysis. Initially, 537 putative metabolites were identified, which were then filtered to 239 metabolites of interest, based on associations with known metabolic pathways. A heatmap comparison of the 239 putatively identified metabolites that were involved in amino acid, secondary metabolite, energy, lipid, sterol, vitamin and cofactor, nucleotide, and peptide metabolism, shows the mean fold-change of metabolites compared to control after drug treatment (Fig. 6). For ritonavir, 50 metabolites showed a significant change compared to control, with 24 metabolites showing ≥1.5-fold increase in abundance, and 26 showing a ≥ 1.5-fold decrease. For pioglitazone and troglitazone, 60 and 49 metabolites showed a significant change in

abundance, respectively. PHH treated with pioglitazone had 31 metabolites that showed a ≥ 1.5-fold increase in abundance and 29 showed a ≥ 1.5-fold decrease. PHH treated with troglitazone had 21 metabolites that showed a ≥ 1.5-fold increase in abundance and 28 that showed a ≥ 1.5-fold decrease.

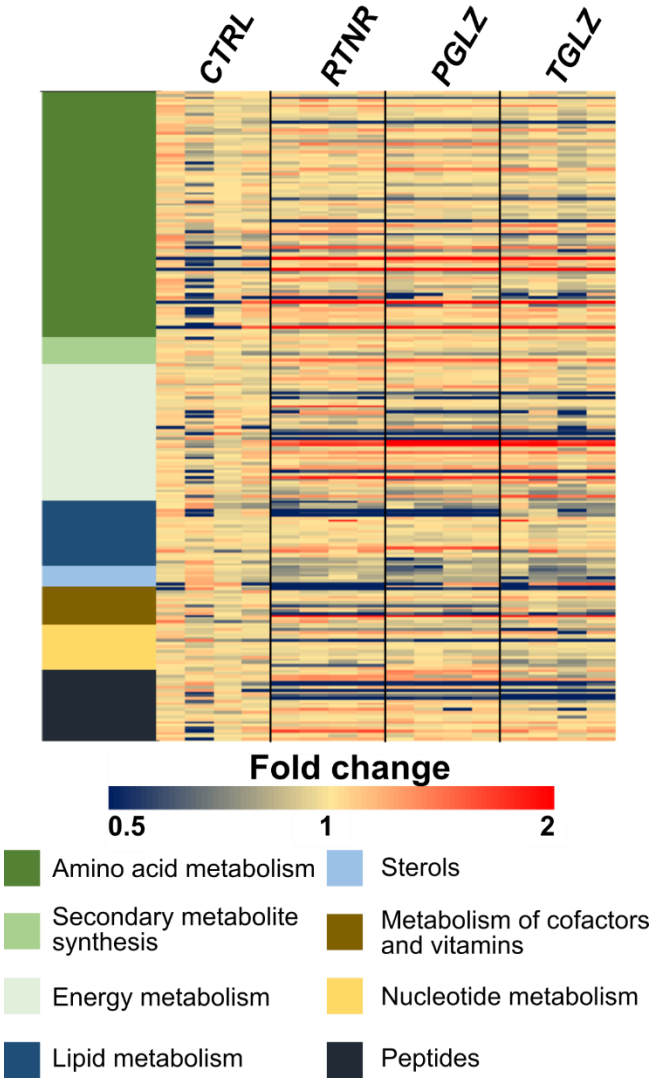

Figure 6: Metabolomics multivariate analysis and heatmap of drug-treated primary human hepatocytes (PHH). Sandwich-cultured PHH were treated with ritonavir 25 µM (RTNR), pioglitazone 100 µM (PGLZ), and troglitazone 12.5 µM (TGLZ) for 24h and compared to untreated control (CTRL) PHH. Metabolites were extracted and analysed using LC-MS metabolomics (n=4). Heatmap of PHH (donor BXW) metabolites from major metabolic pathways following drug treatment comparing the mean fold-change of each metabolite to control PHH. Red, increased abundance; yellow, unchanged abundance; blue, decreased abundance.

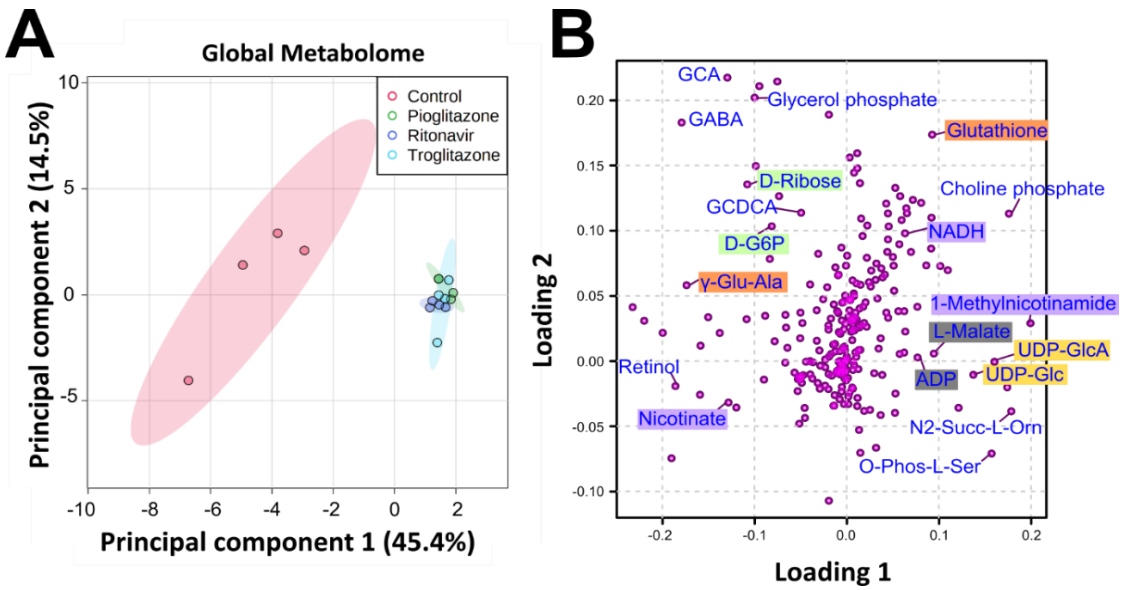

Figure 7: Multivariate analysis of metabolite changes in primary human hepatocytes (PHH) after treatment with drug-induced liver injury (DILI)-associated drugs. (A) A principal component analysis (PCA) of metabolites from control (red), pioglitazone-treated (green), and ritonavir-treated (dark blue), and troglitazone-treated (light blue) PHH. (B) PCA loading plot showing metabolites with a significant contribution to the variation between the drug-treated and control PHH. Metabolites highlighted are those associated with glucose metabolism (green), TCA cycle (grey), nicotinamide metabolism (purple), glucuronidation (yellow), and glutathione metabolism (orange). PCA and loading plot were generated with Metaboanalyst 5.0 with n=4 for each condition.

The metabolomics data of the drug-treated PHH were analysed using PCA of 239 putatively identified metabolites. A PCA plot of the data revealed that the control PHH samples were clearly distinct from the ritonavir-, pioglitazone-, and troglitazone -treated PHH based on principal component 1 (Fig. 7A). This indicated that the drug treatment led to significant metabolite perturbations in PHH at sub-toxic treatment concentrations. However, the three drug treatments clustered strongly together, which indicated that the metabolic perturbations in the PHH were similar for these three drugs. A loading plot, which used the loadings from principal component 1 and 2 from the PCA, identified a number of metabolites associated with glucose metabolism, the TCA cycle, nicotinamide,

glucuronidation, and glutathione metabolism that contributed significantly to the differences observed between the control and drug-treated PHH (Fig. 7B).

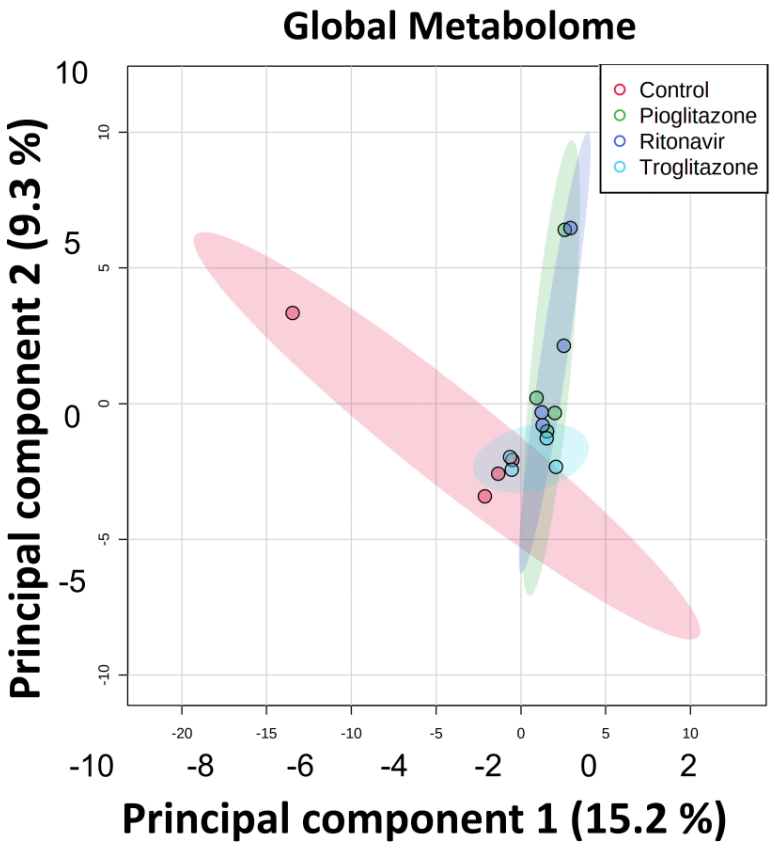

Figure 8: Multivariate analysis of protein changes in primary human hepatocytes (PHH) after treatment with drug-induced liver injury (DILI)-associated drugs. A principal component analysis (PCA) of the DIA proteome from control (red), pioglitazone-treated (green), ritonavir-treated (dark blue), and troglitazone-treated (light blue) PHH. The PCA plot was generated with Metaboanalyst 5.0 with n=4 for each condition.

While a PCA of the whole cell proteome from the DIA proteomics analysis did not identify significant separation between the treatment conditions (Fig. 8), an enrichment analysis identified a number of metabolic pathways that were significantly affected by drug treatment. An enrichment analysis of the top 50 metabolites from principal component 1 demonstrated that pathways associated with glucose metabolism, the TCA

cycle, nicotinamide metabolism, glucuronidation, and glutathione metabolism were significantly affected by drug treatment (Fig. 9).

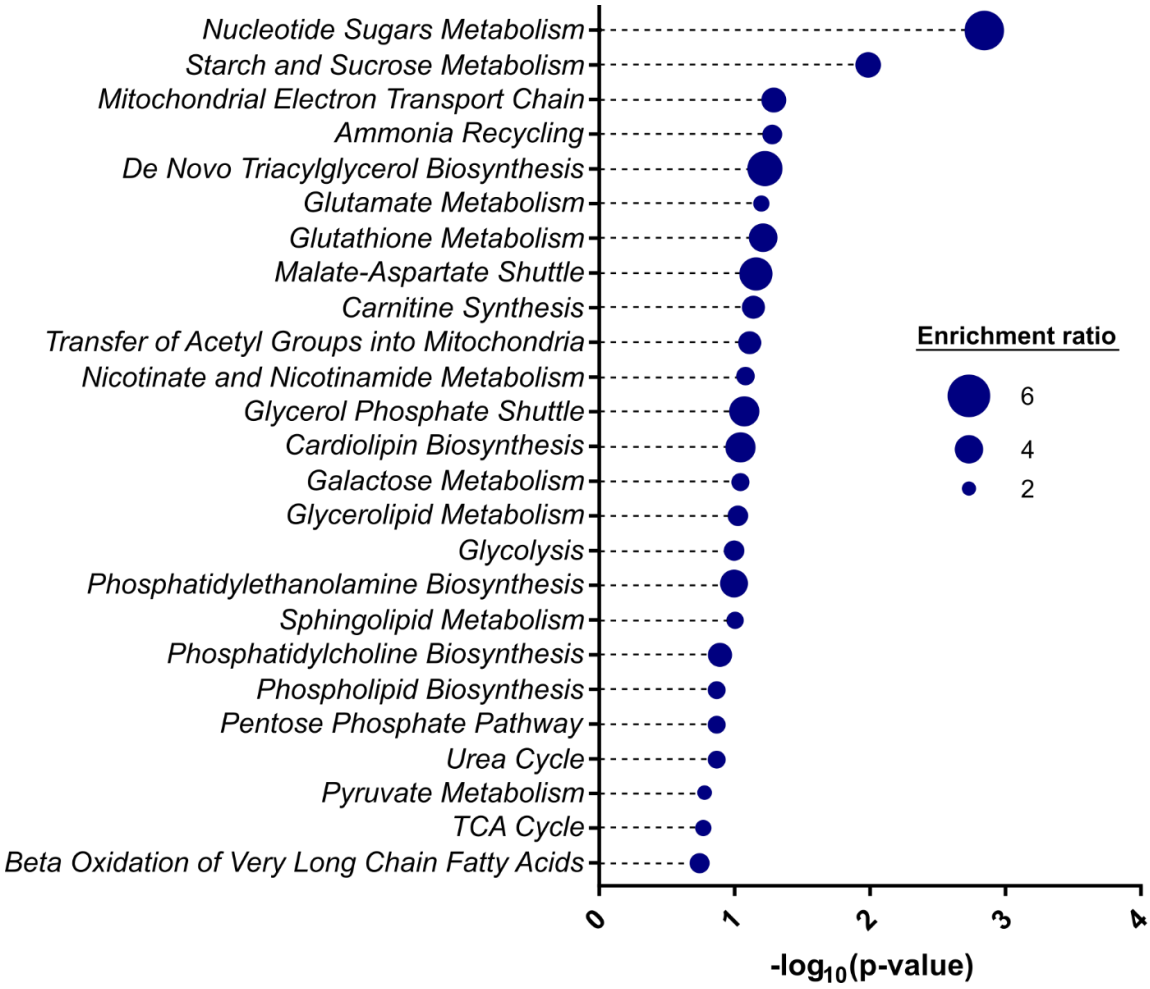

Figure 9: Enrichment analysis of top 50 most altered metabolites from primary human hepatocytes treated with DILI-associated drugs. Enrichment analysis shows the -$\log_{10}$(p-values) of the top 50 most altered metabolites identified by PCA analysis from principal component 1. Diameter of point shows enrichment ratio for each metabolism pathway. Enrichment analysis was performed using MetaboAnalyst 5.0 using SMPDB *homo sapiens* pathway database.

Perturbation of metabolites and protein abundance in major metabolic pathways

Multivariate analysis of the metabolic perturbations induced by ritonavir, pioglitazone, and troglitazone demonstrated that these drugs significantly affected major liver metabolism pathways (glucose metabolism, TCA cycle, nicotinamide metabolism, glucuronidation, and glutathione metabolism). Multi-omics analysis utilising metabolomics and proteomics was applied to holistically study the impact of ritonavir, pioglitazone, and troglitazone treatment of PHH on these metabolic pathways. Analysis of phase I metabolism enzymes from the DIA proteomic analysis was performed due to its significant contribution to xenobiotic metabolism.

Drug treatment had a significant impact on the glucose metabolism pathway, with all drug treatments demonstrating an overall trend towards decreased abundance of glucose metabolism enzymes (Table 1). The abundance of the glucose uptake transporter 10 (GLUT10) showed increased abundance after treatment with ritonavir (Table 1). This transporter showed some degree of increased abundance after treatment with pioglitazone and troglitazone, although these changes were not statistically significant. While a statistically significant change in the abundance of glucokinase (GCK) was not observed, the GCK synthesis product metabolite, D-glucose-6-phosphate, significantly decreased in abundance after all drug treatments (Figs. 10 and 11). The abundance of D-ribose, a product of the pentose phosphate pathway, also was decreased after all drug treatments (Fig. 10 and 11). Phosphoenolpyruvate carboxykinase 1 (PCK1), which synthesises phosphoenolpyruvate, was significantly increased in abundance after treatment with ritonavir, pioglitazone, and troglitazone (Table 1; Fig. 10).

Table 1: Glucose metabolism pathway proteins significantly altered by treatment of primary human hepatocytes (PHH) with ritonavir (25 µM), pioglitazone (100 µM), or troglitazone (12.5 µM). Statistically significant differences are shown in bold and were determined with a one-way ANOVA with significance at a p-value ≤ 0.05 with an n=4 for each condition.

	Ritonavir		**Pioglitazone**		**Troglitazone**	
Proteins	***Fold-change***	***p-value***	***Fold-change***	***p-value***	***Fold-change***	***p-value***
GLUT10	**1.35**	0.0015	1.13	0.2347	1.13	0.2763
GPI	**0.76**	<0.0001	**0.82**	0.0002	**0.85**	0.0007
ALDOA	**0.76**	0.0050	**0.74**	0.0065	**0.78**	0.0090
TPI1	**0.80**	0.0099	0.89	0.1774	0.93	0.5013
PGAM1	0.88	0.0614	**0.85**	0.0228	**0.81**	0.0043
ENO1	0.88	0.0872	**0.84**	0.0166	0.91	0.2222
ENO3	**0.75**	0.0035	0.86	0.1047	0.93	0.5122
LDHA	**0.79**	<0.0001	**0.89**	0.0178	**0.87**	0.0055
PCK1	**1.33**	0.0045	**1.25**	0.0272	**1.29**	0.0107
GOT1	**0.84**	0.0002	**0.84**	0.0002	**0.83**	0.0001
G6PD	**0.80**	0.0145	0.86	0.0920	**0.79**	0.0183
RPE	**0.81**	0.0277	**0.79**	0.0154	**0.81**	0.0309
TKT	**0.84**	0.0318	**0.85**	0.0419	0.95	0.7066
TALDO1	**0.78**	0.0017	**0.85**	0.0209	0.92	0.2626

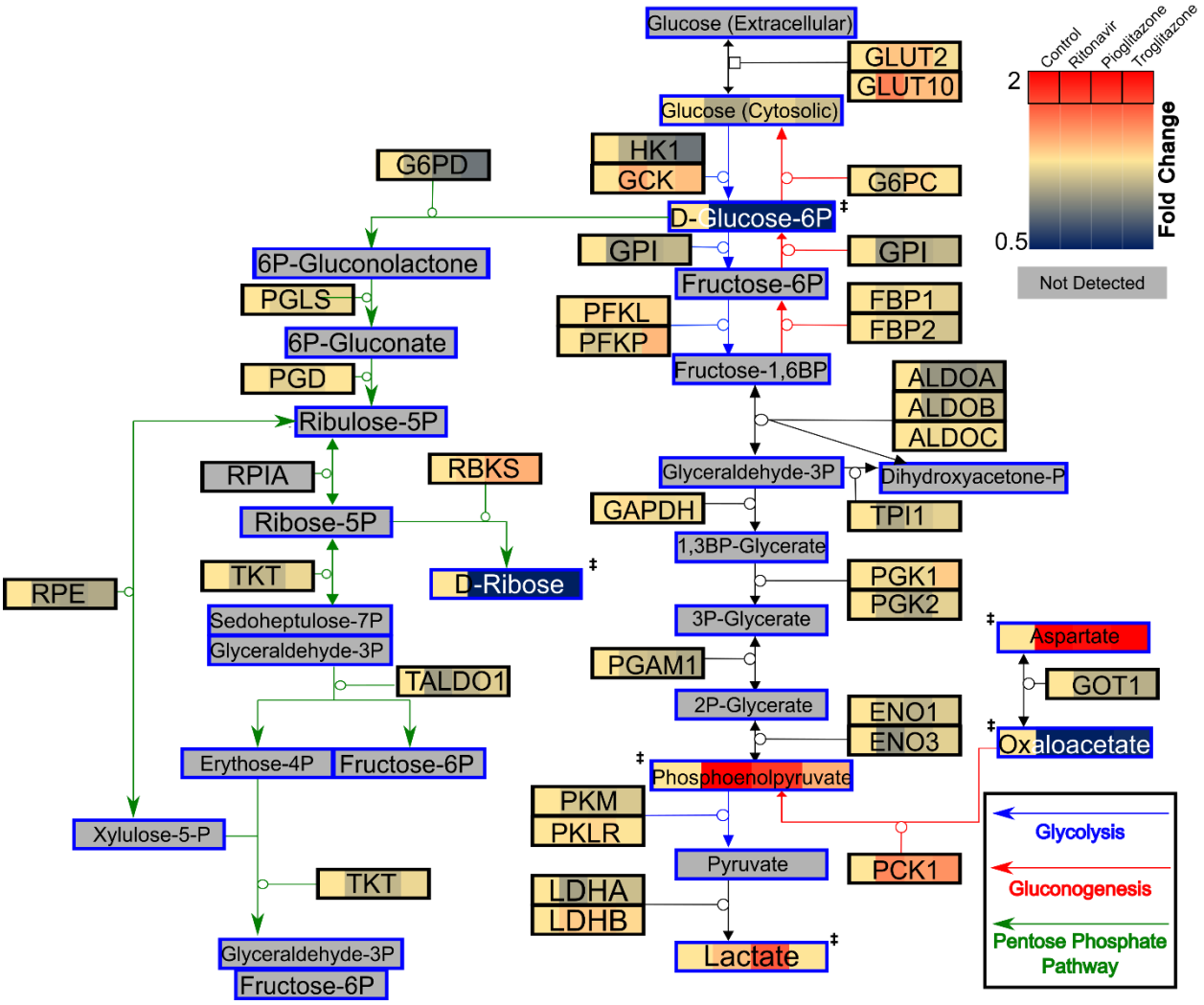

Figure 10: Glucose metabolism pathway of metabolite and protein perturbations in drug-treated primary human hepatocytes (PHH). Glucose metabolic pathway with alterations in metabolite and protein abundance shown by the heatmap for each drug treatment compared to untreated control. Heatmap ranges were from a 2-fold increase in abundance (red) to a 2-fold decrease in abundance (blue), with yellow depicting no change in abundance. ‡ denotes a significant change in metabolite abundance determined with a p-value ≤ 0.05 when compared to untreated control with an n=4 for each condition.

Furthermore, phosphoenolpyruvate itself was significantly increased in abundance after treatment with ritonavir, with a trend towards an increased abundance after treatment with pioglitazone and troglitazone (Fig. 11). All drug treatments resulted in a decreased abundance of glutamic-oxaloacetic transaminase 1 (GOT1; Table 1 and Fig. 10), which synthesises aspartate. The abundance of aspartate was significantly increased following treatment with pioglitazone and troglitazone, with a trend towards an increased abundance after treatment with ritonavir (Fig. 11). Lactate dehydrogenase A (LDHA) abundance was significantly decreased after all drug treatments (Fig. 10), but the only significant change in lactate abundance was an increase after treatment with pioglitazone (Fig. 11).

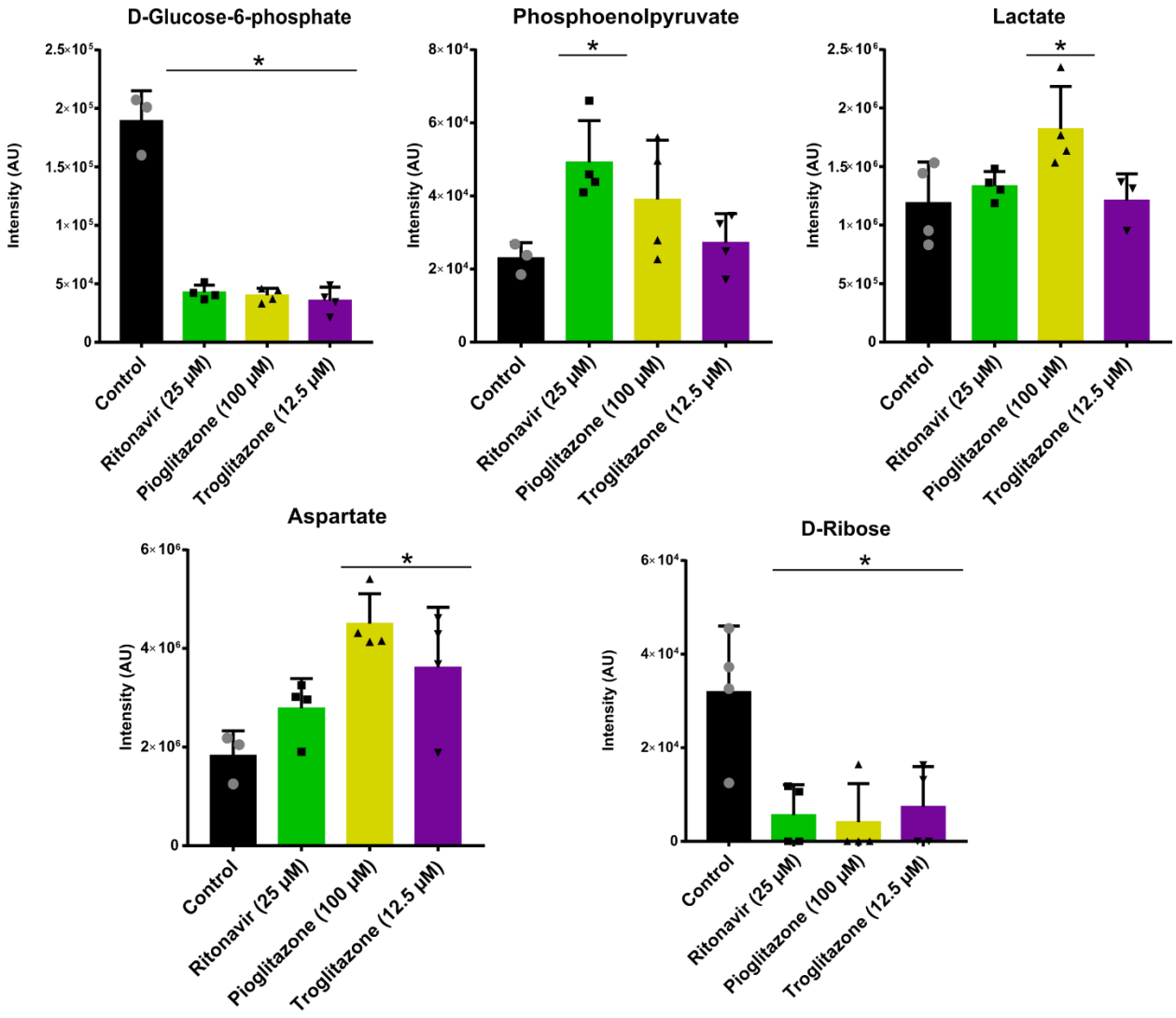

Figure 11: Metabolites with significantly altered abundance from the glucose metabolism pathway in drug-treated primary human hepatocytes (PHH). LCMS untargeted metabolomics was used to identify alterations in metabolite abundance after a 24-h treatment with ritonavir, pioglitazone, or troglitazone (mean ± SD in quadruplicate). * Statistically significant differences were determined with a one-way ANOVA with significance at a p-value ≤ 0.05 with an n=4 for each condition.

Multi-omics characterisation of perturbations in the TCA cycle identified five significantly altered metabolites and three significantly altered proteins as a result of drug treatment. The changes to protein abundance observed were minor increases (< 25%) in the abundance of enzymes in the section of the TCA cycle that converts isocitrate to fumarate (Table 2).

Table 2: TCA cycle pathway proteins significantly altered by treatment of primary human hepatocytes (PHH) with ritonavir (25 µM), pioglitazone (100 µM), or troglitazone (12.5 µM). Statistically significant differences are shown in bold and were determined with a one-way ANOVA with significance at a p-value ≤ 0.05 with an n=4 for each condition.

	Ritonavir		**Pioglitazone**		**Troglitazone**	
Proteins	***Fold-change***	***p-value***	***Fold-change***	***p-value***	***Fold-change***	***p-value***
IDH2	1.15	0.2006	1.08	0.6911	**1.26**	0.0210
OGDH	**1.17**	0.0182	1.09	0.2424	1.12	0.1279
SDHB	**1.20**	0.0362	1.12	0.0853	**1.19**	0.0064

However, the metabolite changes that were observed included large increases and decreases in the abundance of several TCA cycle metabolites (Fig 12). Succinate was significantly decreased in abundance by all three drug treatments (Fig. 12) while there was no change to succinate-CoA ligases, enzymes that catalyse the interconversion of succinate and succinate-CoA (Table 2). Although fumarate was not detected, malate, which is synthesised from fumarate, was significantly increased in abundance after all drug treatments (Fig. 12). Oxaloacetate was significantly decreased in abundance after all drug treatments. Finally, adenosine diphosphate (ADP) was significantly increased in abundance after all three drug treatments.

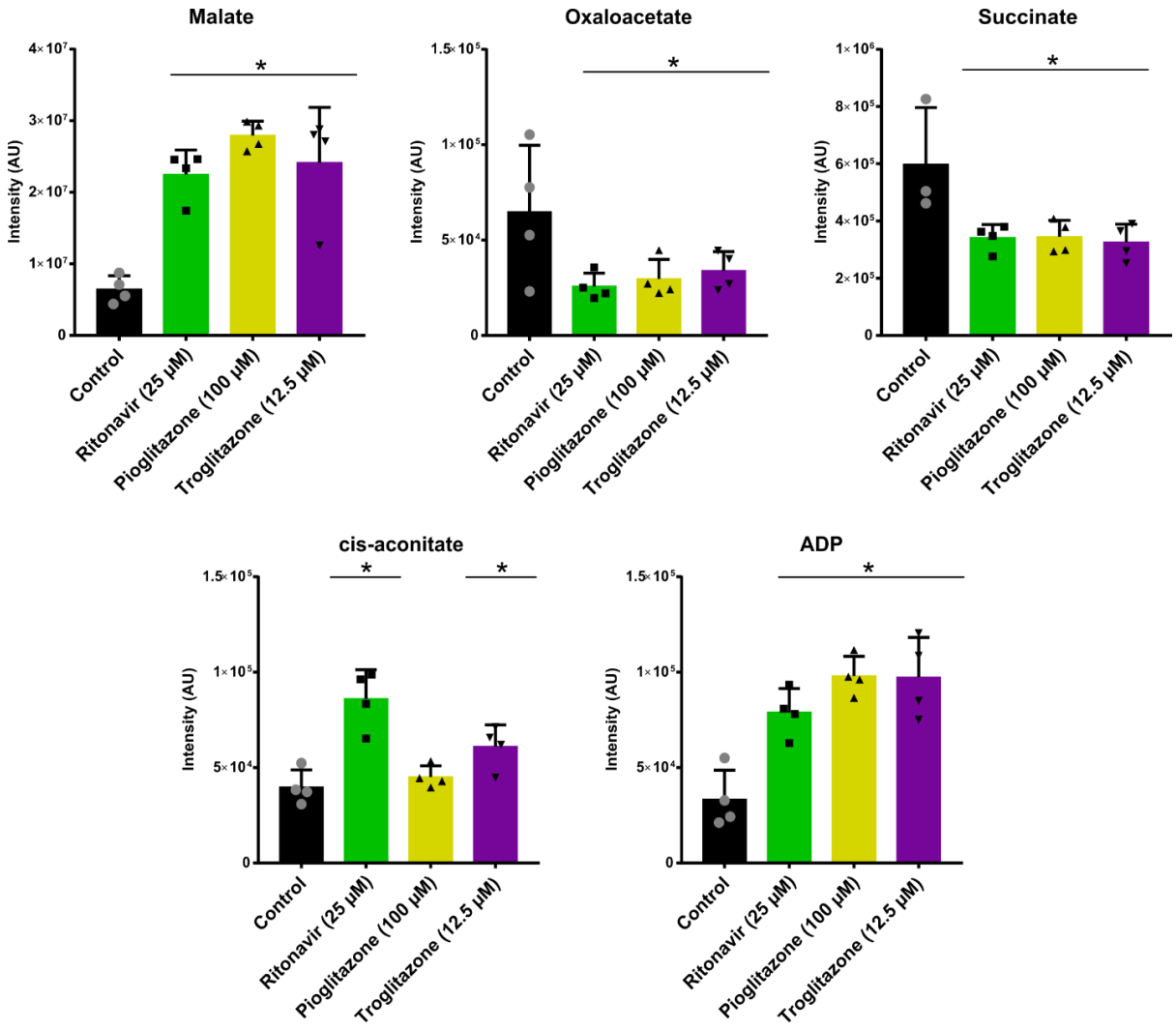

Figure 12: Metabolites with significantly altered abundance from the TCA cycle metabolism pathway in drug-treated primary human hepatocytes (PHH). LCMS untargeted metabolomics was used to identify alterations in metabolite abundance after a 24-h treatment with ritonavir, pioglitazone, or troglitazone (mean ± SD in quadruplicate). * Statistically significant differences were determined with a one-way ANOVA with significance at a p-value ≤ 0.05 with an n=4 for each condition.

Drug treatment with ritonavir, pioglitazone, and troglitazone all impacted the nicotinamide metabolism pathway. The nicotinamide metabolism pathway demonstrated an overall trend towards increased synthesis of nicotinamide and 1-methylnicotinamide following drug exposure across all drug treatments (Fig. 13).

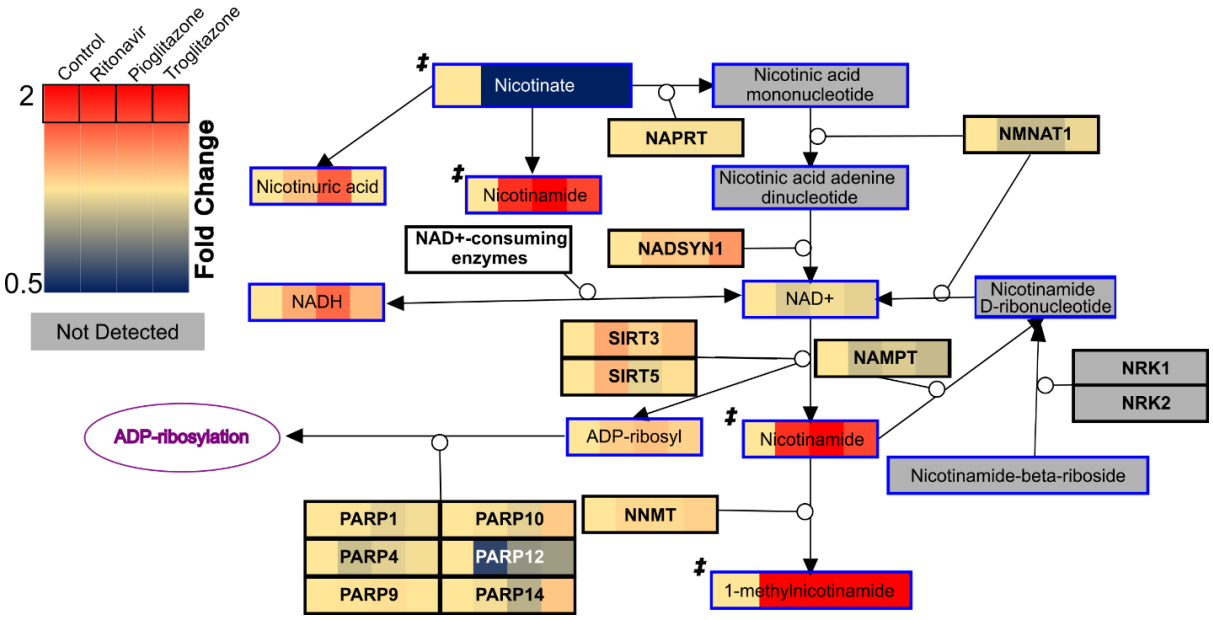

Figure 13: Nicotinamide metabolism pathway of metabolite and protein perturbations in drug-treated primary human hepatocytes (PHH). Nicotinamide metabolism pathway with alterations in metabolite and protein abundance shown by the heatmap for each drug treatment compared to untreated control (mean ± SD in quadruplicate). Heatmap ranges were from a 2-fold increase in abundance (red) to a 2-fold decrease in abundance (blue), with yellow depicting no change in abundance. ‡ denotes a significant change in metabolite abundance determined with a p-value ≤ 0.05 when compared to untreated control with an n=4 for each condition.

NAD-dependent deacetylase sirtuin-3 (SIRT3) and -5 (SIRT5), which synthesises nicotinamide, were not significantly altered in abundance, however, ritonavir did induce a significant increase in the abundance of nicotinamide as well as an increase in 1-methylnicotinamide abundance (Fig. 14). Pioglitazone and troglitazone also significantly increased the abundance of 1-methylnicotinamide. Additionally, pioglitazone and troglitazone also appeared to increase nicotinamide abundance as well, however, not to

a statistically significant degree. Nicotinamide phosphoribosyltransferase (NAMPT), which converts nicotinamide to nicotinamide-D-ribonucleoside, showed a trend towards a decreased abundance for all drug treatments, with ritonavir and troglitazone inducing a statistically significant decrease as determined by a one-way ANOVA. Finally, all three drug treatments caused a significant decrease in nicotinate, a precursor of nicotinamide and 1-methylnicotinamide synthesis (Fig. 14).

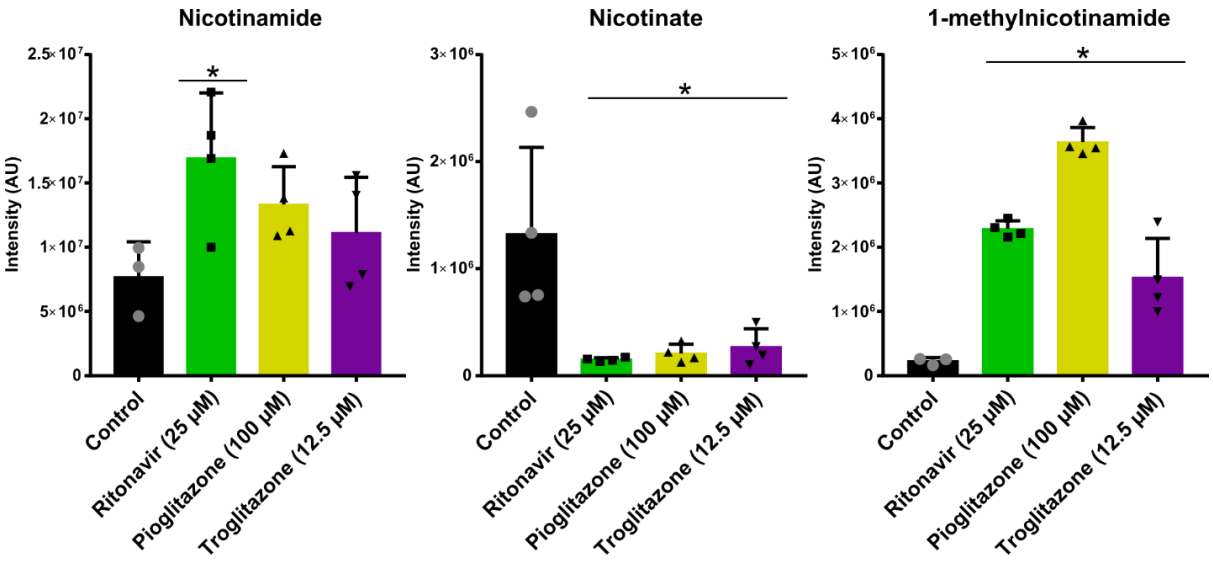

Figure 14: Metabolites with significantly altered abundance from the nicotinamide metabolism pathway in drug-treated primary human hepatocytes (PHH). LCMS untargeted metabolomics was used to identify alterations in metabolite abundance after a 24-h treatment with ritonavir, pioglitazone, or troglitazone (mean ± SD in quadruplicate). * Statistically significant differences were determined with a one-way ANOVA with significance at a p-value ≤ 0.05 with an n=4 for each condition.

All three drug treatments had a significant effect on the abundance of phase I metabolism enzymes with eight CYP and four aldehyde dehydrogenase (ALDH) enzymes significantly increased in abundance (Fig. 15). Additionally, while not all phase I enzymes showed a statistically significant increase in abundance, there was a pathway-wide trend towards an increased abundance; only six of the 34 enzymes demonstrated any decrease

in abundance by the drug treatments. CYP2B6 was the only phase I enzyme that was significantly increased in abundance for all three drug treatments. However, each drug treatment induced an increase in at least five phase I enzymes. Ritonavir caused seven phase I enzymes to be significantly increased in abundance, while pioglitazone and troglitazone caused an increase in the abundance of five and nine phase I enzymes, respectively.

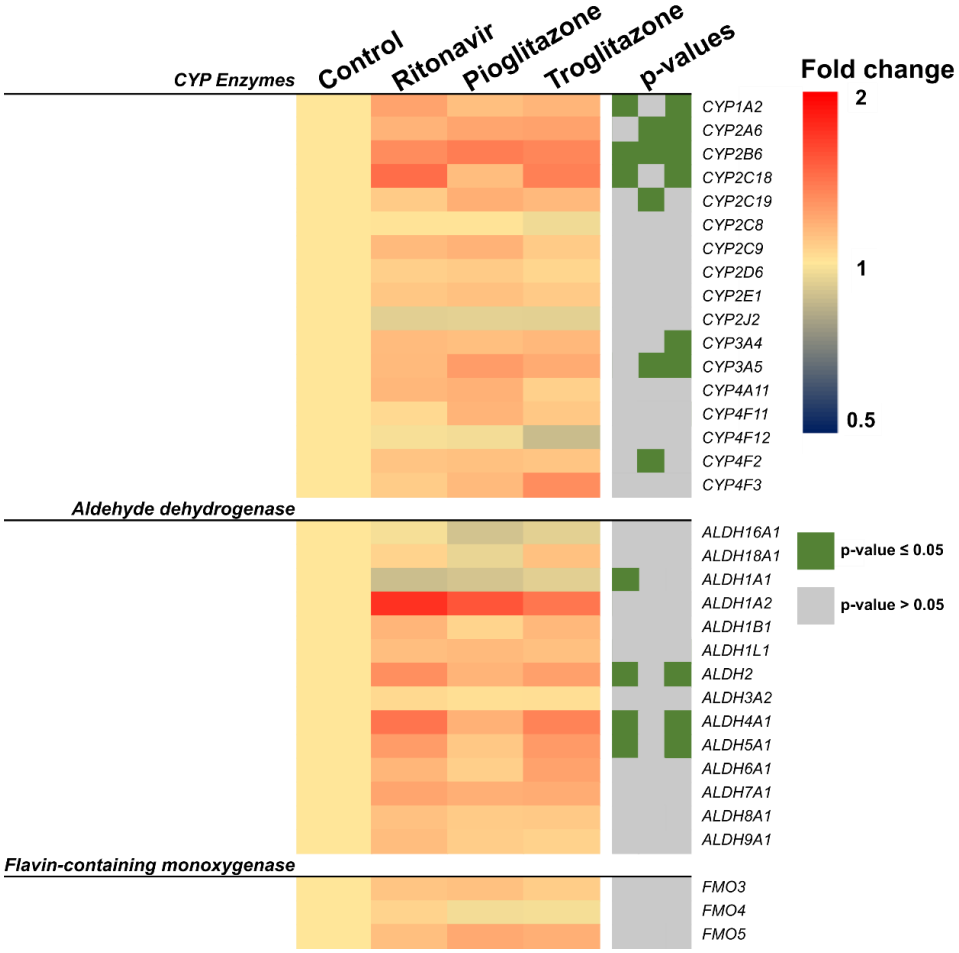

Figure 15: Heatmap of changes to phase I enzyme abundance in drug-treated primary human hepatocytes (PHH). Heatmap depicts the changes in abundance of CYP enzymes, aldehyde dehydrogenases, and flavin-containing monooxygenases after a 24-h treatment with ritonavir (25 µM), pioglitazone (100 µM), or troglitazone (12.5 µM). Statistically significant changes in each enzyme are shown by p-values of ≤0.05 (dark green) or >0.05 (grey) determined by one-way ANOVA (n=4).

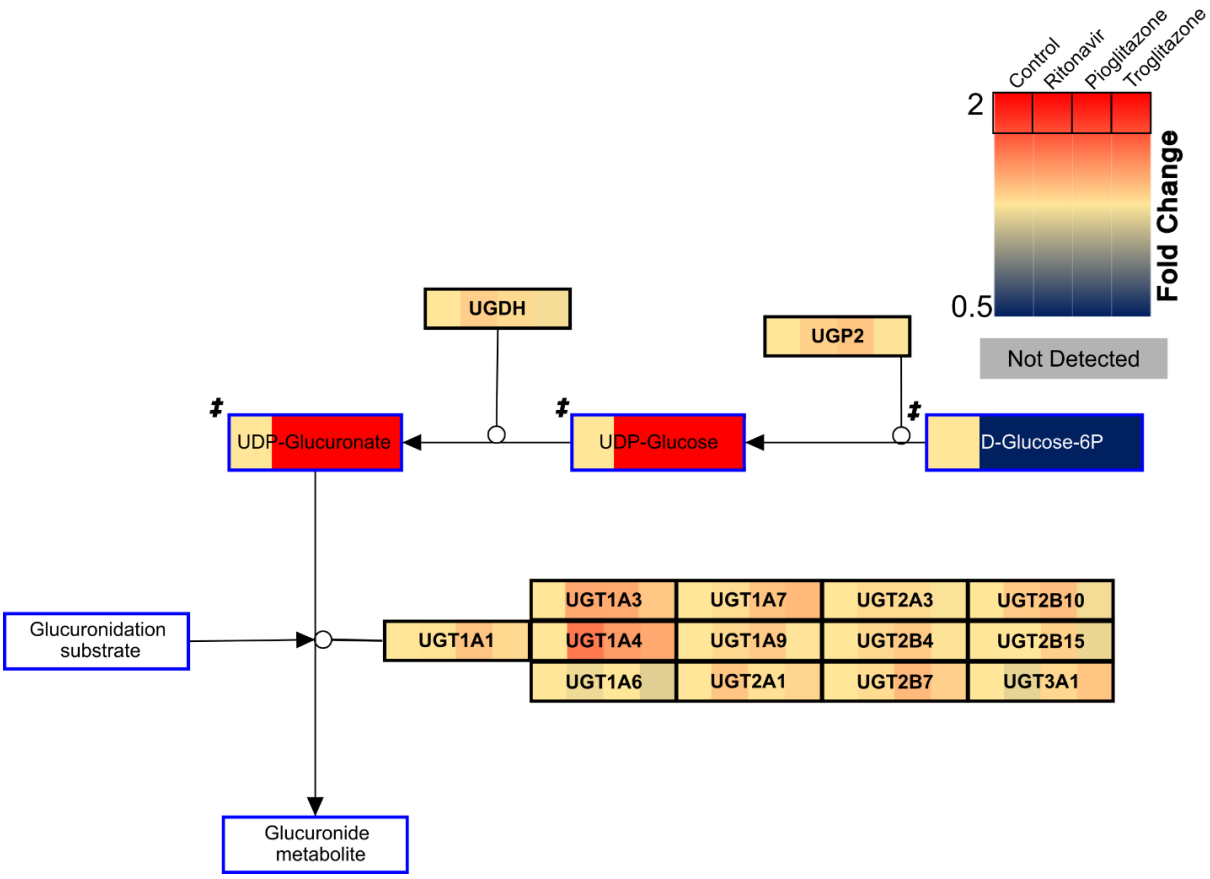

Figure 16: Phase II glucuronidation metabolism pathway of metabolite and protein perturbations in drug-treated primary human hepatocytes (PHH). Phase II glucuronidation metabolism pathway with alterations in metabolite and protein abundance shown by the heatmap for each drug treatment compared to untreated control. Heatmap ranges were from a 2-fold increase in abundance (red) to a 2-fold decrease in abundance (blue), with yellow depicting no change in abundance. ‡ denotes a significant change in metabolite abundance determined with a p-value ≤ 0.05 when compared to untreated control with an n=4 for each condition.

For glucuronidation metabolism, the three metabolites of this pathway showed significant changes in their abundance after all drug treatments, with a shift towards an increased abundance of uridine diphosphate (UDP) conjugated metabolites (Fig. 16). D-glucose-6-phosphate was reduced by over 4-fold for all drug treatments, while UDP-glucose and UDP-glucuronate increased by up to 11-fold, with the greatest increase associated with pioglitazone (Fig. 16). In contrast, while 12 of the 13 uridine 5'-diphospho-

glucuronosyltransferase (UGT) enzymes showed a trend towards increased abundance after all drug treatments, only UGT2A1 showed a statistically significant increase after treatment with ritonavir (Fig. 16).

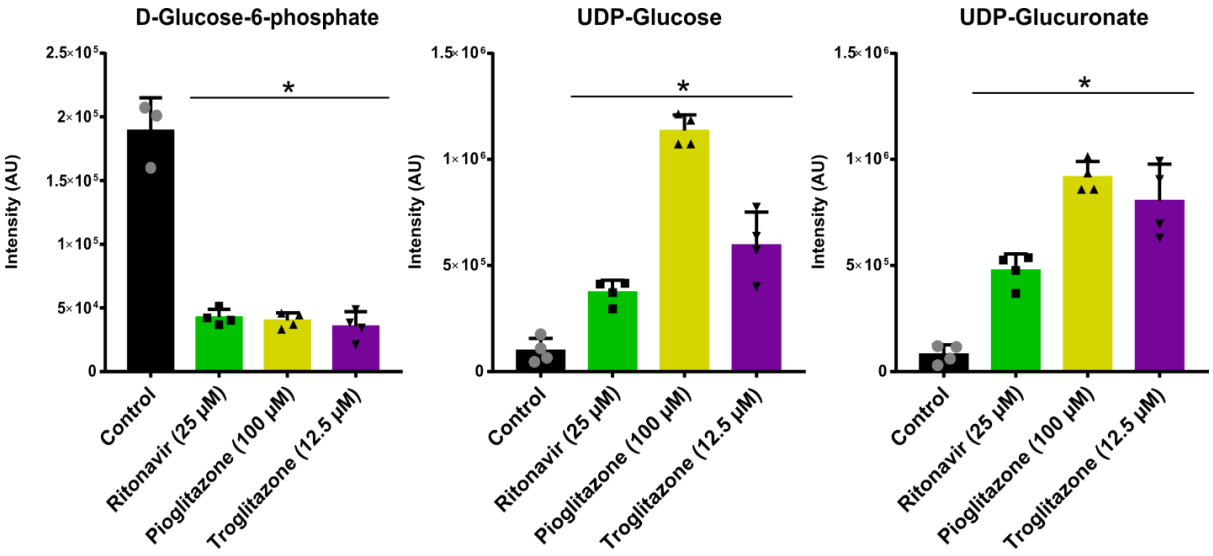

Figure 17: Metabolites with significantly altered abundance from glucuronidation metabolism pathway in drug-treated primary human hepatocytes (PHH). LCMS untargeted metabolomics was used to identify alterations in metabolite abundance after a 24-h treatment with ritonavir, pioglitazone, or troglitazone (mean ± SD in quadruplicate). * Statistically significant differences were determined with a one-way ANOVA with significance at a p-value ≤ 0.05 with an n=4 for each condition.

Glutathione metabolism, an oxidative stress and conjugation pathway, had six proteins and one metabolite that demonstrated significantly altered abundance by the drug treatments. The abundance of gamma-glutamylcyclotransferase (GGCT), an enzyme that converts L-γ-glutamyl-containing peptides to 5-oxoproline, was significantly lower (2-fold) in ritonavir-treated PHH (Table 3). However, 5-oxoproline showed the opposite trend, and was significantly increased in abundance after drug treatment with ritonavir (Figs. 18). Additionally, the ritonavir drug treatment induced a significant increase in the abundance of glutathione peroxidase 4 (GPX4) and glutathione S-transferase kappa 1 (GSTK1), and a significant decrease in the abundance of glutathione S-

transferase omega 1 (GSTO1). All drug treatments induced a significant decrease in glutathione synthetase (GSS) and alanine aminopeptidase (ANPEP) (Table 3).

Table 3: Glutathione metabolism pathway proteins significantly altered by treatment of primary human hepatocytes (PHH) with ritonavir (25 µM), pioglitazone (100 µM), or troglitazone (12.5 µM). Statistically significant differences are shown in bold and were determined with a one-way ANOVA with significance at a p-value ≤ 0.05 with an n=4 for each condition.

	Ritonavir		Pioglitazone		Troglitazone	
	Fold-change	***p-value***	***Fold-change***	***p-value***	***Fold-change***	***p-value***
GGCT	**0.51**	0.0132	0.63	0.0569	0.60	0.0599
GSS	**0.73**	<0.0001	**0.80**	0.0012	**0.75**	0.0002
ANPEP	**0.89**	0.0127	**0.86**	0.0025	**0.83**	0.0007
GPX4	**1.28**	0.0057	1.10	0.4194	1.04	0.8777
GSTK1	**1.25**	0.0060	1.08	0.4688	1.11	0.2532
GSTO1	**0.86**	0.0404	0.4844	0.2823	1.01	0.9895

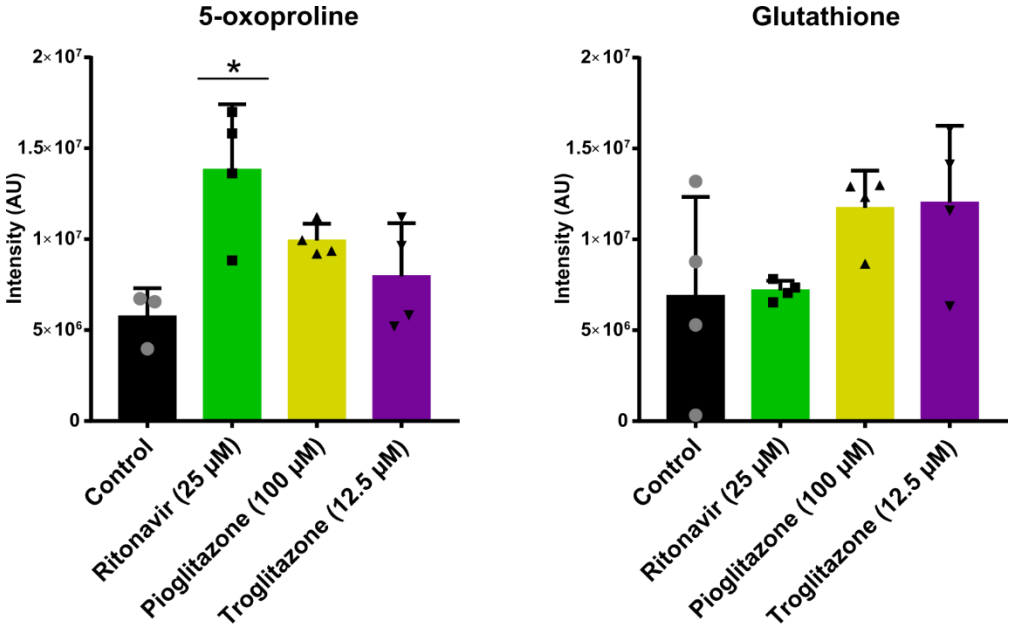

Figure 18: Important metabolites with altered abundance from the glutathione metabolism pathway in drug-treated primary human hepatocytes (PHH). LCMS untargeted metabolomics was used to identify alterations in metabolite abundance after a 24-h treatment with ritonavir, pioglitazone, or troglitazone (mean ± SD in quadruplicate). * Statistically significant differences were determined with a one-way ANOVA with significance at a p-value ≤ 0.05 with an n=4 for each condition.

Discussion

The research presented used DIA proteomics to compare the proteomic profiles of differentiated HepaRG™ cells to two PHH donors (BXW and JHY). The proteomic profiles were compared for the whole cell proteome and the major metabolic pathways of PHH and HepaRG™ cells. In addition, multi-omics techniques were utilised to characterise and compare changes to the proteome and metabolome of PHH after treatment with drugs associated with DILI. This study demonstrated that while PHH and HepaRG™ cells show some similarities in their proteomes, there are significant variations in protein abundance, especially proteins from the major metabolic pathways. Furthermore, this study demonstrated that the combination of metabolomics and proteomics allowed for characterisation of perturbations to major metabolic pathways after treatment with drugs associated with DILI.

Comparison between the proteomes from the two PHH donors and HepaRG™ cells indicated that there was a strong similarity in the abundance of proteins in the whole cell proteome and major metabolic pathways for both PHH donors. However, for the major metabolic pathways, 82% of the proteins detected showed a difference in abundance in HepaRG™ cells compared to PHH, which is 6.7-fold greater than the number of differences between donors (Figs. 4 and 5). Donors were expected to demonstrate relatively similar metabolic behaviour, but a small amount of variation due to interdonor variability is known to lead to variations in protein expression between individual donors (44). The difference in protein abundance of major metabolic pathways between HepaRG™ cells and PHH suggests that HepaRG™ cells may have some limitations in their capacity to replicate the metabolic behaviour of PHH. However, the degree to which

these differences in abundance may impact the functional metabolic behaviour of HepaRG cells, in comparison to PHH, is also dependent on the phenotypic nature of the proteins. Different protein variants may have inherently different metabolic properties, as exemplified by the N-acetyltransferase 2 slow and fast acetylator, or glucokinase regulatory protein variants (45, 46). The proteomics methodology utilised in this study would not detect such protein variants, and only provides a measure of protein abundance, not function. Therefore, in order to comprehensively understand how the metabolic functionality of HepaRG cells differ from PHH, additional functional assays would be necessary.

Liver injury has been demonstrated previously to have a significant effect on several major metabolic pathways including glucose metabolism, the TCA cycle, nicotinamide, phase I, glucuronidation, and glutathione metabolism (18-21, 47-51). Multivariate and enrichment analysis demonstrated that the changes to the metabolome after drug treatment significantly affected several of these pathways (Figs. 7 and 8). From these pathways, a total of 37 proteins and 16 metabolites were found to be significantly altered in abundance after drug treatment compared to control (Tables 1-3; Figs. 9-18). The changes in abundance of metabolites and proteins from these pathways are likely intrinsically linked to the mechanism(s) of hepatotoxicity for these DILI-associated drugs. The drug treatments were shown to have a significant effect on the energy metabolism pathways of PHH, affecting the homeostasis of glucose metabolism, the TCA cycle, and nicotinamide metabolism. D-glucose-6-phosphate, utilised by the glucose metabolism and glucuronidation pathways, and malate and oxaloacetate, utilised in the TCA cycle, showed significant changes in abundance (Figs. 11, 12, and 17). Three notable glucose

metabolism proteins that were affected included LHDA, glucose-6-phosphate isomerase (GPI), and GLUT10. While the increased abundance of GLUT10 would likely drive increased glucose uptake and D-glucose-6-phosphate synthesis, it is unlikely to be beneficial in the presence of ritonavir. Ritonavir is a known inhibitor of glucose uptake transporters with 50% inhibition occurring at 8.2 μM for glucose transporters (52). However, since troglitazone and pioglitazone caused a similar decrease in D-glucose-6-phosphate abundance, it is unlikely that inhibition of glucose transporters is the sole cause behind the decreased abundance of D-glucose-6-phosphate.The significantly increased synthesis of UDP-glucose and UDP-glucuronate to supply the cofactor for glucuronidation is a likely explanation for the decrease in D-glucose-6-phosphate abundance (Figs. 16 and 17). In addition, ritonavir, pioglitazone, and troglitazone also caused a 24%, 18%, and 15% decrease in GPI, the enzyme that converts D-glucose-6-phosphate to D-fructose-6-phosphate. While the decrease in abundance of GPI may further impact the cells capacity to maintain glycolytic homeostasis, the direction of the interconversion between D-glucose-6-phosphate and D-fructose-6-phosphate mediated by GP1, and how the decreased abundance of GP1 would affect the abundance of D-fructose-6-phosphate, is unclear.

Ritonavir, pioglitazone, and troglitazone demonstrated uniform impact on the abundance of ADP, malate, and succinate, which indicates significant perturbations to mitochondrial respiration. The high abundance of ADP and malate could potentially have resulted from the inhibition or suppression of state 3 respiration, which relies on complex I (53). Complex I consumes malate as a substrate and is known to be inhibited by thiazolidinediones through disassembly of this complex (54, 55). It was, therefore,

expected that both troglitazone and pioglitazone would cause dysregulation of mitochondrial respiration through complex I inhibition, which could lead to the accumulation of malate and ADP. Additionally, a significant decrease in D-ribose abundance was observed after ritonavir, pioglitazone, and troglitazone treatments (Fig. 11). D-ribose is readily phosphorylated by ribokinase (RBKS), which transfers a phosphate from ATP to D-ribose and produces ADP and ribose-5-phosphate. The significant decrease observed in the abundance of D-ribose and increase in ADP may be a result of this pathway. For the thiazolidinediones, this shift may be due to increased expression of phosphoribosyl pyrophosphate synthetase, an essential enzyme of the nucleotide metabolism pathways (56). As both thiazolidinediones are known to induce the expression of a number of proteins, it was expected that an increase in nucleotide metabolism would occur to supply gene expression pathways (57-60). Furthermore, ritonavir is known to induce the expression of a number of proteins and, therefore, the decrease observed in the abundance of D-ribose in ritonavir-treated PHH could also be explained by phosphorylation of D-ribose to ribose-5-phosphate, which is subsequently converted to phosphoribosyl pyrophosphate to supply nucleotide metabolism pathways (61, 62). The decreased abundance of succinate may be attributable to thiazolidinediones not inhibiting complex II, which utilises succinate for respiration and as such, is depleted as a means of compensation for the inhibition of complex I (55, 63). Less is known, however, about the impact of ritonavir on mitochondrial processes. While ritonavir is known to cause mitochondrial damage and has off-target inhibitory effects, there is no clear evidence that ritonavir affects specific mitochondrial complexes or specific respiration pathways (64, 65). Additionally, the decrease in succinate and increase in

malate abundance also may be attributed to the drug treatments causing an increased abundance of succinate dehydrogenase B (SDHB), which may have led to a greater conversion of succinate to fumarate and then, subsequently to malate (Fig. 12).

The alterations in the nicotinamide metabolism pathways reflect an increase in synthesis of protective metabolites and their precursors. The significant increase in 1-methylnicotinamide abundance by up to 16-fold, which occurred for all treatments, is likely a response to the oxidative stress induced by the drug treatments (Fig. 14). 1-Methylnicotinamide is associated with a reduction in reactive oxygen species (ROS) and protection against oxidative stress, particularly in reducing the generation of mitochondrial ROS and glycoxidative stress (50, 51). This is reinforced by the decreased abundance of nicotinic acid, which is known to support protection against oxidative stress through conversion to subsequent metabolites of the nicotinamide pathway (66). Perturbations in the major metabolic pathways make it clear that these three drugs have significant potential to cause hepatocellular injury by impairing glucose metabolism, mitochondrial respiration, and increasing oxidative stress.

The abundance of metabolites and, potentially, proteins of the phase I and phase II metabolic pathways was expected to be significantly altered in order to metabolise and inactivate the drugs tested. An increase in phase II metabolism may have occurred due to the observed increase in abundance of glucuronide metabolites (Figs. 16 and 17) and glutathione S-transferase enzymes (Table 3). Increases in phase I enzymes were expected; all three drugs are known inducers of CYP enzyme expression and are also substrates for several CYP enzymes (67, 68). Interestingly, ritonavir and pioglitazone, well-known inducers of CYP3A4, caused only a 1.13-fold increase in CYP3A4 protein

abundance (p-value =0.088 and 0.103, respectively), with only troglitazone causing a statistically significant increase. Furthermore, pioglitazone and troglitazone, as PPARγ agonists, are known to activate pathways that protect against oxidative stress. Troglitazone is known to induce ALDH2 expression, which explains the increased abundance seen for this enzyme (59). Treatment with ritonavir had the most prominent effect on the glutathione metabolism pathway out of the three drug treatments. Ritonavir in known to induce the endoplasmic reticulum (ER) and oxidative stress, which may explain the increased abundance of GSTK1 and GPX4 (Table 3) (64, 69). GSTK1 and GPX4 are protective against ER and oxidative stress and may increase the expression of these enzymes, which may be a protective response against ritonavir treatment (70, 71). In addition, GGCT, an enzyme involved in the degradation of glutathione, was decreased in abundance after treatment with ritonavir (Table 3). This may have occurred as a response mechanism in order to conserve glutathione for antioxidative and phase II metabolism pathways. However, since there was no significant change in the abundance of glutathione, it is unclear whether GGCT decreased for this reason.

PHH have significant similarities in gene expression to liver tissue and offer an excellent *in vitro* model for metabolic studies, which may provide insight into *in vivo* behaviour (6, 72). However, the translational capacity of this study may be limited due to the relatively short exposure period compared to the duration of treatment used clinically. The onset of DILI occurs over longer time periods, in the range of several days to 6 months and, with the exception of acute poisoning, is not usually seen within the 24-h exposure time used for this study (73, 74). The 24-h time period was a limitation of the sandwich-cultured PHH system, which shows diminishing functionality over days in

culture and, therefore, weeks or months of exposure would not be possible (75). Additionally, while the concentration of ritonavir used in this study was similar to standard total serum concentrations of 15 µM used clinically, pioglitazone was used at almost a 30-fold higher concentration than what is clinically observed after a 45 mg dose (76, 77). While the specific liver concentration of pioglitazone is unknown, drug concentrations can be up to 98-fold higher in liver tissue than in serum and, therefore, the high concentration used in this *in vitro* study could occur clinically (78). Troglitazone, has a C_{max} of up to 4.5 µM after a single oral dose. The 12.5 µM concentration of troglitazone used in this study is only 3-fold greater and, therefore, would be a reasonable treatment concentration in regard to liver studies (79).

In conclusion, by using proteomics and metabolomics, the differences in the proteomes of PHH and HepaRG were compared, in addition to identifying metabolic perturbations to PHH after treatment with DILI-associated drugs. The data revealed that while there is some degree of similarity in the proteomes of PHH and HepaRG™ cells, there is still a large portion of the HepaRG™ proteome that significantly differs in abundance, and this difference is prominent among proteins associated with major metabolic pathways of the liver. While this is not an absolute indicator that HepaRG™ cells are inadequate models for liver behaviour, it does imply that they may possess some limitations as an *in vitro* liver model, especially regarding metabolic studies. Furthermore, the use of multi-omics has allowed extensive characterisation of the metabolic perturbations that could lead to DILI. Ritonavir, pioglitazone, and troglitazone caused dysregulation of energy metabolism, induced protective oxidative stress responses, and increased the abundance of several phase I and II metabolites and proteins. These data

demonstrate the value presented by omics, which offers a platform through which *in vitro* models can be assessed for their similarities to *in vivo* conditions. In addition, omics provides insight into the mechanism(s) by which drugs associated with severe liver injury may exert hepatotoxic effects. By obtaining a greater depth of knowledge, more appropriate and translational *in vitro* models can be selected that will facilitate the development of safer drugs by avoiding the characteristic metabolomics and proteomics signatures associated with DILI.

References

1. Mitra V, Metcalf J. Metabolic functions of the liver. *Anaesth Intensive Care*. 2012;13(2):54-55.
2. Lodish H, Berk A, Zipursky S, Matsudaira P, Baltimore D, Darnell J. Molecular Cell Biology. 29. New York: W.H. Freeman & Co.; 2000. p. 126-28.
3. Vilei MT, Granato A, Ferraresso C, Neri D, Carraro P, Gerunda G, et al. Comparison of pig, human and rat hepatocytes as a source of liver specific metabolic functions in culture systems--implications for use in bioartificial liver devices. *Int J Artif Organs*. 2001;24(6):392-6.
4. Wang L, Prasad B, Salphati L, Chu X, Gupta A, Hop CECA, et al. Interspecies variability in expression of hepatobiliary transporters across human, dog, monkey, and rat as determined by quantitative proteomics. *Drug Metab Dispos*. 2015;43(3):367-74.
5. Yabuuchi H, Tanaka K, Maeda M, Takemura M, Oka M, Ohashi R, et al. Cloning of the dog bile salt export pump (BSEP; ABCB11) and functional comparison with the human and rat proteins. *Biopharm Drug Dispos*. 2008;29(8):441-48.
6. Hart SN, Li Y, Nakamoto K, Subileau EA, Steen D, Zhong XB. A comparison of whole genome gene expression profiles of HepaRG cells and HepG2 cells to primary human hepatocytes and human liver tissues. *Drug Metab Dispos*. 2010;38(6):988-94.
7. Rogue A, Lambert C, Spire C, Claude N, Guillouzo A. Interindividual variability in gene expression profiles in human hepatocytes and comparison with HepaRG cells. *Drug Metab Dispos*. 2012;40(1):151-58.
8. Parent R, Marion MJ, Furio L, Trépo C, Petit MA. Origin and characterization of a human bipotent liver progenitor cell line. *Gastroenterology*. 2004;126(4):1147-56.
9. Nelson LJ, Morgan K, Treskes P, Samuel K, Henderson CJ, LeBled C, et al. Human hepatic hepaRG cells maintain an organotypic phenotype with high intrinsic CYP450 activity/metabolism and significantly outperform standard HepG2/C3A cells for pharmaceutical and therapeutic applications. *Basic Clin Pharmacol Toxicol*. 2017;120(1):30-37.
10. Sison-Young RLC, Mitsa D, Jenkins RE, Mottram D, Alexandre E, Richert L, et al. Comparative proteomic characterization of 4 human liver-derived single cell culture models reveals significant variation in the capacity for drug disposition, bioactivation, and detoxication. *Toxicol Sci*. 2015;147(2):412-24.
11. Mesnage R, Biserni M, Balu S, Frainay C, Poupin N, Jourdan F, et al. Integrated transcriptomics and metabolomics reveal signatures of lipid metabolism dysregulation in HepaRG liver cells exposed to PCB 126. *Arch Toxicol*. 2018;92(8):2533-47.

12. Rodrigues RM, Laxmikanth K, Chaudhari U, Sachinidis A, Zahedi RP, Sickmann A, et al. Omics-based responses induced by bosentan in human hepatoma HepaRG cell cultures. *Arch Toxicol*. 2018;92(6):1939-52.

13. Bell CC, Hendriks DFG, Moro SML, Ellis E, Walsh J, Renblom A, et al. Characterization of primary human hepatocyte spheroids as a model system for drug-induced liver injury, liver function and disease. *Scientific Reports*. 2016;6(1):25187.

14. Seeger B, Mentz A, Knebel C, Schmidt F, Bednarz H, Niehaus K, et al. Assessment of mixture toxicity of (tri)azoles and their hepatotoxic effects in vitro by means of omics technologies. *Arch Toxicol*. 2019;93(8):2321-33.

15. Vogel C, Marcotte EM. Insights into the regulation of protein abundance from proteomic and transcriptomic analyses. *Nat Rev Genet*. 2012;13(4):227-32.

16. Cuykx M, Beirnaert C, Rodrigues RM, Laukens K, Vanhaecke T, Covaci A. Untargeted liquid chromatography-mass spectrometry metabolomics to assess drug-induced cholestatic features in HepaRG® cells. *Toxicol Appl Pharmacol*. 2019;379:114666.

17. Cuykx M, Claes L, Rodrigues RM, Vanhaecke T, Covaci A. Metabolomics profiling of steatosis progression in HepaRG® cells using sodium valproate. *Toxicol Lett*. 2018;286:22-30.

18. Noor MA, Flint OP, Maa JF, Parker RA. Effects of atazanavir/ritonavir and lopinavir/ritonavir on glucose uptake and insulin sensitivity: demonstrable differences in vitro and clinically. *AIDS*. 2006;20(14):1813-21.

19. Okuno A, Ikeda K, Shiota M, Fujiwara T, Yoshioka S, Sugano T, et al. Acute effect of troglitazone on glucose metabolism in the absence or presence of insulin in perfused rat hindlimb. *Metabolism*. 1997;46(6):716-21.

20. Hong MKG. Investigation of troglitazone hepatotoxicity by a metabolomics approach [Doctoral]. Guildford: University of Surrey (United Kingdom). 2012.

21. Kalavalapalli S, Bril F, Koelmel JP, Abdo K, Guingab J, Andrews P, et al. Pioglitazone improves hepatic mitochondrial function in a mouse model of nonalcoholic steatohepatitis. *Am J Physiol Endocrinol Metab*. 2018;315(2):E163-E73.

22. Jonathan P. Jackson KMF, Robert L. St. ClaireIII, Chris B. Black, Kenneth R. Brouwer. Cholestatic drug induced liver injury: a function of bile salt export pump inhibition and farnesoid x receptor antagonism. *Appl In Vitro Toxicol*. 2018;4(3):265-79.

23. Alvarez-Requejo A, Carvajal A, Begaud B, Moride Y, Vega T, Arias LH. Under-reporting of adverse drug reactions. Estimate based on a spontaneous reporting scheme and a sentinel system. *Eur J Clin Pharmacol*. 1998;54(6):483-8.

24. Montastruc P, Damase-Michel C, Lapeyre-Mestre M, Puget C, Damase L, Hurstel JF, et al. A prospective intensive study of adverse drug reactions in urban general practice. *Clin Drug Investig*. 1995;10(2):117-22.

25. Moride Y, Haramburu F, Requejo AA, Begaud B. Under-reporting of adverse drug reactions in general practice. *Brit J Clin Pharmacol*. 1997;43(2):177-81.

26. Heeley E, Riley J, Layton D, Wilton LV, Shakir SA. Prescription-event monitoring and reporting of adverse drug reactions. *Lancet*. 2001;358(9296):1872-3.

27. Lewis MA, Kühl-Habich D, Rosen J. Drug use and adverse event monitoring in German children. *Int J Clin Pharmacol Ther*. 2001;39:507-12.

28. Klopotowska JE, Wierenga PC, Smorenburg SM, Stuijt CCM, Arisz L, Kuks PFM, et al. Recognition of adverse drug events in older hospitalized medical patients. *Eur J Clin Pharmacol*. 2013;69(1):75-85.

29. Nebeker JR, Hoffman JM, Weir CR, Bennett CL, Hurdle JF. High rates of adverse drug events in a highly computerized hospital. *Ann Intern Med*. 2005;165(10):1111-16.

30. Creek DJ, Chua HH, Cobbold SA, Nijagal B, MacRae JI, Dickerman BK, et al. Metabolomics-based screening of the malaria box reveals both novel and established mechanisms of action. *Antimicrob Agents Chemother*. 2016;60(11):6650-63.

31. Creek DJ, Jankevics A, Burgess KEV, Breitling R, Barrett MP. IDEOM: an excel interface for analysis of LC–MS-based metabolomics data. *Bioinformatics*. 2012;28(7):1048-49.

32. Chambers MC, Maclean B, Burke R, Amodei D, Ruderman DL, Neumann S, et al. A cross-platform toolkit for mass spectrometry and proteomics. *Nat Biotechnol*. 2012;30(10):918-20.

33. Smith CA, Want EJ, O'Maille G, Abagyan R, Siuzdak G. XCMS: processing mass spectrometry data for metabolite profiling using nonlinear peak alignment, matching, and identification. *Anal Chem*. 2006;78(3):779-87.

34. Scheltema RA, Jankevics A, Jansen RC, Swertz MA, Breitling R. PeakML/mzMatch: a file format, java library, R library, and tool-chain for mass spectrometry data analysis. *Anal Chem*. 2011;83(7):2786-93.

35. Beaudoin JJ, Bezençon J, Sjöstedt N, Fallon JK, Brouwer KLR. Role of organic solute transporter alpha/beta in hepatotoxic bile acid transport and drug interactions. *Toxicol Sci*. 2020;176(1):34-45.

36. Batth TS, Francavilla C, Olsen JV. Off-line high-ph reversed-phase fractionation for in-depth phosphoproteomics. *J Proteome Res*. 2014;13(12):6176-86.

37. Birrell GW, Challis MP, De Paoli A, Anderson D, Devine SM, Heffernan GD, et al. Multi-omic Characterization of the Mode of Action of a Potent New Antimalarial Compound, JPC-3210, Against Plasmodium falciparum. *Mol Cell Proteomics*. 2020;19(2):308-25.

38. Cox J, Mann M. MaxQuant enables high peptide identification rates, individualized p.p.b.-range mass accuracies and proteome-wide protein quantification. *Nat Biotechnol*. 2008;26(12):1367-72.

39. Pang Z, Chong J, Zhou G, de Lima Morais DA, Chang L, Barrette M, et al. MetaboAnalyst 5.0: narrowing the gap between raw spectra and functional insights. *Nucleic Acids Res*. 2021.

40. Raudvere U, Kolberg L, Kuzmin I, Arak T, Adler P, Peterson H, et al. g:Profiler: a web server for functional enrichment analysis and conversions of gene lists (2019 update). *Nucleic Acids Res*. 2019;47(W1):W191-W98.

41. Merico D, Isserlin R, Stueker O, Emili A, Bader GD. Enrichment Map: a network-based method for gene-set enrichment visualization and interpretation. *PLoS One*. 2010;5(11):e13984.

42. Shannon P, Markiel A, Ozier O, Baliga NS, Wang JT, Ramage D, et al. Cytoscape: a software environment for integrated models of biomolecular interaction networks. *Genome Res*. 2003;13(11):2498-504.

43. Consortium TU. UniProt: the universal protein knowledgebase in 2021. *Nucleic Acids Res*. 2020;49(D1):D480-D89.

44. Khatri R, Fallon JK, Rementer RJB, Kulick NT, Lee CR, Smith PC. Targeted quantitative proteomic analysis of drug metabolizing enzymes and transporters by nano LC-MS/MS in the sandwich cultured human hepatocyte model. *J Pharmacol Toxicol Methods*. 2019;98:106590.

45. Agúndez JA, Olivera M, Martínez C, Ladero JM, Benítez J. Identification and prevalence study of 17 allelic variants of the human NAT2 gene in a white population. *Pharmacogenet*. 1996;6(5):423-8.

46. López Rodríguez M, Fernandes Silva L, Vangipurapu J, Modi S, Kuusisto J, Kaikkonen MU, et al. Functional variant in the GCKR gene affects lactate levels differentially in the fasting state and during hyperglycemia. *Sci Rep*. 2018;8(1):15989.

47. Sugiyama Y, Taketomi S, Shimura Y, Ikeda H, Fujita T. Effects of pioglitazone on glucose and lipid metabolism in Wistar fatty rats. *Drug Res*. 1990;40(3):263-7.

48. Zhang LQ, Nsumu M, Huang P, Heruth DP, Riordan SM, Shortt K, et al. Novel protective role of nicotinamide phosphoribosyltransferase in acetaminophen-induced acute liver injury in mice. *Am J Pathol*. 2018;188(7):1640-52.

49. Wang S, Wan T, Ye M, Qiu Y, Pei L, Jiang R, et al. Nicotinamide riboside attenuates alcohol induced liver injuries via activation of SirT1/PGC-1α/mitochondrial biosynthesis pathway. *Redox Biol*. 2018;17:89-98.

50. Tanaka Y, Kume S, Araki H, Nakazawa J, Chin-Kanasaki M, Araki S, et al. 1-Methylnicotinamide ameliorates lipotoxicity-induced oxidative stress and cell death in kidney proximal tubular cells. *Free Radic Biol Med*. 2015;89:831-41.

51. Országhová Z, Uličná O, Liptáková A, Zitňanová I, Muchová J, Watala C, et al. Effects of N1-methylnicotinamide on oxidative and glycooxidative stress markers in rats with streptozotocin-induced diabetes mellitus. *Redox Rep*. 2012;17(1):1-7.

52. Hresko RC, Hruz PW. HIV protease inhibitors act as competitive inhibitors of the cytoplasmic glucose binding site of GLUTs with differing affinities for GLUT1 and GLUT4. *PLoS One*. 2011;6(9):e25237.

53. Korzeniewski B. 'Idealized' state 4 and state 3 in mitochondria vs. rest and work in skeletal muscle. *PLoS One*. 2015;10(2):e0117145-e45.

54. García-Ruiz I, Solís-Muñoz P, Fernández-Moreira D, Muñoz-Yagüe T, Solís-Herruzo JA. Pioglitazone leads to an inactivation and disassembly of complex I of the mitochondrial respiratory chain. *BMC Biol*. 2013;11(1):88.

55. Brunmair B, Staniek K, Gras F, Scharf N, Althaym A, Clara R, et al. Thiazolidinediones, like metformin, inhibit respiratory complex I: a common mechanism contributing to their antidiabetic actions? *Diabetes*. 2004;53(4):1052-9.

56. Liu Y, Yan X, Mao G, Fang L, Zhao B, Liu Y, et al. Metabonomic profiling revealed an alteration in purine nucleotide metabolism associated with cardiac hypertrophy in rats treated with thiazolidinediones. *J Proteome Res*. 2013;12(12):5634-41.

57. Yin QQ, Pei JJ, Xu S, Luo DZ, Dong SQ, Sun Ma, et al. Pioglitazone improves cognitive function via increasing insulin sensitivity and strengthening antioxidant defense system in fructose-drinking insulin resistance rats. *PLoS One*. 2013;8(3):e59313.

58. Chung SS, Kim M, Youn BS, Lee NS, Park JW, Lee IK, et al. Glutathione peroxidase 3 mediates the antioxidant effect of peroxisome proliferator-activated receptor gamma in human skeletal muscle cells. *Mol Cell Biol*. 2009;29(1):20-30.

59. Crabb DW, Pinaire J, Chou WY, Sissom S, Peters JM, Harris RA, et al. Peroxisome proliferator-activated receptors (PPAR) and the mitochondrial aldehyde dehydrogenase (ALDH2) promoter in vitro and in vivo. *Alcohol Clin Exp Res*. 2001;25(7):945-52.

60. Bogacka I, Xie H, Bray GA, Smith SR. Pioglitazone induces mitochondrial biogenesis in human subcutaneous adipose tissue in vivo. *Diabetes*. 2005;54(5):1392-9.

61. Lum PY, He YD, Slatter JG, Waring JF, Zelinsky N, Cavet G, et al. Gene expression profiling of rat liver reveals a mechanistic basis for ritonavir-induced hyperlipidemia. *Genomics*. 2007;90(4):464-73.

62. Foisy MM, Yakiwchuk EM, Hughes CA. Induction effects of ritonavir: implications for drug interactions. *Ann Pharmacother*. 2008;42(7):1048-59.

63. Sanz MN, Sánchez-Martín C, Detaille D, Vial G, Rigoulet M, El-Mir MY, et al. Acute mitochondrial actions of glitazones on the liver: a crucial parameter for their antidiabetic properties. *Cell Physiol Biochem*. 2011;28(5):899-910.

64. Ganta KK, Chaubey B. Endoplasmic reticulum stress leads to mitochondria-mediated apoptosis in cells treated with anti-HIV protease inhibitor ritonavir. *Cell Biol Toxicol*. 2019;35(3):189-204.

65. Tricarico P, Franca R, Pacor S, Ceglia V, Crovella S, Celsi F. HIV protease inhibitors apoptotic effect in SH-SY5Y neuronal cell line. *Cell Physiol Biochem*. 2016;39:1463-70.

66. Dou X, Shen C, Wang Z, Li S, Zhang X, Song Z. Protection of nicotinic acid against oxidative stress-induced cell death in hepatocytes contributes to its beneficial effect on alcohol-induced liver injury in mice. *J Nutr Biochem*. 2013;24(8):1520-28.

67. Sahi J, Black CB, Hamilton GA, Zheng X, Jolley S, Rose KA, et al. Comparative effects of thiazolidinediones on in vitro P450 enzyme induction and inhibition. *Drug Metab Dispos*. 2003;31(4):439-46.

68. Foisy M, Yakiwchuk E, Hughes C. Induction effects of ritonavir: implications for drug interactions. *Ann Pharmacother*. 2008;42:1048-59.

69. Gratton R, Tricarico PM, Guimaraes RL, Celsi F, Crovella S. Lopinavir/ritonavir treatment induces oxidative stress and caspase-independent apoptosis in human glioblastoma U-87 MG cell line. *Curr HIV Res*. 2018;16(2):106-12.

70. Liu M, Chen H, Wei L, Hu D, Dong K, Jia W, et al. Endoplasmic reticulum (ER) localization is critical for DsbA-L protein to suppress ER stress and adiponectin down-regulation in adipocytes. *J Biol Chem*. 2015;290(16):10143-48.

71. Ran Q, Liang H, Gu M, Qi W, Walter CA, Roberts LJ, II, et al. Transgenic mice overexpressing glutathione peroxidase 4 are protected against oxidative stress-induced apoptosis. *J Biol Chem*. 2004;279(53):55137-46.

72. Gupta R, Schrooders Y, Hauser D, van Herwijnen M, Albrecht W, ter Braak B, et al. Comparing in vitro human liver models to in vivo human liver using RNA-Seq. *Arch Toxicol*. 2021;95(2):573-89.

73. Cosmin Sebastian Voican, M.D., Ph.D. ,, Emmanuelle Corruble, M.D., Ph.D. ,, Sylvie Naveau, M.D., Ph.D. , and, Gabriel Perlemuter, M.D., Ph.D. Antidepressant-induced liver injury: a review for clinicians. *Am J Psychiatry*. 2014;171(4):404-15.

74. Kullak-Ublick GA, Andrade RJ, Merz M, End P, Benesic A, Gerbes AL, et al. Drug-induced liver injury: recent advances in diagnosis and risk assessment. *Gut*. 2017;66(6):1154-64.

75. Bell CC, Dankers ACA, Lauschke VM, Sison-Young R, Jenkins R, Rowe C, et al. Comparison of hepatic 2D sandwich cultures and 3D spheroids for long-term toxicity applications: a multicenter study. *Toxicol Sci*. 2018;162(2):655-66.

76. Shelton MJ, Hewitt RG, Adams J, Della-Coletta A, Cox S, Morse GD. Pharmacokinetics of ritonavir and delavirdine in human immunodeficiency virus-infected patients. *Antimicrob Agents Chemother*. 2003;47(5):1694-9.

77. Christensen ML, Meibohm B, Capparelli EV, Velasquez-Mieyer P, Burghen GA, Tamborlane WV. Single- and multiple-dose pharmacokinetics of pioglitazone in adolescents with type 2 diabetes. *J Clin Pharmacol*. 2005;45(10):1137-44.

78. Venuto CS, Markatou M, Woolwine-Cunningham Y, Furlage R, Ocque AJ, DiFrancesco R, et al. Paritaprevir and ritonavir liver concentrations in rats as

assessed by different liver sampling techniques. *Antimicrob Agents Chemother*. 2017;61(5):e02283-16.

79. Loi CM, Young M, Randinitis E, Vassos A, Koup JR. Clinical pharmacokinetics of troglitazone. *Clin Pharmacokinet*. 1999;37(2):91-104.

Chapter 3

Multi-omics Analysis of *In Vitro* Primary Human Hepatocytes after Treatment with Cholestatic Drugs

Abstract

Cholestasis is one of the most common forms of drug-induced liver injury (DILI) and can occur as the sole DILI phenotype or as a comorbidity with other DILI phenotypes. Cholestasis is characterised by impaired bile flow from the liver and may be induced through a number of different mechanisms. The C-DILI™ and B-CLEAR® assays were used to evaluate a panel of DILI-associated drugs to determine which drugs possessed cholestatic hepatotoxic potential and could impair bile acid transport, respectively. Primary human hepatocytes (PHH) and HepaRG™ cells were treated with the drugs that showed cholestatic hepatotoxic potential and impaired bile acid transport. These cells were then analysed using targeted metabolomics and proteomics to identify changes to the abundance of bile acid-associated metabolites and proteins. Metabolomics identified that the treatment with cholestatic drugs induced a cellular depletion of several bile acids, including taurocholate and glycocholate, in both PHH and HepaRG™ cells. In addition, increased abundance of several phase I metabolism enzymes was observed, with a prominent increase in the cellular abundance of CYP3A4, CYP3A5 and cytochrome P450 oxidoreductase. It is likely that the decreased cellular abundance of bile acids is due to increased phase I metabolism as part of a protective cellular mechanism against cholestatic liver injury.

Introduction

Population-based studies across a variety of demographics have identified annual rates of drug-induced liver injury (DILI) occurring in the range of 3 to 24 cases per 100,000 patients (1-5). Of the various DILI phenotypes, one of the most common is cholestatic

liver injury, which is characterised by impaired bile flow from the liver. Cholestasis accounts for 42% of DILI cases, occurring as either a comorbidity with other injury phenotypes, or as the sole liver injury phenotype (6). Cholestatic liver injury can be further categorised into several sub-phenotypes including acute cholestasis, which can present with or without hepatitis, or chronic cholestasis in the forms of vanishing bile duct syndrome, primary sclerosing cholangitis, or mild non-specific bile duct injury (7, 8).

Cholestatic liver injury can be induced by a variety of different causative agents such as antibiotics, non-steroidal anti-inflammatory drugs (NSAIDs), immune suppressants, diabetes medications, and herbal dietary supplements (1, 4, 8, 9). The three broad mechanisms by which a drug may induce cholestasis are impaired hepatocellular transport of bile acids, disrupted hepatocellular structure, and altered bile canalicular dynamics (10). Impaired bile acid transport has been implicated as a key mechanism through which a variety of well-known cholestatic drugs induce cholestasis. Troglitazone, a potent inhibitor of several bile acid transporters including the bile salt export pump (BSEP), Na^+-taurocholate co-transporting polypeptide (NTCP), and multidrug resistance-associated proteins 2, 3, and 4 (MRP2, MRP3, MRP4, respectively), is a prominent example of a cholestatic DILI drug. Troglitazone induced severe cholestasis with a liver failure rate of up to 8.3 cases per 100,000 patients (11, 12). Additionally, ethinyl estradiol, a synthetic estrogen, not only has the capacity to impair bile acid transport, but also impacts hepatocellular structure by decreasing sinusoidal membrane fluidity (11, 13). Furthermore, estradiol-17β-D-glucuronide, a cholestatic glucuronide derivative of estradiol, has been shown to disrupt the tight junctions between hepatocytes, further compromising hepatocellular structure (14). Collectively, these

examples illustrate the toxicological impact that drug treatments can have on healthy liver structure and biliary transport.

It is vital to understand the impact that cholestatic drugs have on intracellular metabolite and protein abundance, particularly bile acids and their associated enzymes and transporters, in order to elucidate the toxicological mechanism(s) of cholestatic DILI. While there has been a significant body of work investigating cholestasis-associated changes in metabolites, the majority of this research has used animal models or focused on extracellular metabolites, such as those in serum or urine, rather than assessing intracellular metabolites (15-17). While animal models allow for controlled induction of cholestasis and collection of a variety of biological samples, species variations can be a significant limitation in understanding cholestasis in humans. The impact of such variation is best illustrated by the differences in bile acid composition in Sprague-Dawley (SD) rats compared to humans. SD rats have a three times greater total plasma bile acid concentration than humans, with cholate and muricholic acid comprising 30% and 22% of the rat plasma bile acid pool compared to 11% and 0.7% in humans, respectively (18). The transport capacity of BSEP is also subject to species variation with rat BSEP exhibiting a two-fold greater V_{max} in transporting taurocholate compared to humans (19). Furthermore, while serum and urinary metabolites can be used for the development of diagnostic biomarkers of liver injury, analysis of the cellular metabolite alterations in hepatocytes can provide a more comprehensive insight into the biological perturbations that are intrinsically linked to cholestatic DILI, and the cellular mechanism(s) that lead to cholestasis (17, 20).

Proteomics and metabolomics are invaluable analytical techniques that can characterise metabolic changes and mechanisms that can lead to cholestatic DILI. Proteomics analysis has been used to describe the impact of treatment with DILI-associated drugs, such as nevirapine and bosentan, on the proteome of a cell (21-23). LC-MS proteomics of nevirapine-treated HepG2 cells identified impaired mitochondrial function, with altered abundance of 13 mitochondrial proteins after drug treatment. The abundance of vital mitochondrial enzymes such as glyceraldehyde-3-phosphate dehydrogenase (GAPDH) and phosphoenolpyruvate carboxykinase (PEPCK) were significantly decreased after nevirapine treatment (21). Using metabolomic and proteomic techniques, bosentan was shown to impair mitochondrial function, alter the phosphorylation state, increase ceramide synthesis, cause endoplasmic reticulum stress, and alter the homeostasis of glucose, lipids, and cholesterol (22, 23). There is an imperative need to elucidate the toxicological mechanisms that result in cholestatic DILI to allow for the identification of biological changes that could be utilised clinically or during drug development as a biomarker for early detection and prevention of cholestatic DILI.

This study utilises a multi-faceted approach of multi-omics and plate-based assays to determine the hepatotoxic characteristics and mechanisms of several DILI-associated drugs using *in vitro* liver models. The C-DILI™ and B-CLEAR® plate-based assays allowed for determination of which DILI-associated drugs had the potential to cause cholestatic DILI and affect bile acid transport. Additionally, targeted bile acid metabolomics revealed reduced cellular bile acid abundance, and proteomics identified several enzymes which had altered cellular abundance, including increases to the

abundance of CYP3A4 and cytochrome P450 oxidoreductase (POR), which may be responsible for the decreased cellular abundance of bile acid.

Material and methods

Materials

Undifferentiated HepaRG™ cells were acquired from Biopredic International under a material transfer agreement and HepaRG™ Maintenance/Metabolism Media was purchased from Biopredic international. Cryoplateable human hepatocytes were acquired from BioIVT along with all QualGro™ Media and additives. Hepatocytes from the BXW, WID, WWQ, and XVN donors were Transporter Certified™ and hepatocytes from the YNM donor were cryoplateable. PHH were acquired from both female and male donors with an age range of 22 to 73. The HuH-7 human hepatoma cell line (JCRB0403) were acquired from the National Institute of Environmental Health Sciences, which originally sourced the cells from Sekisui Xenotech. Acetaminophen, amiodarone, diclofenac, ethinyl estradiol, pioglitazone, and ritonavir were acquired from Merck with all except acetaminophen being acquired as pharmaceutical secondary standards. Fialuridine, troglitazone, stavudine, and zidovudine were acquired from Cayman Chemicals. Dimethyl sulfoxide (DMSO), HPLC grade chloroform, LC-MS grade methanol (MeOH), sodium dodecyl sulphate (SDS), fetal bovine serum (FBS), and trifluoroacetic acid were also purchased from Merck. LC-MS grade acetonitrile (ACN), 0.25% trypsin-EDTA phenol red, Percoll, Dulbecco's phosphate buffer saline (PBS), Dulbecco's modified Eagle's medium (DMEM), streptomycin, Hanks' Balanced Salt Solution (HBSS), and chenodeoxycholic acid (CDCA) were purchased from ThermoFisher Scientific. Ammonium carbonate was purchased from Rowe Scientific. Matrigel® was purchased from Bio-Strategy.

Cell Culture

Undifferentiated HepaRG™ cells were cultured in a T75 culture flask and differentiated per the supplier's protocol. On day 0, differentiated HepaRG™ cells were passaged using 0.25% w/v trypsin-EDTA. The cells were plated on either 24- or 96-well BioCoat™ Collagen I-coated plates (Corning®) with $4x10^5$ and $0.8x10^5$ cells seeded per well, respectively. Media was changed every 2-3 days with the cells overlaid on day 3 using HepaRG™ Maintenance/Metabolism Media supplemented with 0.25 mg/mL of Matrigel® and used for experimentation on day 7.

Transporter Certified™ cryoplateable human hepatocytes were thawed and transferred to a 50 mL Falcon Conical Centrifuge tube containing 45 mL of QualGro™ Thawing Media that included 30% v/v Percoll®. This was centrifuged at 100 *g* for 8 min. The QualGro™ Thawing Media was aspirated and the cell pellet was resuspended in QualGro™ Seeding Media at 0.8 $x10^6$ cells/ml. The human hepatocytes were plated onto either 24- or 96-well collagen I-coated plates with $4x10^5$ and 0.56 $x10^5$ cells seeded per well, respectively. Media was changed daily with hepatocytes overlaid on day 1 using QualGro™ Overlay Media supplemented with 0.25 mg/mL of Matrigel®, and sandwich-cultured hepatocytes were used for experimentation on day 4.

HuH-7 cells were cultured in a T75 culture flask in a culture media of Dulbecco's modified Eagle's medium (DMEM, ThermoFisher Scientific) containing 10% fetal bovine serum, 100 U/ml penicillin, and 100 µg/ml streptomycin (ThermoFisher Scientific). The T75 culture flask of HuH-7 cells was passaged in the same manner as HepaRG™ cells. The long-term culturing of HuH-7 cells for use in the B-CLEAR® transport assay was described previously by Kang *et al*., 2019 (24).

C-DILI™ hepatotoxicity assay

Day 7 differentiated HepaRG™ cells and day 4 primary human hepatocytes (PHH) cultured on 96-well plates were used to perform the C-DILI™ hepatotoxicity assay. The PHH were treated using the C-DILI™ Culture Media and C-DILI™ Sensitisation Media as described in the supplier's protocol. HepaRG™ cells were cultured in HepaRG™ Maintenance/Metabolism Media with the cells in the sensitised condition supplemented with the proprietary C-DILI™ sensitization additives to mimic the conditions of the PHH media. The HepaRG™ cells and PHH were treated with drugs at five different concentrations prepared by a 1:1 serial dilution four times for each drug (highest and lowest concentrations are listed in Table 1). The highest concentrations were based on the maximal solubility of the drugs in a DMSO stock solution. Control groups in both media conditions were treated with 0.1% v/v DMSO with all drug treatments containing 0.1% v/v DMSO.

Table 1: Maximum and minimum drug treatment concentrations for C-DILI™ assay for primary human hepatocytes (PHH) and HepaRG™ cells

	Drug Concentration (µM)			
	PHH		***HepaRG™***	
	Initial	*Lowest*	*Initial*	*Lowest*
Acetaminophen	5000	312.5	5000	312.5
Amiodarone	125	7.8125	125	7.8125
Diclofenac	500	31.25	500	31.25
Ethinyl Estradiol	100	6.25	200	12.5
Fialuridine	250	15.625	250	15.625
Pioglitazone	500	31.25	500	31.25
Ritonavir	250	15.625	250	15.625
Stavudine	500	31.25	500	31.25
Troglitazone	100	6.25	200	12.5
Zidovudine	500	31.25	500	31.25

After a 24 h incubation, cholestatic hepatotoxicity of the drug-treated cells was determined by comparison of ATP and lactate dehydrogenase (LDH) levels to the control. ATP abundance was quantified using a CellTiter-Glo® (Promega - G7572) luminescent cell viability assay and the hepatotoxicity that occurred was quantified as % of control determined by:

$$\%\ of\ Control = \frac{Drug\ treament\ ATP\ signal - Background}{DMSO\ control\ ATP\ signal - Background} \times 100\%$$

Similarly, LDH abundance was determined by CytoTox-ONE™ (Promega - G7891) homogeneous membrane integrity assay and the hepatotoxicity that occurred was, again, quantified as % of control determined by:

$$\%\ of\ Control = \frac{Drug\ treament\ LDH\ signal - Background}{DMSO\ control\ LDH\ signal - Background} \times 100\%$$

A comparison of the drug-treated culture media and the sensitisation media samples was used to identify which drugs had the capacity to cause cholestatic DILI. Drugs that showed a statistically greater hepatotoxicity for the sensitisation media condition were determined to cause cholestatic hepatotoxicity. Statistically significant differences between culture and sensitization media conditions were determined for a *p*-value ≤ 0.05 using a Student's *t*-test calculated using GraphPad Prism 7. The drug treatment concentrations used in subsequent studies were the highest concentrations that were determined to be sub-toxic based on an *in vitro* C-DILI™ hepatotoxicity study (Appendix 3).

B-CLEAR® transport assay

The B-CLEAR® transport assay (BioIVT) was performed as described previously using [^{3}H]-taurocholate (24). HuH-7 cells were treated for 24 h with several DILI-associated drugs [acetaminophen (1 mM), amiodarone (12.5 µM and 25 µM), diclofenac (100 µM), ethinyl estradiol (50 µM), fialuridine (100 µM), pioglitazone (100 µM), ritonavir (25 µM), and troglitazone (25 µM and 75 µM)] in 0.1% v/v DMSO with a 0.1% DMSO control. A total of six wells were treated with each drug. Of the six drug treatment replicate wells, three wells were washed with Ca^{2+}-containing Hanks' Balanced Salt Solution (HBSS) (Ca^{2+} +), and the remaining three wells were washed with Ca^{2+}-free HBSS (Ca^{2+}

-). The cells washed with Ca^{2+}-containing HBSS maintained canalicular tight junctions and the contents of the canaliculi were retained. In contrast, the cells washed with Ca^{2+}-free HBSS did not retain the canalicular contents due to the absence of Ca^{2+}, which disrupted the tight junctions. The biliary excretion index (BEI), a measure of biliary transport, was calculated using the following equation:

$$BEI\ (\%) = \frac{Substrate\ Accumulation\ (Ca^{2+}+)\ - Substrate\ Accumulation(Ca^{2+}-)}{Substrate\ Accumulation\ (Ca^{2+}+)}$$

Statistical significance was calculated using a two-way analysis of variance (ANOVA) with *post hoc* Dunnett's test with significance at a *p*-value ≤ 0.05.

Drug treatment with drugs associated with DILI and metabolomics extraction

PHH cultured on a 24-well plate were treated with drugs in 0.1% v/v DMSO at concentrations described in Table 2. Following the 24 h incubation, the media was aspirated and cells were washed three times with 1 mL PBS. The cells were collected from the well by the addition of 350 µL MeOH:ddH_2O (6:1) and scraping with a pipette tip. The cells were then transferred to a Safe-Lock microcentrifuge tube (Eppendorf®) containing 100 µL of chloroform to produce a monophasic 2:6:1 chloroform:MeOH:water (C:M:W) extraction mixture. To collect any residual metabolites or cell debris, the wells of the plate were washed with 1 mL of BuOH:MeOH (3:1), transferred to another microcentrifuge tube and dried to completion using a CentriVap Benchtop Centrifugal Vacuum Concentrator (Labconco). The dried BuOH:MeOH extraction was reconstituted using the C:M:W extraction mixture to consolidate the extracted lipids. This pooled extraction mix was centrifuged at 21,600 *g* for 10 min to pellet insoluble components and

transferred to LC-MS vials for analysis. Controls were treated with 0.1% v/v DMSO. Extraction of media samples was performed as above; however, the 450 µL C:M:W extraction solution used 50 µL of the culture media from drug-treated cells instead of water. A statistically significant difference between control and drug-treated cells was determined for a *p*-value ≤ 0.05 using a one-way ANOVA with *post hoc* Dunnett's test.

Table 2: Drug treatment concentrations of primary human hepatocytes (PHH) and HepaRG™ cells for metabolomics and proteomics studies of DILI

	Drug Concentration (µM)		
	PHH		***HepaRG™***
Type of study	*Metabolomics*	*Proteomics*	*Bile acid metabolite time course*
Amiodarone	12.5	-	-
Diclofenac	50	50	250
Ethinyl Estradiol	25	25	100
*Free fatty acid**	1000	-	-
Fialuridine	100	-	-
Pioglitazone	100	100	250
Ritonavir	25	25	50
Troglitazone	12.5	12.5	100

*Free fatty acid mixture contained oleic acid and palmitic acid at a ratio of 2:1

24-hour time course drug treatment

HepaRG™ cells cultured in a 24-well plate format were treated with HepaRG™ Maintenance/Metabolism Media containing drugs at concentrations described in Table 2. At t=0 h, day 7 HepaRG™ cells had their media aspirated and replaced with drug-treated

media. The HepaRG cells were treated with diclofenac, ethinyl estradiol, pioglitazone, ritonavir, and troglitazone. Controls were treated with 0.1% v/v DMSO with all drug treatments containing 0.1% v/v DMSO. A higher concentration was selected in comparison to PHH as the HepaRG™ cells appeared to be less sensitive to drug treatment based on the C-DILI data. Cell and media extracts were collected at time t=1 h, 4 h, 8 h, 16 h, and 24 h with untreated t=1 h extracts used as a baseline for intracellular and extracellular metabolite abundance. Metabolite extraction from both the cell and media was performed using the C:M:W methodology described previously. A statistically significant difference between control and drug-treated cells was determined for a *p*-value ≤ 0.05 using a two-way ANOVA with *post hoc* Dunnett's test for each metabolite.

Liquid chromatography-mass spectrometry metabolomic analysis

Drug-treated PHH and HepaRG™ cells were analysed using hydrophilic interaction liquid chromatography (HILIC) with high resolution mass spectrometry as described previously to detect glycine, taurine, taurochenodeoxycholate (TCDCA), and glycochenodeoxycholate (GCDCA) (25). The samples were injected using an Ultimate U3000 liquid chromatography (LC) system (Dionex) fitted with a ZIC-pHILIC column (5 µm, 4.6 by 150 mm; Merck®) at ambient temperature with an injection volume of 10 µL. Chromatography was performed using 20 mM aqueous ammonium carbonate (A) and acetonitrile (ACN) (B) as the mobile phases. A 30 min gradient at a flow rate of 0.300 mL/min was run starting at 80% B decreasing to 5% B over 21 min followed by a 3 min wash at 5% B and an 8 min re-equilibration phase at 80% B. The samples were detected by a Q-Exactive Orbitrap mass spectrometer (ThermoFisher Scientific) using a heated electrospray ionisation (HESI) source at 3.5 kV operating in both positive and negative

ion mode with rapid switching. A mass range of 85 to 1,275 *m/z* was used over the full 32 min run with an additional mass range of 65 to 975 *m/z* from the 13.5 min to the 17 min time point for detection of glycine with a mass resolution of 35,000 used for both ranges.

A second LC-MS method using reverse phase chromatography was used to detect glycocholate (GCA), taurocholate, cholate (CA), and chenodeoxycholate (CDCA). Using the LC-MS system mentioned above, 10 µL of sample was injected in an Express C8 column (2.7 µm, 2.1 x 100 mm; Avantis). Chromatography was performed using 20 mM ammonium formate (A) and ACN (B) as the mobile phases. An 8-min gradient at a flow rate of 0.250 mL/min was run starting at 30% B increasing to 98% B over 3.5 min and remaining at 98% B for 1 min followed by a 0.5-min transition to 30% for a 3-min wash and re-equilibration. The samples were detected by a Q-Exactive Orbitrap mass spectrometer (ThermoFisher Scientific) using a heated electrospray ionisation (HESI) source at 3.5 kV operating in negative ion mode. A mass range of 100 to 1,250 *m/z* was used over the full 8-min run with a mass resolution of 70,000 used.

LC-MS data were processed in a targeted manner using Quan Browser and XCalibur™ 4.0 software. Peaks for all metabolites except glycine were detected using the negative ion mode output from their respective runs with peak identification performed using exact mass and retention times as follows: glycine (*m/z*=76.0399, Retention time (RT)=15.50 min), taurine (*m/z*=124.0068, RT=15 min), GCDCA (*m/z*=448.3063, RT=4.20 min), TCDCA (*m/z*=498.2889, RT=3.80), GCA (*m/z*=464.3012, RT=4.40), taurocholate (*m/z*=514.2839, RT=4.21), CDCA (*m/z*=391.2848, RT=4.00), and CA (*m/z*=407.2798, RT=2.90) with a 60s RT window.

Proteomic data-independent analysis

PHH cultured on a 24-well plate were treated at drug concentrations described in Table 2. Protein was collected from hepatocytes by addition of 200 µL of 5% w/v SDS and denatured by heating to 95° C for 10 min. Hepatocyte lysates were processed and digested using S-Trap™ mini columns (ProtiFi) following the manufacturer's protocol. The final samples were solubilised in 2% aqueous acetonitrile (ACN) with 0.1% trifluoroacetic acid.

A pooled lysate of drug-treated samples (Sample A) and a pooled lysate of untreated PHH and 100 µM CDCA-treated PHH (Sample B) were used to generate a treatment-specific (Library A) and OSTα/β up-regulated (Library B) protein spectral library (26). Both sample A and B were digested and processed as described above; however, once the samples had been eluted from the S-Trap™ column, the samples were fractionated. High-pH reversed phase fractionation was performed as described by Batth T.S, *et al* 2014 to generate 12 fractions for sample A and sample B (27).

LC-MS/MS analysis of the pooled library and drug-treated samples were performed as described by Birrell G.W *et al* 2020 (28). The pooled library samples were analysed with a data-dependent acquisition method, and the drug-treated samples were analysed with a DIA acquisition method. Analysis was performed using an Ultimate U3000 Nano LC system (Dionex) coupled to a Q-Exactive Orbitrap mass spectrometer. Samples were loaded on to a reversed-phase Acclaim™ PepMap™ trap column (100 µM x 2 cm; Dionex) at a flow rate of 15 µL/min. Analytes were eluted from the trap column into a reversed-phase LC Packings capillary column (75 µM x 50 cm; Dionex). MS/MS was operated in data-dependent mode at a resolution of 70,000 over the *m/z* range of

375-1575 in positive ion mode. Fragmentation was performed for the top 20 most abundant precursors with a normalised collision energy of 27.0 with a 15 ms activation time and dynamic enabled exclusion. DIA MS/MS analysis was performed in data-independent mode using previously mentioned settings for the mass spectrometer with a 25-fixed window setup of 24 *m/z* precursor isolation over a *m/z* range of 375-975.

Sample A and sample B were analysed using MaxQuant version 16.0.5 as previously described (29). The samples were searched against *Homo sapiens* (UP000005640, release version June 29, 2020) Uniprot FASTA database to generate two proteome libraries, library A and B, respectively. The output from MaxQuant for library A and B were combined in Spectronaut™ 13.0 to generate a single library (PHH spectral library) to be used for DIA analysis. The combined library contained 82,361, which allowed for 6,944 proteins to be identified.

The drug-treated samples using the PHH spectral library were processed with Spectronaut™ 13.0. Processing of the drug-treated spectra was performed using default Spectronaut™ settings (Manual for Spectronaut™ 13.0, available on Biognosis website). Quantification in Spectronaut used default settings except for minor group quantity set to sum precursor quantity. The data filtering setting was q-value sparse and global normalisation was performed using median values. The output was then filtered to a targeted list of 80 proteins related to transport, phase I and II metabolism, and bile acid metabolism. Of the 80 proteins in the targeted list, 56 were detected by DIA analysis (Appendix 4). A statistically significant difference in protein abundance between control and drug-treated cells was determined for a p-value ≤ 0.05 using a one-way ANOVA with *post hoc* Dunnett's test.

Statistical analysis

All Student's *t*-tests, as well as one-way and two-way ANOVAs with *post hoc* Dunnett's test were performed using GraphPad Prism 7.

Results

Cholestatic potential of DILI-associated drugs

The potential for cholestatic hepatotoxicity was determined using the C-DILI™ assay for ten DILI-associated drugs by assessing the difference in hepatotoxicity observed over a concentration range for the two different media conditions (Appendix 3). Cholestatic hepatotoxicity was determined to have occurred when there was a significantly greater decrease in intracellular ATP and a greater increase in extracellular LDH for PHH or HepaRG™ cells cultured in the sensitisation media compared to those cultured in the standard media.

HepaRG™ cells exposed to ethinyl estradiol (200 µM), ritonavir (250 µM), or troglitazone (100 µM) exhibited cholestatic hepatotoxicity (Fig. 1A). Cholestatic hepatotoxicity was observed in PHH treated with diclofenac (500 µM), ethinyl estradiol (100 µM), ritonavir (125 µM), or troglitazone (50 µM) (Fig. 1B and 1C). Compared to PHH, HepaRG™ cells required higher concentrations of ethinyl estradiol, ritonavir, or troglitazone to cause a significant decrease in cell viability, and diclofenac did not cause any significant change in cell viability for HepaRG™ cells.

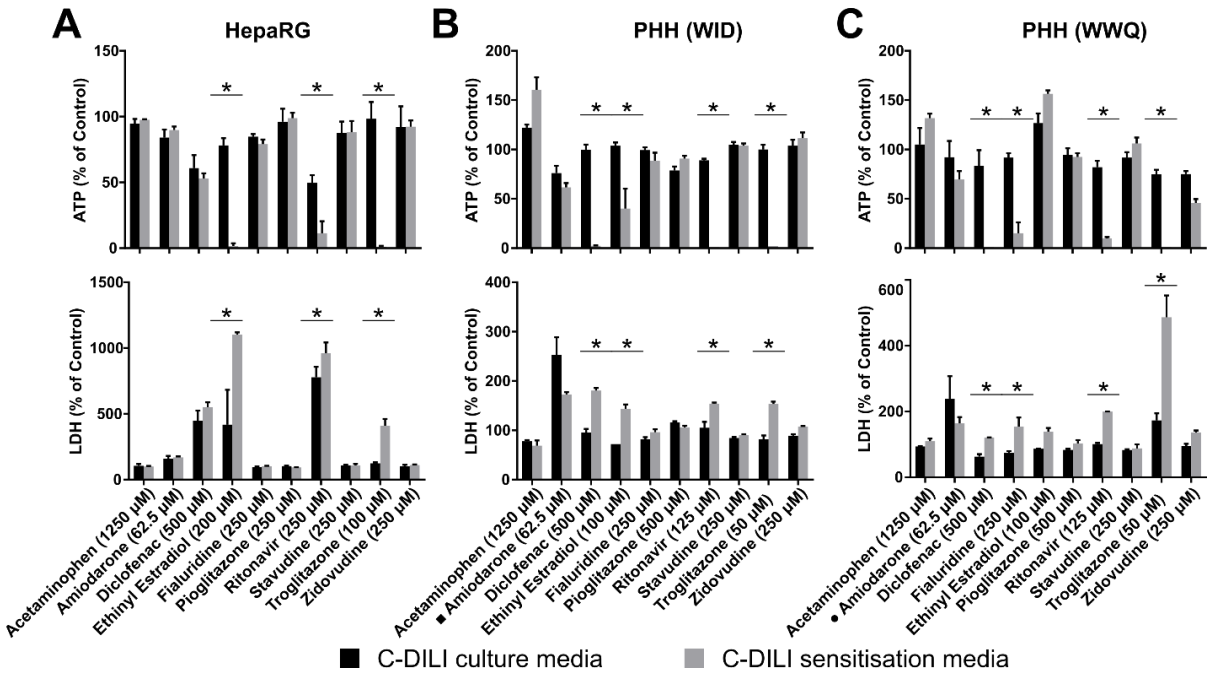

Figure 1: C-DILI™ assay for characterisation of bile acid-dependent toxicity of drug-treated HepaRG™ cells and primary human hepatocytes (PHH). (A) HepaRG™ cells and PHH, donor (B) WID and (C) WWQ, were treated with 10 DILI-associated drugs (acetaminophen, amiodarone, diclofenac, ethinyl estradiol, fialuridine, pioglitazone, ritonavir, stavudine, troglitazone, and zidovudine). Treatment concentrations started at approximately the maximum solubility for a 1000x DMSO stock, with the exception of diclofenac, and concentrations were halved in each subsequent treatment. Bile acid-dependent toxicity was determined to be present when a significantly greater toxic response was observed in the C-DILI™ sensitisation media (grey) compared to the C-DILI standard media (black). A decrease in ATP (% of control) and an increase in LDH (% of control) indicated toxicity and the lowest concentration that demonstrated significant toxicity, if any, is shown. * p-value ≤ 0.05 as determined with a Student's *t*-test (n = 3 for PHH; n=4 for HepaRG™ cells). ■ PHH donor BXW was used instead of WID and ● donor XVN was used in place of WWQ.

Effect of drug treatment on bile acid transport in HuH-7 cells

The B-CLEAR® assay was used to determine if bile acid transport was impaired by drug treatment of HuH-7 cells with the DILI-associated drugs (11, 30). The assay measured the uptake of [^{3}H]-taurocholate from media and its accumulation within the cell and efflux into the canaliculi. The B-CLEAR® assay was performed using HuH-7 cells as they were a more accessible model and were demonstrated to be an adequate model of ABC transporter function by Kang et al (2019)(24). Ethinyl estradiol (50 µM), pioglitazone (100 µM), and ritonavir (25 µM) significantly altered taurocholate transport (Fig. 2A). Ethinyl estradiol and pioglitazone reduced the BEI from 43% to 34% and 6%, respectively. Neither drug affected total cell and canaliculi accumulation of [^{3}H]-taurocholate, however, both drugs caused a greater fraction to be retained within the cell due to impaired efflux into the canaliculi (Fig. 2B). Ritonavir, which caused the BEI to decrease to 10%, showed a larger fraction of the [^{3}H]-taurocholate accumulated within the cell after treatment. In addition, the total amount of [^{3}H]-taurocholate accumulated within both the cell and canaliculi decreased from 31 pmol/mg protein in the control to 24 pmol/mg protein after treatment with ritonavir. This indicated that ritonavir impaired uptake of [^{3}H]-taurocholate in addition to impairing its biliary efflux.

Troglitazone, a known NTCP and BSEP inhibitor, did not initially appear to affect bile acid transport at 25 µM (Fig. 2A)(31). However, when the concentration of troglitazone was increased to 75 µM, it had a profound effect on bile acid transport (Fig. 2C). At 75 µM, troglitazone reduced the BEI to 24% and total [^{3}H]-taurocholate accumulation in the cell and the canaliculi was decreased from 58 pmol/mg protein in the control to 7.5 pmol/mg protein, demonstrating significantly impaired uptake and efflux.

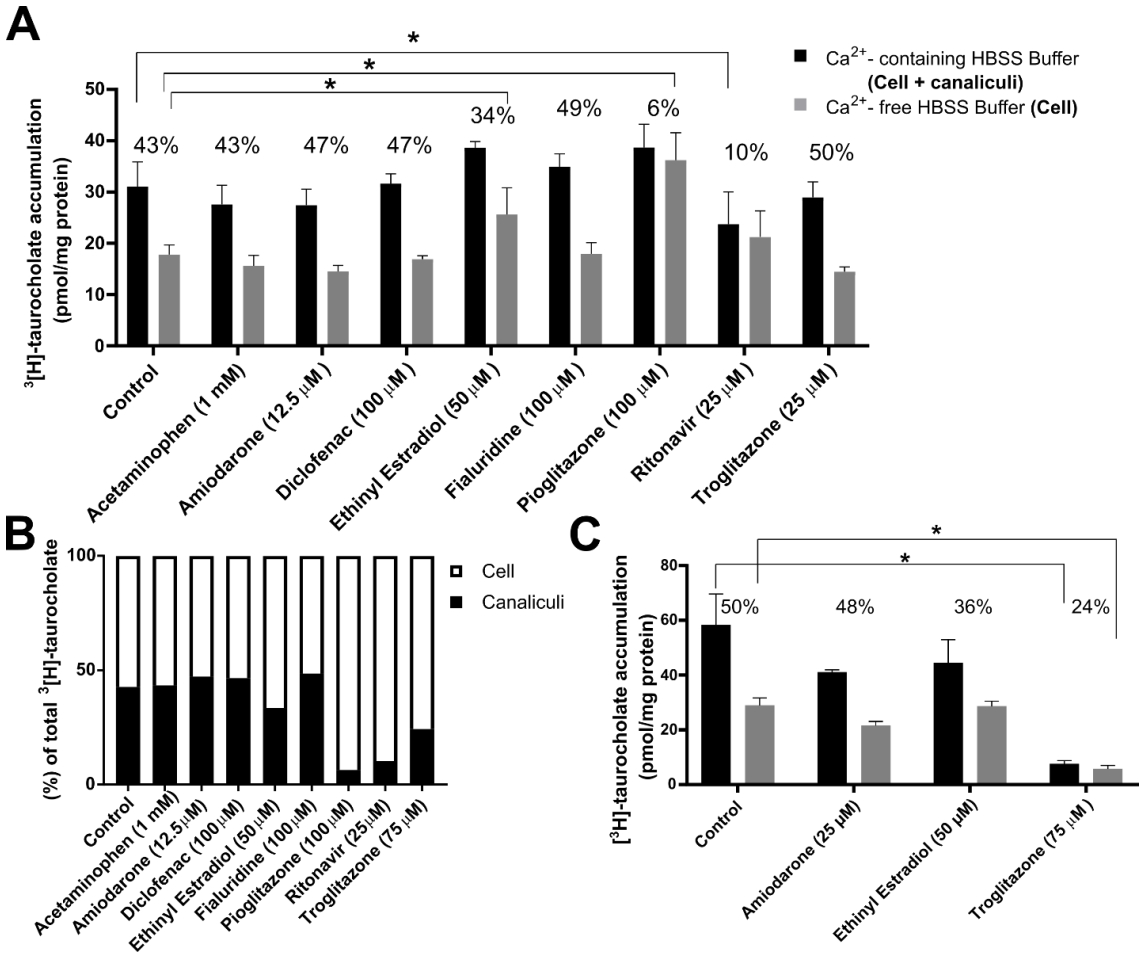

Figure 2: ^{3}[H]-taurocholate B-CLEAR® transport assay using long-term cultured HuH-7 cells after 24-h drug treatment. Total (cell plus canaliculi) ^{3}[H]-taurocholate accumulation (Ca^{2+}-containing HBSS) compared to cellular ^{3}[H]-taurocholate accumulation (Ca^{2+}-free HBSS) after 24-h exposure to (A) acetaminophen (1 mM), amiodarone (12.5 µM), diclofenac (100 µM), ethinyl estradiol (50 µM), fialuridine (100 µM), pioglitazone (100 µM), ritonavir (25 µM), or troglitazone (25 µM) with a 0.1%v/v DMSO control. (B) Mean proportion of ^{3}[H]-taurocholate localisation in the cells and canalicular compartment. (C) Repeated B-CLEAR® transport assay using increased concentrations for amiodarone (25 µM) and troglitazone (75 µM), ethinyl estradiol (50 µM) treatment was repeated at previous concentrations. The biliary excretion index (BEI %) is included above each condition. *p ≤ 0.05 as determined with a two-way ANOVA (n = 3).

Liquid chromatography-mass spectrometry analysis of cellular bile acids after drug treatment of PHH

After a 24-h drug treatment with free fatty acid (FFA) (1 mM), fialuridine (100 µM), amiodarone (12.5 µM), diclofenac (50 µM), ethinyl estradiol (25 µM), pioglitazone (100 µM), ritonavir (25 µM), or troglitazone (12.5 µM), cellular bile acids and related metabolites from PHH were analysed by targeted LC-MS metabolomics (Fig. 3). A 0.1% v/v DMSO treatment was used as a control with FFA, fialuridine, and amiodarone as negative treatment controls for cholestatic hepatotoxicity based on the outcomes of the C-DILI™ and B-CLEAR® assays (Figs. 1 and 2).

Ritonavir significantly depleted cellular taurocholate (4.8% and 8.8% of control), GCA (1.25% and 5.3% of control), TCDCA (9.8% and 14.1% of control), and GCDCA (5.3% and 13.2% of control) compared to control for donors BXW and XVN, respectively (Fig. 3). Pioglitazone demonstrated a similar capacity to significantly reduce taurocholate (5.6% and 2.3% of control), GCA (3.9% and 3.6% of control), TCDCA (3.5% and 3.9% of control), and GCDCA (4.5% and 6% of control) for donors BXW and XVN, respectively. However, no significant changes in taurine, glycine, or CDCA were observed in either donor after treatment with ritonavir or pioglitazone. Ethinyl estradiol, diclofenac, and troglitazone induced less depletion of the four bile acids in comparison to pioglitazone and ritonavir drug treatments. In addition, for the PHH donor XVN, ethinyl estradiol, diclofenac, and troglitazone did not cause a statistically significant decrease in the abundance of bile acids. Amiodarone, which was expected to be a negative control across both donors, also significantly reduced taurocholate (38%) and glycocholate (26.3%) for donor BXW compared to control. Interestingly, fialuridine caused a significant increase in

cellular taurocholate (160.7% and 401.8%) in donor BXW and XVN, respectively, compared to control, and significantly increased TCDCA (209.1%) and CDCA (287.8%) compared to control in donor BXW. CA was not altered significantly in any of the PHH extracts.

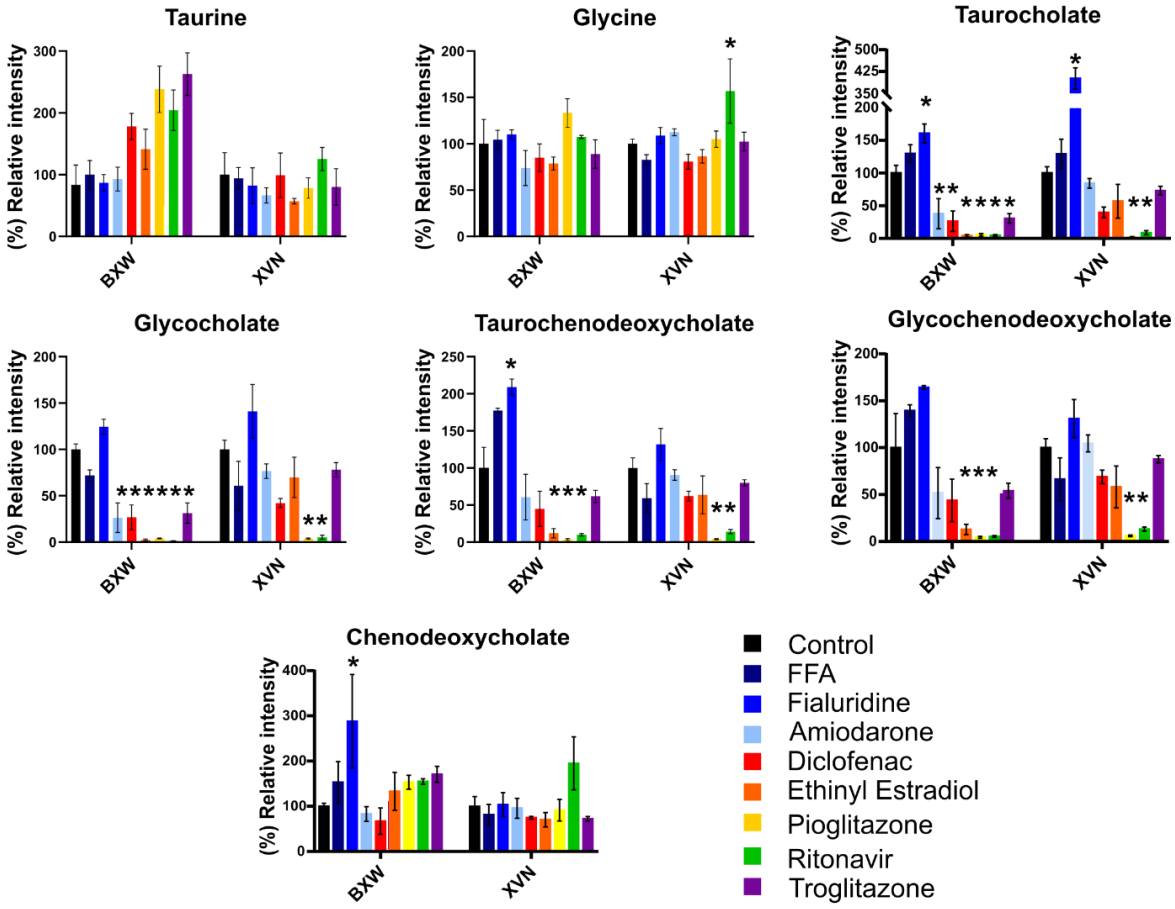

Figure 3: Levels of primary bile acid metabolites in drug-treated primary human hepatocytes (PPH). LC-MS analysis of cellular primary bile acid metabolites; taurine, glycine, taurocholate, glycocholate, taurochenodeoxycholate, glycochenodeoxycholate, and chenodeoxycholate in drug-treated PHH donors BXW and XVN. PHH were treated with 0.1% v/v DMSO control (black), 1 mM free fatty acid (FFA) (navy), 100 µM fialuridine (blue), 12.5 µM amiodarone (pale blue), 50 µM diclofenac (red), 25 µM ethinyl estradiol (orange), 100 µM pioglitazone (yellow), 25 µM ritonavir (green), and 12.5 µM troglitazone (purple) over 24 h (mean ± SD in quadruplicate). * p-value ≤ 0.05 vs control as determined with a one-way ANOVA.

Time course of bile acid abundance in HepaRG™ cells after drug treatment

The change in abundance of bile acids and related metabolites in HepaRG™ cells was characterised over several time points for a 24-h period using targeted LC-MS metabolomics (Fig. 4). No significant changes in abundance were observed for cellular or extracellular glycine or TCDCA for any of the drug treatments across any time point. At 24 h, cellular taurocholate was significantly decreased in abundance by all drug treatments. Extracellular taurocholate was only significantly increased at the 24-h time point by ritonavir and pioglitazone. Additionally, all drugs decreased cellular GCA, CDCA, and CA at 24 h. However, beginning at 16 h, only extracellular CDCA was decreased by the ritonavir and troglitazone drug treatments. The cellular abundance of GCDCA was decreased by all drug treatments at 24 h except for diclofenac. Cellular taurine was significantly decreased at 8 h for pioglitazone, ritonavir, and troglitazone. Ethinyl estradiol caused a significant decrease in cellular taurine at 16 h. Extracellular taurine was significantly increased in abundance by troglitazone after 8 h.

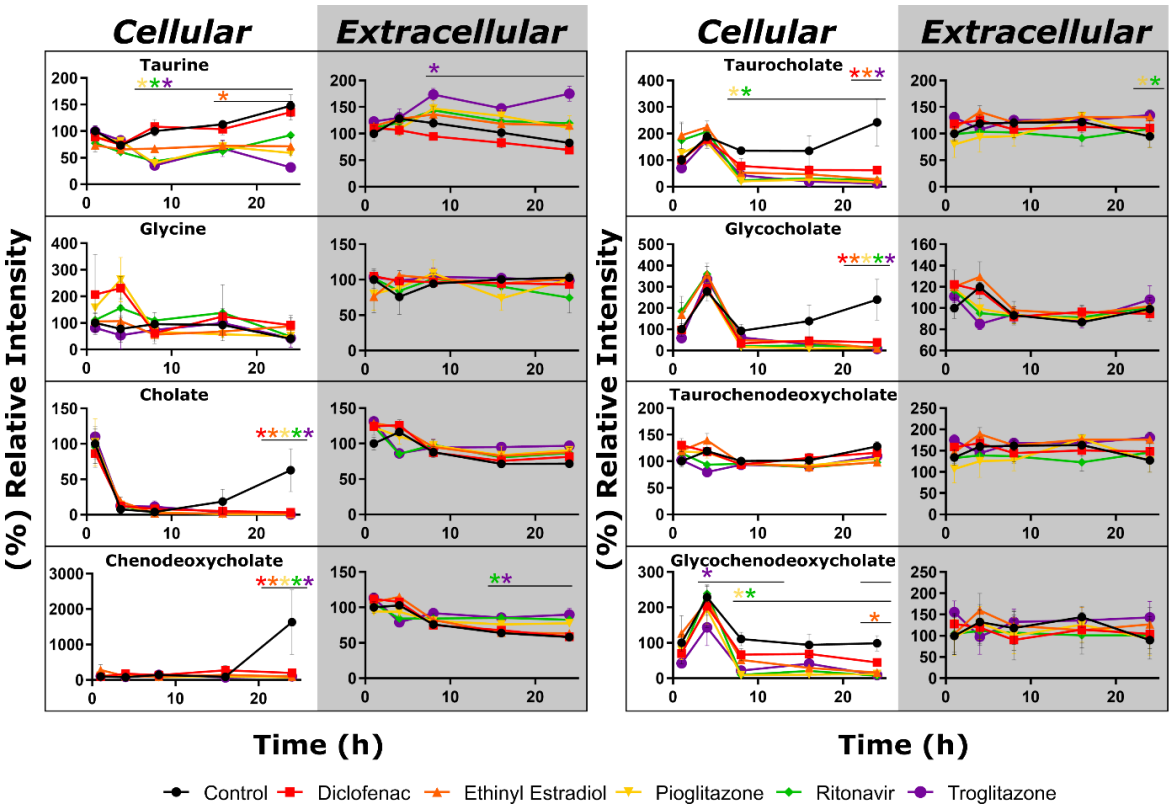

Figure 4: Bile acid kinetics in drug-treated HepaRG™ cells over a 24-h time course. LC-MS analysis of cellular and extracellular primary bile acid metabolites; taurine, glycine, taurocholate, glycocholate, taurochenodeoxycholate, glycochenodeoxycholate, and chenodeoxycholate in drug-treated HepaRG™ cells. Cells were treated with 0.1% v/v DMSO control (black), 250 µM diclofenac (red), 100 µM ethinyl estradiol (orange), 250 µM pioglitazone (yellow), 50 µM ritonavir (green), and 100 µM troglitazone (purple) over 24 h. Intensity represents the mean (n = 4) LC-MS peak area relative to control at the first time point (1 h). * p-value ≤ 0.05 vs control as determined with a one-way ANOVA where the black line indicates subsequent time points in which the p-value remained ≤ 0.05.

Drug-induced changes in drug metabolism and the bile acid-associated proteome in PHH

The proteome of drug-treated PHH was analysed using DIA LC-MS proteomics, from which the changes to a selection of 56 drug metabolism and bile acid-associated proteins was analysed (Appendix 4). Protein levels from all drug treatments were compared, with data normalised to the YNM donor 0.1%v/v DMSO control (Fig. 5). A significant donor-dependent difference in the abundance of proteins was evident from

comparison of the BXW and YNM controls. Therefore, a second comparison was performed for the BXW donor drug treatments and the BXW donor 0.1%v/v DMSO control (Fig. 6).

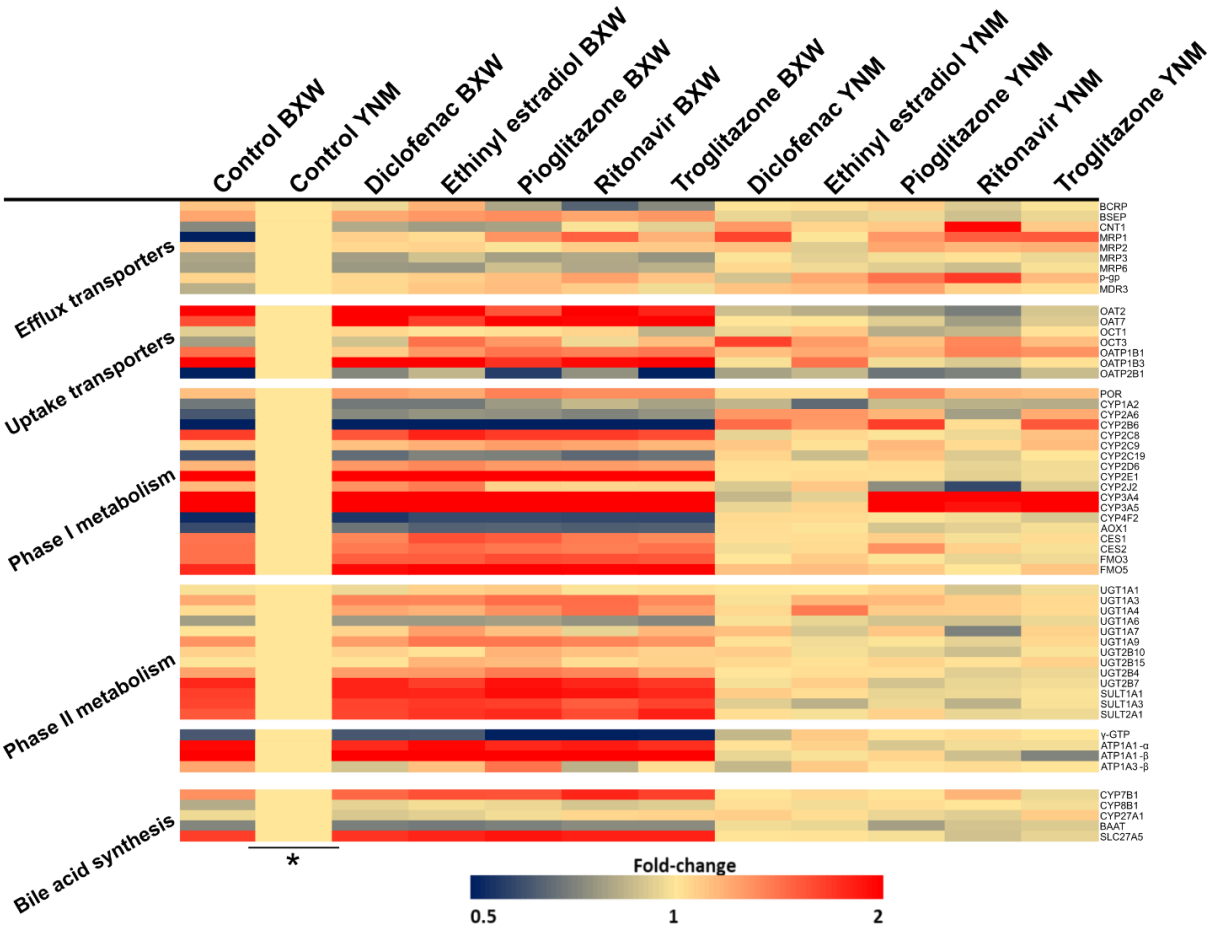

Figure 5: Heatmap of protein levels involved in drug and bile acid transport, detoxification and primary bile acid synthesis in drug-treated primary human hepatocytes (PHH). Heatmap of target proteins after 24-h treatment with 0.1% v/v DMSO control, 50 µM diclofenac, 25 µM ethinyl estradiol, 100 µM pioglitazone, 25 µM ritonavir, or 12.5 µM troglitazone. Red, increased abundance; yellow, unchanged abundance; blue, decreased abundance. * Heatmap shows the fold-change compared to control of donor YNM for each protein.

When comparing drug treatments to their matched donor controls (Figs. 5 and 6), there was a trend for drug metabolism and bile acid-associated proteins to be significantly increased in response to drug treatment. Across all drug treatments, 68-75% of significantly altered proteins were drug metabolism and bile acid-associated proteins with a majority of these proteins increasing in abundance.

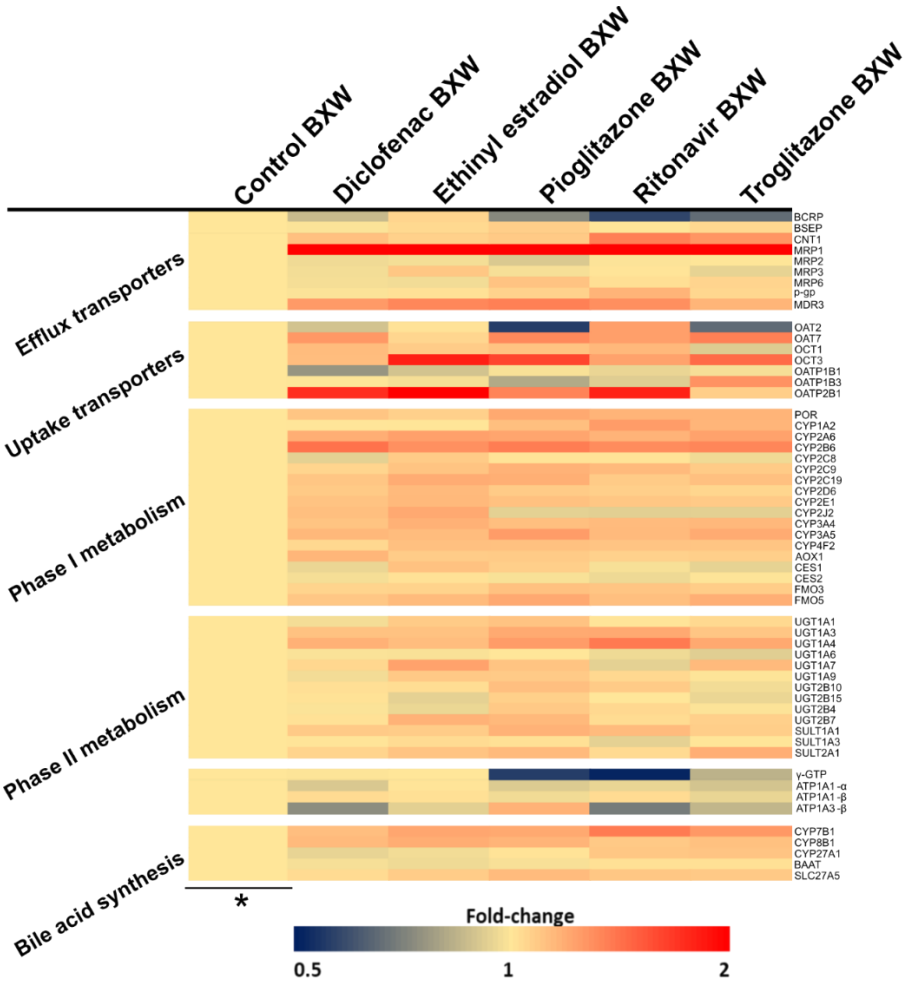

Figure 6: Heatmap of protein levels involved in drug and bile acid transporters, detoxification and primary bile acid synthesis in drug-treated primary human hepatocytes (PHH) from donor BXW. Heatmap of target proteins after 24-h treatment with 0.1% v/v DMSO control, 50 µM diclofenac, 25 µM ethinyl estradiol, 100 µM pioglitazone, 25 µM ritonavir, or 12.5 µM troglitazone. Red, increased abundance; yellow, unchanged abundance; blue, decreased abundance. * Heatmap shows the fold-change compared to control of donor BXW for each protein.

Diclofenac, pioglitazone, ritonavir, and troglitazone induced an increase in the abundance of phase I metabolism enzymes with significant increases in the abundance of POR for both donors with the exception of diclofenac (Fig. 7). All drug treatments demonstrated a significant increase in some phase I CYP metabolism enzymes with CYP2A6, CYP2B6, CYP3A4, and CYP3A5 being most prominently affected. Furthermore, pioglitazone, ritonavir, and troglitazone increased the abundance of CYP3A4 and CYP3A5 for at least one donor, by up to 3.1- and 2.7-fold, respectively. Treatment with pioglitazone, ritonavir, and troglitazone did affect transporters proteins, and bile acid synthesis enzymes, however; these changes were not as consistent between donors nor as prominent (Fig. 7).

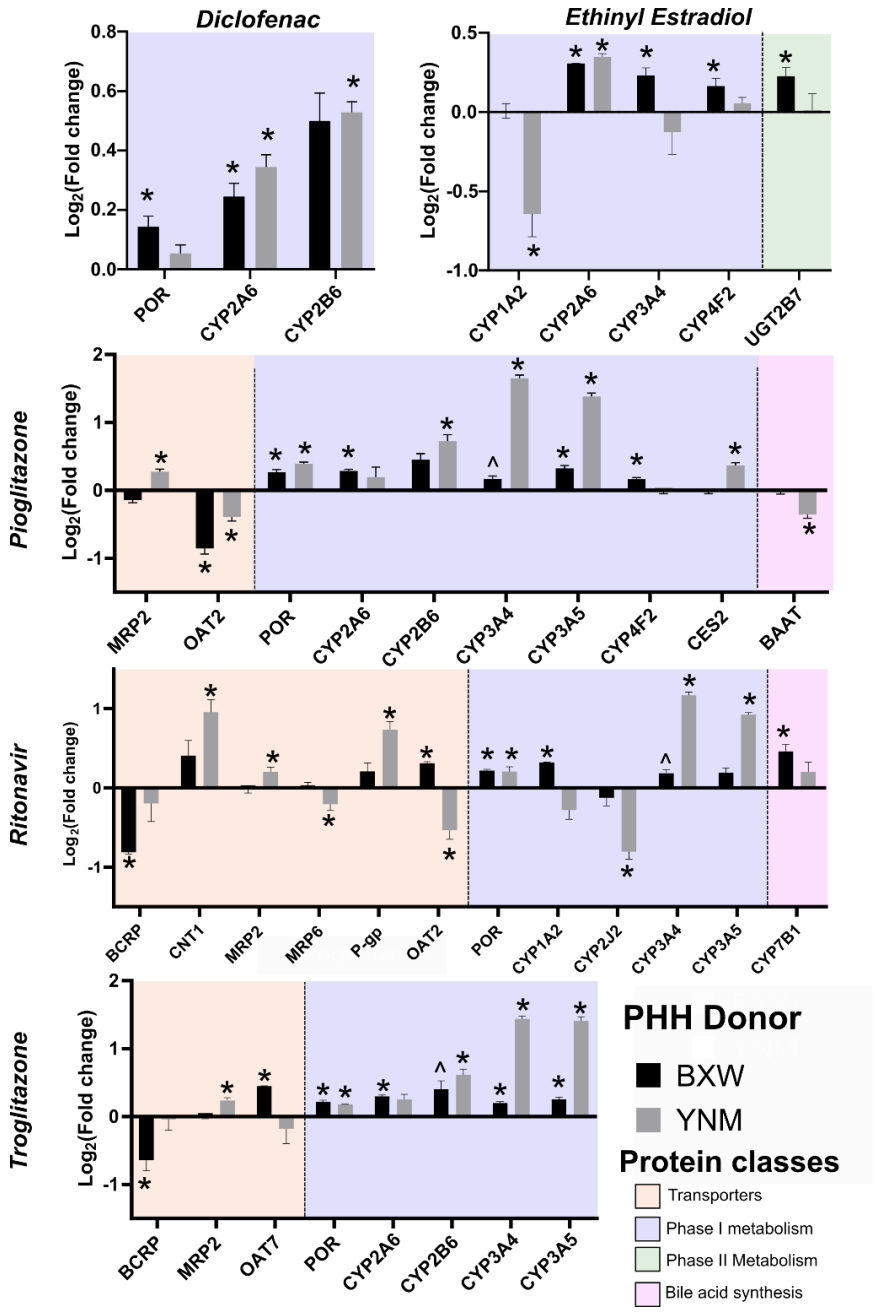

Figure 7: Changes in abundance of drug and bile acid transporters, detoxification, and primary bile acid synthesis-related proteins in drug-treated primary human hepatocytes (PHH) with cholestasis-associated drugs. Data are presented as the $\log_2$(fold change) of transporter and protein abundance relative to 0.1% DMSO control of the respective PHH donor, BXW (black) or YNM (grey)(mean ± SD in quadruplicate). Proteins that had a significant alteration in abundance included transporters (orange), phase I metabolism enzymes (blue), phase II metabolism enzymes (green), and bile acid synthesis proteins (pink). * p-value ≤ 0.05 and ^ p-value ≤ 0.1 vs control for at least one donor determined by a one-way ANOVA (n = 4).

Discussion

This chapter identified several drugs that were shown to have a capacity to induce cholestatic liver injury and offered insight into the perturbations to the bile acid-associated metabolome and proteome of PHH as a result of treatment with DILI-associated drugs. C-DILI™ and B-CLEAR® assays were used to identify which drugs had the potential to induce cholestatic hepatotoxicity as well as impair bile acid transport. Metabolite and protein extracts from PHH treated with these drugs were analysed to characterise the biological perturbations to bile acid homeostasis that may result in cholestatic DILI.

The C-DILI™ assay was used to determine which drugs could induce cholestatic hepatotoxicity in a bile acid-dependent. The C-DILI™ assay used cells cultured in sensitisation media, which causes them to be more susceptible to cholestatic hepatotoxicity and demonstrate a lower cell viability at a given drug concentration when exposed to drugs with cholestatic potential (32). The assay identified diclofenac, ethinyl estradiol, ritonavir, and troglitazone as capable of causing cholestatic hepatotoxicity, which is consistent with previous literature (Figs. 1B and C)(13, 33-35). The other drugs that showed no cholestatic hepatotoxic potential (acetaminophen, amiodarone, and fialuridine) are more commonly associated with hepatotoxicity pathways involving oxidative stress, mitochondrial dysfunction, and dysregulation of lipid metabolism and, therefore, are unlikely to give a positive result for the C-DILI™ assay (36-38). It is worth noting that pioglitazone, a thiazolidinedione, demonstrated no bile acid-dependant toxicity at 10x the dose of troglitazone, with which it shares structural similarities. However, the difference in toxicity in consistent with previous observations and clinical data indicating that only troglitazone causes significant hepatotoxicity (39, 40). This technique is primarily

designed to be used with PHH, however, it is clear that the hepatic-like cell line, HepaRG™, was also capable of determining cholestatic hepatotoxicity using the C-DILI™ methodology (Fig. 1A)(41). This could allow for the use of a more affordable and accessible *in vitro* cell model for performing the C-DILI™ assay, in comparison to transporter certified PHH. However, it must be noted that HepaRG™ cells did demonstrate a reduced sensitivity to the drug treatments, requiring a higher dose for the cholestatic hepatotoxicity to be evident. The HepaRG™ cells may be more resilient because they are a cancer-derived cell line, which is known to possess de-regulated cell death signalling pathways (42, 43). In addition, it was previously shown that the proteome of HepaRG™ cells has a significant number of proteins present in different abundances from the drug metabolism, bile acid synthesis, and transport pathways when compared to PHH, which may also be a contributing factor (Chapter 2).

One of the main mechanisms through which cholestasis can be induced is the impairment of bile acid transporters (10). The B-CLEAR® assay was performed to determine whether any of the drugs associated with cholestatic hepatotoxicity in the C-DILI™ assay impaired bile acid transport as part of their mechanism of hepatotoxicity. Ethinyl estradiol, pioglitazone, ritonavir, and troglitazone all demonstrated significant capacity to impair bile acid transport, however, the initial treatment concentration for troglitazone, 25 µM, was insufficient to alter BEI (Fig. 2A). Inhibition of bile acid transport by troglitazone was achieved at a treatment concentration of 75 µM (Fig. 2B). While several of the other drugs reduced the BEI, only ritonavir and 75 µM troglitazone decreased both BEI and total accumulation of [^{3}H]-taurocholate (Ca^{2+}-containing HBSS buffer), which indicated that both bile acid uptake and efflux were inhibited. The increased

concentration needed for troglitazone to impair bile acid transport shows that there is a concentration dependence. Ritonavir, pioglitazone, and troglitazone are all well-known inhibitors of BSEP, the major efflux transporter of taurocholate, and NTCP, the major uptake transporter of taurocholate, and were expected to affect bile acid transport (9, 44, 45). However, it is unclear why pioglitazone, a known NTCP inhibitor, only affected efflux, while troglitazone affected both although this may explain why troglitazone exhibited cholestatic hepatotoxicity in the C-DILI™ assay whereas pioglitazone did not. Ethinyl estradiol is also a known inhibitor of BSEP; although it does affect NTCP expression, it is not known to directly inhibit NTCP (46). Diclofenac showed cholestatic hepatotoxicity in PHH, but it did not exhibit transport inhibition. However, this may be due to an insufficient treatment concentration, similar to troglitazone, because diclofenac did not cause toxicity in HepaRG™ cells at 500 µM which, like HuH-7 cells used in the B-CLEAR® assay, are a cancer derived cell line that may be less sensitive to drug treatment., Diclofenac may affect bile acid transport at a higher dose, or if transporter certified PHH were used as it has been shown previously to inhibit bile acid transport, though at concentrations up to 100x greater than ritonavir, pioglitazone, or troglitazone (47).

Metabolomics and proteomics analysis of bile acids demonstrated that there were significant alterations in the abundance of bile acids and bile acid-related proteins after treatment with cholestatic drugs. The common trend seen for both the bile acids of PHH and HepaRG™ cells was a consistent decrease in abundance of cellular bile acids. All drug treatments that were considered to be cholestatic (diclofenac, ethinyl estradiol, pioglitazone, ritonavir, and troglitazone) either caused no change in bile acid abundance or a significant decrease (Figs. 3 and 4). As these changes to bile acids were not

observed for amiodarone or fialuridine, it is unlikely that this decrease in bile acids is the result of general hepatocellular injury (Fig. 3). From the time course study with HepaRG™ cells, it appeared that after the media change, the HepaRG™ cells undergo a time-dependent change in the cellular abundance of bile acids that likely occurs to re-establish bile acid homeostasis between the cellular, canaliculi, and extracellular compartments. The drug-treated cells were unable to restore bile acids to homeostatic levels as seen in the untreated control (Fig. 4). Over the 24-h treatment period, the control cells demonstrated an increase in several bile acids whereas the drug-treated cells did not produce the same increase in bile acids over time. Cholate, a bile acid that is metabolized to various conjugated forms, did not increase in abundance over the 24-h period in the drug-treated samples, while it increased to 63% of initial abundance for the control (Fig. 4). This may indicate that after a media change with drug-treated media, bile acid homeostatic mechanisms are significantly affected. This could be due to impaired bile acid synthesis. Ritonavir has been associated with impaired bile acid synthesis and increased cholesterol abundance, a precursor to bile acids (48). Furthermore, thiazolidinediones are known to activate peroxisome proliferator-activated receptor alpha (PPARα), which is associated with impaired expression of bile acid synthesis enzymes (49, 50). However, from the proteomics analysis it is unlikely that the suppression of the gene expression of bile synthesis enzymes is the cause of the decrease seen in bile acids as only pioglitazone and ritonavir affected the abundance of one bile acid synthesis enzymes each (Fig. 7). Based on the data from the B-CLEAR® assay, it is unlikely that altered transport is the primary mechanism responsible for the cellular depletion of bile

acids. While ethinyl estradiol, pioglitazone, ritonavir, and troglitazone decreased the BEI, only ritonavir and troglitazone demonstrated impaired bile acid uptake.

A common trend that occurred for all drug treatments that may have resulted in the decrease in abundance of bile acids is the increased abundance of several CYP enzymes including CYP3A4 and CYP3A5. CYP3A4 and CYP3A5, which metabolise bile acids, were significantly increased in abundance in PHH after ethinyl estradiol, pioglitazone, ritonavir, and troglitazone treatment for at least one PHH donor, if not both (51-53). While the abundance of CYP3A4 and CYP3A5 increased in both donors, it did not increase to the same extent. The less significant increase in the abundance of CYP3A4 and CYP3A5 observed for BXW compared to YNM may be due to the higher baseline abundance of these enzymes in the BXW control (Fig. 5). The increased abundance of CYP3A4 and CYP3A5 is likely to have resulted in the increased abundance of POR observed with pioglitazone, ritonavir, and troglitazone. POR is an oxidoreductase enzyme that is essential for CYP3A4 and CYP3A5 metabolism because POR supplies the electrons required for CYP3A4 metabolic activity (54, 55). CYP3A4 and CYP3A5 rapidly metabolise bile acids, including cholate, and the increased expression after drug treatment may have resulted in significant increased metabolism of bile acids (56). Furthermore, CYP2B6 is also associated with bile acid metabolism, however, CYP3A4 and, to a lesser extent, CYP3A5, are considered the primary metabolisers of bile acids (52). The increased expression of phase I metabolism enzymes has been strongly associated with a protective mechanism against cholestasis (51). The inhibition of efflux of bile acids into the canaliculi that was observed in the B-CLEAR® assay after treatment with some drugs may have led to cellular accumulation of bile acids (Fig. 2). Either in response to the

presence of xenobiotics or accumulation of bile acids, the expression of CYP3A4 and CYP3A5 was increased. Several of the drug treatments are known to induce the expression of CYP3A4 and CYP3A5 and these CYPs also may be induced by bile acids via FXR- and PXR-mediated pathways (51, 57). CYP3A4 and CYP3A5 would be capable of metabolising the bile acids to prevent cellular accumulation of bile acids and cholestatic liver injury.

A limitation of the multi-omics methods used is that they only offer information about metabolite and protein abundance. The abundance and presence of a protein does not directly correlate to a given level of metabolic activity as it may be inactivated by the drug treatments. The activity of proteins may be impaired by inhibition and, for transporters, translocation from the membrane or impairment of translocation to the membrane. This is well illustrated by BSEP, for which only 40% of total hepatocellular BSEP is present on the canalicular membrane (58). As such, if a drug treatment were to inhibit BSEP localisation or directly inhibit the transporter without altering protein abundance, bile acid transport would be affected in a manner that could not be identified by proteomics. The importance of considering this limitation is illustrated by estradiol-17β-D-glucuronide, an estradiol conjugate, which can internalise MRP2 (59). This would cause a decrease in MRP2-mediated efflux without altering the cellular abundance of MRP2. The inhibition of bile acid transporters through altered localisation or direct inhibition of transporters by ethinyl estradiol, pioglitazone, ritonavir, and troglitazone may be the reason that significant impairment of bile acid transport was observed (Fig. 2) without significant impact on the abundance of bile acid transporters (Fig. 7). In order to overcome such limitations, proteomics was coupled with the B-CLEAR® assay to account

for inhibition of biliary transport that is not the result of altered bile acid transporter abundance. However, further assays that could determine the inhibition of specific bile acid transporters, or the use of immunofluorescence microscopy to characterise changes in the localisation of bile acid transporters, would be valuable in ascertaining the specific mechanisms involved. The use of PHH also introduced the common issue inherent to primary cells of interdonor variability, which can be seen in the difference between donors in Figs. 3, 5, and 7. Such variability is a well-known confounding factor, especially among cells as metabolically active as PHH (60, 61). While the use of HepaRG™ and HuH-7 cells allows for reproducible *in vitro* models without such variability, the potential trade-off is the metabolic competency of these models (Chapter 2). Therefore, future studies would benefit from a greater number of PHH donors to compensate for interdonor variability, however, this may not be feasible due to the costs involved with using PHH.

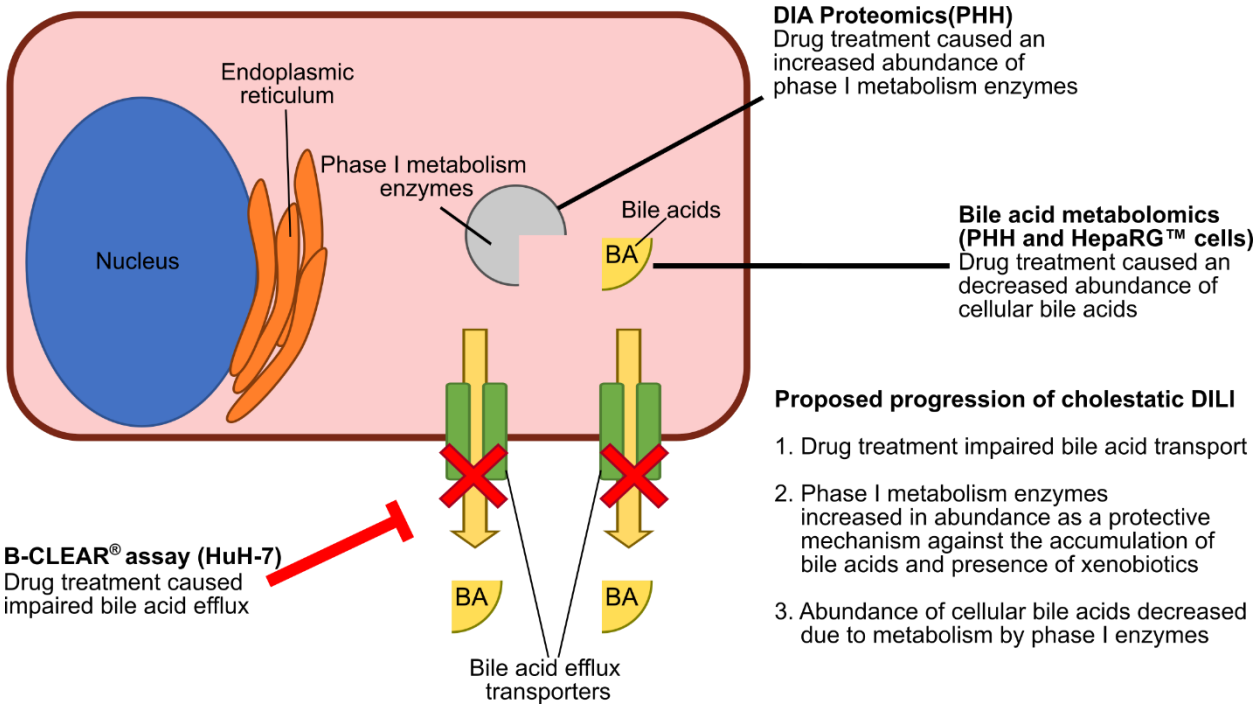

Figure 8: Proposed mechanism of the progression of cholestatic DILI in hepatocytes and hepatic-derived cells after treatment with DILI associated drugs. The proposed progression of cholestatic DILI involved an inhibition of bile acid transport with the abundance of phase I metabolism enzymes increased as a protective mechanism against cellular bile acid accumulation and cholestatic liver injury.

This study applied a combination of plate-based assays, proteomics, and metabolomics to obtain in-depth insight into the perturbations that drugs associated with cholestatic DILI may induce in PHH and hepatic-like cell lines. The C-DILI™ and B-CLEAR® assays allowed for determination of drugs that could cause cholestatic hepatotoxicity and impair bile acid transport. From the C-DILI™ assay, it was determined that diclofenac, ethinyl estradiol, ritonavir, and troglitazone had significant potential to cause cholestatic DILI. Additionally, ethinyl estradiol, pioglitazone, ritonavir, and troglitazone significantly impaired bile acid transport using the B-CLEAR® assay with HuH-7 cells. Targeted metabolomics of PHH and HepaRG cells treated with cholestatic drugs demonstrated a common behaviour of decreasing the cellular abundance of several

bile acids. Proteomics analysis of drug-treated PHH revealed that the abundance of CYP3A4, CYP3A5, and POR was significantly increased for pioglitazone, ritonavir, and troglitazone, the drugs which caused the greatest decrease in bile acids. The B-CLEAR® assay demonstrated impairment in the bile acid transport capacity of cells treated with ethinyl estradiol, pioglitazone, ritonavir, and troglitazone, which could have resulted in cellular bile acid accumulation and cholestatic liver injury. Therefore, the depletion of bile acids observed in the metabolomic analysis of PHH and HepaRG™ cells may be the result of increased expression of CYP3A4 and CYP3A5 as a protective mechanism against xenobiotics and cholestatic liver injury (Fig. 8). Using a multi-faceted approach to study cholestatic DILI has enabled characterisation of the potential for several DILI-associated drugs to induce cholestatic hepatotoxicity, alter bile acid transport, and impact the abundance of bile acid metabolites and associated proteins. This approach revealed that the cholestatic liver injury induced by the cholestatic drugs studied was likely driven by impaired bile acid transport. Based on the metabolomics and proteomics results, cellular bile acids were depleted, which may have been due to increased phase I metabolism of bile acids as a protective mechanism against cholestatic liver injury. Knowledge of the mechanisms that cause cholestatic DILI, and the mechanisms that hepatocytes employ to protect against cholestasis, can be utilised to develop safer drugs with minimal cholestatic potential.

References

1. Bjornsson ES, Bergmann OM, Bjornsson HK, Kvaran RB, Olafsson S. Incidence, presentation, and outcomes in patients with drug-induced liver injury in the general population of Iceland. *Gastroenterology*. 2013;144(7):1419-25.
2. Sgro C, Clinard F, Ouazir K, Chanay H, Allard C, Guilleminet C, et al. Incidence of drug-induced hepatic injuries: a French population-based study. *Hepatology*. 2002;36(2):451-55.
3. Suk KT, Kim DJ, Kim CH, Park SH, Yoon JH, Kim YS, et al. A prospective nationwide study of drug-induced liver injury in Korea. *Am J Gastroenterol*. 2012;107(9):1380-7.
4. Shen T, Liu Y, Shang J, Xie Q, Li J, Yan M, et al. Incidence and etiology of drug-induced liver injury in mainland China. *Gastroenterology*. 2019;156(8):2230-41.e11.
5. Goldberg DS, Forde KA, Carbonari DM, Lewis JD, Leidl KBF, Reddy KR, et al. Population-representative incidence of drug-induced acute liver failure based on an analysis of an integrated health care system. *Gastroenterology*. 2015;148(7):1353-61.e3.
6. Licata A, Minissale MG, Calvaruso V, Craxi A. A focus on epidemiology of drug-induced liver injury: analysis of a prospective cohort. *Eur Rev Med Pharmacol Sci*. 2017;21(1 Suppl):112-21.
7. Lu RJ, Zhang Y, Tang FL, Zheng ZW, Fan ZD, Zhu SM, et al. Clinical characteristics of drug-induced liver injury and related risk factors. *Exp Ther Med*. 2016;12(4):2606-16.
8. Sundaram V, Björnsson ES. Drug-induced cholestasis. *Hepatol C ommun*. 2017;1(8):726-35.
9. Funk C, Pantze M, Jehle L, Ponelle C, Scheuermann G, Lazendic M, et al. Troglitazone-induced intrahepatic cholestasis by an interference with the hepatobiliary export of bile acids in male and female rats. Correlation with the gender difference in troglitazone sulfate formation and the inhibition of the canalicular bile salt export pump (Bsep) by troglitazone and troglitazone sulfate. *Toxicology*. 2001;167(1):83-98.
10. Gijbels E, Vilas-Boas V, Deferm N, Devisscher L, Jaeschke H, Annaert P, et al. Mechanisms and in vitro models of drug-induced cholestasis. *Arch Toxicol*. 2019;93(5):1169-86.
11. Morgan RE, van Staden CJ, Chen Y, Kalyanaraman N, Kalanzi J, Dunn RT, II, et al. A multifactorial approach to hepatobiliary transporter assessment enables improved therapeutic compound development. *Toxicol Sci*. 2013;136(1):216-41.
12. Graham DJ, Drinkard CR, Shatin D. Incidence of idiopathic acute liver failure and hospitalized liver injury in patients treated with troglitazone. *Am J Gastroenterol*. 2003;98(1):175-9.

13. Simon FR, Fortune J, Iwahashi M, Gartung C, Wolkoff A, Sutherland E. Ethinyl estradiol cholestasis involves alterations in expression of liver sinusoidal transporters. *Am J Pathol*. 1996;271(6 Pt 1):G1043-52.

14. Mottino AD, Hoffman T, Crocenzi FA, Sánchez Pozzi EJ, Roma MG, Vore M. Disruption of function and localization of tight junctional structures and Mrp2 in sustained estradiol-17beta-D-glucuronide-induced cholestasis. *Am J Physiol Gastrointest Liver Physiol*. 2007;293(1):G391-402.

15. Muchova L, Vanova K, Zelenka J, Lenicek M, Petr T, Vejrazka M, et al. Bile acids decrease intracellular bilirubin levels in the cholestatic liver: implications for bile acid-mediated oxidative stress. *J Cell Mol Med*. 2011;15(5):1156-65.

16. Yu H, Li Y, Xu Z, Wang D, Shi S, Deng H, et al. Identification of potential biomarkers in cholestasis and the therapeutic effect of melatonin by metabolomics, multivariate data and pathway analyses. *Int J Mol Med*. 2018;42(5):2515-26.

17. Ma Z, Wang X, Yin P, Wu R, Zhou L, Xu G, et al. Serum metabolome and targeted bile acid profiling reveals potential novel biomarkers for drug-induced liver injury. *Medicine (Baltimore)*. 2019;98(31):e16717-e17.

18. Thakare R, Alamoudi JA, Gautam N, Rodrigues AD, Alnouti Y. Species differences in bile acids I. Plasma and urine bile acid composition. *J Appl Toxicol*. 2018;38(10):1323-35.

19. Wang L, Prasad B, Salphati L, Chu X, Gupta A, Hop CECA, et al. Interspecies variability in expression of hepatobiliary transporters across human, dog, monkey, and rat as determined by quantitative proteomics. *Drug Metab Dispos*. 2015;43(3):367-74.

20. Sun J, Schnackenberg LK, Beger RD. Studies of acetaminophen and metabolites in urine and their correlations with toxicity using metabolomics. *Drug Metab Lett*. 2009;3(3):130-36.

21. Paemanee A, Sornjai W, Kittisenachai S, Sirinonthanawech N, Roytrakul S, Wongtrakul J, et al. Nevirapine induced mitochondrial dysfunction in HepG2 cells. *Sci Rep*. 2017;7:1-11.

22. Rodrigues RM, Laxmikanth K, Chaudhari U, Sachinidis A, Zahedi RP, Sickmann A, et al. Omics-based responses induced by bosentan in human hepatoma HepaRG cell cultures. *Arch Toxicol*. 2018;92(6):1939-52.

23. Cuykx M, Beirnaert C, Rodrigues RM, Laukens K, Vanhaecke T, Covaci A. Untargeted liquid chromatography-mass spectrometry metabolomics to assess drug-induced cholestatic features in HepaRG® cells. *Toxicol Appl Pharmacol*. 2019;379:114666.

24. Kang HE, Malinen MM, Saran C, Honkakoski P, Brouwer KLR. Optimization of canalicular ABC transporter function in HuH-7 cells by modification of culture conditions. *Drug Metab Dispos*. 2019;47(10):1222-30.

25. Creek DJ, Chua HH, Cobbold SA, Nijagal B, MacRae JI, Dickerman BK, et al. Metabolomics-based screening of the malaria box reveals both novel and

established mechanisms of action. *Antimicrob Agents Chemother*. 2016;60(11):6650-63.

26. Beaudoin JJ, Bezençon J, Sjöstedt N, Fallon JK, Brouwer KLR. Role of organic solute transporter alpha/beta in hepatotoxic bile acid transport and drug interactions. *Toxicol Sci*. 2020;176(1):34-45.

27. Batth TS, Francavilla C, Olsen JV. Off-line high-ph reversed-phase fractionation for in-depth phosphoproteomics. *J Proteome Res*. 2014;13(12):6176-86.

28. Birrell GW, Challis MP, De Paoli A, Anderson D, Devine SM, Heffernan GD, et al. Multi-omic Characterization of the Mode of Action of a Potent New Antimalarial Compound, JPC-3210, Against Plasmodium falciparum. *Mol Cell Proteomics*. 2020;19(2):308-25.

29. Cox J, Mann M. MaxQuant enables high peptide identification rates, individualized p.p.b.-range mass accuracies and proteome-wide protein quantification. *Nat Biotechnol*. 2008;26(12):1367-72.

30. Garzel B, Yang H, Zhang L, Huang SM, Polli JE, Wang H. The role of bile salt export pump gene repression in drug-induced cholestatic liver toxicity. *Drug Metab Dispos*. 2014;42(3):318-22.

31. Kemp DC, Zamek-Gliszczynski MJ, Brouwer KLR. Xenobiotics inhibit hepatic uptake and biliary excretion of taurocholate in rat hepatocytes. *Toxicol Sci*. 2005;83(2):207-14.

32. Jonathan P. Jackson KMF, Robert L. St. ClaireIII, Chris B. Black, Kenneth R. Brouwer. Cholestatic drug induced liver injury: a function of bile salt export pump inhibition and farnesoid x receptor antagonism. *Appl In Vitro Toxicol*. 2018;4(3):265-79.

33. Sarkar U, Ravindra KC, Large E, Young CL, Rivera-Burgos D, Yu J, et al. Integrated assessment of diclofenac biotransformation, pharmacokinetics, and omics-based toxicity in a three-dimensional human liver-immunocompetent coculture system. *Drug Metab Dispos*. 2017;45(7):855-66.

34. Griffin LM, Watkins PB, Perry CH, St. Claire RL, Brouwer KLR. Combination lopinavir and ritonavir alter exogenous and endogenous bile acid disposition in sandwich-cultured rat hepatocytes. *Drug Metab Dispos*. 2013;41(1):188-96.

35. Chang JH, Sangaraju D, Liu N, Jaochico A, Plise E. Comprehensive evaluation of bile acid homeostasis in human hepatocyte co-culture in the presence of troglitazone, pioglitazone, and acetylsalicylic acid. *Mol Pharm*. 2019;16(10):4230-40.

36. Hinson JA, Roberts DW, James LP. Mechanisms of acetaminophen-induced liver necrosis. *Handb Exp Pharmacol*. 2010(196):369-405.

37. Vitins AP, Kienhuis AS, Speksnijder EN, Roodbergen M, Luijten M, van der Ven LT. Mechanisms of amiodarone and valproic acid induced liver steatosis in mouse in vivo act as a template for other hepatotoxicity models. *Arch Toxicol*. 2014;88(8):1573-88.

38. Lee EW, Lai Y, Zhang H, Unadkat JD. Identification of the mitochondrial targeting signal of the human equilibrative nucleoside transporter 1 (hENT1): implications for interspecies differences in mitochondrial toxicity of fialuridine. *J Biol Chem*. 2006;281(24):16700-06.

39. Vella A, de Groen PC, Dinneen SF. Fatal hepatotoxicity associated with troglitazone. *Ann Intern Med*. 1998;129(12):1080.

40. Rachek LI, Yuzefovych LV, Ledoux SP, Julie NL, Wilson GL. Troglitazone, but not rosiglitazone, damages mitochondrial DNA and induces mitochondrial dysfunction and cell death in human hepatocytes. *Toxicol Appl Pharmacol*. 2009;240(3):348-54.

41. Jackson JP, Brouwer KR. The C-DILI™ assay: an integrated in vitro approach to predict cholestatic hepatotoxicity. In: Vinken M, editor. Experimental Cholestasis Research. New York, NY: Springer New York; 2019. p. 75-85.

42. Todaro M, Lombardo Y, Francipane MG, Alea MP, Cammareri P, Iovino F, et al. Apoptosis resistance in epithelial tumors is mediated by tumor-cell-derived interleukin-4. *Cell Death Differ*. 2008;15(4):762-72.

43. Morin PJ. Drug resistance and the microenvironment: nature and nurture. *Drug Resist Updat*. 2003;6(4):169-72.

44. McRae MP, Lowe CM, Tian X, Bourdet DL, Ho RH, Leake BF, et al. Ritonavir, Saquinavir, and Efavirenz, but Not Nevirapine, Inhibit Bile Acid Transport in Human and Rat Hepatocytes. *Journal of Pharmacology and Experimental Therapeutics*. 2006;318(3):1068-75.

45. Dong Z, Ekins S, Polli JE. Quantitative NTCP pharmacophore and lack of association between DILI and NTCP Inhibition. *Eur J Pharm Sci*. 2015;66:1-9.

46. Micheline D, Emmanuel J, Serge E. Effect of ursodeoxycholic acid on the expression of the hepatocellular bile acid transporters (Ntcp and Bsep) in rats with estrogen-induced cholestasis. *J Pediatr Gastroenterol Nutr*. 2002;35(2):185-91.

47. Zhang J, He K, Cai L, Chen YC, Yang Y, Shi Q, et al. Inhibition of bile salt transport by drugs associated with liver injury in primary hepatocytes from human, monkey, dog, rat, and mouse. *Chem Biol Interact*. 2016;255:45-54.

48. Cao R, Hu Y, Wang Y, Gurley EC, Studer EJ, Wang X, et al. Prevention of HIV protease inhibitor-induced dysregulation of hepatic lipid metabolism by raltegravir via endoplasmic reticulum stress signaling pathways. *J Pharmacol Exp Ther*. 2010;334(2):530-39.

49. Orasanu G, Ziouzenkova O, Devchand PR, Nehra V, Hamdy O, Horton ES, et al. The peroxisome proliferator-activated receptor-gamma agonist pioglitazone represses inflammation in a peroxisome proliferator-activated receptor-alpha-dependent manner in vitro and in vivo in mice. *J Am Coll Cardiol*. 2008;52(10):869-81.

50. Li T, Chiang JYL. Regulation of bile acid and cholesterol metabolism by PPARs. *PPAR Res*. 2009;2009:501739.

51. Chen J, Zhao KN, Chen C. The role of CYP3A4 in the biotransformation of bile acids and therapeutic implication for cholestasis. *Ann Transl Med*. 2014;2(1):7-7.

52. Furster C, Wikvall K. Identification of CYP3A4 as the major enzyme responsible for 25-hydroxylation of 5beta-cholestane-3alpha,7alpha,12alpha-triol in human liver microsomes. *Biochim Biophys Acta*. 1999;1437(1):46-52.

53. Li T, Apte U. Bile acid metabolism and signaling in cholestasis, inflammation, and cancer. *Adv Pharmacol*. 2015;74:263-302.

54. Flück CE, Mullis PE, Pandey AV. Reduction in hepatic drug metabolizing CYP3A4 activities caused by P450 oxidoreductase mutations identified in patients with disordered steroid metabolism. *Biochem Biophys Res Commun*. 2010;401(1):149-53.

55. Flück CE, Pandey AV. Chapter 3H - P450 Oxidoreductase Deficiency (PORD). In: New MI, Lekarev O, Parsa A, Yuen TT, O'Malley BW, Hammer GD, editors. Genetic Steroid Disorders. San Diego: Academic Press; 2013. p. 125-43.

56. Bodin K, Lindbom U, Diczfalusy U. Novel pathways of bile acid metabolism involving CYP3A4. *Biochim Biophys Acta Mol Cell Biol Lipids*. 2005;1687(1):84-93.

57. Luo G, Cunningham M, Kim S, Burn T, Lin J, Sinz M, et al. CYP3A4 induction by drugs: correlation between a pregnane X receptor reporter gene assay and CYP3A4 expression in human hepatocytes. *Drug Metab Dispos*. 2002;30(7):795-804.

58. Wakabayashi Y, Lippincott-Schwartz J, Arias IM. Intracellular trafficking of bile salt export pump (ABCB11) in polarized hepatic cells: constitutive cycling between the canalicular membrane and rab11-positive endosomes. *Mol Biol Cell*. 2004;15(7):3485-96.

59. Mottino AD, Cao J, Veggi LM, Crocenzi F, Roma MG, Vore M. Altered localization and activity of canalicular Mrp2 in estradiol-17β-D-glucuronide–induced cholestasis. *Hepatology*. 2002;35(6):1409-19.

60. Rogue A, Lambert C, Spire C, Claude N, Guillouzo A. Interindividual variability in gene expression profiles in human hepatocytes and comparison with HepaRG cells. *Drug Metab Dispos*. 2012;40(1):151-58.

61. Wiśniewski JR, Vildhede A, Norén A, Artursson P. In-depth quantitative analysis and comparison of the human hepatocyte and hepatoma cell line HepG2 proteomes. *J Proteomics*. 2016;136:234-47.

Chapter 4

Lipidomics Characterisation of Steatosis-Induced Changes to Lipid Profiles in Human Hepatocytes

Abstract

Steatotic liver injury can present as numerous different injury phenotypes and may result from a variety of causative stimuli. Non-alcoholic steatohepatitis (NASH) is a severe form of liver injury with significant mortality rate that can be induced by a variety of stimuli including prescription medications. Identifying changes in the cellular lipid profiles of hepatocytes from patients with NASH or hepatocytes treated with drugs that cause steatotic drug-induced liver injury (DILI) may allow for the identification of characteristic lipid signatures. This study aimed to identify lipid signatures that are characteristic of steatotic liver injury by combining LC-MS-based lipidomics and multivariate analysis. Lipidomics analysis of hepatocytes obtained from patients with NASH identified increases in the total cellular abundance of phosphatidylcholine, phosphatidylethanolamine, phosphatidylglycerol, phosphatidylinositol, and phosphatidylserine lipids. Furthermore, lipidomics and multivariate analysis of *in vitro* primary human hepatocytes treated with steatogenic drugs identified several lipids that may be predictive of steatotic liver injury, a majority of which were phospholipids. Phospholipids were demonstrated to be characteristically altered in steatotic hepatocytes and may a unique and characteristic lipid signature for steatotic liver injury.

Introduction

Non-alcoholic fatty liver disease (NAFLD), commonly defined as the vesicular accumulation of neutral lipids within hepatocytes, is a prevalent issue that affects an estimated 25% of the global population (1). The primary risk factors for NAFLD include obesity, type II diabetes, and the metabolic syndrome. In addition, hepatitis infections and

certain medications also may be contributing factors (2, 3). Certain prescription drugs also have the potential to be a causative factor of NALFD (4-7). NAFLD can progress to non-alcoholic steatohepatitis (NASH), which is a more severe sub-type of NAFLD with a mortality rate 6.5-times higher than NAFLD. Although the risk of disease progression and the development of advanced fibrosis is unclear, one study demonstrated that progression to NASH occurred in as many as 59% of biopsy-confirmed NAFLD patients (1). The prevalence and severity of NAFLD and NASH makes it of vital importance to identify characteristic, specific, and sensitive biomarkers for these disease states.

Drug-induced liver injury (DILI) is a potential, non-obesity related cause of NAFLD and NASH (8). DILI has an annual global prevalence ranging from 13.9 to 19.1 of cases per 100,000 individuals, with 64% of DILI cases presenting with liver steatosis (9-12). The presentation of steatosis in DILI patients is troubling as 73% of patients who presented with steatotic histological features required a liver transplant or had a fatal outcome (12). A variety of drugs including amiodarone, methotrexate, nonsteroidal anti-inflammatory drugs (NSAIDs), and valproate have all been associated with NAFLD and NASH (5, 13-15). Additionally, cationic amphiphilic drugs, including amiodarone, have been linked to phospholipidosis, defined as the accumulation of excess phospholipids in the lysosomes of hepatocytes (4, 16). Various *in vitro* models have been used to study DILI and NAFLD/NASH including primary human hepatocytes (PHH) and immortalised hepatic-like cell lines such as HepaRG™ and HepG2 (17-20). To develop an accurate and deeper understanding of the pathology of NAFLD/NASH and DILI with altered lipid abundance, it is imperative to utilise *in vitro* models that have sufficient metabolic competency and can offer translational insight into *in vivo* steatotic conditions.

In vitro modelling has provided valuable insight into the biochemical changes that occur during the development of NAFLD and NASH. These have included studies demonstrating that increased dietary lipids can lead to lipid accumulation and increased hepatic free fatty acids (FFA). This increase in FFA can induce oxidative stress within cells and enhance inflammatory responses resulting in NASH or liver cirrhosis (17, 21, 22). The most common method to induce steatosis in *in vitro* cultures is by the addition of FFA, such as oleic and palmitic acid, to the culture media (17, 18, 23). However, this method primarily simulates steatosis induced by a high-fat diet and does not adequately emulate other potential causes of NAFLD or NASH. The prevalence and severity of NAFLD and NASH illustrates the need for *in vitro* models that accurately reproduce the relevant histological and metabolic changes that occur in both NAFLD and NASH. To obtain the greatest value from a metabolically competent *in vitro* liver model, sufficiently quantitative and descriptive analytical techniques are required. Metabolomics and lipidomics, which is a subset of metabolomics, have been implemented in classifying several DILI phenotypes and their potential mechanism(s) of injury (24, 25). Characteristic metabolite and lipid profiles can be generated from drug-treated *in vitro* cultures, which can then be used to categorise various drugs by their liver injury phenotype(s) (24, 26). In addition to general phenotypic classifications, metabolomics and lipidomics have been successfully applied to generate lipid fingerprints for different drugs identifying potential diagnostic biomarkers of DILI (27).

In this study, lipid profiles from PHH *in vitro* liver models and hepatocytes from patients diagnosed with NASH were characterised using untargeted liquid chromatography-mass spectrometry (LC-MS) lipidomics. Using these techniques and

multivariate analysis, this study investigated the perturbations to the lipid profile of NASH PHH and compared them to the profiles of healthy control PHH and *in vitro*-induced steatotic (IVIS) PHH. Analysis of the changes to these profiles revealed that the increased total abundance of certain phospholipid classes is characteristic of NASH. Furthermore, untargeted lipidomics and multivariate analysis were used to characterise changes to the lipid profiles of *in vitro* PHH treated with drugs associated with DILI. The changes to the drug-treated lipidomes were assessed using sparse partial least-squares discriminant analysis (sPLS-DA) and receiver operating characteristic (ROC) curve analysis to identify and evaluate potentially predictive lipids for steatotic DILI.

Materials and methods

Materials

Undifferentiated HepaRG™ cells were acquired from Biopredic International under a material transfer agreement and HepaRG™ Maintenance/Metabolism Media was purchased from Biopredic International. Cryoplateable human hepatocytes were acquired from BioIVT along with all QualGro™ Media. Hepatocytes from female donors (BXW, JPR, OSI, and YNM) ranged in age from 48-76 years, while hepatocytes from male donors (GWD, IWM, JHY, and XVN) ranged in age from 46-74 years (Appendix 2). Acetaminophen, amiodarone, diclofenac, ethinyl estradiol, pioglitazone, and ritonavir were acquired from Merck with all except acetaminophen being acquired as pharmaceutical secondary standards. Fialuridine, troglitazone, stavudine, and zidovudine were acquired from Cayman Chemicals. Dimethyl sulfoxide (DMSO), HPLC grade chloroform, HPLC grade butanol (ButOH), LC-MS grade methanol (MeOH), LC-MS grade isopropanol, oleic acid, palmitic acid, and trifluoroacetic acid were also purchased from Merck. LC-MS grade acetonitrile (ACN), 0.25% trypsin-EDTA phenol red, Percoll, Dulbecco's phosphate buffer saline (PBS), chenodeoxycholic acid (CDCA), formic acid, Hoechst 33342, Alexa Fluor™ 488, BODIPY 493/503, and saponin were purchased from ThermoFisher Scientific. Ammonium carbonate was purchased from Rowe Scientific. Matrigel® was purchased from Bio-Strategy.

Cell Culture

Undifferentiated HepaRG™ cells were acquired from Biopredic International under a material transfer agreement. HepaRG™ cells were cultured in a T75 Culture Flask (Corning®) and differentiated per the supplier's protocol. On day 0, differentiated

HepaRG™ cells were passaged using 0.25% w/v trypsin-EDTA (Gibco™). The cells were plated on either 24- or 96-well BioCoat™ Collagen I-coated plates (Corning®) with $4x10^5$ and $0.8x10^5$ cells seeded per well, respectively. Media was changed every 2-3 days with the cells overlaid on day 3 using HepaRG™ Maintenance/Metabolism Media supplemented with 0.25 mg/mL of Matrigel® (Corning® – 356234) and used for experimentation on day 7.

Transporter Certified™ cryoplateable human hepatocytes (BioIVT) were thawed and transferred to a 50 mL Falcon Conical Centrifuge tube containing 45 mL of QualGro™ Thawing Media (BioIVT) that included 30% v/v Percoll® (ThermoFisher Scientific). This was centrifuged at 100 *g* for 8 min. The QualGro™ Thawing Media was aspirated and the cell pellet was resuspended in QualGro™ Seeding Media (BioIVT) at $0.8\ x10^6$ cells/ml. The human hepatocytes were plated onto either 24- or 96-well collagen I-coated plates with $4x10^5$ and $0.56\ x10^5$ cells seeded per well, respectively. Media was changed daily with hepatocytes overlaid on day 1 using QualGro™ Overlay Media (BioIVT) supplemented with 0.25 mg/mL of Matrigel®; sandwich-cultured hepatocytes were used for experimentation on day 4.

Fluorescent imaging of steatosis and phospholipidosis

Day 7 differentiated HepaRG™ cells and day 4 primary human hepatocytes (PHH) cultured on 96-well plates were incubated in compound-containing media for 24 hours (Table 1). The drug treatment concentrations used were the highest concentrations that were determined to be sub-toxic based on an in vitro C-DILI™ hepatotoxicity study (Appendix 3). Controls were treated with 0.1% v/v DMSO.

Table 1: Treatment Concentrations for HepaRG and Primary Human Hepatocytes (PHH)

Treatment Compound	**Treatment Concentration (µM)**	
	HepaRG	***PHH***
Acetaminophen	1000	1000
Amiodarone	25	12.5
Diclofenac	250	50
Ethinyl Estradiol	100	25
Fialuridine	100	100
Pioglitazone	250	100
Ritonavir	50	25
Stavudine	125	125
Troglitazone	100	10
Zidovudine	125	125
Free fatty acids *	1000	1000

*Free fatty acid mixture contained oleic acid and palmitic acid at a ratio of 2:1

After incubation, cells were fixed with 4% w/v paraformaldehyde in PBS for 15 min and then stained for 30 min with 2 µg/mL BODIPY 493/503 (Invitrogen™), 1 µg/ml Hoechst 33342 (ThermoFisher Scientific), and 4 µg/ml Alexa Fluor™ 488 (ThermoFisher Scientific) in 0.05% w/v saponin (ThermoFisher Scientific) to stain the vesicular neutral lipids, nuclei, and actin filaments, respectively. Intracellular vesicular lipid abundance was determined with an Operetta® high-content imaging system (PerkinElmer®) and Harmony high-content imaging and analysis software 4.8 using total lipid area per total cell area determined based on the BODIPY 493/503 lipid staining and Alexa Fluor™ 488 cell

staining. A significant increase in intracellular vesicular lipid abundance was determined by comparing treatment conditions to control with a one-way analysis of variance (ANOVA).

DILI drug treatment and lipid extraction

PHH cultured on a 24-well plate were treated with compounds at the concentrations listed above in Table 1. Drug treatments used concentrations that were the highest concentrations that were determined to be sub-toxic based on an *in vitro* C-DILI™ hepatotoxicity study (Appendix 3). Controls were treated with 0.1% v/v DMSO. Following the 24-hour incubation, the media was aspirated, and the cells were washed three times with 1 mL PBS. The cells were collected from the well by the addition of 350 µL MeOH:ddH_2O (6:1) and scraping with a pipette tip. The cells were then transferred to a Safe-Lock microcentrifuge tube (Eppendorf®) containing 100 µL of chloroform to produce a monophasic 2:6:1 chloroform:methanol:water (C:M:W) extraction mixture. To collect any residual metabolites or cell debris, the wells of the plate were washed with 1 mL of BuOH:MeOH (3:1), transferred to another microcentrifuge tube and dried to completion using a CentriVap Benchtop Centrifugal Vacuum Concentrator (Labconco). The dried BuOH:MeOH extraction was reconstituted using the C:M:W extraction mixture to consolidate the extracted lipids. This pooled extraction mix was centrifuged at 21,600 *g* for 10 min to pellet any insoluble components and then the supernatant was dried and reconstituted in 100 µL of BuOH:MeOH:ddH_2O (9:9:2) and centrifuged at 21,600 *g* for 10 min at 4 °C.

Lipid extraction of clinical and in vitro-induced steatotic PHH samples

IVIS PHH were generated by supplementing the culture media with a proprietary mixture of lipids (QualGro-FTL) from BioIVT on day 1 and cultured as previously described using supplemented media until day 5. On day 5, lipids were extracted by the addition of 320 µL MeOH and scraping with a pipette tip. The PHH were then transferred to a microcentrifuge tube containing 640 µL of chloroform to produce a 960 µL solution of MeOH:CCl_4 (1:2). Preparation of the sample continued as previously described.

PHH that were collected from healthy controls and patients presenting with NASH were supplied by BioIVT. The PHH were thawed and made into a cell suspension of $0.8x10^6$ cells/mL. From this suspension, 625 µL ($0.5x10^6$ cells) was transferred into microcentrifuge tubes. The PHH were pelleted at 21,600 *g* for 10 min, the media was aspirated, and the cells were washed with 1 mL of PBS three times. Lipids were extracted by the addition of 960 µL of methanol:chloroform (1:2). After addition of the extraction solution, the NASH PHH were treated the same as the IVIS PHH.

Liquid chromatography-mass spectrometry lipidomics analysis

Lipidomic samples were analysed in an untargeted manner using reverse phase chromatography with high resolution mass spectrometry as described previously (28). The samples were injected using an Ultimate U3000 LC system fitted with a C8 Ascentis Express® column (2.7 µm, 2.1 by 100 mm; Merck®) at 40° C with an injection volume of 10 µL. Chromatography was performed using 40% aqueous isopropanol with 8 mM ammonium carbonate and 2 mM formic acid (A) and 98% aqueous isopropanol with 8 mM ammonium carbonate and 2 mM formic acid (B) as the mobile phases. A 30-min

gradient at a flow rate of 0.2 mL/min was run starting at 0% B increasing stepwise to 100% B over 25 min followed by a 2-min wash at 100% B and a 3-min re-equilibration phase at 0% B. The samples were detected by Q-Exactive Orbitrap MS (ThermoFisher Scientific). A mass range of 140 to 1,300 *m/z* was used over the full 30 min with a mass resolution of 70,000 used for both ranges.

LC-MS data were processed in a targeted manner using IDEOM software to perform targeted identification of glycerolipids, fatty acids, and phospholipids based on accurate mass and retention time from the IDEOM database (29). The LC-MS raw file conversion was performed using ProteoWizard and XCMS (30, 31). Mzmatch.R was then used for alignment and filtering of peaks with an intensity cut-off of 100,000, relative standard deviation of less than 0.8, and peak shape noise filter of greater than 0.8 (32). Relative quantification of LC-MS peaks was based on peak height, and total ion current (TIC) for each lipid class was calculated by the sum of peak heights for all detected putative lipids in that class.

Statistical analysis

One-way ANOVA with *post hoc* Dunnett's test was performed using GraphPad Prism 7. Principal component analysis (PCA), partial least squares discrimination analysis (PLS-DA), sparse PLS-DA (sPLS-DA) and receiver operating characteristic (ROC) curve analysis was performed using MetaboAnalyst 5.0 (33).

Results

Comparative analysis of lipid profiles in hepatocytes from patients with NASH and IVIS PHH

The comparison of NASH to healthy control and IVIS PHH was performed to identify differences in the lipid profiles that were markers of NASH. IVIS PHH were included to identify differences that may have resulted primarily from exposure to a high-fat environment. Untargeted lipidomics using reverse-phase exact mass LC-MS analysis identified 374 lipids including 20 fatty acids, 150 glycerolipids, and 224 phospholipids. For the NASH PHH, the mean abundance of 149 lipids exhibited a >2-fold increase compared to control, and 42 lipids exhibited a >2-fold decrease. In comparison, the IVIS samples exhibited 58 lipids that had a >2-fold increase and 47 that had a >2-fold decrease in abundance (Fig. 1A). For NASH PHH, 49 neutral lipids (FFA and glycerolipids) were increased in abundance and 31 were decreased in abundance. For IVIS PHH, 52 neutral lipids increased and 4 decreased in abundance (Fig. 1B). There was a significant increase in phospholipids in the lipidome of NASH PHH; 100 phospholipids were increased in abundance and only 11 phospholipids were decreased in abundance (Fig. 1B).

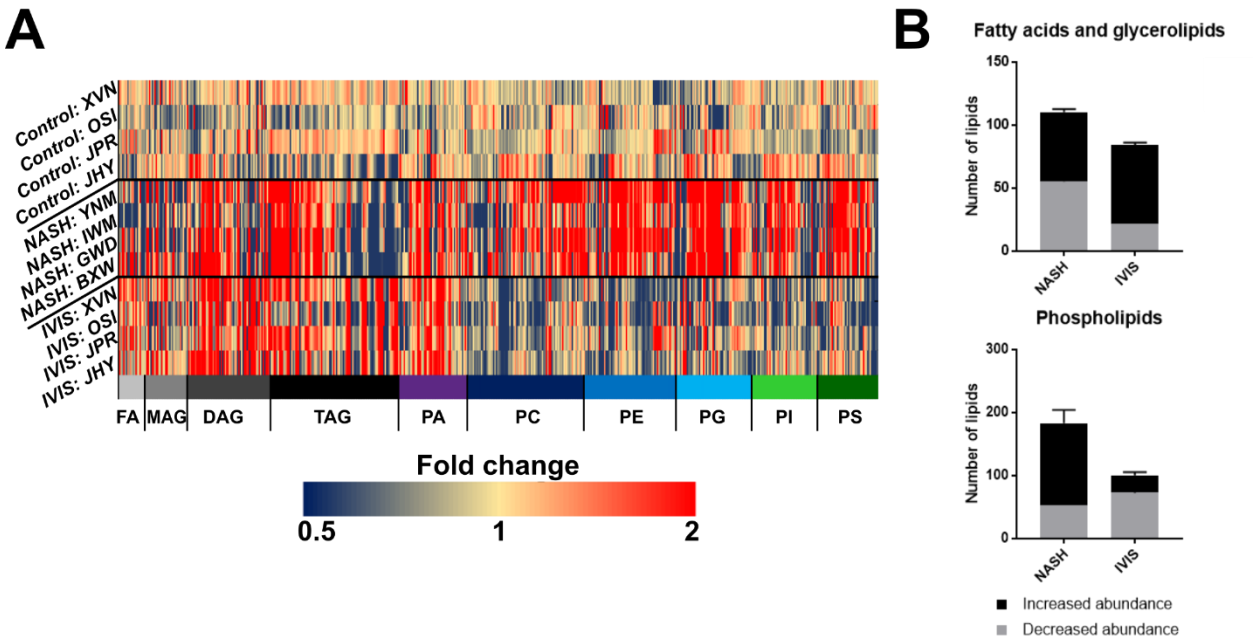

Figure 1: Comparison of untargeted lipidomic profiles in primary human hepatocytes (PHH) from patients with non-alcoholic steatohepatitis (NASH), healthy controls, and control PHH with *in vitro*-induced steatosis (IVIS). (A) Heatmap of all identified lipids across the fatty acid, glycerolipid, and phospholipid classes with rows grouped by lipid class and then by increasing molecular mass of lipids. The heatmap shows the fold-change in abundance compared to mean abundance in control donors for each lipid species. Red, increased abundance; yellow, unchanged abundance; blue, decreased abundance. (B) Total number of lipids for each donor that shows a >2-fold increase or decrease in lipid abundance compared to the mean abundance in control donors for each lipid species.

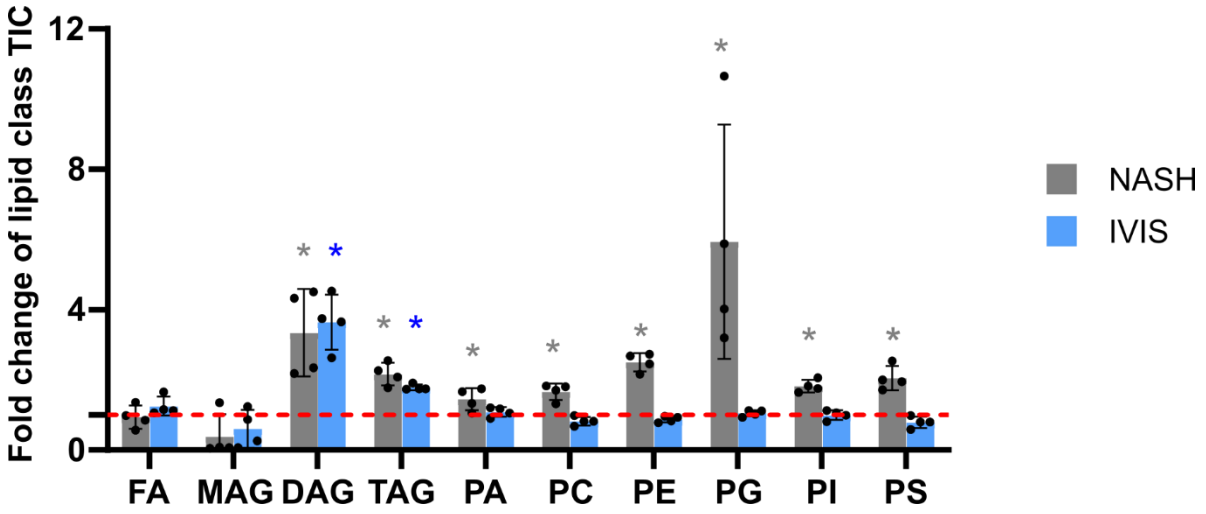

Figure 2: Fold change in total ion current (TIC) of lipid classes in primary human hepatocytes (PHH) from patients with non-alcoholic steatohepatitis (NASH) and PHH with *in vitro*-induced steatosis (IVIS) compared to control. The fold change in TIC of the fatty acid (FA), monoglyceride (MAG), diglyceride (DAG), triglyceride (TAG), Phosphatidic acid (PA), Phosphatidylcholine (PC), phosphatidylethanolamine (PE), phosphatidylglycerol (PG), phosphatidylinositol (PI), and phosphatidylserine (PS) lipid classes was generated by the summation of the peak intensities for each lipid species in a given lipid class for NASH PHH and IVIS SCHH compared to control SCHH. One-way ANOVA was used to determine statistically significance differences, * p-value ≤ 0.05.

In contrast, in IVIS PHH, 6 phospholipids were increased in abundance and 43 phospholipids were decreased. The total change to lipid class abundance was determined by the change observed in TIC for a given lipid class (Fig. 2). Diglycerides (DAG) and triglycerides (TAG) were significantly increased in total abundance compared to control for both NASH (DAG: 3.3-fold, TAG: 2.2-fold increase) and IVIS PHH (DAG: 3.6-fold, TAG: 1.8-fold increase). However, several classes of phospholipids only showed an increase in abundance for NASH PHH. Phosphatidic acid (PA), Phosphatidylcholine (PC), phosphatidylethanolamine (PE), phosphatidylglycerol (PG), phosphatidylinositol (PI), and phosphatidylserine (PS) all exhibited significant increases in their total class abundance in NASH PHH ranging from a 1.4-fold to a 5.9-fold increase in lipid class TIC.

Multivariate analysis of NASH-related lipids

The lipidomics data generated were processed into two separate lipid datasets, which were grouped as fatty acids and glycerolipids in one dataset and phospholipids in the other. The ‘Fatty acids and glycerolipids’ dataset contained 150 lipids and the ‘Phospholipids’ dataset contained 224 lipids. PCA plots of the two datasets showed that the *in vivo* NASH PHH strongly separated from both the control and IVIS samples over principal component 1 for both datasets (Fig. 3A). This suggests that there are significant differences in the lipid profile of NASH PHH compared to healthy PHH that was not reproduced by culturing PHH in a high-fat environment. While the presence of NASH appeared to be the primary factor for separation across the ‘Fatty acids and glycerolipids’ dataset for principal component 1, it should be noted that there was a donor-dependent effect. NASH PHH donors YNM and IWM demonstrated a noticeable separation from donors BXW and GWD (Fig. 3A). PLS-DA (Fig. 3B) was performed to generate a set of important feature lipids from component 1 for both datasets (Fig. 3C). These lipids strongly contributed to the differences observed in the lipid profiles of NASH PHH compared to control and IVIS PHH lipid profiles. While the PLS-DA scores plot for both datasets demonstrated separation of NASH PHH from control and IVIS PHH across component 1, the phospholipid dataset demonstrated a much stronger separation between NASH and IVIS PHH. For component 1 of the ‘Fatty acids and glycerolipids’ dataset, 66% (31/47) and 21% (9/47) of lipids with a variable importance in projection (VIP) score ≥ 1 were TAGs and DAGs, respectively. For component 1 of the ‘Phospholipids’ dataset, the PG, PE, and PC lipid classes had the most significant contribution to the variance in lipid profiles between NASH PHH, and control and IVIS

PHH. For the ‘Phospholipids’ dataset, 31% (17/55), 31% (17/55) and 20% (11/55) of phospholipids with a VIP score ≥ 1were PC, PG and PE, respectively (Appendix 6).

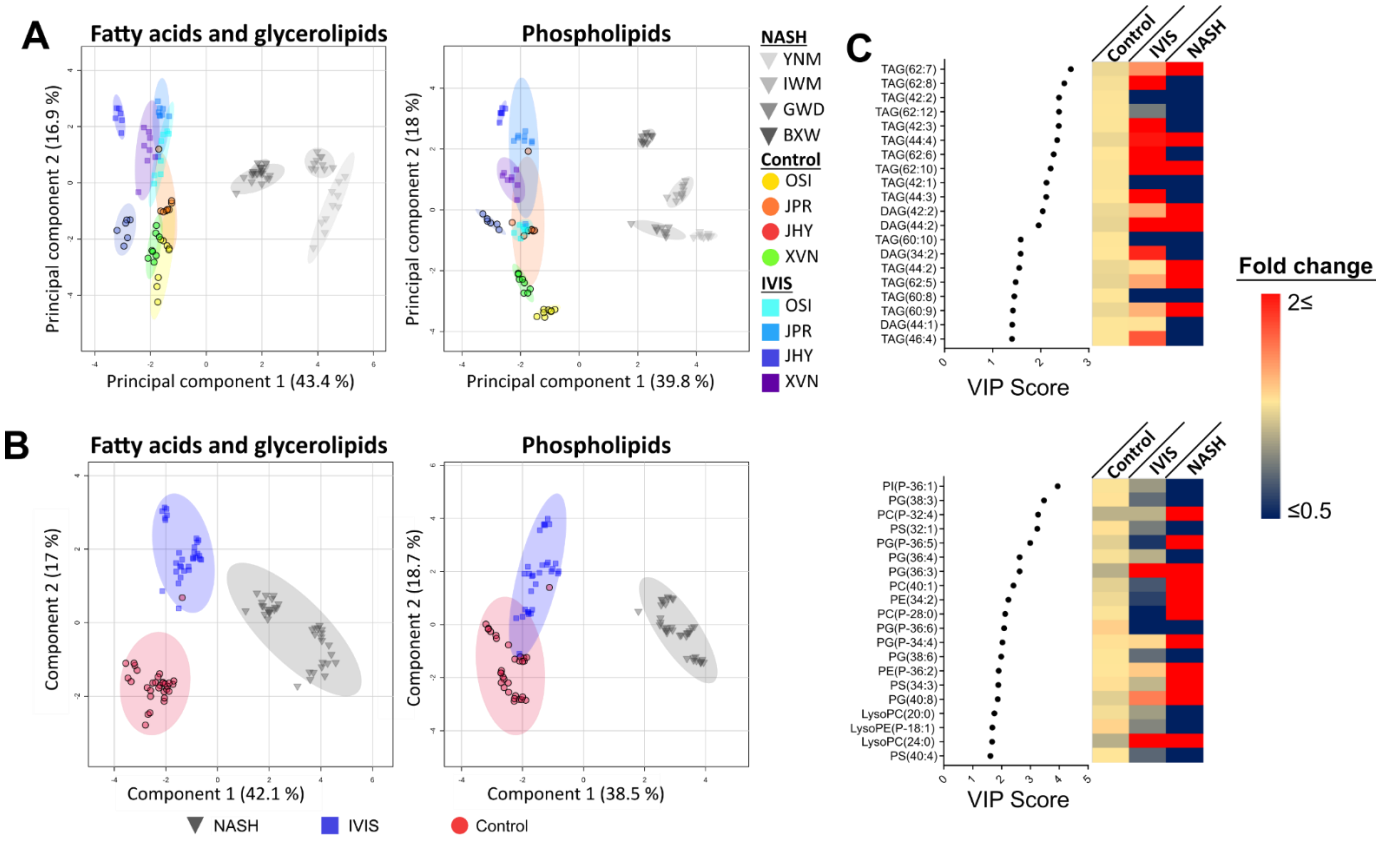

Figure 3: Multivariate analysis of LC-MS lipidomics profiles of non-alcoholic steatohepatitis (NASH), healthy controls, and control primary human hepatocytes (PHH) with *in vitro*-induced steatosis (IVIS). (A) Principal component analysis (PCA) plot of PHH lipids was separated into two datasets of 'Fatty acids and glycerolipids', and 'Phospholipids'. PHH samples were grouped by condition and donor: NASH (BXW, GWD, IWM, YNM), control (JHY, JPR, OSI, XVN), and IVIS (JHY, JPR, OSI, XVN). (B) Partial least squares-discriminant analysis (PLS-DA) scores plot of PHH lipids was separated into two datasets: fatty acids and glycerolipids, and phospholipids. PHH samples were grouped by condition. (C) List of top 20 important lipids by variable's importance in projection (VIP) scores and heatmap of relative abundance of component 1 from both datasets. Heatmap shows maximum change at 2-fold increase (red) or decrease (blue). PCA and PLS-DA analysis were performed using MetaboAnalyst 5.0.

BODIPY plate assay of DILI drug panel for identification of in vitro steatotic-DILI

In order to determine whether a combination of lipidomics and multivariate analysis could generate a set of lipids that could discriminate between healthy hepatocytes, steatotic DILI, and steatosis induced by culturing in a high-fat environment, a panel of DILI-associated drugs were selected from clinical reports and previous literature. Acetaminophen, amiodarone, diclofenac, ethinyl estradiol, fialuridine, pioglitazone, ritonavir, stavudine, troglitazone, and zidovudine were selected due to their reported association with DILI (34-41). A 1 mM FFA treatment was used as a positive control, which simulates a high-fat environment. BODIPY staining of neutral lipids was performed after HepaRG™ and PHH were treated with the DILI-associated drugs to determine their steatogenic potential (Fig. 4). Method validation was conducted with HepaRG™ cells, which showed tolerance to relatively high drug concentrations before loss of cell viability (Appendix 3). Lower treatment concentrations were used for PHH than HepaRG™ cells due to cell viability concerns.

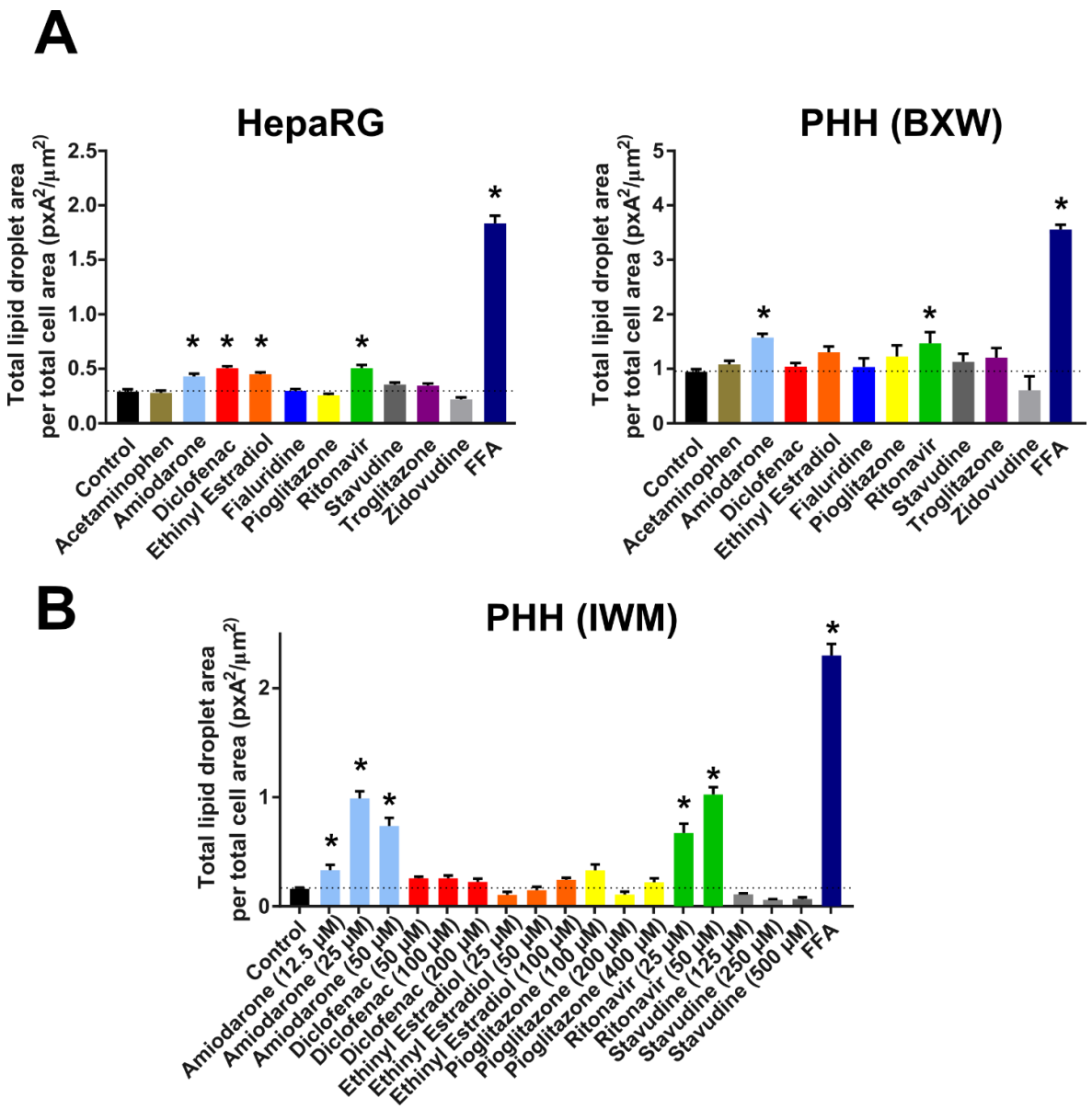

Figure 4: BODIPY staining of HepaRG cells and primary human hepatocytes (PHH) for *in vitro* drug-induced intracellular lipid accumulation. Cellular staining was performed using BODIPY 493/503, Hoechst 33342, and Alexa Fluor™ 488 to stain vesicular neutral lipids, nuclei, and actin filaments, respectively. The cells were imaged using an Operetta® high-content imaging system with image analysis performed using Harmony high-content imaging and analysis software 4.8. (A) Screening of DILI-associated drugs in both HepaRG cells and PHH. Donor BXW was used for initial PHH analysis. (B) Effect of concentration on drug-induced intracellular lipid accumulation. Donor IWN was used for concentration-dependent analysis. Dotted line indicates level of untreated control. Significant changes from control were determined by one-way ANOVA, * p- value ≤ 0.05.

Amiodarone (25 µM), diclofenac (250 µM), ethinyl estradiol (100 µM) and ritonavir (50 µM) demonstrated a significant increase in lipid accumulation in HepaRG™ cells (Fig. 4A). However, the PHH donor BXW only demonstrated a significant increase in lipid accumulation for the amiodarone (12.5 µM) and ritonavir (25 µM) treatments. To assess the concentration dependence and whether the initial treatment concentrations of diclofenac and ethinyl estradiol were insufficient, the study was repeated in PHH using donor IWM at multiple concentrations (1x, 2x, and 4x the initial treatment concentrations) for amiodarone, diclofenac, ethinyl estradiol, pioglitazone, and stavudine (Fig. 4B). However, only 1x and 2x the initial ritonavir concentration was used due to solubility limitations. Pioglitazone and stavudine were included as negative controls. Compared to control, amiodarone and ritonavir increased lipid accumulation by up to 6.2- and 6.4-fold, respectively, with an apparent concentration dependence. Ethinyl estradiol showed a concentration-dependent trend of lipid accumulation, with a 2.3-fold increase in lipid accumulation when comparing the lowest and highest treatment concentrations, although lipid accumulation failed to reach statistical significance compared to control. Interestingly, no significant lipid accumulation across the three treatment concentrations was observed for diclofenac.

Identification of intracellular lipids predictive of steatotic-based liver injury

Based on the BODIPY data, amiodarone and ritonavir were considered steatogenic. Untargeted MS lipidomics was used to analyse the lipid profiles of PHH treated with amiodarone and ritonavir. Lipidomics analysis identified noticeable changes in the lipidome of PHH (BXW and XVN donors) following treatment with amiodarone and ritonavir (Fig. 5A). While both drugs caused similar increases in lipid accumulation in the BODIPY study, the overall changes in the lipid profiles between

amiodarone and ritonavir were noticeably different. Ritonavir decreased the abundance of a large portion of lipids relative to control with increases occurring primarily in long-chain TAG and lysophospholipids. Amiodarone showed similar increases in long-chain TAG and lysophospholipids. In addition, amiodarone increased the abundance of medium-chain TAG, DAG, and phosphatidic acid. The changes observed after amiodarone treatment showed greater similarity to the lipid profiles of the diclofenac and ethinyl estradiol drug treatments. Additionally, there were indications of interdonor variability in the changes to the lipidome in response to drug treatment. A larger number of lipids decreased to a greater degree in donor BXW, and a larger number of lipids increased to a greater degree in donor XVN across the amiodarone and ritonavir drug treatments (Fig. 5A).

An sPLS-DA plot, using the lipidomics data from both PHH donors, was generated using ten metabolites per component. This analysis was conducted to identify the lipid species that showed the greatest variance between control, FFA-treated, and steatotic DILI PHH (amiodarone- and ritonavir-treated PHH) (Fig. 5B). Based on the sPLS-DA plot, component 1 had a strong capacity to differentiate FFA-treated PHH from control and DILI PHH. In contrast, component 2 showed some capacity to differentiate DILI and control PHH, but minimal capacity to differentiate FFA-treated PHH from either. A ROC curve analysis was performed using the ten lipids from component 1 and 2 to generate a set of predictive lipids for distinguishing steatotic DILI (DILI PHH) from healthy controls (control PHH) and high-fat-induced steatosis (FFA-treated PHH). Using the combined donor dataset, an area under the curve (AUC) of 0.993 was achieved (95% CI: 0.893-1) when differentiating DILI from control PHH, indicating that these 20 lipids were strongly predictive of steatotic DILI (Fig. 5C). The lipidomics data of PHH treated with diclofenac, ethinyl estradiol,

fialuridine, and FFA were then used to further test the predictive capacity of this model. The model was able to correctly identify FFA-treated PHH as negative for steatotic DILI in 100% of replicates with a mean probability of 0.9978 for the BXW donor and 0.9995 for the XVN donor (Table 1). The diclofenac and ethinyl estradiol treatments were determined to be positive for inducing steatotic DILI in 75% of the BXW donor replicates with a mean probability of 0.7769 and 0.8696, respectively (Table 1). However, for the XVN donor, the model only determined diclofenac to be capable of inducing steatotic DILI in 50% of replicates with a mean probability of 0.5682. For the XVN donor, ethinyl estradiol was not determined to be steatogenic. Fialuridine was predicted to be negative for steatotic DILI in 100% of replicates for both donors with a mean probability of 0.9962 for the BXW donors and 0.8689 for the XVN donor. Using ROC curve analysis, the capacity for each lipid from component 1 and 2 to distinguish DILI from control and FFA-treatment was assessed for each drug treatment (Table 2). In addition, the NASH PHH lipidome also was assessed using these lipids and ROC curve analysis with comparisons to control PHH and IVIS PHH lipid profiles.

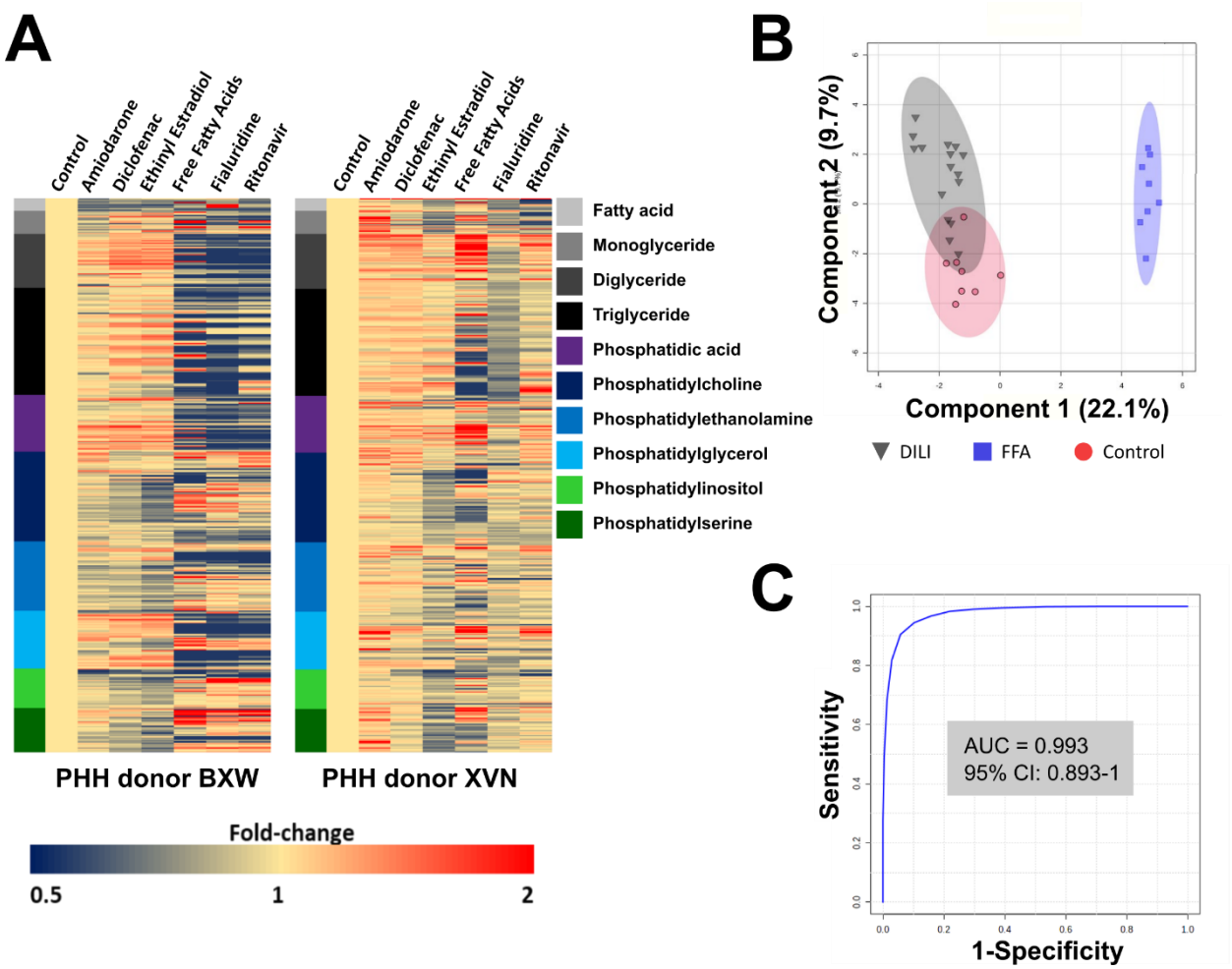

Figure 5: Lipidomics heatmap and multivariate analysis of drug-treated PHH. PHH were treated with amiodarone, diclofenac, ethinyl estradiol, FFA, fialuridine and ritonavir for a 24-hour period. Lipids were extracted and analysed using untargeted LC-MS lipidomics. (A) Heatmap of PHH donor BXW and XVN lipid profiles following drug treatment. Red, increased abundance; yellow, unchanged abundance; blue, decreased abundance. (B) Using combined PHH dataset (donors BXW and XVN), a sparse partial least squares-discriminant analysis (sPLS-DA) of lipids from control PHH (red), DILI PHH (grey) (amiodarone- and ritonavir-treated PHH), and FFA-treated PHH (blue). sPLS-DA components contained ten lipids for each component. (C) Receiver-operating characteristic (ROC) curve analysis of classification performance using component 1 and 2 lipids from the sPLS-DA to generate a predictive model, which was assessed for the ability to separate DILI PHH samples from control PHH samples. Lipidomics data were normalised with the mean control of the respective donor for each lipid species. sPLS-DA and ROC curve analysis was performed using MetaboAnalyst 5.0.

Table 1: ROC curve analysis predictive classification of drug-treated PHH using lipids selected from sPLS-DA. The sPLS-DA component 1 and 2 lipids were used to generate a predictive model for identifying steatotic DILI using the amiodarone- and ritonavir-treated PHH lipid profiles as a training data set. Diclofenac, ethinyl estradiol, and fialuridine drug treatments, with FFA as a negative control, were used as the test data set and classified using this model. The correct prediction is given as the fraction of total replicates to which the designation matches the expected classification. The mean probability was calculated from the individual replicates' classification probabilities for correctly classified replicates. ROC curve predictive modelling was performed using MetaboAnalyst 5.0.

		Correct Prediction		**Mean Probability**	
Treatment Condition	**Expected classification**	***BXW***	***XVN***	***BXW***	***XVN***
Diclofenac	DILI (Steatotic)	3/4	2/4	0.7769	0.5682
Ethinyl Estradiol	DILI (Steatotic)	3/4	0/4	0.8696	-*****
FFA	Non-DILI (Steatotic)	4/4	4/4	0.9978	0.9995
Fialuridine	Non-DILI (Steatotic)	4/4	4/4	0.9962	0.8689

***** Mean probability for ethinyl estradiol treatment of XVN PHH could not be calculated as no replicates gave the expected classification based on lipidomics data and published literature.

When using component 1 lipids to compare drug-treated PHH to FFA-treated PHH, all drug treatments, except fialuridine, were able to achieve a ROC curve AUC of 1.00 with the ROC curve AUC of fialuridine ranging from 0.75 to 1.00 depending on the lipid. The $\log_2$(fold change) of all drug treatments showed a consistent trend across all ten lipids. However, the lipids showed a poorer performance for NASH PHH with only five of the ten lipids detected and ROC curve AUC values ranging from 0.56 to 0.95. In addition, two of the five lipids showed the opposite trend in $\log_2$(fold change) compared to the drug treatments. When using component 2 lipids to compare drug-

treated PHH to healthy control PHH, the ROC curve AUC values for the lipids showed greater variability across all treatments with amiodarone, ritonavir, diclofenac, ethinyl estradiol, and fialuridine having AUCs ranging from 0.70-0.92, 0.72-1.00, 0.55-0.97, 0.67-1.00, and 0.58-1.00, respectively. The trend in the $\log_2$(fold change) for four of the ten lipids was consistent across all drug treatments. For amiodarone and ritonavir, the positive steatotic DILI controls, nine of the ten lipids showed a consistent trend. LysoPG(24:0), however, showed an opposing trend in its $\log_2$(fold change) for amiodarone and ritonavir. LysoPG(24:0) increased for the amiodarone treatment and decreased for the ritonavir and other drug treatments. Diclofenac had the same trend in $\log_2$(fold change) as amiodarone and ritonavir for the other nine lipids. Ethinyl estradiol shared a trend in $\log_2$(fold change) with amiodarone and ritonavir for seven of the other nine lipids. Finally, fialuridine demonstrated the fewest similarities to the changes observed in amiodarone and ritonavir with only five of the other nine lipids showing consistent trends. Ethinyl estradiol and fialuridine showed a decrease in PG(36:1), which deviated from the increase observed for amiodarone and ritonavir. Additionally, PS(32:1) deviated from the changes observed with amiodarone and ritonavir for the ethinyl estradiol treatment and LysoPE(P-24:1), PA(P-36:5) and TAG(46:0) deviated for the fialuridine treatment. Component 2 demonstrated marginally better performance than component 1 for NASH PHH with eight of the ten lipids from component 2 detected in the lipidome of NASH PHH. Additionally, five of the eight detected lipids in the lipidome of NASH PHH demonstrated the same trends as those in PHH after treatment with amiodarone and ritonavir.

Table 2: Combined PHH (donors BXW and XVN) ROC curve AUC values and Log_2(fold change) of sPLS-DA component 1 and 2 lipids for drug-treated PHH and combined NASH PHH. The ROC curve AUC value for the 20 lipids from the sPLS-DA component 1 and 2 are shown when comparing drug treatments to free fatty acids (FFA; component 1) and to control (component 2). Log_2 (fold change) values show the mean change in abundance after drug treatment compared to FFA and control for component 1 and 2, respectively. The NASH PHH lipidome also was assessed using these lipids and ROC curve analysis with comparisons to control PHH and IVIS PHH lipid profiles. Positive log_2 (fold change) values describe an increase in lipid abundance while negative values describe a decrease in lipid abundance. The lipid of components 1 and 2 were from the fatty acid, monoglyceride (MAG), triglyceride (TAG), phosphatidic acid (PA), phosphatidylcholine (PC), phosphatidylethanolamine (PE), phosphatidylglycerol (PG), phosphatidylinositol (PI), and phosphatidylserine (PS) lipid classes. Lipidomics data were normalised with the mean control of the respective donor for each lipid species, and ROC curve analysis was performed using MetaboAnalyst 5.0 with the steatotic DILI training data set shown in bold. N/D: not detected.

	ROC curve AUC						**Log_2 (fold change)**					
	Amiodarone	**Ritonavir**	Diclofenac	Ethinyl estradiol	Fialuridine	NASH	**Amiodarone**	**Ritonavir**	Diclofenac	Ethinyl estradiol	Fialuridine	NASH
Component 1	***Drug treatment vs FFA***											
TAG(64:7)	**1.00**	**1.00**	1.00	1.00	0.94	N/D	**3.6**	**4.1**	3.6	3.2	2.3	N/D
TAG(62:9)	**1.00**	**1.00**	1.00	1.00	1.00	N/D	**4.1**	**4.1**	3.9	3.9	2.7	N/D
TAG(64:8)	**1.00**	**1.00**	1.00	1.00	0.75	N/D	**3.7**	**4.0**	3.5	3.2	1.3	N/D
TAG(64:6)	**1.00**	**1.00**	1.00	1.00	0.94	N/D	**0.9**	**4.0**	3.8	3.5	2.5	N/D
TAG(62:11)	**1.00**	**1.00**	1.00	1.00	0.81	N/D	**3.6**	**3.3**	3.6	3.7	1.7	N/D
MAG(16:1)	**1.00**	**1.00**	1.00	1.00	1.00	0.78	**-1.7**	**-2.5**	-2.0	-2.2	-2.1	-0.7
Oleic acid	**1.00**	**1.00**	1.00	1.00	1.00	0.74	**-1.9**	**-2.7**	-2.2	-2.4	-2.3	-0.7
TAG(62:10)	**1.00**	**1.00**	1.00	1.00	0.88	0.58	**3.6**	**3.5**	3.7	3.6	2.0	-0.4
TAG(54:3)	**1.00**	**1.00**	1.00	1.00	1.00	0.56	**-1.5**	**-1.7**	-1.5	-1.5	-1.8	-0.2
TAG(62:8)	**1.00**	**1.00**	1.00	1.00	0.95	0.95	**4.0**	**4.2**	4.0	3.9	2.7	-2.6

Component 2	***Drug treatment vs Control***											
LysoPG(24:0)	**0.84**	**1.00**	0.94	0.95	0.91	N/D	**0.3**	**-1.1**	-0.5	-0.7	-0.5	N/D
LysoPI(P-20:0)	**0.81**	**1.00**	0.97	1.00	0.92	0.64	**-0.4**	**-0.9**	-0.5	-0.6	-0.4	-0.7
PS(32:1)	**0.92**	**1.00**	0.70	0.83	1.00	1.00	**0.3**	**0.9**	0.1	-0.5	0.7	3.2
LysoPI(P-20:1)	**0.73**	**1.00**	0.94	0.98	0.94	N/D	**-0.4**	**-1.0**	-0.5	-0.7	-0.5	N/D
Linoleic acid	**0.78**	**0.94**	0.83	0.89	0.84	0.62	**-0.4**	**-0.9**	-0.4	-0.6	-0.5	-0.6
LysoPE(P-24:1)	**0.91**	**0.91**	0.58	0.67	0.80	0.77	**0.3**	**0.3**	0.1	0.2	-0.2	0.9
PG(36:1)	**0.84**	**0.80**	0.55	0.73	0.58	0.56	**0.6**	**0.4**	0.1	-0.2	-0.1	-1.1
PA(P-36:5)	**0.78**	**0.94**	0.77	0.83	0.95	0.92	**-0.1**	**-0.3**	-0.1	-0.2	0.3	0.5
TAG(46:0)	**0.81**	**0.72**	0.61	0.75	0.59	0.90	**-0.2**	**-0.1**	-0.1	-0.2	0.0	2.7
PC(P-38:6)	**0.70**	**0.95**	0.67	0.88	0.80	0.88	**-0.2**	**-0.4**	-0.1	-0.4	-0.3	-0.8

Discussion

This study demonstrated that there are significant changes in the lipidome of PHH that occur in patients with NASH compared to healthy controls, and that these changes cannot be replicated by exposure to culture conditions that simulate a high-fat environment, as with IVIS PHH. Furthermore, changes in the hepatocellular lipidome in PHH from patients with NASH demonstrate some similarity to changes in PHH in response to treatment with several of the steatogenic drugs tested in this study. However, the significance of such similarities is unclear as the *in vivo* NASH PHH were obtained without a known causative factor. For both conditions, while the abundance and distribution of neutral lipids was impacted, lipidomics and multivariate analysis identified that the most specific and significant lipid changes involved phospholipids.

PHH from patients with NASH have a significantly increased abundance of total PA, PC, PE, PG, PI, and PS compared to IVIS and healthy control PHH, showing up to a 5.9-fold increase compared to healthy control PHH. Additionally, unlike neutral lipids such as DAG and TAG, where a significant increase was observed for the NASH and IVIS PHH, the changes in the abundance of these phospholipid classes were not replicated in the IVIS PHH. These unique, NASH-associated alterations in phospholipids indicate that they may be useful biomarkers for NASH. The impact to the phospholipidome has been reported previously with increased levels of phospholipids occurring in patients with NAFLD and NASH compared to healthy patients (42-44). The total abundance (TIC) of PE and PS increased by up to 2.5- and 2-fold, respectively, compared to control, showing the greatest increase of all the phospholipid classes. A comparable change was detected in the plasma lipidome of NAFLD and NASH patients (42). Healthy subjects had a mean

PE plasma concentration of 170 µg/ml while patients with NAFLD or NASH had mean plasma concentrations of 210 and 250 µg/ml, respectively. For PS, a similar increase was observed with healthy subjects having a mean PS plasma concentration of 95 µg/ml, and NAFLD or NASH patients had a mean plasma concentration of 170 µg/ml (42). These data suggest that the intracellular changes in the lipidome that were observed in patients with NASH may also affect the abundance of plasma phospholipids. These phospholipids may be useful as serum biomarkers for NASH because they are related to intracellular perturbations of the hepatocellular lipidome. However, a limitation of this data is that it does not offer insight into the causative factors of NASH. The NASH samples were supplied with a NASH score and patient characteristics. While this information is valuable, a suspected cause of NASH was not supplied, only that it was not alcohol related. Therefore, there is no known association between the observed NASH and a drug, or any other factor that might be the causative stimuli. Thus, while the increase in phospholipids could be diagnostic of NASH (Fig. 3C), this increase may only represent a general NASH diagnosis and may not be predictive of a specific causative factor.

Untargeted lipidomics and multivariate analysis of *in vitro* lipidomes were used to identify lipids that may be predictive of steatotic DILI. As with the NASH PHH, phospholipids showed a significant capacity to discriminate between healthy PHH and PHH with injury-induced steatosis. Of the lipids identified as discriminatory based on sPLS-DA, eight of the ten lipids identified were phospholipids or lysophopholipids. There was a significant similarity in the changes to the abundance of these phospholipids for amiodarone, ritonavir, diclofenac, and ethinyl estradiol. Most notable based on Fig. 5A was the decrease in abundance of a number of PC and PE phospholipids for PHH donor

BXW. A similar change in plasma PC and PE has been observed after treatment with valproate, a drug reported to induce steatosis in rats and epileptic children (45, 46). Multivariate analysis of the lipidome of rat plasma identified a decrease in certain PC phospholipids that may act as a predictive biomarker for valproate-induced steatotic liver injury (45). Furthermore, linoleic acid, which was identified by the sPLS-DA study to be a potentially discriminatory biomarker for steatotic DILI, was decreased by 24-47% across all drug treatments with a 35% decrease in NASH PHH (Table 2). Linoleic acid has been shown previously to decrease in abundance in liver tissue from NASH patients due to oxidation (47). While linoleic acid may not be solely predictive of steatotic DILI, it may still offer a biomarker for steatosis or NASH induced by increased oxidative stress. However, the other lipids from component 2 showed a poorer performance for NASH PHH with only eight of the ten lipids detected, and five of the eight lipids showed consistent trends in their abundance compared to the drug treatments. This indicates that these ten lipids are unlikely to show the same capacity to identify hepatocytes with NASH.

The sPLS-DA and ROC curve analysis showed that there is a strong potential for lipidomics to identify lipids which are characteristic of steatotic DILI. However, this current study is limited by the small number of PHH donors and drugs determined to be steatogenic. This limits the robustness and confidence in the predictive capacity of the 20 selected lipids. The use of BODIPY to determine a drug's steatogenic capacity was likely a factor that reduced the number of drugs deemed to be steatogenic. From the BODIPY study, only amiodarone and ritonavir appeared to be steatogenic at the selected concentrations over a 24-hour drug treatment. Therefore, only these two drugs were used as positive treatments for steatotic DILI. Yet, upon lipidomics analysis of several drug

treatments, it appeared that diclofenac and ethinyl estradiol also had steatogenic properties (Fig. 5A). This is consistent with observations from animal studies in rats and canines (48-50). Furthermore, for at least the BXW donor, three out of the four diclofenac and ethinyl estradiol replicates were considered positive for steatotic DILI. BODIPY only stains neutral lipids that have accumulated into vesicles. Therefore, it has a limited capacity to characterise more complex forms of altered lipid metabolism, especially regarding phospholipid metabolism. It is likely that the use of BODIPY to screen for steatogenic drugs lacked sensitivity and may have led to false negatives. Additionally, interdonor variability also needs to be addressed. There was notable variation in lipid profiles between donors for both the NASH and the steatotic DILI studies. The fatty acids and glycerolipids PCA plot (Fig. 3A) showed distinct separation of PHH donors YNM and IWM from the GWD and BXW donors. With NASH scores and genders varying in a similar manner between each pairing, the only identified common factor was age. The YNM and IWM donors were in their 40s, while the GWD and BXW donors were in their 70s (Appendix 2). Differences also were seen in the lipidomics heatmaps for the steatotic DILI study (Fig 5A) and the ROC curve analysis predictions (Table 1). This variance is likely due to the well-known phenotypic variations that occur between the proteomes of donors and impacts the metabolic behaviour of hepatocytes (51, 52). While the sPLS-DA study did identify a number of potentially characteristic lipids, a larger number of donors will be required for future studies to overcome the impact of interdonor variability and identify robust and specific lipids that are characteristic of steatotic liver injury.

This study, using untargeted lipidomics, reinforced that phospholipids are characteristically increased in NASH patients and are also increased in *in vitro* PHH after

treatment with steatogenic drugs. All phospholipid classes showed an increased total abundance (TIC) in PHH from NASH patients. This characteristic increase could not be replicated by culturing PHH *in vitro* in a high-fat environment (IVIS PHH). This prominent change to the intracellular phospholipidome of NASH PHH is similar to changes previously seen in the plasma lipidome of NAFLD and NASH patients (42). Furthermore, phospholipids demonstrated the potential to discriminate between steatotic DILI and healthy control PHH. In addition, phospholipids also had some capacity to distinguish steatotic DILI from steatosis induced by exposure to a high-fat environment. Amiodarone and ritonavir were used to identify ten lipids that had some capacity to distinguish healthy control PHH from PHH treated with steatogenic drugs. Of these ten lipids, eight were phospholipids or lysophospholipids. While this study has shown that the increase in cellular phospholipids observed in NASH patients and *in vitro* PHH culutures treated with steatogenic drugs, further investigation is needed. In order to determine if these lipids may offer any predictive capacity for a drugs steatotic nature during drug development, a much larger sample size of steatogenic drugs and PHH donors is required. Identifying lipids with this predictive capacity would be invaluable because it may offer more comprehensive options for toxicological screening during drug development. Furthermore, as there appears to be an intrinsic link between the lipid profiles of serum and hepatocytes, the perturbations to the lipid profiles observed in this study could be used to diagnosis NAFLD/NASH, and to determine whether a drug was a causative factor for inducing steatotic liver injury.

References

1. Younossi ZM, Koenig AB, Abdelatif D, Fazel Y, Henry L, Wymer M. Global epidemiology of nonalcoholic fatty liver disease—meta-analytic assessment of prevalence, incidence, and outcomes. *Hepatology*. 2016;64(1):73-84.
2. Kneeman JM, Misdraji J, Corey KE. Secondary causes of nonalcoholic fatty liver disease. *Therap Adv Gastroenterol*. 2012;5(3):199-207.
3. Dash A, Figler RA, Sanyal AJ, Wamhoff BR. Drug-induced steatohepatitis. *Expert Opin Drug Metab Toxicol*. 2017;13(2):193-204.
4. Anthérieu S, Rogue A, Fromenty B, Guillouzo A, Robin MA. Induction of vesicular steatosis by amiodarone and tetracycline is associated with up-regulation of lipogenic genes in heparg cells. *Hepatology*. 2011;53(6):1895-905.
5. Vitins AP, Kienhuis AS, Speksnijder EN, Roodbergen M, Luijten M, van der Ven LT. Mechanisms of amiodarone and valproic acid induced liver steatosis in mouse in vivo act as a template for other hepatotoxicity models. *Arch Toxicol*. 2014;88(8):1573-88.
6. Ito M, Suzuki J, Sasaki M, Watanabe K, Tsujioka S, Takahashi Y, et al. Development of nonalcoholic steatohepatitis model through combination of high-fat diet and tetracycline with morbid obesity in mice. *Hepatol Res*. 2006;34(2):92-8.
7. Langman G, Hall PM, Todd G. Role of non-alcoholic steatohepatitis in methotrexate-induced liver injury. *J Gastroenterol Hepatol*. 2001;16(12):1395-401.
8. Rabinowich L, Shibolet O. Drug induced steatohepatitis: an uncommon culprit of a common disease. *BioMed Res Int*. 2015;2015:168905.
9. Bjornsson ES, Bergmann OM, Bjornsson HK, Kvaran RB, Olafsson S. Incidence, presentation, and outcomes in patients with drug-induced liver injury in the general population of Iceland. *Gastroenterology*. 2013;144(7):1419-25.
10. Sgro C, Clinard F, Ouazir K, Chanay H, Allard C, Guilleminet C, et al. Incidence of drug-induced hepatic injuries: a French population-based study. *Hepatology*. 2002;36(2):451-55.
11. Suk KT, Kim DJ, Kim CH, Park SH, Yoon JH, Kim YS, et al. A prospective nationwide study of drug-induced liver injury in Korea. *Am J Gastroenterol*. 2012;107(9):1380-7.
12. Kleiner DE, Chalasani NP, Lee WM, Fontana RJ, Bonkovsky HL, Watkins PB, et al. Hepatic histological findings in suspected drug-induced liver injury: systematic evaluation and clinical associations. *Hepatology*. 2014;59(2):661-70.
13. Scott DA, Gholson CF, Netchvolodoff CV, Ray M, Gonzalez E, Bacon BR. Incidental microvesicular steatosis due to valproic acid anticonvulsant therapy. *Am J Gastroenterol*. 1991;86(4):500-2.

14. Utzeri E, Usai P. Role of non-steroidal anti-inflammatory drugs on intestinal permeability and nonalcoholic fatty liver disease. *World J Gastroenterol*. 2017;23(22):3954-63.

15. Dalaklioglu S, Genc GE, Aksoy NH, Akcit F, Gumuslu S. Resveratrol ameliorates methotrexate-induced hepatotoxicity in rats via inhibition of lipid peroxidation. *Hum Exp Toxicol*. 2013;32(6):662-71.

16. Halliwell WH. Cationic amphiphilic drug-induced phospholipidosis. *Toxicol Pathol*. 1997;25(1):53-60.

17. Cui W, Chen SL, Hu KQ. Quantification and mechanisms of oleic acid-induced steatosis in HepG2 cells. *Am J Transl Res*. 2010;2(1):95-104.

18. Gómez-Lechón MJ, Donato MT, Martínez-Romero A, Jiménez N, Castell JV, O'Connor JE. A human hepatocellular in vitro model to investigate steatosis. *Chem Biol Interact*. 2007;165(2):106-16.

19. Saito J, Okamura A, Takeuchi K, Hanioka K, Okada A, Ohata T. High content analysis assay for prediction of human hepatotoxicity in HepaRG and HepG2 cells. *Toxicol In Vitro*. 2016;33:63-70.

20. Wobser H, Dorn C, Weiss TS, Amann T, Bollheimer C, Büttner R, et al. Lipid accumulation in hepatocytes induces fibrogenic activation of hepatic stellate cells. *Cell Research*. 2009;19(8):996-1005.

21. Liu J, Han L, Zhu L, Yu Y. Free fatty acids, not triglycerides, are associated with non-alcoholic liver injury progression in high fat diet induced obese rats. *Lipids Health Dis*. 2016;15(1):27.

22. Dowman JK, Tomlinson JW, Newsome PN. Pathogenesis of non-alcoholic fatty liver disease. *QJM*. 2010;103(2):71-83.

23. Sharma S, Mells JE, Fu PP, Saxena NK, Anania FA. GLP-1 analogs reduce hepatocyte steatosis and improve survival by enhancing the unfolded protein response and promoting macroautophagy. *PLoS One*. 2011;6(9):e25269.

24. García- Cañaveras JC, Castell JV, Donato MT, Lahoz A. A metabolomics cell-based approach for anticipating and investigating drug-induced liver injury. *Sci Rep*. 2016;6(1):27239.

25. Cuykx M, Claes L, Rodrigues RM, Vanhaecke T, Covaci A. Metabolomics profiling of steatosis progression in HepaRG® cells using sodium valproate. *Toxicol Lett*. 2018;286:22-30.

26. Ramirez T, Strigun A, Verlohner A, Huener H-A, Peter E, Herold M, et al. Prediction of liver toxicity and mode of action using metabolomics in vitro in HepG2 cells. *Archives of toxicology*. 2018;92(2):893-906.

27. Goracci L, Valeri A, Sciabola S, Aleo MD, Moritz W, Lichtenberg J, et al. A novel lipidomics-based approach to evaluating the risk of clinical hepatotoxicity potential of drugs in 3D human microtissues. *Chem Res Toxicol*. 2020;33(1):258-70.

28. Aurelio L, Scullino CV, Pitman MR, Sexton A, Oliver V, Davies L, et al. From sphingosine kinase to dihydroceramide desaturase: a structure-activity relationship (SAR) study of the enzyme inhibitory and anticancer activity of 4-((4-(4-chlorophenyl)thiazol-2-yl)amino)phenol (SKI-II). *J Med Chem*. 2016;59(3):965-84.

29. Creek DJ, Jankevics A, Burgess KEV, Breitling R, Barrett MP. IDEOM: an excel interface for analysis of LC–MS-based metabolomics data. *Bioinformatics*. 2012;28(7):1048-49.

30. Chambers MC, Maclean B, Burke R, Amodei D, Ruderman DL, Neumann S, et al. A cross-platform toolkit for mass spectrometry and proteomics. *Nat Biotechnol*. 2012;30(10):918-20.

31. Smith CA, Want EJ, O'Maille G, Abagyan R, Siuzdak G. XCMS: processing mass spectrometry data for metabolite profiling using nonlinear peak alignment, matching, and identification. *Anal Chem*. 2006;78(3):779-87.

32. Scheltema RA, Jankevics A, Jansen RC, Swertz MA, Breitling R. PeakML/mzMatch: a file format, java library, R library, and tool-chain for mass spectrometry data analysis. *Anal Chem*. 2011;83(7):2786-93.

33. Pang Z, Chong J, Zhou G, de Lima Morais DA, Chang L, Barrette M, et al. MetaboAnalyst 5.0: narrowing the gap between raw spectra and functional insights. *Nucleic Acids Res*. 2021.

34. James LP, Mayeux PR, Hinson JA. Acetaminophen-induced hepatotoxicity. *Drug Metab Dispos*. 2003;31(12):1499-506.

35. Donato MT, Martínez-Romero A, Jiménez N, Negro A, Herrera G, Castell JV, et al. Cytometric analysis for drug-induced steatosis in HepG2 cells. *Chem Biol Interact*. 2009;181(3):417-23.

36. Aithal GP, Ramsay L, Daly AK, Sonchit N, Leathart JB, Alexander G, et al. Hepatic adducts, circulating antibodies, and cytokine polymorphisms in patients with diclofenac hepatotoxicity. *Hepatology*. 2004;39(5):1430-40.

37. Simon FR, Fortune J, Iwahashi M, Gartung C, Wolkoff A, Sutherland E. Ethinyl estradiol cholestasis involves alterations in expression of liver sinusoidal transporters. *Am J Pathol*. 1996;271(6 Pt 1):G1043-52.

38. Manning FJ, Swartz MN, National Academies P. Review of the fialuridine (FIAU) clinical trials. 1995.

39. Terelius Y, Figler RA, Marukian S, Collado MS, Lawson MJ, Mackey AJ, et al. Transcriptional profiling suggests that Nevirapine and Ritonavir cause drug induced liver injury through distinct mechanisms in primary human hepatocytes. *Chem Biol Interact*. 2016;255:31-44.

40. Masubuchi Y. Metabolic and non-metabolic factors determining troglitazone hepatotoxicity: a review. *Drug Metab Pharmacokinet*. 2006;21(5):347-56.

41. May LD, Lefkowitch JH, Kram MT, Rubin DE. Mixed hepatocellular-cholestatic liver injury after pioglitazone therapy. *Ann Intern Med*. 2002;136(6):449-52.

42. Ma DWL, Arendt BM, Hillyer LM, Fung SK, McGilvray I, Guindi M, et al. Plasma phospholipids and fatty acid composition differ between liver biopsy-proven nonalcoholic fatty liver disease and healthy subjects. *Nutr Diabetes*. 2016;6(7):e220-e20.

43. García-Cañaveras JC, Donato MT, Castell JV, Lahoz A. A comprehensive untargeted metabonomic analysis of human steatotic liver tissue by RP and HILIC chromatography coupled to mass spectrometry reveals important metabolic alterations. *J Proteome Res*. 2011;10(10):4825-34.

44. Gorden DL, Myers DS, Ivanova PT, Fahy E, Maurya MR, Gupta S, et al. Biomarkers of NAFLD progression: a lipidomics approach to an epidemic. *J Lipid Res*. 2015;56(3):722-36.

45. Goda K, Saito K, Muta K, Kobayashi A, Saito Y, Sugai S. Ether-phosphatidylcholine characterized by consolidated plasma and liver lipidomics is a predictive biomarker for valproic acid-induced hepatic steatosis. *J Toxicol Sci*. 2018;43(6):395-405.

46. Xu S, Chen Y, Ma Y, Liu T, Zhao M, Wang Z, et al. Lipidomic profiling reveals disruption of lipid metabolism in valproic acid-induced hepatotoxicity. *Front Pharmacol*. 2019;10(819).

47. Feldstein AE, Lopez R, Tamimi TAR, Yerian L, Chung YM, Berk M, et al. Mass spectrometric profiling of oxidized lipid products in human nonalcoholic fatty liver disease and nonalcoholic steatohepatitis. *J Lipid Res*. 2010;51(10):3046-54.

48. Obert LA, Sobocinski GP, Bobrowski WF, Metz AL, Rolsma MD, Altrogge DM, et al. An immunohistochemical approach to differentiate hepatic lipidosis from hepatic phospholipidosis in rats. *Toxicol Pathol*. 2007;35(5):728-34.

49. Chahardahcherik M, Shahriari A, Asadian P, Esmaeilzadeh S. Preventive effect of omega-3 fatty acids on ethinyl estradiolinduced hepatosteatosis in female wistar rat. *Iran J Vet Med*. 2013;7(2):129-34.

50. Selvaraj S, Oh JH, Spanel R, Länger F, Han HY, Lee EH, et al. The pathogenesis of diclofenac induced immunoallergic hepatitis in a canine model of liver injury. *Oncotarget*. 2017;8(64):107763-824.

51. Rogue A, Lambert C, Spire C, Claude N, Guillouzo A. Interindividual variability in gene expression profiles in human hepatocytes and comparison with HepaRG cells. *Drug Metab Dispos*. 2012;40(1):151-58.

52. Wiśniewski JR, Vildhede A, Norén A, Artursson P. In-depth quantitative analysis and comparison of the human hepatocyte and hepatoma cell line HepG2 proteomes. *J Proteomics*. 2016;136:234-47.

Chapter 5

Conclusion and future directions

Research Summary

Drug-induced liver injury (DILI) is a constant challenge during drug development and when using medicines for the clinical treatment of patients. DILI has been observed to affect anywhere from 200,000 to 1.8 million individuals annually, however, it is difficult to identify the true prevalence of DILI with up to 94% of adverse drug reactions going unreported (1-6). The avenue with the greatest potential to reduce the development of future drugs that induce DILI, and offer early detection of DILI in patients, is to develop a comprehensive understanding of the mechanism(s) of injury of current DILI-associated drugs. DILI-associated drugs commonly have complicated and multi-faceted mechanism(s) of hepatotoxicity, and a holistic approach that assesses functional changes as well as changes in the abundance of metabolites and proteins is necessary. Multi-omic approaches, especially when using metabolomics, lipidomics, and proteomics, can provide multi-faceted, quantitative, and descriptive analysis of toxicological effects and already has shown significant potential in elucidating the pathways by which drugs cause liver injury (7-11). This thesis has further demonstrated this potential by revealing the impact that DILI-associated drugs can have on the proteome and metabolome of major liver metabolic pathways induced by DILI-associated drugs, characterising the impact of these drugs on bile acid homeostasis, and revealing the perturbations such drugs can induce on the lipidome of PHH.

Characterisation and application of alternative in vitro liver models

The choice of analytical technique is vital to obtaining the greatest amount of information possible, however, the biological model utilised is just as important. *In vitro* models are the most practical, accessible, and ethical platform for performing

toxicological studies, however, not all models are equal. While animal primary hepatocytes may offer a cost-efficient and accessible option, there are a number of limitations that may reduce the translational capacity to *in vivo* human conditions. These limitations can result from variations in metabolic behaviour, bile acid composition, and transporter expression (12-15). The *in vitro* cell type that offers the greatest similarity to human liver tissue is primary human hepatocytes (PHH) (16), although PHH suffer from some limitations including interdonor variability and high costs (17). Therefore, alternatives such as HepaRG™, HuH-7, and HepG2 cells are often used due to the lower cost and accessibility. This thesis characterised the similarities in the proteomes of PHH and HepaRG™ cells, as well as the similarities between PHH from two different donors. While the proteome of HepaRG™ cells did possess similarities to the proteome of PHH, the variations between proteomes indicated that HepaRG™ cells may not be suitable as a ubiquitous surrogate for PHH. However, in Chapter 3 it was demonstrated that for specific studies, alternative cell lines such as HepaRG™ or HuH-7 cells can be successfully used as surrogates for PHH in certain assays such as the C-DILI™ and B-CLEAR® assays. Studies using *in vitro* liver model alternatives provide qualitative information, but precise concentration-response characteristics may vary, as was observed when HepaRG™ cells were used in place of PHH for the C-DILI™ and BODIPY-staining assays. The results of these studies revealed that four drugs demonstrated steatogenic potential for HepaRG™ cells but only two drugs appeared to be steatogenic for PHH. With a plethora of *in vitro* liver models available, including organ-on-a-chip, organoids, HuH-7, HepaRG™, and pluripotent stem cell-derived hepatocyte-like cells, it would be invaluable to compare the proteomes of these models to PHH, and even to liver

tissue itself, to determine which would be most suitable as a surrogate for PHH as an alternative *in vitro* liver model for a given metabolism- or transport-based study. A model system such as 3D PHH spheroid cultures may offer a better in vivo-like metabolic phenotype and improved longevity over 2D sandwich-cultured human hepatocytes, which were used as the primary in vitro liver cell model in this thesis (18). However, transporter expression, localization and function has not been thoroughly examined in 3D PHH spheroid cultures. Furthermore, a significant limitation of 3D PHH spheroid cultures is the cell yield. Where a single well of a 2D culture may yield anywhere from $4x10^4$ to $1x10^6$ cells, a single PHH spheroid may consist of only $1.5x10^3$ cells (19). Performing metabolomics with 3D PHH spheroid cultures would require pooling several wells, as such analytical techniques usually require upwards of $1x10^4$ cells for analysis (20). Due to this requirement, some previous studies have pooled PHH spheroids from over 600 wells to achieve sufficient cell numbers for metabolomics analysis (21). However, with recent advances in single spheroid metabolomics technologies, 3D PHH spheroid cultures may soon become a more practical and viable in vitro model for metabolomics-based studies (22).

Furthermore, while proteomics offers significant insight into the abundance of proteins within a proteome, due to biochemical variations that can affect the functional behaviour of a protein, the proteomic profile may not be completely representative of the functionality of an *in vitro* liver model. Therefore, it would be ideal to perform functional assays for HepaRG™ cells as well as other alternative *in vitro* liver models to gain holistic insight into the metabolic functionality of these alternative models compared to PHH and

liver tissue. While PHH serve as an invaluable *in vitro* model for liver tissue, there are more accessible alternatives that, when used appropriately, can act as surrogates for PHH in toxicological studies allowing for valuable insights at a lower cost. However, in order to make the determination about whether a model is suitable for a given study, it is vital that it is well characterised, especially with regard to the metabolic competency of the proteome.

Multi-omics analysis of metabolic perturbations induced by DILI

The power of multi-omics was demonstrated by its capacity to characterise the biological perturbations to the abundance of metabolites and proteins in response to treatment with drugs associated with DILI. Perturbations to the abundance of metabolites and proteins associated with major metabolic pathways and bile acid metabolism were characterised, which offered insight into the potential mechanisms and progression of various DILI phenotypes including cholestatic DILI. Through multi-omics analysis, perturbations to glucose metabolism, the TCA cycle, and nicotinamide metabolism were identified and associated with the known effects of pioglitazone, troglitazone, and ritonavir on impaired mitochondrial respiration and induction of significant oxidative stress. By combining both metabolomics and proteomics, a greater depth of information was obtained compared to more focused approaches, as the entire metabolic mechanism, including reactive metabolites, catalytic enzymes, and nutrient transporters, were analysed. These omics studies identified perturbations to metabolites such as ADP, malate, and succinate that may be a result of inhibition or suppression of state 3 respiration, which relies on complex I (23). The thiazolidinedione drug class, which includes pioglitazone and troglitazone, is known to inhibit state 3 respiration by disassembly of complex I (24, 25). Whereas

previous studies identified the impact of thiazolidinediones on complex I using activity assays and western blots, the work in this thesis demonstrated that metabolomics had the capacity to identify perturbations in the abundance of metabolites that is consistent with inhibition of complex I and state 3 respiration.

Metabolomics studies demonstrated that diclofenac, ethinyl estradiol, pioglitazone, ritonavir, and troglitazone induced a decreased cellular abundance of several bile acids in both PHH and HepaRG™ cells after a 24-h exposure. Based on the proteomics analysis, this depletion may have been due to increased phase I metabolism of bile acids, which is a known protective pathway against cholestasis (26). However, a primary limitation of the whole cell proteomics and metabolomics methodologies was that it quantifies only the sum change in the abundance of metabolites and proteins. Cellular metabolism can be inhibited without alterations in the abundance of proteins or metabolic intermediates and, therefore, further studies are needed to assess the functional state of hepatocytes after drug treatment. Functional assays such as the B-CLEAR® assay provide specific insight into functional changes to the cell, such as altered biliary transport. Furthermore, it would be beneficial to expand the number and types of functional assays to determine the impact that DILI-associated drugs may have on protein localisation or direct inhibition of enzyme or transporter activity. Interestingly, ritonavir, which appeared to induce a depletion of cellular bile acids via increased CYP3A4 and CYP3A5 metabolism, is a known CYP3A4 and CYP3A5 inhibitor and inducer (27, 28). The interplay of these properties of ritonavir would be important to characterise to holistically understand the impact on bile acid homeostasis. Furthermore, the phosphorylation of the proteins could not be determined by the applied methods. Post-translational

modifications, such as phosphorylation, is a vital determinant of the functionality of many proteins and is known to be affected by some of the drug treatments (29). It would also be highly valuable to perform future studies over a variety of time-points because the impact of DILI-associated drugs may be time-dependent, as demonstrated for bile acids in the HepaRG™ cell time-course study. Finally, the addition of transcriptomics to the multi-omics approach would be invaluable as it would allow for a complete and holistic characterisation of the impact of DILI-associated drugs from transcription to metabolism. Previous work already has described drug-induced changes to gene expression, which may result in mitochondrial dysfunction, cholestasis, or steatosis (30, 31). Linking changes in gene expression directly to protein and metabolite abundance will offer a comprehensive insight into the perturbations to the functional state of hepatocytes when exposed to DILI-associated drugs.

Identification of liver injury-associated lipids

The changes observed in the proteins and metabolites of pathways associated with energy or bile acid metabolism, or changes to the hepatocellular lipidome, may not only offer mechanistic insight but potential clinical biomarkers for diagnosis of liver injury, including DILI. The potential for this was best demonstrated in Chapter 4, as non-alcoholic steatohepatitis (NASH) is a significant clinical issue that is caused by numerous factors including DILI-associated drugs and has a significant mortality rate (32-37). Lipidomics profiling and multivariate analysis of hepatocytes from NASH patients, and PHH treated with steatotic DILI-associated drugs, allowed for the characterisation of changes to specific lipid classes that are representative of steatotic liver injury, and determination lipid signatures associated with steatotic liver injury. The increase in the abundance of

hepatocellular phospholipids in NASH PHH mirrors the previously observed increases in serum phosphatidylserine and phosphatidylethanolamine in patients suffering from NASH (38). From this, it could be inferred that the change to the lipid profile of serum is intrinsically linked to changes in the cellular lipidome of hepatocytes in patients with NASH. However, the NASH PHH that were analysed in this thesis had no clear indication of a causative agent and so it is unclear whether DILI might have been a factor. Expanding upon the concept that changes to hepatocellular metabolites can result in changes to the serum metabolome and proteome, there is a significant potential to identify translational diagnostic biomarkers for steatogenic DILI. Previous work has shown that metabolites such as malate, which was shown to increase in abundance after drug treatment in Chapter 2, has the potential to act as a translational markers for liver failure and could be predictive of the risk of mortality (39). A limitation towards identifying robust and specific metabolites that are indicative of DILI from the research presented in this thesis is the limited number of donors and drugs used. To robust and specific metabolites which can be associated with DILI, it is imperative that they are validated with a much larger sample size including a wide variety of demographics to ensure that such metabolites are predictive for the general population. Finally, analysis of hepatocytes or serum obtained from patients suffering from clearly documented DILI would be invaluable in ascertaining the translational potential of these metabolites and whether they are predictive in serum.

Concluding Remarks

This thesis has offered new insights into the behaviour of DILI-associated drugs by utilising multi-omics techniques and multivariate analysis. The research encompassed the characterisation of the proteomes of *in vitro* liver models, determination of

perturbations in the metabolites and proteins associated with energy metabolism, detoxification, and bile acid homeostasis, and the identification of metabolites with predictive potential for drugs that cause steatotic liver injury. It was shown, under *in vitro* conditions, that the DILI-associated drugs pioglitazone, troglitazone, and ritonavir impaired mitochondrial respiration and increased the abundance of proteins associated with protection against oxidative stress. Furthermore, the research presented also investigated the specific liver injury phenotypes of cholestasis and steatosis using omics techniques and multivariate analysis. Diclofenac, ethinyl estradiol, pioglitazone, ritonavir, and troglitazone were shown to possess cholestatic properties and significantly impacted bile acid homeostasis, reducing the abundance of cellular bile acids over a 24-h drug treatment. The decrease in the abundance of bile acids was likely due, in part, to increased metabolism of cellular bile acids by CYP3A4 and CYP3A5. Finally, lipidomics identified hepatocellular increases in phospholipids and, in combination with multivariate analysis, identified and evaluated lipid signatures that are associated with drug-induced steatotic liver injury. While the robustness of the lipid signatures requires further validation, it did demonstrate that there is significant future potential to utilise a lipidomics and multivariate-based approach to identify lipid profiles that are indicative of steatotic DILI.

In the context of understanding DILI, in vitro models, and metabolic perturbations, it is evident that a multi-faceted approach is highly beneficial. While technologies such as transcriptomics, proteomics, metabolomics, plate-based assays, and various imaging techniques are invaluable techniques, alone they offer incomplete insights. Transcriptomics can allow for a better understanding of signalling pathways and how cells

respond to stimuli through gene expression, however, it is not a reliable indicator of protein abundance or activity because degradation and inhibition of proteins, for example, also affect protein abundance and activity. Similarly, proteomics, while offering a measure of protein abundance, does not account for changes in activity due to inhibition or direct interactions between xenobiotics and metabolites. Therefore, it is vital to investigate DILI, and any other metabolic system, using the most holistic approach possible to accurately characterise actual metabolic function and alterations in the abundance of biomolecules. A multifaceted approach that included the analysis of proteins, metabolites, and functional assays was utilized in Chapter 3 to demonstrate the value and necessity of such an approach. In Chapter 3, proteomics identified an increase in phase I metabolism enzymes but, due to their promiscuous nature, metabolomics analysis was necessary to identify the impact on the abundance of cellular bile acids. In addition, proteomics analysis did not identify any changes in the abundance of transporter proteins, however, the B-CLEAR® assay demonstrated that hepatocellular transport was severely affected. Furthermore, any model utilised must be determined to be fit for purpose. A common in vitro technique for simulating steatotic liver injury involves culturing PHH in a high-fat environment, however, this has been demonstrated to only reproduce the histological features of steatosis and increases in neutral lipids (21). The analysis of the lipidome of NASH PHH in Chapter 4, as well as previous clinical data, demonstrated that such an approach does not reproduce the significant increases observed in the phospholipidome of hepatocytes and serum of patients with NASH (38, 40, 41). As demonstrated through the utilisation of HuH-7 cells for the B-CLEAR® assay, the most sophisticated models are not always necessary but, whichever in vitro model is used must be metabolically

competent for the given purpose. As demonstrated in this dissertation, the application of multi-omics, functional assays, and multi-variate analysis has an immense capacity to allow researchers to develop a holistic insight into the mechanisms of DILI and the effects of DILI on the metabolome, lipidome, and proteome of hepatocytes. Applications of this novel work will aid in improving the diagnosis and management of clinical DILI, and the development of new drugs with limited DILI liability.

References

1. Bjornsson ES, Bergmann OM, Bjornsson HK, Kvaran RB, Olafsson S. Incidence, presentation, and outcomes in patients with drug-induced liver injury in the general population of Iceland. *Gastroenterology*. 2013;144(7):1419-25.
2. Sgro C, Clinard F, Ouazir K, Chanay H, Allard C, Guilleminet C, et al. Incidence of drug-induced hepatic injuries: a French population-based study. *Hepatology*. 2002;36(2):451-55.
3. Suk KT, Kim DJ, Kim CH, Park SH, Yoon JH, Kim YS, et al. A prospective nationwide study of drug-induced liver injury in Korea. *Am J Gastroenterol*. 2012;107(9):1380-7.
4. Shen T, Liu Y, Shang J, Xie Q, Li J, Yan M, et al. Incidence and etiology of drug-induced liver injury in mainland China. *Gastroenterology*. 2019;156(8):2230-41.e11.
5. Goldberg DS, Forde KA, Carbonari DM, Lewis JD, Leidl KBF, Reddy KR, et al. Population-representative incidence of drug-induced acute liver failure based on an analysis of an integrated health care system. *Gastroenterology*. 2015;148(7):1353-61.e3.
6. Torello Iserte J, Castillo Ferrando JR, Lainez MM, Garcia Morillas M, Arias Gonzalez A. Adverse reactions to drugs reported by the primary care physicians of Andalusia. Analysis of underreporting. *Aten Primaria*. 1994;13(6):307-11.
7. Xie Z, Chen E, Ouyang X, Xu X, Ma S, Ji F, et al. Metabolomics and cytokine analysis for identification of severe drug-induced liver injury. *J Proteome Res*. 2019;18(6):2514-24.
8. Cuykx M, Beirnaert C, Rodrigues RM, Laukens K, Vanhaecke T, Covaci A. Untargeted liquid chromatography-mass spectrometry metabolomics to assess drug-induced cholestatic features in HepaRG® cells. *Toxicol Appl Pharmacol*. 2019;379:114666.
9. Cuykx M, Claes L, Rodrigues RM, Vanhaecke T, Covaci A. Metabolomics profiling of steatosis progression in HepaRG® cells using sodium valproate. *Toxicol Lett*. 2018;286:22-30.
10. Rodrigues RM, Laxmikanth K, Chaudhari U, Sachinidis A, Zahedi RP, Sickmann A, et al. Omics-based responses induced by bosentan in human hepatoma HepaRG cell cultures. *Arch Toxicol*. 2018;92(6):1939-52.
11. García- Cañaveras JC, Castell JV, Donato MT, Lahoz A. A metabolomics cell-based approach for anticipating and investigating drug-induced liver injury. *Sci Rep*. 2016;6(1):27239.
12. Vilei MT, Granato A, Ferraresso C, Neri D, Carraro P, Gerunda G, et al. Comparison of pig, human and rat hepatocytes as a source of liver specific metabolic functions in culture systems--implications for use in bioartificial liver devices. *Int J Artif Organs*. 2001;24(6):392-6.

13. Thakare R, Alamoudi JA, Gautam N, Rodrigues AD, Alnouti Y. Species differences in bile acids I. Plasma and urine bile acid composition. *J Appl Toxicol*. 2018;38(10):1323-35.

14. Wang L, Prasad B, Salphati L, Chu X, Gupta A, Hop CECA, et al. Interspecies variability in expression of hepatobiliary transporters across human, dog, monkey, and rat as determined by quantitative proteomics. *Drug Metab Dispos*. 2015;43(3):367-74.

15. Li N, Bi YA, Duignan DB, Lai Y. Quantitative expression profile of hepatobiliary transporters in sandwich cultured rat and human hepatocytes. *Mol Pharm*. 2009;6(4):1180-89.

16. Godoy P, Hewitt NJ, Albrecht U, Andersen ME, Ansari N, Bhattacharya S, et al. Recent advances in 2D and 3D in vitro systems using primary hepatocytes, alternative hepatocyte sources and non-parenchymal liver cells and their use in investigating mechanisms of hepatotoxicity, cell signaling and ADME. *Arch Toxicol*. 2013;87(8):1315-530.

17. Khatri R, Fallon JK, Rementer RJB, Kulick NT, Lee CR, Smith PC. Targeted quantitative proteomic analysis of drug metabolizing enzymes and transporters by nano LC-MS/MS in the sandwich cultured human hepatocyte model. *J Pharmacol Toxicol Methods*. 2019;98:106590.

18. Cox CR, Lynch S, Goldring C, Sharma P. Current Perspective: 3D Spheroid Models Utilizing Human-Based Cells for Investigating Metabolism-Dependent Drug-Induced Liver Injury. *Front Med*. 2020;2(14).

19. Bell CC, Hendriks DFG, Moro SML, Ellis E, Walsh J, Renblom A, et al. Characterization of primary human hepatocyte spheroids as a model system for drug-induced liver injury, liver function and disease. *Sci Rep*. 2016;6(1):25187.

20. Smith L, Villaret-Cazadamont J, Claus SP, Canlet C, Guillou H, Cabaton NJ, et al. Important Considerations for Sample Collection in Metabolomics Studies with a Special Focus on Applications to Liver Functions. *Metabolites*. 2020;10(3):104.

21. Kozyra M, Johansson I, Nordling Å, Ullah S, Lauschke VM, Ingelman-Sundberg M. Human hepatic 3D spheroids as a model for steatosis and insulin resistance. *Sci Rep*. 2018;8(1):14297.

22. Rusz M, Rampler E, Keppler BK, Jakupec MA, Koellensperger G. Single Spheroid Metabolomics: Optimizing Sample Preparation of Three-Dimensional Multicellular Tumor Spheroids. *Metabolites*. 2019;9(12):304.

23. Korzeniewski B. 'Idealized' state 4 and state 3 in mitochondria vs. rest and work in skeletal muscle. *PLoS One*. 2015;10(2):e0117145-e45.

24. García-Ruiz I, Solís-Muñoz P, Fernández-Moreira D, Muñoz-Yagüe T, Solís-Herruzo JA. Pioglitazone leads to an inactivation and disassembly of complex I of the mitochondrial respiratory chain. *BMC Biol*. 2013;11(1):88.

25. Brunmair B, Staniek K, Gras F, Scharf N, Althaym A, Clara R, et al. Thiazolidinediones, like metformin, inhibit respiratory complex I: a common

mechanism contributing to their antidiabetic actions? *Diabetes*. 2004;53(4):1052-9.

26. Chen J, Zhao KN, Chen C. The role of CYP3A4 in the biotransformation of bile acids and therapeutic implication for cholestasis. *Ann Transl Med*. 2014;2(1):7-7.

27. Luo G, Cunningham M, Kim S, Burn T, Lin J, Sinz M, et al. CYP3A4 induction by drugs: correlation between a pregnane X receptor reporter gene assay and CYP3A4 expression in human hepatocytes. *Drug Metab Dispos*. 2002;30(7):795-804.

28. Rock BM, Hengel SM, Rock DA, Wienkers LC, Kunze KL. Characterization of ritonavir-mediated inactivation of cytochrome P450 3A4. *Mol Pharmacol*. 2014;86(6):665-74.

29. Sanz MN, Sánchez-Martín C, Detaille D, Vial G, Rigoulet M, El-Mir MY, et al. Acute mitochondrial actions of glitazones on the liver: a crucial parameter for their antidiabetic properties. *Cell Physiol Biochem*. 2011;28(5):899-910.

30. Garzel B, Yang H, Zhang L, Huang SM, Polli JE, Wang H. The role of bile salt export pump gene repression in drug-induced cholestatic liver toxicity. *Drug Metab Dispos*. 2014;42(3):318-22.

31. Wolters JEJ, van Breda SGJ, Grossmann J, Fortes C, Caiment F, Kleinjans JCS. Integrated 'omics analysis reveals new drug-induced mitochondrial perturbations in human hepatocytes. *Toxicol Lett*. 2018;289:1-13.

32. Anthérieu S, Rogue A, Fromenty B, Guillouzo A, Robin MA. Induction of vesicular steatosis by amiodarone and tetracycline is associated with up-regulation of lipogenic genes in heparg cells. *Hepatology*. 2011;53(6):1895-905.

33. Vitins AP, Kienhuis AS, Speksnijder EN, Roodbergen M, Luijten M, van der Ven LT. Mechanisms of amiodarone and valproic acid induced liver steatosis in mouse in vivo act as a template for other hepatotoxicity models. *Arch Toxicol*. 2014;88(8):1573-88.

34. Ito M, Suzuki J, Sasaki M, Watanabe K, Tsujioka S, Takahashi Y, et al. Development of nonalcoholic steatohepatitis model through combination of high-fat diet and tetracycline with morbid obesity in mice. *Hepatol Res*. 2006;34(2):92-8.

35. Langman G, Hall PM, Todd G. Role of non-alcoholic steatohepatitis in methotrexate-induced liver injury. *J Gastroenterol Hepatol*. 2001;16(12):1395-401.

36. Younossi ZM, Koenig AB, Abdelatif D, Fazel Y, Henry L, Wymer M. Global epidemiology of nonalcoholic fatty liver disease—meta-analytic assessment of prevalence, incidence, and outcomes. *Hepatology*. 2016;64(1):73-84.

37. Rafiq N, Bai C, Fang Y, Srishord M, McCullough A, Gramlich T, et al. Long-term follow-up of patients with nonalcoholic fatty liver. *Clin Gastroenterol Hepatol*. 2009;7(2):234-38.

38. Ma DWL, Arendt BM, Hillyer LM, Fung SK, McGilvray I, Guindi M, et al. Plasma phospholipids and fatty acid composition differ between liver biopsy-proven

nonalcoholic fatty liver disease and healthy subjects. *Nutr Diabetes*. 2016;6(7):e220-e20.

39. Yoon KC, Kwon HD, Jo H-S, Choi YY, Seok JI, Kang Y, et al. Explorative study of serum biomarkers of liver failure after liver resection. *Sci Rep*. 2020;10(1):9960.

40. García-Cañaveras JC, Donato MT, Castell JV, Lahoz A. A comprehensive untargeted metabonomic analysis of human steatotic liver tissue by RP and HILIC chromatography coupled to mass spectrometry reveals important metabolic alterations. *J Proteome Res*. 2011;10(10):4825-34.

41. Gorden DL, Myers DS, Ivanova PT, Fahy E, Maurya MR, Gupta S, et al. Biomarkers of NAFLD progression: a lipidomics approach to an epidemic. *J Lipid Res*. 2015;56(3):722-36.

Appendix

Appendix 1

Accepted Manuscript: Analytical and Omics-based Advances in the Study of Drug-Induced Liver Injury. DOI: https://doi.org/10.1093/toxsci/kfab069 (Accessed: 14 July 2021 – Preprint version)

Analytical and Omics-based Advances in the Study of Drug-Induced Liver Injury

Thomas Kralj* (ORCID iD: 0000-0001-6534-4638), Kim L. R. Brouwer† (ORCID iD: 0000-0003-1945-4929), Darren J. Creek* (ORCID iD: 0000-0001-7497-7082)

* Drug Delivery, Disposition and Dynamics, Monash Institute of Pharmaceutical Sciences, Monash University, Parkville Campus, Parkville, Victoria Australia

† Division of Pharmacotherapy and Experimental Therapeutics, UNC Eshelman School of Pharmacy, CB #7569 Beard Hall, University of North Carolina at Chapel Hill, Chapel Hill, NC 27599-7569

Keywords: metabolomics, proteomics, DILI, cholestasis, steatosis, transcriptomics

Running Head: Analytical and Omics-based Advances in the Study of Drug-Induced Liver Injury

Corresponding Authors:

Associate Professor Darren Creek

Drug Delivery, Disposition and Dynamics, Monash University, 381 Royal Parade, Parkville, Victoria 3052, Australia

Phone: +61 424 362 572

Email: Darren.creek@monash.edu

and

Professor Kim Brouwer

Division of Pharmacotherapy and Experimental Therapeutics, UNC Eshelman School of Pharmacy, CB #7569 Beard Hall, University of North Carolina at Chapel Hill, Chapel Hill, NC 27599-7569

Phone: +1 919 962 7030

Email: kbrouwer@unc.edu

Abstract

Drug-induced liver injury (DILI) is a significant clinical issue, affecting 1-1.5 million patients annually, and remains a major challenge during drug development - toxicity and safety concerns are the second highest reason for drug candidate failure. The future prevalence of DILI can be minimised by developing a greater understanding of the biological mechanisms behind DILI. Both qualitative and quantitative analytical techniques are vital to characterising and investigating DILI. A variety of assays are capable of characterising specific aspects of a drug's hepatotoxic nature, with multiplexed assays capable of characterising and scoring a drug's association with DILI. However, an even deeper insight into the perturbations to biological pathways involved in the mechanisms of DILI can be gained through the use of omics-based analytical techniques: genomics, transcriptomics, proteomics, and metabolomics. These omics analytical techniques can offer qualitative and quantitative insight into genetic susceptibilities to DILI, the impact of drug treatment on gene expression, and the effect on protein and metabolite abundance. This review will discuss the analytical techniques that can be applied to characterise and investigate the biological mechanisms of DILI and potential predictive biomarkers.

1.1 Drug-induced Liver Injury

Drug-induced liver injury (DILI) is a type of adverse drug reaction (ADR) that refers to a variety of related conditions resulting from exposure to pharmaceuticals with hepatotoxic potential. In addition, chemicals other than drugs (e.g. plant toxins or mycotoxins, industrial by-products, biocides) can also induce DILI-like conditions, with herbal and dietary supplements accounting for 20% of injury cases in the US and up to 73% in Asia (Navarro et al. 2017). DILI is a globally prevalent issue and various population studies have identified DILI occurrence rates of 14 to 19 cases per 100,000 people annually (Bjornsson et al. 2013; Suk et al. 2012).

In a Finnish cohort, 1.4% of all medical in-patients experienced DILI (Meier et al. 2005). While relatively low, this incidence is still concerning as up to 10.1% of cases may be fatal or require a liver transplant (Chalasani et al. 2008; Idilman et al. 2010; Suk et al. 2012). A study of 1,089 DILI cases in the US found that 9.8% died or required a liver transplant (Hayashi et al. 2017). Of these severe cases, DILI was reported as

the primary cause of death or liver transplant in 64% of patients and contributed to an additional 14% of deaths or liver transplants.

DILI is not just a condition of clinical concern but is also a prevalent problem in drug development, with toxicity and safety concerns being the second highest reason for drug failure (Waring et al. 2015). Hepatotoxicity, a fundamental issue with drug safety, ideally should be detected during the preclinical stages of testing using *in vitro* methods and animal models. However, there are numerous limitations with the use of animal models to assess DILI, including high costs, ethical issues, and poor translation between species, whereby numerous drugs have been misidentified in pre-clinical animal models as either safe or toxic for humans (Van Norman 2019). In the preclinical phase of drug development, the attrition rate of drug candidates due to safety concerns is 40% (Waring et al. 2015). Post-market surveillance reveals that even with major preclinical and clinical efforts to screen out compounds with DILI liability, many DILI-associated drugs still reach the market. An analysis of 1,036 Food and Drug Administration (FDA)-approved drugs found that 192 drugs (19%) have strong DILI concerns, and only 62 (6%) of these drugs have been discontinued. For the remaining drugs assessed, 278 (27%) have minor DILI concerns, 254 (25%) have ambiguous DILI concerns, and 312 (30%) have no DILI concerns (Chen et al. 2016).

Understanding the mechanism(s) of DILI based on a thorough examination of known DILI-associated drugs may be useful in preventing drugs with hepatotoxic potential from reaching the market. With that goal in mind, representative *in vitro* models have been combined with investigative omics techniques, such as transcriptomics, proteomics, and metabolomics to identify characteristics of drugs with potential to cause DILI. These approaches provide an alternative to the use of animal models, thus reducing the reliance on costly *in vivo* models during drug development.

1.2 Common Drug-Induced Liver Injury Phenotypes

DILI has been simplified into three general classes: hepatocellular, mixed, and cholestatic liver injury. These phenotypes are classified clinically based on serum enzyme ratios with hepatocellular liver injury being the most prevalent injury phenotype followed by cholestatic liver injury (Table 1). Clinically, idiosyncratic DILI is the most common phenotype, where a combination of patient biological characteristics leads to DILI susceptibility from a given drug. Additionally, idiosyncratic DILI presents

without a clear relationship between dose or dosage regimen and severity of injury (Fontana 2014). Hepatocellular liver injury acts as a catch-all class containing any form of DILI that is not cholestatic in nature, including acute hepatic necrosis, acute hepatitis, chronic hepatitis, hepatic steatosis with lactic acidosis, and non-alcoholic fatty liver disease (NAFLD) (Kleiner 2009). Of these liver injury phenotypes, steatosis, the accumulation of lipids within hepatocytes, is one of the most prevalent forms of hepatocellular injury occurring in 64% of DILI cases (Kleiner et al. 2014).

1.2.1 Steatosis

Drug-induced steatosis is a form of NAFLD caused by drugs such as amiodarone, and tetracycline (Antherieu et al. 2011; Vitins et al. 2014). Steatosis is a concerning occurrence as a DILI phenotype because 73% of patients who required a liver transplant or had a fatal outcome exhibited steatosis as a histological feature (Kleiner et al. 2014). Lipid droplet accumulation may occur as microvesicles or macrovesicles. Both forms of steatosis may occur with or without lobular inflammation, however, liver injury severity often correlates with the degree of inflammation (Chan 2015; Yeh and Brunt 2014).

Drugs induce hepatic lipid accumulation by multiple, diverse mechanisms (Figure 1). Steatosis is likely to result from impairment in the capacity of mitochondria to perform fatty acid oxidation (FAO), impaired microsomal triglyceride transfer proteins (MTTP), a drug-induced increase in uptake of fatty acids, and/or direct stimulation of lipid synthesis within the liver through activation of lipogenic transcription factors (Blas-García et al. 2010; Schadinger et al. 2005; Serviddio et al. 2011)

1.2.2 Cholestasis

Cholestatic liver injury results from the reduction or impairment of bile acid transport, occurring as hepatocellular or canalicular bile stasis, or significant duct loss, which then leads to cholestasis (Onofrio and Hirschfield 2020). Cholestatic phenotypes are classified as either acute or chronic cholestatic liver injury, and the specific form of cholestasis is determined by the levels of serum liver enzymes (Padda et al. 2011; Sundaram and Björnsson 2017). While specific mechanistic and causal links of drug-induced cholestasis remain poorly characterised for many drugs, altered bile acid transport is a primary cause (Figure 2) (Crocenzi et al. 2003; Garzel et al. 2014; Morgan et al. 2010; Morgan et al. 2013; Mottino et al. 2002). Cholestatic drugs

may directly inhibit bile acid transporters, alter gene expression and/or modify the localisation of bile acid transporters (Figure 2).

1.3 Analytical Techniques for Investigation of Drug-Induced Liver Injury

Identifying the potential for drugs to cause DILI, and the mechanisms by which this occurs, has been the focus of continued investigations using *in vitro* models. These studies can range from simple plate-based methods such as the B-CLEAR® transporter assay, or microscope imaging-based assays, to more complex studies using multiple parameters to characterise the various facets of DILI. There are a number of versatile analytic techniques that are applicable for DILI studies including studies of cell viability or function, and analysis of the abundance, function, or localisation of specific biomolecules (Table 2).

1.3.1 Plate-based assays

Plate-based studies of transporter function are particularly valuable for DILI research because the impairment of hepatocellular transport can result in a loss of hepatocyte homeostasis and the accumulation of toxic xenobiotics or endogenous molecules. This loss of functional transporters may lead to cholestasis or other forms of liver injury (Garzel et al. 2014; Morgan et al. 2010; Morgan et al. 2013). The impact that a drug has on hepatocyte transporters, such as the bile salt export pump (BSEP), may be quantified using a transport assay such as B-CLEAR®, a plate-based assay (Kemp et al. 2005). This transport assay has been used to gain insight regarding the accumulation of drugs in hepatocytes and the impact of cholestasis-associated drugs such as troglitazone and bosentan. These well-known cholestasis-associated drugs decreased the uptake of taurocholate, a substrate of the sodium taurocholate cotransporting polypeptide (NTCP), and estradiol-17β-D-glucuronide, an organic anion transporting polypeptide (OATP) substrate (Kemp et al. 2005). Thus, a plate-based assay can be used to identify whether a drug has the potential to impair hepatic transporters and disrupt hepatocellular bile acid homeostasis, which may contribute to DILI.

Previous work has shown that a compound's potential to cause cholestatic DILI does not necessarily correlate with its capacity to inhibit the BSEP transporter because of the involvement of other transporters and compensatory mechanisms in hepatocytes. Thus, more sophisticated hepatotoxic plate-based assays have been

developed (Chan and Benet 2017; Morgan et al. 2013). By appropriately challenging hepatocytes with the addition of free fatty acids (FFA) and exogenous bile acids to the culture media, drugs capable of inducing cholestatic DILI will have a much more profound hepatotoxic effect. This was illustrated in a study using C-DILI™, a plate-based hepatotoxicity specific assay, to compare cyclosporin A (CysA) and troglitazone, both potent BSEP inhibitors (CysA, IC_{50}=0.5 μM; troglitazone, IC_{50}=3 μM) (Jonathan P. Jackson 2018; Morgan et al. 2013). While both drugs are capable of inhibiting BSEP, the C-DILI™ assay demonstrated a greater potential for cholestatic liver injury caused by troglitazone compared to CysA, which has been reflected in clinical studies (Ganschow et al. 2006; Jagannath and Rai 2000; Jonathan P. Jackson 2018; Reuben et al. 2010).

1.3.2 Image-based assays

Image-based assays are ideal for visualising and quantifying the localisation and abundance of organelles and various biomolecules. These assays can provide information about the impact that DILI-associated drugs may have on transporter localisation or on steatosis or phospholipidosis. Immunofluorescence microscopy assays (IFAs) are a common and powerful imaging tool for assessing transporter localisation and abundance. IFAs utilise affinity-based biology (antibodies) coupled with fluorescent reporters and can be performed in two ways: direct, with conjugation directly to the antibody targeting a specific protein; or indirect, where a secondary antibody/fluorophore conjugate that targets the anti-protein immunoglobulin class (such as anti-IgG) (Kang et al. 2019; Malinen et al. 2019; Román et al. 2003). The added benefit of these techniques is the variety of fluorophores available for multiplexing assays, allowing the investigation of multiple proteins in a single assay. IFAs have been used to demonstrate the capacity for estradiol 17β-d-glucuronide and CysA to cause the internalisation of the BSEP transporter in primary rat hepatocytes, which leads to a disruption in hepatocyte homeostasis (Crocenzi et al. 2003; Román et al. 2003). Lipid staining dyes, such as the fluorescent dye, BODIPY, or the colorimetric dye, Oil Red O, are used to assess the accumulation of neutral lipid droplets and can be used to detect drug-induced steatosis (Figure 1) (Fam et al. 2018; Jiang et al. 2012; Liu et al. 2014; Ohsaki et al. 2010). Additionally, clinical data for steatogenic drugs correlates well with their ability to cause *in vitro* steatosis; drugs

such as amiodarone, methotrexate, tamoxifen, and tetracycline have steatogenic properties both in clinical and *in vitro* studies (Chen et al. 2016; Donato et al. 2009).

The detection of phospholipidosis is commonly performed using electron microscopy to identify lamellar inclusions within hepatocytes; however, this is a labour-intensive, low-throughput assay requiring expert training. Phospholipidosis may potentially be identified with lysosomal dyes such as β-BODIPY C_{12}-HPC, HCS LipidTOX™, or LysoTracker™, which can detect an increased volume and abundance of lysosomal vesicles, the accumulation site of phospholipids when phospholipidosis is induced (Funk and Krise 2012). The use of image-based detection assays for acylglycerides and phospholipids allows for high-throughput screening of drugs to identify their potential to cause steatosis or phospholipidosis (Donato et al. 2012; Funk and Krise 2012).

1.3.3 High-content multiple parameter assays

Recently, high-content plate-based assays were developed in which various assays using fluorescent probes, antibodies, and reactive dyes were combined to characterise the nature of a drug's hepatotoxic behaviour across several parameters (Kawaguchi et al. 2020). These parameters can assess the production of reactive oxygen species and changes in glutathione abundance, changes to membrane permeability, formation of biliary canaliculi, lipid accumulation, bile-acid dependant toxicity, and impairment of mitochondrial membrane potential and mitochondrial toxicity (Kawaguchi et al. 2020; Saito et al. 2016). Furthermore, using receiver operating characteristic analysis can allow for the outcomes of these assays to grade the hepatotoxic potential of the drugs tested (Kawaguchi et al. 2020).

1.4 Application of Omics to Investigate Drug-Induced Liver Injury

Omics is a broad term that encompasses the four fields of genomics, transcriptomics, proteomics, and metabolomics. Each of these fields offers powerful tools that can be used to investigate the underlying mechanisms that cause DILI. This may range from genetic susceptibilities or changes in gene expression after drug treatment, to perturbations of biochemical pathways identified from changes in protein and metabolite abundance.

1.4.1 Genomics

Genomics was one of the first omics fields to be developed. Genomics is the science of characterising an organism's genetic code, focussing on evolutionary relationships, genome structure and correlating gene sequences with biological functions of the organism (Aronson and Rehm 2015). Genomics is a powerful tool in the DILI field; research has concentrated on identifying single nucleotide polymorphisms (SNPs) – gene variants that may lead to increased susceptibility to DILI (Andrade et al. 2009). A common cause of susceptibility comes from SNPs within immune-related genes, such as the human leukocyte antigen (HLA) gene or genes related to cytokines (Lucena et al. 2011; Petros et al. 2016; Singer et al. 2010; Spraggs et al. 2011). Amoxicillin-clavulanate, lapatinib, and lumiracoxib have all been associated with specific HLA gene variants that have resulted in a greater susceptibility of patients to DILI. Amoxicillin-clavulanate was associated with three haplotypes for susceptibility to DILI; HLA class II *DRB1*15:01-DQB1*06:02*, which is known to indicate susceptibility to other drugs as well, and HLA class I *A*02:01* (Andrade et al. 2004; Lucena et al. 2011). Lapatinib and lumiracoxib also were found to increase susceptibility to DILI in patients with the *HLA-DQA1*02:01* and *HLA-DQA1*01:02* genotypes, respectively. These variants were associated with a significantly increased occurrence of DILI versus control populations after treatment with lapatinib (71% vs 21%) and lumiracoxib (77% vs 46%) (Singer et al. 2010; Spraggs et al. 2011). Furthermore, gene variants related to cytokines such as interleukin (IL)-4, IL-10, and Tumour Necrosis Factor (TNF)-α are associated with increased incidence of idiosyncratic DILI. IL-4 and IL-10 phenotypic susceptibilities were identified after treatment with diclofenac. The SNPs responsible for these susceptibilities, IL-10-A627C (Odds ratio (OR): 2.84), and IL-4-T590C (OR: 2.6), demonstrated a significant association with diclofenac-induced liver injury, with the greatest effect occurring when both SNPs were present (OR: 5.3) (Aithal et al. 2004). A similar trend also was observed with a gene variant of TNF-α, in which the TNF-α-G308A variant was identified to correlate as a risk factor for hepatitis induced by anti-tuberculosis drugs including isoniazid, rifampicin, and pyrazinamide (Kim et al. 2012). Genetic variants of phase II liver enzymes also introduce susceptibility to DILI, primarily because many of these gene variants exhibit reduced activity. N-acetyltransferase 2 (NAT2) is a phase II N-acetylation enzyme known to have several alleles in the human population. Patients with the *NAT2*5*, *NAT2*6*, and *NAT2*7*

alleles are referred to as "slow acetylators", in which the rate at which patients with these alleles acetylate their substrates is reduced in comparison to patients with other NAT2 alleles (Agúndez et al. 1996). These slow acetylation variants increase susceptibility to isoniazid and rifampicin-induced liver injury from 4- to 28-fold in Japanese patients (Ohno et al. 2000). Additionally, for a population of 24 Singaporean patients treated with isoniazid, there was a significant correlation between DILI and slow *NAT2* variants (OR: 13.9) (Chan et al. 2017). Isoniazid and rifampicin are both substrates of NAT2, and the DILI observed among those with the slow acetylation variant is likely due to prolonged exposure to higher plasma concentrations of the anti-tuberculosis drug (Kumar et al. 2017; Touré et al. 2016). Furthermore, double null genotypes of the glutathione S-transferase genes *(GSTT1-GSTM1*) have been identified as risk factors for DILI induced by tacrine, troglitazone, NSAIDs, and amoxicillin-clavulanate (OR: 3.7, 2.8, 5.61, and 2.8, respectively) (Lucena et al. 2008; Simon et al. 2000; Watanabe et al. 2003).

1.4.2 Transcriptomics

Transcriptomics is the next layer down from genomics and, instead of assessing variations in gene sequences and their association with DILI susceptibilities, it can be used to identify changes to genetic expression profiles that occur in response to treatment with DILI-associated drugs. Transcriptomics involves the use of microarrays or, more recently, RNA sequencing (RNA-seq), which allows for the characterisation of a biological system's transcriptome and changes to this transcriptome in response to stimuli. RNA-seq is commonly used in the pharmaceutical industry to investigate the potential for DILI. Recent animal studies showed that the larger dynamic range of RNA-seq can capture a greater number of differentially expressed genes with improved coverage of pathways that are relevant to hepatotoxicity compared to microarrays (Rao et al. 2019).

There is significant application of transcriptomics in drug development through the application of toxicogenomics for safety screening of new chemical entities (Liu et al. 2019). It is important to understand how the transcriptome of hepatocytes changes with exposure to a drug with DILI potential because this information can provide predictive and mechanistic insight into DILI. Transcriptomics has been used to generate predictive *in vitro* models for detecting DILI, with a predictive accuracy of 73% when comparing drugs strongly associated with severe and no incidence of DILI

(Jennen et al. 2014; Kohonen et al. 2017). These models primarily focus on analysing variations in the expression of genes related to general cell injury such as apoptosis, necrosis, and inflammation (Jennen et al. 2014; Rodrigues et al. 2016).

Transcriptomics also has been used to identify mechanistic perturbations that may result in hepatotoxicity associated with a specific drug. For example, several DILI-associated drugs, including ethinyl estradiol and ritonavir, impair BSEP gene expression in an farnesoid X receptor (FXR)-dependant manner, which may be mechanistically linked to their cholestatic liver injury phenotype (Garzel et al. 2014). In another example, CysA down-regulates OATP1B1, NTCP, Cytochrome P450 (CYP)3A4, and bile acid-CoA:amino acid N-acyltransferase (BAAT) (Wolters et al. 2016). Valproic acid suppresses the expression of several ATP-synthases, fatty acid transporters, and other mitochondrial genes leading to mitochondrial dysfunction, steatosis and hepatotoxicity (Wolters et al. 2018). Transcriptomics can be applied to determine the hepatocellular responses that may protect from fatal hepatotoxicity and allow for recovery from DILI. In a study of mouse models using acetaminophen (APAP) to induce both non-lethal DILI and DILI resulting in fatal liver failure, the non-lethal dose increased expression of *Myc*, *Bag3*, and *Btc,* which did not occur at a lethal dose. These genes are related to cell survival, as well as protective, repair, and stress responses; *Bag3* has anti-apoptotic activities and *Btc* induces cell survival and may explain how fatal liver failure is mitigated at lower doses (Li et al. 2018). Additionally, betacellulin, the protein encoded by *Btc*, is present in serum and could potentially be used as a biomarker to predict a patient's likelihood of recovery from DILI.

A recent development in transcriptomics is single cell RNA-seq, which allows for individual cells to be sequenced. This can be invaluable when there is heterogeneity between cells, a known characteristic of hepatocytes (Halpern et al. 2017; MacParland et al. 2018). The impact this heterogeneity could have on a hepatocyte's response to injury was shown in cholestatic mice in which several heterogenous groups of cholestatic hepatocytes were identified and shown to differentially regulate genes that affected their lipid metabolism and localisation, cholesterol esterification, and inflammatory-related gene expression (Chang et al. 2019). Single cell RNA-seq is therefore a vital tool for investigating and characterising how cell heterogeneity can affect and alter a biological system's response to toxic stimuli.

1.4.3 Proteomics

The study of proteins through the use of immunoassays or proteomic mass spectrometry is vital in understanding, quantifying, and characterising proteins within biological systems. Proteomics has long been used to detect DILI in patients because the primary clinical assay for identification of DILI is detection of elevated aspartate aminotransferase (AST) and alanine aminotransferase (ALT) liver enzymes in the blood. This concept of using serum proteins to detect liver injury has been further developed, improving the accuracy and sensitivity for detecting DILI. The accuracy that can be achieved by detecting elevations of apolipoprotein E (89%) is a notable improvement on the current clinical standard method of detecting changes in AST, ALT, and bilirubin (81%); however, further improvement to the detection accuracy for DILI is achieved when detecting changes in apolipoprotein E, inter-alpha-trypsin inhibitor, gelsolin, complement component C7, and serum amyloid P-component proteins in mice (95%) (van Swelm et al. 2012). Furthermore, detection assays for a specific DILI-associated drug have been proposed. APAP-induced liver injury is detectable by quantification of urinary levels of calmodulin in humans, which correlate with plasma APAP concentrations (r= 0.97) and was detectable before any ALT elevations in blood occurred (van Swelm et al. 2012). An assay for the detection of diclofenac-induced liver injury was developed *in vitro* and validated in patients with diclofenac-mediated DILI. A patient would be considered positive for diclofenac-mediated DILI if the levels of ITGB3-expressing cells in whole blood decreased below 60%, a decrease not observed in other DILI patients or other forms of liver injury not associated with a drug treatment (Dragoi et al. 2018). These new proteomic-based detection methods could prove to be vital tools in reducing the large number of DILI cases that are not clinically identified, and potentially could enable clinicians to intervene earlier before severe DILI occurs (Klopotowska et al. 2013; Nebeker et al. 2005).

An even greater strength of proteomics is the ability to investigate biological perturbations induced by DILI-associated compounds in order to identify mechanisms of toxicity. For example, HepaRG cells dosed with the mycotoxins deoxynivalenol (DON) and zearalenone (ZEA) exhibited a change in the abundance of up to 96 proteins, depending on dosing format and duration of exposure. The proteins that were significantly altered by DON and ZEA exposure included proteins related to cellular

metabolic processes, stress response pathways, and cellular development and proliferation (Smith et al. 2018). Most notable was the significant decrease in abundance of DNA topoisomerase 1 and DNA topoisomerase 2-alpha, both shown previously to be affected as part of the broader mycotoxin mechanism of toxicity (Cosimi et al. 2009; Ostry 2008; Smith et al. 2018). Nevirapine (NVP), a non-nucleoside reverse-transcriptase inhibitor, has been associated with a high rate of DILI, with 5-12% of treated patients experiencing NVP associated-liver injury (Dieterich et al. 2004; Martín-Carbonero et al. 2003). Dosing HepG2 cells with NVP led to mitochondrial dysfunction, as indicated by altered abundance of 13 mitochondrial proteins (Paemanee et al. 2017). Important mitochondrial enzymes such as glyceraldehyde-3-phosphate dehydrogenase (GAPDH) and phosphoenolpyruvate carboxykinase (PEPCK) showed a 2.2- and 12.2-fold decrease in abundance following NVP exposure (Paemanee et al. 2017; Pilon et al. 2002).

1.4.4 Metabolomics

Metabolomics is capable of characterising and determining changes in the metabolism of a biological system, which allows for identification of small molecular biomarkers and mechanistic insight into DILI. Metabolomic analysis is primarily performed using mass spectrometry and, in some instances, nuclear magnetic resonance. There has been a variety of studies performed using metabolomics to identify serum biomarkers of DILI for use in pathology, and for discovery of *in vitro* biomarkers that predict DILI, as well as for characterisation of the injury phenotype. Several serum biomarkers have been identified and proposed for clinical use in DILI diagnosis based on metabolites from primary and secondary bile acid biosynthesis, α-linolenic acid metabolism, and glycerophospholipid metabolism (Ma et al. 2019; Xie et al. 2019). A significant increase in serum levels of palmitic acid, TCDCA, glycocholate (GCA), and tauroursodexycholate (TUDCA), in addition to a significant decrease in serum lysophosphatidylethanolamine levels, were observed in DILI patients compared to healthy controls. Additionally, the severity of DILI corresponded with increased serum levels of glycine and taurine conjugates [GCA, taurocholate, TUDCA, glycochenodeoxycholate, and taurodeoxycholate], with decreased serum levels of chenodeoxycholate, deoxycholate, and lithocholate also corresponding to more severe DILI pathology (Ma et al. 2019; Xie et al. 2019). The serum bile acids that increased in response to DILI were sensitive and specific differentiators of DILI

compared to healthy controls, while the decreased serum bile acids were poor serum biomarkers of DILI (Ma et al. 2019). One limitation of the serum biomarkers is that their capacity to differentiate between DILI and other forms of liver injury has yet to be established.

MetaMap®-Tox is an excellent example of metabolomics being applied to identify the toxicological mode of action of compounds. MetaMap®-Tox is a database of serum metabolites from Wistar rats treated with compounds that have known toxicological modes of action. These metabolites were analysed and categorised to produce a database of biomarkers that can be used to determine a novel compound's toxicological mode of action (Mattes et al. 2013; van Ravenzwaay et al. 2007; van Ravenzwaay et al. 2016). This toxicological biomarker database has been applied to identify the potential toxicological mode of action of drugs such as phenytoin, lamivudine, zidovudine, and phenobarbital (Kamp et al. 2012; Mattes et al. 2014).

In vitro metabolomic studies can be used to classify DILI-associated drugs based on general hepatotoxic mechanisms through the combined use of metabolomics analysis and Principal Component Analysis (PCA)-based clustering (García- Cañaveras et al. 2016; Ramirez et al. 2018). PCA comparisons of metabolomic data may identify metabolite biomarkers of DILI phenotypes such as oxidative stress, steatosis, and phospholipidosis. Metabolite biomarkers could then be applied to predict the likely mechanism of hepatotoxicity based on metabolite fingerprints generated from DILI-associated drugs with known mechanisms of hepatotoxicity (García- Cañaveras et al. 2016). A notable example was the use of lipidomics, a form of metabolomics, for the classification of steatogenic drugs by the increase in total triglycerides, diglycerides and phospholipids, and a metabolite profile indicating oxidative stress distinguishing between well-known mechanisms involving impaired β-oxidation and mitochondrial dysfunction (Cuykx et al. 2018; Donato and Gómez-Lechón 2012; García- Cañaveras et al. 2016; Masarone et al. 2018). Additionally, lipidomic analysis of drug-treated 3D human microtissues allowed for a lipid fingerprint to be generated that showed that alterations to triacylglycerides and lysophosphatidylcholines abundance was indicative of a higher DILI risk. The lipidomics profile of the drugs tested in this study correlated with its DILIrank classification for their potential to cause DILI with those of higher risk showing similar changes to their lipid profiles (Goracci et al. 2020). APAP is a drug that has been

repeatedly studied for toxicity- and mechanism-related biomarkers. From mouse hepatic extracts, metabolomic studies have shown that APAP treatment results in glutathione depletion. The depletion of glutathione can lead to depletion of glutathione precursor metabolites such as hypotaurine and methionine, reflecting a cellular response to protect against APAP-induced oxidative stress. In addition, mitochondrial dysfunction was observed due to impaired ATP synthesis and up-regulation of energy-related pathways indicated by the depletion of glucose and glycogen and the elevation of D-3-hydroxybutyrate (Kyriakides et al. 2016). These changes show the capacity for metabolomics to use metabolites as predictive and descriptive biomarkers of DILI.

1.5 Summary and Future Directions

DILI is an important safety concern for numerous drugs prescribed to patients as well as for drugs in development. For decades, animal models and *in vitro* plate-based assays have acted as the primary barrier for detection of potentially toxic drugs prior to first-in-human trials. With advancing technologies including sophisticated, human-relevant *in vitro* models, *in silico* tools, and even artificial intelligence (AI), there is an abundance of new approaches that can identify safety concerns earlier in drug development. However, for these models to achieve the greatest benefit, they need to be coupled with powerful analytical techniques that offer both a profound breadth and depth of information about biochemical changes due to toxic stimuli. Genomics, transcriptomics, proteomics, and metabolomics provide the technology to allow this to be achieved. For sophisticated, human-relevant models, the greatest benefit in using these models is achieved when an equally sophisticated analytical technique can determine the mechanism responsible for DILI for each drug. Furthermore, for development of accurate *in silico* or AI models, which could predict DILI based on a chemical structure, extensive information will be required about DILI-associated mechanisms of existing compounds, and this 'big data' can be obtained through robust omics analysis. Previous investigations using omics techniques have shown that these are immensely powerful analytical tools which can provide highly relevant mechanistic and predictive insight into DILI. It is imperative that an interdisciplinary and intersectoral approach is taken towards expanding the implementation of omics in pharmacological and toxicology to achieve the incredible potential that this analytical approach offers to revolutionise drug safety.

Financial Support:

The authors acknowledge PharmAlliance (an alliance between the Pharmacy Schools of Monash University, the University of North Carolina at Chapel Hill, and University College London) for financial support for this research. DJC is supported by an NHMRC Career Development Fellowship #APP1148700. KLRB is supported, in part, by the National Institute of General Medical Sciences of the National Institutes of Health under Award Number R35 GM122576.

Conflicts of Interest:

Dr Kim L.R. Brouwer is a co-inventor of the sandwich-cultured hepatocyte technology for quantification of biliary excretion (B-CLEAR®) and related technologies, which have been licensed exclusively to Qualyst Transporter Solutions, acquired by BioIVT.

1.6 References

Agúndez JA, Olivera M, Martínez C, Ladero JM, Benítez J. 1996. Identification and prevalence study of 17 allelic variants of the human NAT2 gene in a white population. *Pharmacogenetics (Lond.)*. 6(5):423-428.

Aithal GP, Ramsay L, Daly AK, Sonchit N, Leathart JB, Alexander G, Kenna JG, Caldwell J, Day CP. 2004. Hepatic adducts, circulating antibodies, and cytokine polymorphisms in patients with diclofenac hepatotoxicity. *Hepatology*. 39(5):1430-1440.

Andrade RJ, Lucena MI, Alonso A, García-Cortés M, García-Ruiz E, Benitez R, Fernández MC, Pelaez G, Romero M, Corpas R et al. 2004. HLA class II genotype influences the type of liver injury in drug-induced idiosyncratic liver disease. *Hepatology*. 39(6):1603-1612.

Andrade RJ, Robles M, Ulzurrun E, Lucena MI. 2009. Drug-induced liver injury: Insights from genetic studies. *Pharmacogenomics*. 10:1467-1487.

Antherieu S, Rogue A, Fromenty B, Guillouzo A, Robin MA. 2011. Induction of vesicular steatosis by amiodarone and tetracycline is associated with up-regulation of lipogenic genes in HepaRG cells. *Hepatology*. 53(6):1895-1905.

Aronson SJ, Rehm HL. 2015. Building the foundation for genomics in precision medicine. *Nature*. 526(7573):336-342.

Bjornsson ES, Bergmann OM, Bjornsson HK, Kvaran RB, Olafsson S. 2013. Incidence, presentation, and outcomes in patients with drug-induced liver injury in the general population of iceland. *Gastroenterology*. 144(7):1419-1425.

Blas-García A, Apostolova N, Ballesteros D, Monleón D, Morales JM, Rocha M, Victor VM, Esplugues JV. 2010. Inhibition of mitochondrial function by efavirenz increases lipid content in hepatic cells. *Hepatology*. 52(1):115-125.

Chalasani N, Fontana RJ, Bonkovsky HL, Watkins PB, Davern T, Serrano J, Yang H, Rochon J. 2008. Causes, clinical features, and outcomes from a prospective study of drug-induced liver injury in the united states. *Gastroenterology*. 135(6):1924-1934.

Chan A. 2015. Nonalcoholic steatohepatitis (nash). Non-neoplastic liver pathology. PathologyOutlines.

Chan R, Benet LZ. 2017. Measures of bsep inhibition in vitro are not useful predictors of DILI. *Toxicol. Sci.* 162(2):499-508.

Chan SL, Chua APG, Aminkeng F, Chee CBE, Jin S, Loh M, Gan SH, Wang YT, Brunham LR. 2017. Association and clinical utility of nat2 in the prediction of isoniazid-induced liver injury in singaporean patients. *PloS ONE*. 12(10):e0186200.

Chang N, Tian L, Ji X, Zhou X, Hou L, Zhao X, Yang Y, Yang L, Li L. 2019. Single-cell transcriptomes reveal characteristic features of mouse hepatocytes with liver cholestatic injury. Cells. 8(9):1069.

Chen M, Suzuki A, Thakkar S, Yu K, Hu C, Tong W. 2016. Dilirank: The largest reference drug list ranked by the risk for developing drug-induced liver injury in humans. *Drug Discov. Today*. 21(4):648-653.

Cosimi S, Orta L, Mateos S, Cortés F. 2009. The mycotoxin ochratoxin a inhibits DNA topoisomerase II and induces polyploidy in cultured CHO cells. *Toxicol. In Vitro*. 23(6):1110-1115.

Crocenzi FA, Mottino AD, Cao J, Veggi LM, Pozzi EJS, Vore M, Coleman R, Roma MG. 2003. Estradiol-17β-D-glucuronide induces endocytic internalization of Bsep in rats. *Am. J. Physiol. Gastrointest. Liver Physiol*. 285(2):G449-G459.

Cuykx M, Claes L, Rodrigues RM, Vanhaecke T, Covaci A. 2018. Metabolomics profiling of steatosis progression in HepaRG® cells using sodium valproate. *Toxicol. Lett*. 286:22-30.

Dieterich DT, Robinson PA, Love J, Stern JO. 2004. Drug-induced liver injury associated with the use of nonnucleoside reverse-transcriptase inhibitors. *Clin. Infect. Dis*. 38 Suppl 2:S80-S89.

Donato MT, Gómez-Lechón MJ. 2012. Drug-induced liver steatosis and phospholipidosis: Cell-based assays for early screening of drug candidates. *Curr. Drug Metab*. 13(8):1160-1173.

Donato MT, Martínez-Romero A, Jiménez N, Negro A, Herrera G, Castell JV, O'Connor J-E, Gómez-Lechón MJ. 2009. Cytometric analysis for drug-induced steatosis in HepG2 cells. *Chem. Biol. Interact*. 181(3):417-423.

Donato MT, Tolosa L, Jiménez N, Castell JV, Gómez-Lechón MJ. 2012. High-content imaging technology for the evaluation of drug-induced steatosis using a multiparametric cell-based assay. *J. Biomol. Screen*. 17(3):394-400.

Dragoi D, Benesic A, Pichler G, Kulak NA, Bartsch HS, Gerbes AL. 2018. Proteomics analysis of monocyte-derived hepatocyte-like cells identifies integrin beta 3 as

a specific biomarker for drug-induced liver injury by diclofenac. *Front. Pharmacol*. 9:699-699.

Fam TK, Klymchenko AS, Collot M. 2018. Recent advances in fluorescent probes for lipid droplets. *Materials*. 11(9):1768.

Fontana RJ. 2014. Pathogenesis of idiosyncratic drug-induced liver injury and clinical perspectives. *Gastroenterology*. 146(4):914-928.

Fontana RJ, Seeff LB, Andrade RJ, Björnsson E, Day CP, Serrano J, Hoofnagle JH. 2010. Standardization of nomenclature and causality assessment in drug-induced liver injury: Summary of a clinical research workshop. *Hepatology*. 52(2):730-742.

Funk RS, Krise JP. 2012. Cationic amphiphilic drugs cause a marked expansion of apparent lysosomal volume: Implications for an intracellular distribution-based drug interaction. *Mol. Pharm*. 9(5):1384-1395.

Ganschow R, Albani J, Grabhorn E, Richter A, Burdelski M. 2006. Tacrolimus-induced cholestatic syndrome following pediatric liver transplantation and steroid-resistant graft rejection. *Pediatr. Transplant*. 10(2):220-224.

García- Cañaveras JC, Castell JV, Donato MT, Lahoz A. 2016. A metabolomics cell-based approach for anticipating and investigating drug-induced liver injury. *Sci. Rep*. 6(1):27239.

Garzel B, Yang H, Zhang L, Huang S-M, Polli JE, Wang H. 2014. The role of bile salt export pump gene repression in drug-induced cholestatic liver toxicity. *Drug Metab. Dispos*. 42(3):318-322.

Halpern KB, Shenhav R, Matcovitch-Natan O, Toth B, Lemze D, Golan M, Massasa EE, Baydatch S, Landen S, Moor AE et al. 2017. Single-cell spatial reconstruction reveals global division of labour in the mammalian liver. *Nature*. 542(7641):352-356.

Hayashi PH, Rockey DC, Fontana RJ, Tillmann HL, Kaplowitz N, Barnhart HX, Gu J, Chalasani NP, Reddy KR, Sherker AH et al. 2017. Death and liver transplantation within 2 years of onset of drug-induced liver injury. *Hepatology*. 66(4):1275-1285.

Idilman R, Bektas M, Cinar K, Toruner M, Cerit ET, Doganay B, Erden E, Bozkaya H, Bahar K, Karayalcin S et al. 2010. The characteristics and clinical outcome of drug-induced liver injury: A single-center experience. Journal of clinical *Gastroenterology*. 44(6):e128-132.

Jagannath S, Rai R. 2000. Rapid-onset subfulminant liver failure associated with troglitazone. *Ann. Intern. Med.* 132(8):677-677.

Jennen D, Polman J, Bessem M, Coonen M, van Delft J, Kleinjans J. 2014. Drug-induced liver injury classification model based on in vitro human transcriptomics and in vivo rat clinical chemistry data. *Syst. Biol.* 2(4):63-70.

Jiang L, Gu Y, Ye J, Liu F, Zhao Y, Wang C, Xu Y, Cao X, Zhang L, Dong W et al. 2012. Resveratrol prevents hepatic steatosis induced by hepatitis C virus core protein. *Biotech. Lett.* 34(12):2205-2212.

Jonathan P. Jackson KMF, Robert L. St. ClaireIII, Chris B. Black, Kenneth R. Brouwer. 2018. Cholestatic drug induced liver injury: A function of bile salt export pump inhibition and farnesoid X receptor antagonism. *Appl. In Vitro Toxicol.* 4(3):265-279.

Kamp H, Fabian E, Groeters S, Herold M, Krennrich G, Looser R, Mattes W, Mellert W, Prokoudine A, Ruiz-Noppinger P et al. 2012. Application of in vivo metabolomics to preclinical/toxicological studies: Case study on phenytoin-induced systemic toxicity. *Bioanalysis.* 4(18):2291-2301.

Kang HE, Malinen MM, Saran C, Honkakoski P, Brouwer KLR. 2019. Optimization of canalicular abc transporter function in HuH-7 cells by modification of culture conditions. *Drug Metab. Dispos.* 47(10):1222-1230.

Kawaguchi M, Nukaga T, Sekine S, Takemura A, Susukida T, Oeda S, Kodama A, Hirota M, Kouzuki H, Ito K. 2020. Mechanism-based integrated assay systems for the prediction of drug-induced liver injury. *Toxicol. Appl. Pharmacol.* 394:114958.

Kemp DC, Zamek-Gliszczynski MJ, Brouwer KLR. 2005. Xenobiotics inhibit hepatic uptake and biliary excretion of taurocholate in rat hepatocytes. *Toxicol. Sci.* 83(2):207-214.

Kim S-H, Kim S-H, Yoon HJ, Shin DH, Park SS, Kim Y-S, Park J-S, Jee Y-K. 2012. TNF-α genetic polymorphism −308G/A and antituberculosis drug-induced hepatitis. *Liver Int.* 32(5):809-814.

Kleiner DE. 2009. The pathology of drug-induced liver injury. *Semin Liver Dis.* 29(04):364-372.

Kleiner DE, Chalasani NP, Lee WM, Fontana RJ, Bonkovsky HL, Watkins PB, Hayashi PH, Davern TJ, Navarro V, Reddy R et al. 2014. Hepatic histological findings in

suspected drug-induced liver injury: Systematic evaluation and clinical associations. *Hepatology*. 59(2):661-670.

Klopotowska JE, Wierenga PC, Smorenburg SM, Stuijt CCM, Arisz L, Kuks PFM, Dijkgraaf MGW, Lie-A-Huen L, de Rooij SE, group Ws. 2013. Recognition of adverse drug events in older hospitalized medical patients. *Eur. J. Clin. Pharmacol*. 69(1):75-85.

Kohonen P, Parkkinen JA, Willighagen EL, Ceder R, Wennerberg K, Kaski S, Grafström RC. 2017. A transcriptomics data-driven gene space accurately predicts liver cytopathology and drug-induced liver injury. *Nat. Commun*. 8(1):15932.

Kumar AH, Ramesh K, Kannan T, Sudha V, Haribabu H, Lavanya J, Swaminathan S, Ramachandran G. 2017. N-acetyltransferase gene polymorphisms & plasma isoniazid concentrations in patients with tuberculosis. *Indian J. Med. Res*. 145(1):118.

Kyriakides M, Maitre L, Stamper BD, Mohar I, Kavanagh TJ, Foster J, Wilson ID, Holmes E, Nelson SD, Coen M. 2016. Comparative metabonomic analysis of hepatotoxicity induced by acetaminophen and its less toxic meta-isomer. *Arch. Toxicol*. 90(12):3073.

Li C, Ming Y, Hong W, Tang Y, Lei X, Li X, Mao Y. 2018. Comparison of hepatic transcriptome profiling between acute liver injury and acute liver failure induced by acetaminophen in mice. *Toxicol. Lett*. 283:69-76.

Licata A, Minissale MG, Calvaruso V, Craxi A. 2017. A focus on epidemiology of drug-induced liver injury: Analysis of a prospective cohort. *Eur Rev Med Pharmacol Sci*. 21(1 Suppl):112-121.

Liu F, Wang C, Zhang L, Xu Y, Jang L, Gu Y, Cao X, Zhao X, Ye J, Li Q. 2014. Metformin prevents hepatic steatosis by regulating the expression of adipose differentiation-related protein. *Int J Mol Med*. 33(1):51-58.

Liu Z, Huang R, Roberts R, Tong W. 2019. Toxicogenomics: A 2020 vision. *Trends Pharmacol. Sci*. 40(2):92-103.

Lu R-J, Zhang Y, Tang F-L, Zheng Z-W, Fan Z-D, Zhu S-M, Qian X-F, Liu N-N. 2016. Clinical characteristics of drug-induced liver injury and related risk factors. *Exp. Ther. Med*. 12(4):2606-2616.

Lucena MI, Andrade RJ, Martínez C, Ulzurrun E, García-Martín E, Borraz Y, Fernández MC, Romero-Gomez M, Castiella A, Planas R et al. 2008.

Glutathione s-transferase M1 and T1 null genotypes increase susceptibility to idiosyncratic drug-induced liver injury. *Hepatology*. 48(2):588-596.

Lucena MI, Molokhia M, Shen Y, Urban TJ, Aithal GP, Andrade RJ, Day CP, Ruiz-Cabello F, Donaldson PT, Stephens C et al. 2011. Susceptibility to amoxicillin-clavulanate-induced liver injury is influenced by multiple HLA class I and II alleles. *Gastroenterology*. 141(1):338-347.

Ma Z, Wang X, Yin P, Wu R, Zhou L, Xu G, Niu J. 2019. Serum metabolome and targeted bile acid profiling reveals potential novel biomarkers for drug-induced liver injury. *Medicine (Baltimore)*. 98(31):e16717-e16717.

MacParland SA, Liu JC, Ma XZ, Innes BT, Bartczak AM, Gage BK, Manuel J, Khuu N, Echeverri J, Linares I et al. 2018. Single cell RNA sequencing of human liver reveals distinct intrahepatic macrophage populations. *Nat Commun*. 9(1):4383.

Malinen MM, Ito K, Kang HE, Honkakoski P, Brouwer KLR. 2019. Protein expression and function of organic anion transporters in short-term and long-term cultures of HuH-7 human hepatoma cells. *Eur J Pharm Sci*. 130:186-195.

Martín-Carbonero L, Nunez M-J, González-Lahoz J, Soriano V. 2003. Incidence of liver injury after beginning antiretroviral therapy with efavirenz or nevirapine. HIV clinical trials. 4:115-120.

Masarone M, Rosato V, Dallio M, Gravina AG, Aglitti A, Loguercio C, Federico A, Persico M. 2018. Role of oxidative stress in pathophysiology of nonalcoholic fatty liver disease. *Oxid. Med. Cell. Longev*. 2018:9547613-9547613.

Mattes W, Davis K, Fabian E, Greenhaw J, Herold M, Looser R, Mellert W, Groeters S, Marxfeld H, Moeller N et al. 2014. Detection of hepatotoxicity potential with metabolite profiling (metabolomics) of rat plasma. *Toxicol. Lett.* 230(3):467-478.

Mattes WB, Kamp HG, Fabian E, Herold M, Krennrich G, Looser R, Mellert W, Prokoudine A, Strauss V, van Ravenzwaay B et al. 2013. Prediction of clinically relevant safety signals of nephrotoxicity through plasma metabolite profiling. *BioMed Res. Int*. 2013:202497.

Meier Y, Cavallaro M, Roos M, Pauli-Magnus C, Folkers G, Meier PJ, Fattinger K. 2005. Incidence of drug-induced liver injury in medical inpatients. *Eur. J. Clin. Pharmacol*. 61(2):135-143.

Morgan RE, Trauner M, van Staden CJ, Lee PH, Ramachandran B, Eschenberg M, Afshari CA, Qualls CW, Jr, Lightfoot-Dunn R, Hamadeh HK. 2010. Interference

with bile salt export pump function is a susceptibility factor for human liver injury in drug development. *Toxicol. Sci.* 118(2):485-500.

Morgan RE, van Staden CJ, Chen Y, Kalyanaraman N, Kalanzi J, Dunn RT, II, Afshari CA, Hamadeh HK. 2013. A multifactorial approach to hepatobiliary transporter assessment enables improved therapeutic compound development. *Toxicol. Sci.* 136(1):216-241.

Mottino AD, Cao J, Veggi LM, Crocenzi F, Roma MG, Vore M. 2002. Altered localization and activity of canalicular MRP2 in estradiol-17β-D-glucuronide–induced cholestasis. *Hepatology*. 35(6):1409-1419.

Navarro VJ, Khan I, Björnsson E, Seeff LB, Serrano J, Hoofnagle JH. 2017. Liver injury from herbal and dietary supplements. *Hepatology*. 65(1):363-373.

Nebeker JR, Hoffman JM, Weir CR, Bennett CL, Hurdle JF. 2005. High rates of adverse drug events in a highly computerized hospital. *Ann. Intern. Med.* 165(10):1111-1116.

Ohno M, Yamaguchi I, Yamamoto I, Fukuda T, Yokota S, Maekura R, Ito M, Yamamoto Y, Ogura T, Maeda K et al. 2000. Slow N-acetyltransferase 2 genotype affects the incidence of isoniazid and rifampicin-induced hepatotoxicity. *Int. J. Tuberc. Lung Dis.* 4:256-261.

Ohsaki Y, Shinohara Y, Suzuki M, Fujimoto T. 2010. A pitfall in using bodipy dyes to label lipid droplets for fluorescence microscopy. *Histochem. Cell Biol.* 133(4):477-480.

Onofrio FQ, Hirschfield GM. 2020. The pathophysiology of cholestasis and its relevance to clinical practice. *Clin. Liver Dis.* 15(3):110-114.

Ostry V. 2008. Alternaria mycotoxins: An overview of chemical characterization, producers, toxicity, analysis and occurrence in foodstuffs. World Mycotoxin Journal. 1(2):175-188.

Padda MS, Sanchez M, Akhtar AJ, Boyer JL. 2011. Drug-induced cholestasis. *Hepatology*. 53(4):1377-1387.

Paemanee A, Somjai W, Kittisenachai S, Sirinonthanawech N, Roytrakul S, Wongtrakul J, Smith DR. 2017. Nevirapine induced mitochondrial dysfunction in HepG2 cells. *Sci. Rep* 7:1-11.

Petros Z, Lee M-TM, Takahashi A, Zhang Y, Yimer G, Habtewold A, Amogne W, Aderaye G, Schuppe-Koistinen I, Mushiroda T et al. 2016. Genome-wide

association and replication study of anti-tuberculosis drugs-induced liver toxicity. *BMC Genomics*. 17(1):755.

Pilon AA, Lum JJ, Sanchez-Dardon J, Phenix BN, Douglas R, Badley AD. 2002. Induction of apoptosis by a nonnucleoside human immunodeficiency virus type 1 reverse transcriptase inhibitor. *Antimicrob. Agents Chemother*. 46(8):2687-2691.

Ramirez T, Strigun A, Verlohner A, Hans-Albrecht H, Peter E, Herold M, Bordag N, Mellert W, Walk T, Spitzer M et al. 2018. Prediction of liver toxicity and mode of action using metabolomics in vitro in HepG2 cells. *Arch. Toxicol*. 92(2):893-906.

Rao MS, Van Vleet TR, Ciurlionis R, Buck WR, Mittelstadt SW, Blomme EAG, Liguori MJ. 2019. Comparison of rna-seq and microarray gene expression platforms for the toxicogenomic evaluation of liver from short-term rat toxicity studies. *Front. Genet*. 9(636).

Reuben A, Koch DG, Lee WM. 2010. Drug-induced acute liver failure: Results of a U.S. Multicenter, prospective study. *Hepatology*. 52(6):2065-2076.

Rodrigues RM, Heymans A, De Boe V, Sachinidis A, Chaudhari U, Govaere O, Roskams T, Vanhaecke T, Rogiers V, De Kock J. 2016. Toxicogenomics-based prediction of acetaminophen-induced liver injury using human hepatic cell systems. *Toxicol. Lett*. 240(1):50-59.

Román ID, Fernández-Moreno MD, Fueyo JA, Roma MG, Coleman R. 2003. Cyclosporin a induced internalization of the bile salt export pump in isolated rat hepatocyte couplets. *Toxicol. Sci*. 71(2):276-281.

Saito J, Okamura A, Takeuchi K, Hanioka K, Okada A, Ohata T. 2016. High content analysis assay for prediction of human hepatotoxicity in HepaRG and HepG2 cells. *Toxicol. In Vitro*. 33:63-70.

Schadinger SE, Bucher NLR, Schreiber BM, Farmer SR. 2005. Pparγ2 regulates lipogenesis and lipid accumulation in steatotic hepatocytes. *Am. J. Physiol. Endocrinol. Metab*. 288(6):E1195-E1205.

Serviddio G, Bellanti F, Vendemiale G, Altomare E. 2011. Mitochondrial dysfunction in nonalcoholic steatohepatitis. *Expert Rev Gastroenterol Hepatol*. 5(2):233-244.

Simon T, Becquemont L, Mary-Krause M, de Waziers I, Beaune P, Funck-Brentano C, Jaillon P. 2000. Combined glutathione-s-transferase M1 and T1 genetic

polymorphism and tacrine hepatotoxicity. *Clin. Pharmacol. Ther.* 67(4):432-437.

Singer JB, Lewitzky S, Leroy E, Yang F, Zhao X, Klickstein L, Wright TM, Meyer J, Paulding CA. 2010. A genome-wide study identifies hla alleles associated with lumiracoxib-related liver injury. *Nat* Genet. 42(8):711-714.

Smith M-C, Timmins-Schiffman E, Coton M, Coton E, Hymery N, Nunn BL, Madec S. 2018. Differential impacts of individual and combined exposures of deoxynivalenol and zearalenone on the HepaRG human hepatic cell proteome. *J. Proteomics*. 173:89-98.

Spraggs CF, Budde LR, Briley LP, Bing N, Cox CJ, King KS, Whittaker JC, Mooser VE, Preston AJ, Stein SH et al. 2011. HLA-DQA1*02:01 is a major risk factor for lapatinib-induced hepatotoxicity in women with advanced breast cancer. *J. Clin. Oncol*. 29(6):667-673.

Suk KT, Kim DJ, Kim CH, Park SH, Yoon JH, Kim YS, Baik GH, Kim JB, Kweon YO, Kim BI et al. 2012. A prospective nationwide study of drug-induced liver injury in korea. *Am. J. Gastroenterol*. 107(9):1380-1387.

Sundaram V, Björnsson ES. 2017. Drug-induced cholestasis. *Hepatol. Commun*. 1(8):726-735.

Touré A, Cabral M, Niang A, Diop CAK, Garat A, Humbert L, Fall M, Diouf A, Broly F, Lhermitte M et al. 2016. Prevention of isoniazid toxicity by NAT2 genotyping in senegalese tuberculosis patients. *Toxicol. Rep*. 3:826 - 831.

Van Norman GA. 2019. Limitations of animal studies for predicting toxicity in clinical trials: Is it time to rethink our current approach? *JACC: Basic to Translational Science*. 4(7):845-854.

van Ravenzwaay B, Cunha GC-P, Leibold E, Looser R, Mellert W, Prokoudine A, Walk T, Wiemer J. 2007. The use of metabolomics for the discovery of new biomarkers of effect. *Toxicol. Lett*. 172(1):21-28.

van Ravenzwaay B, Sperber S, Lemke O, Fabian E, Faulhammer F, Kamp H, Mellert W, Strauss V, Strigun A, Peter E et al. 2016. Metabolomics as read-across tool: A case study with phenoxy herbicides. *Regul. Toxicol. Pharmacol*. 81:288-304.

van Swelm RPL, Laarakkers CMM, van der Kuur EC, Morava-Kozicz E, Wevers RA, Augustijn KD, Touw DJ, Sandel MH, Masereeuw R, Russel FGM. 2012. Identification of novel translational urinary biomarkers for acetaminophen-

induced acute liver injury using proteomic profiling in mice. *PloS ONE*. 7(11):e49524.

Vitins AP, Kienhuis AS, Speksnijder EN, Roodbergen M, Luijten M, van der Ven LT. 2014. Mechanisms of amiodarone and valproic acid induced liver steatosis in mouse in vivo act as a template for other hepatotoxicity models. *Arch. Toxicol*. 88(8):1573-1588.

Waring MJ, Arrowsmith J, Leach AR, Leeson PD, Mandrell S, Owen RM, Pairaudeau G, Pennie WD, Pickett SD, Wang J et al. 2015. An analysis of the attrition of drug candidates from four major pharmaceutical companies. *Nat. Rev. Drug Discov*. 14(7):475-486.

Watanabe I, Tomita A, Shimizu M, Sugawara M, Yasumo H, Koishi R, Takahashi T, Miyoshi K, Nakamura K, Izumi T et al. 2003. A study to survey susceptible genetic factors responsible for troglitazone-associated hepatotoxicity in japanese patients with type 2 diabetes mellitus. *Clin. Pharmacol. Ther*. 73(5):435-455.

Wolters JEJ, van Breda SGJ, Grossmann J, Fortes C, Caiment F, Kleinjans JCS. 2018. Integrated 'omics analysis reveals new drug-induced mitochondrial perturbations in human hepatocytes. *Toxicol. Lett*. 289:1-13.

Wolters JEJ, van Herwijnen MHM, Theunissen DHJ, Jennen DGJ, Van den Hof WFPM, de Kok TMCM, Schaap FG, van Breda SGJ, Kleinjans JCS. 2016. Integrative "-omics" analysis in primary human hepatocytes unravels persistent mechanisms of cyclosporine a-induced cholestasis. *Chem. Res. Toxicol*. 29(12):2164-2174.

Xie Z, Chen E, Ouyang X, Xu X, Ma S, Ji F, Wu D, Zhang S, Zhao Y, Li L. 2019. Metabolomics and cytokine analysis for identification of severe drug-induced liver injury. *J. Proteome Res*. 18(6):2514-2524.

Yeh MM, Brunt EM. 2014. Pathological features of fatty liver disease. *Gastroenterology*. 147(4):754-764.

1.7 Tables & Figures

Table 1: Aetiology of the various clinical classifications of DILI and the clinical criteria used to classify each clinical class of DILI (Fontana et al. 2010; Kleiner et al. 2014; Licata et al. 2017; Lu et al. 2016).

Clinical Classification	R*-Value Range	Prevalence Range
Hepatocellular	R ≥ 5	52 – 59%
Mixed	2 < R < 5	6 – 23%
Cholestatic	R ≤ 2	18 – 29%

$$R = \frac{ALT}{ULN_{ALT}} \div \frac{ALP}{ULN_{ALP}}*.$$

ALT = Alanine aminotransferase, ALP = Alkaline phosphatase, ULN = Upper limit of normal

Table 2: Non-omic based analytical techniques applicable for DILI studies

Assay	Method	Outcome	Advantages/Limitations
Cell viability assay	A spectroscopic change is made to a chemical indicator based on the function of a cell's mitochondria. Viability is commonly measured by the cellular ATP content or the presence of viable mitochondrial enzymes	Quantifies the relative number of functional mitochondria present in a culture	Accessible measurement of cytotoxicity that can be conducted in a high-throughput manner. Measurements are non-specific and are based on biomarkers of viability which may be impacted without permanent cell death
C-DILI™ assay	Comparison of viability of drug-treated control hepatocytes and cholestatic-sensitised hepatocytes	Determines a drug's potential to cause bile acid-mediated hepatotoxicity and its risk of causing cholestatic DILI	Specific assay for high-throughput determination of cholestatic potential of chemicals. Requires use of transporter certified primary human hepatocytes for greatest accuracy
Membrane integrity assay	A spectroscopic change is made to a chemical indicator based on the amount of lactate dehydrogenase (LDH) released from cells due to the loss of cell membrane integrity	Quantifies the amount of LDH released from cells due to loss of cell membrane integrity. In many cases, it is assumed that the loss of integrity is due to cell death	Accessible measurement of cytotoxicity that can be conducted in a high-throughput manner. Measurements are non-specific and rely on the presence of LDH, which has a 6- to 8-hour half-life potentially leading to inaccurate results
Apoptosis assay	A spectroscopic change is made to a chemical indicator based on the caspase-3 and/or -7 abundance within a cell culture	Gives an indication of the relative amount of apoptosis that a cell population is experiencing	Accessible measurement of apoptosis that can be conducted in a high-throughput manner. Cell death occurring through non-apoptotic pathways may be poorly assessed
Western blot	Gel electrophoresis followed by attachment of a primary antibody to a target protein followed by the attachment of a	Determines if a specific protein is present in a biological protein extract, and provides a semi-quantitative	Antibodies are specific and sensitive to target proteins; data are only semi-quantitative. Primary antibodies are expensive and

	secondary antibody	indication of relative abundance	may not be available for all target proteins
B-CLEAR® assay	Comparison of cellular accumulation vs cellular and biliary accumulation of transporter substrates by comparing cells with and without sealed tight junctions forming bile canaliculi	Quantifies functional changes in hepatocyte basolateral (uptake) and canalicular (biliary excretion) transporters	Offers quantitative measurement of changes in transport and cellular concentrations of bile acids and/or xenobiotics. Requires use of transporter certified PHH for greatest accuracy
Transporter localisation	Immunofluorescence microscopy of target transport proteins via the use of primary and fluorescent-labelled secondary antibodies	Assesses the localisation of hepatic transporters	Offers semi-quantitative spatial information about transporter location within cells; cannot be applied to live cells
Neutral lipid staining	Staining of hepatocytes with lipophilic dyes (e.g., BODIPY, Oil Red O) for fluorescence microscopy	Identifies the intracellular accumulation of neutral lipids caused by drug treatment resulting in steatosis	Allows for the accessible and, potentially high-throughput visualisation of neutral lipid accumulation. Degree of accumulation can only be assessed semi-quantitatively, and neutral lipid dyes do not stain phospholipids
Lysosomal staining	Staining of acidic lysosomal environment with dyes (e.g., NBD-PE, HCS LipidTOX™, LysoTracker™) for fluorescence microscopy	Determines whether lysosomes have increased in size or abundance and may be used to identify phospholipidosis	Allows for the accessible and, potentially high-throughput visualisation of changes in lysosomes. Lysosomal changes are semi-quantitative

Figure 1: Mechanisms by which drugs may disrupt lipid transport and metabolism leading to steatosis in hepatocytes. Drug-induced steatosis may result from increased uptake of free fatty acids (FFA) and chylomicrons (CM), impaired fatty acid oxidation (β-oxidation) and resulting esterification of excess FFA to acylglycerides (AG), and impaired export of very low-density lipoproteins (VLDL) by inhibition of microsomal triglyceride transfer proteins (MTTP).

Figure 2: Common mechanisms by which a cholestatic drug may cause impaired bile acid transport including A) direct inhibition of the transporter, B) inhibition of transporter gene expression, and C) internalisation of transporters. Transporters are depicted in green, the nucleus in blue, and bile acids (B) in yellow.

Figure 3: BODIPY staining of primary human hepatocytes (PHH), comparing control to steatotic hepatocytes. Day 5 sandwich cultured PHH untreated (control) or treated with 1 mM free fatty acids for 24 h (steatotic). PHH were stained with BODIPY 493/503 (green), Hoechst 33342 (blue), and Alexa Fluor™ 488 Phalloidin (yellow) and imaged using an Operetta® high-content imaging system.

Figure 4: Schematic representation of a multi-omics workflow for *in vitro* cell-based models to provide transcriptomics, proteomics and metabolomics analysis of biological pathways impacted by addition of drugs associated with DILI.

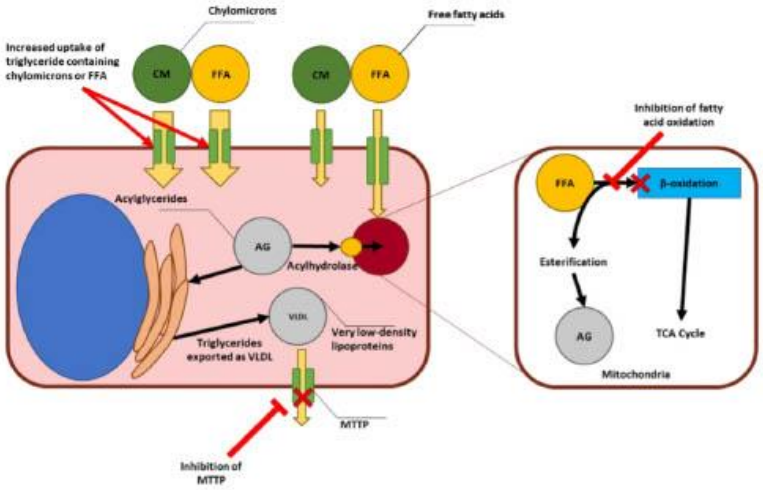

Figure 1: Mechanisms by which drugs may disrupt lipid transport and metabolism leading to steatosis in hepatocytes. Drug-induced steatosis may result from increased uptake of free fatty acids (FFA) and chylomicrons (CM), impaired fatty acid oxidation (β-oxidation) and resulting esterification of excess FFA to acylglycerides (AG), and impaired export of very low-density lipoproteins (VLDL) by inhibition of microsomal triglyceride transfer proteins (MTTP).

160x103mm (300 x 300 DPI)

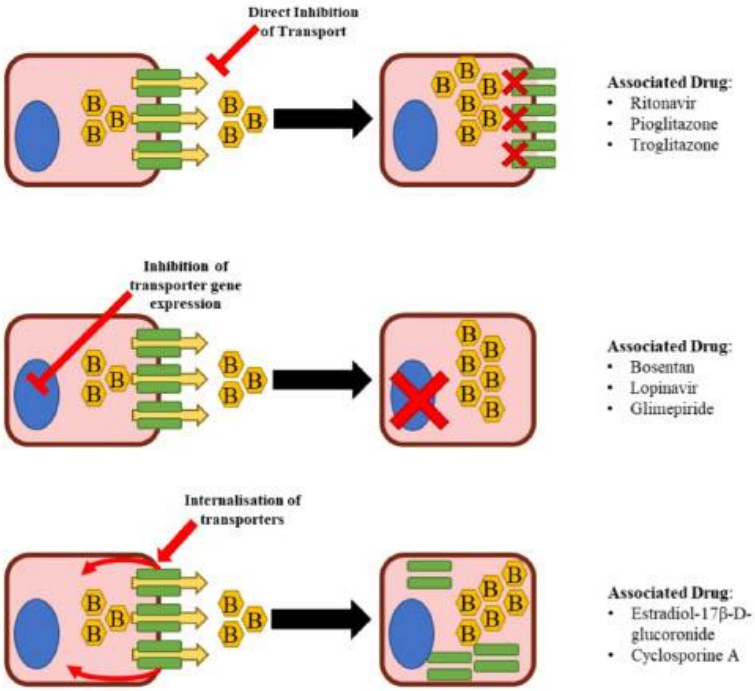

Figure 2: Common mechanisms by which a cholestatic drug may cause impaired bile acid transport including A) direct inhibition of the transporter, B) inhibition of transporter gene expression, and C) internalisation of transporters. Transporters are depicted in green, the nucleus in blue, and bile acids (B) in yellow.

155x141mm (300 x 300 DPI)

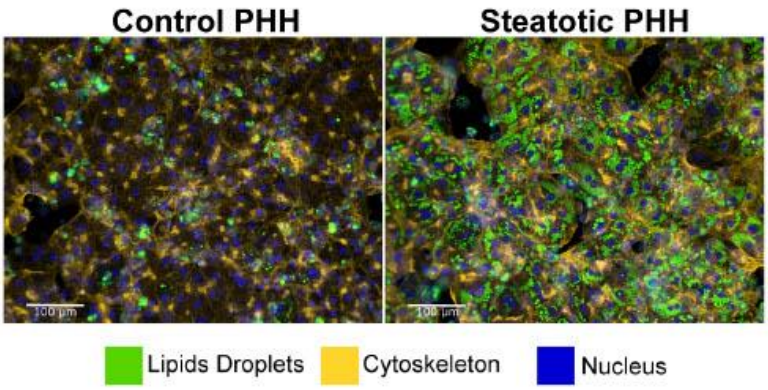

Figure 3: BODIPY staining of primary human hepatocytes (PHH), comparing control to steatotic hepatocytes. Day 5 sandwich cultured PHH untreated (control) or treated with 1 mM free fatty acids for 24 h (steatotic). PHH were stained with BODIPY 493/503 (green), Hoechst 33342 (blue), and Alexa Fluor™ 488 Phalloidin (yellow) and imaged using an Operetta® high-content imaging system.

203x100mm (600 x 600 DPI)

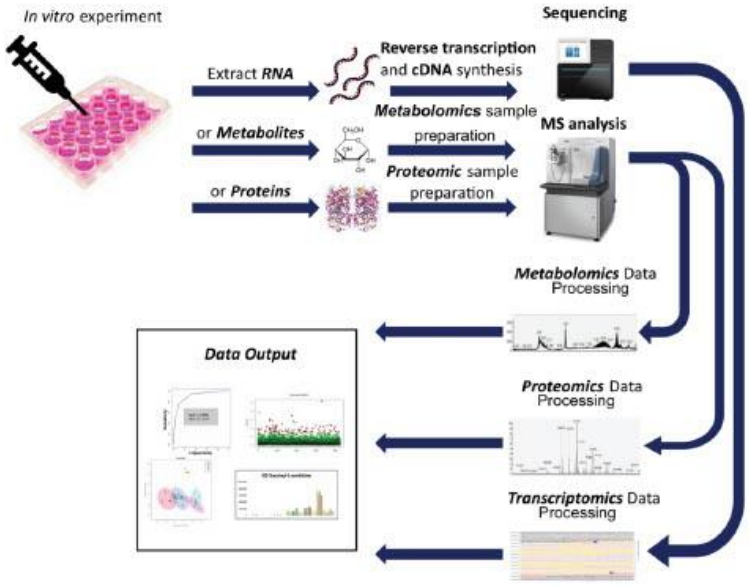

Figure 4: Schematic representation of a multi-omics workflow for in vitro cell-based models to provide transcriptomics, proteomics and metabolomics analysis of biological pathways impacted by addition of drugs associated with DILI.

206x164mm (300 x 300 DPI)

Appendix 2

Primary human hepatocyte (PHH) donor information used in all studies.

Lot Name	Age	Gender	Product type
BXW	Female	73	Transporter certified
GWD	Male	74	Cryoplateable
IWM	Male	46	Transporter certified
JHY	Male	51	Cryoplateable
JPR	Female	76	Cryoplateable
OSI	Female	48	Cryoplateable
WID	Male	71	Transporter certified
WWQ	Male	22	Transporter certified
YNM	Female	48	Cryoplateable
XVN	Male	57	Transporter certified

Appendix 3

Cell viability of drug-treated primary human hepatocytes (PHH) and HepaRG™ cells from the C-DILI™ hepatotoxicity assay for ten drug-induced liver injury (DILI) associated drugs over a range of concentrations. Cell viability of drug-treated PHH (donors WID, WWQ, BXW, and XVN) and HepaRG™ cells after treatment with DILI-associated drugs at five different concentrations. (A) Cell viability determined by cellular ATP abundance using the CellTiter-Glo® luminescent cell viability assay. (B) Cell viability determined by extracellular lactate dehydrogenase (LDH) abundance using the CytoTox-ONE™ homogeneous membrane integrity assay. Data (mean ± SD in triplicate for PHH and quadruplicate for HepaRG™ cells) are expressed as (%)of control.

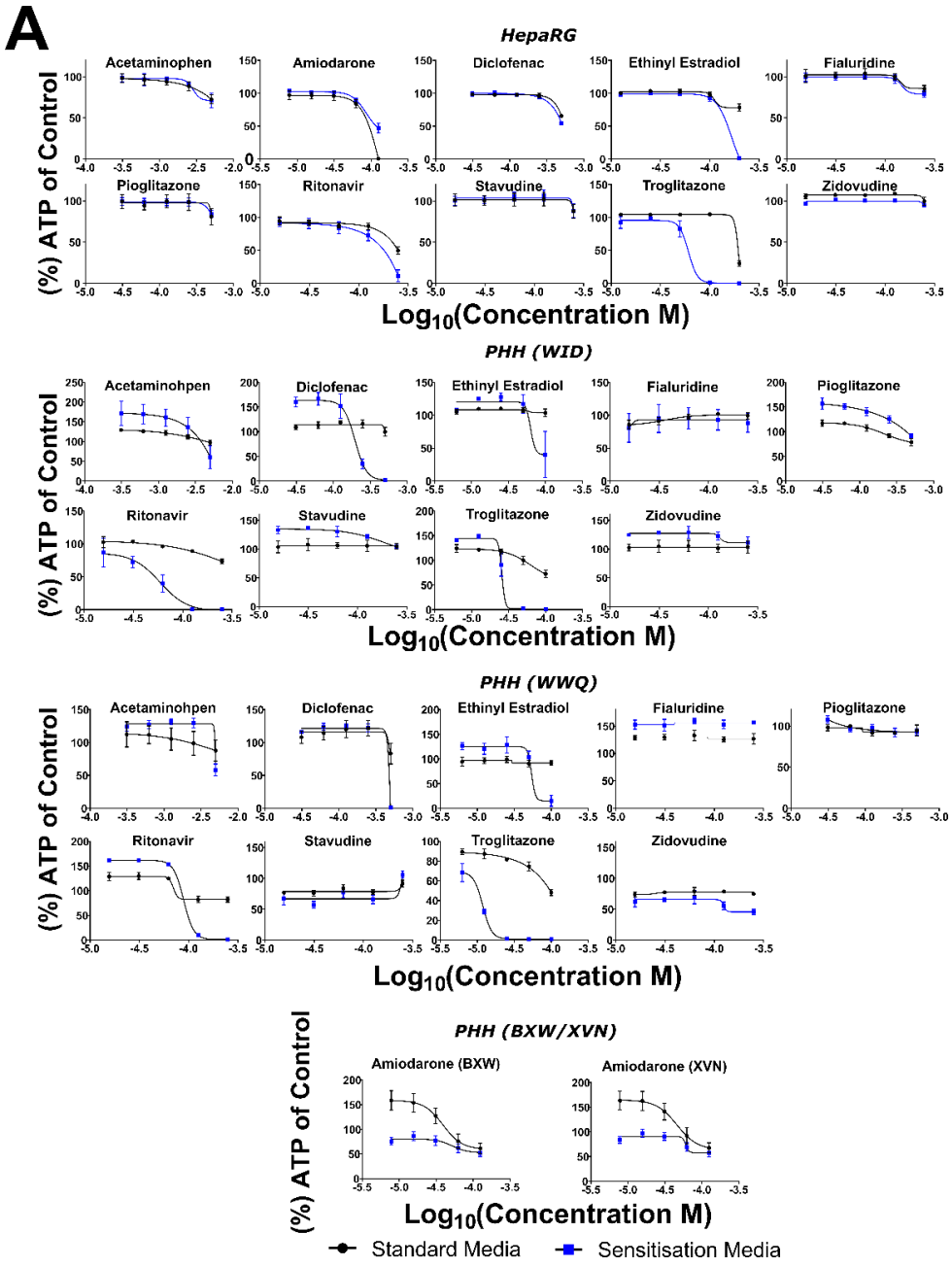
A
HepaRG
Acetaminophen
Amiodarone
Diclofenac
Ethinyl Estradiol
Fialuridine
Pioglitazone
Ritonavir
Stavudine
Troglitazone
Zidovudine
(%) ATP of Control
Log10(Concentration M)
PHH (WID)
Acetaminohpen
Diclofenac
Ethinyl Estradiol
Fialuridine
Pioglitazone
Ritonavir
Stavudine
Troglitazone
Zidovudine
(%) ATP of Control
Log10(Concentration M)
PHH (WWQ)
Acetaminohpen
Diclofenac
Ethinyl Estradiol
Fialuridine
Pioglitazone
Ritonavir
Stavudine
Troglitazone
Zidovudine
(%) ATP of Control
Log10(Concentration M)
PHH (BXW/XVN)
Amiodarone (BXW)
Amiodarone (XVN)
(%) ATP of Control
Log10(Concentration M)
Standard Media
Sensitisation Media

B

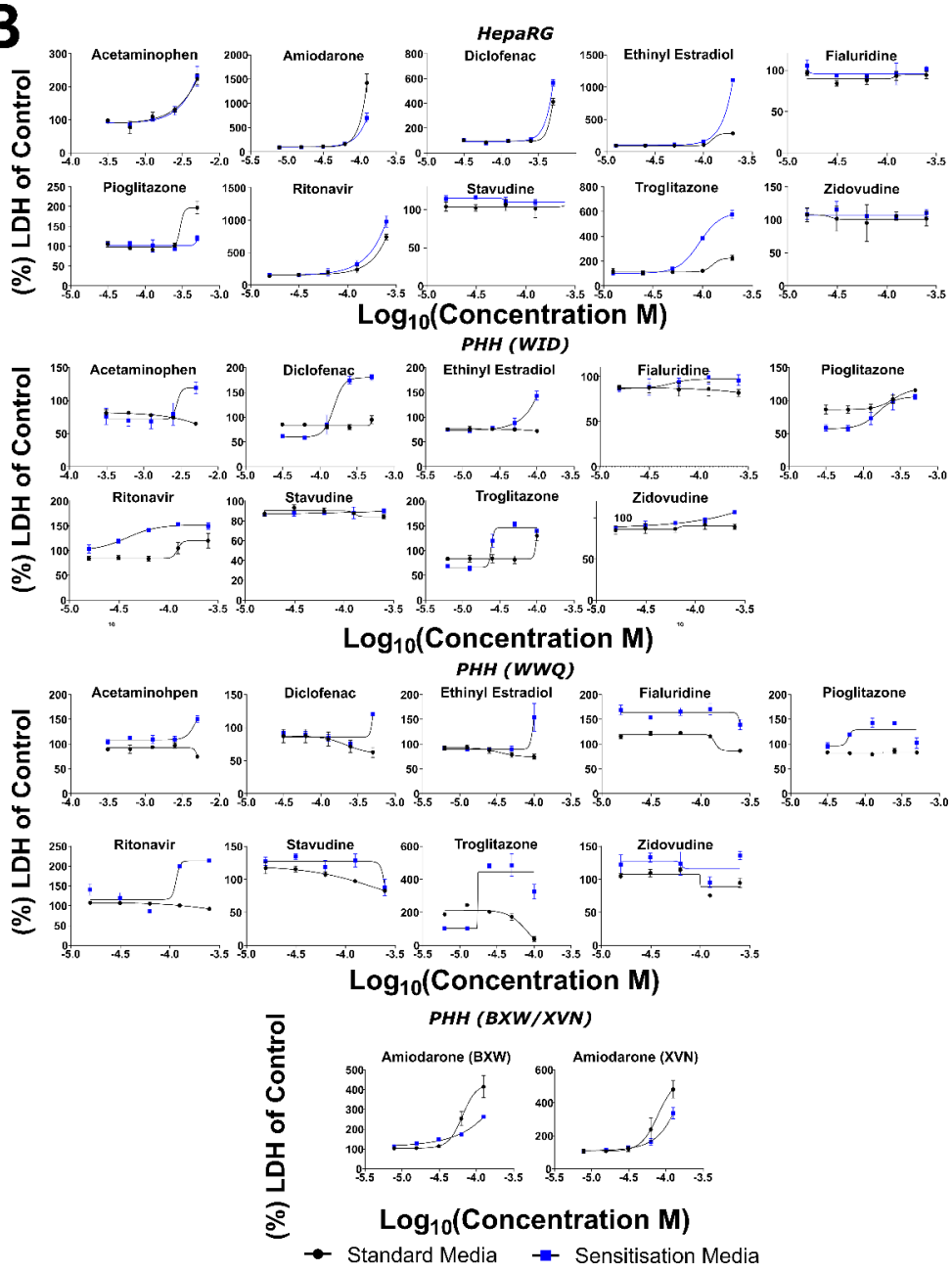
HepaRG
Acetaminophen
Amiodarone
Diclofenac
Ethinyl Estradiol
Fialuridine
Pioglitazone
Ritonavir
Stavudine
Troglitazone
Zidovudine
(%) LDH of Control
Log10(Concentration M)
PHH (WID)
Acetaminophen
Diclofenac
Ethinyl Estradiol
Fialuridine
Pioglitazone
Ritonavir
Stavudine
Troglitazone
Zidovudine
(%) LDH of Control
Log10(Concentration M)
PHH (WWQ)
Acetaminohpen
Diclofenac
Ethinyl Estradiol
Fialuridine
Pioglitazone
Ritonavir
Stavudine
Troglitazone
Zidovudine
(%) LDH of Control
Log10(Concentration M)
PHH (BXW/XVN)
Amiodarone (BXW)
Amiodarone (XVN)
(%) LDH of Control
Log10(Concentration M)
Standard Media
Sensitisation Media

Appendix 4

Pathway histogram and protein association chart for comparison of primary human hepatocyte (PHH) and HepaRG cells for the whole cell and major metabolic pathways proteome. (A) Pathway histogram and protein association chart for the top 100 proteins from the whole cell proteome, which differed most between PHH and HepaRG cells. (B) Pathway histogram and protein association chart for the top 50 proteins from the major metabolic proteome, which differed most between PHH and HepaRG cells. The histogram shows the $-\log_{10}$(p-value) for each pathway that shows different abundance of proteins between PHH and HepaRG cells. A black box denotes that the protein is present in the proteome of the respective pathway.

A

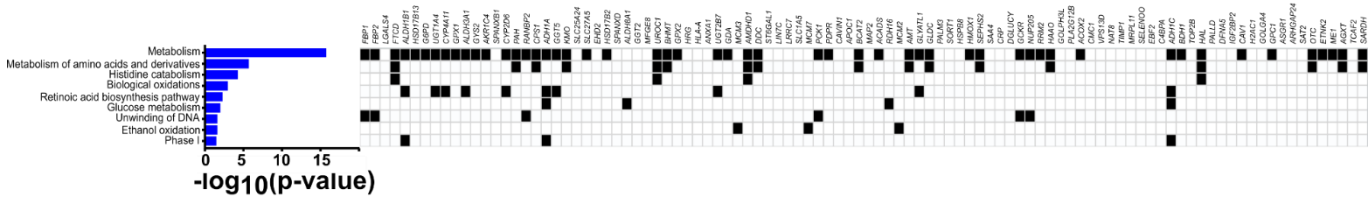
Metabolism
Metabolism of amino acids and derivatives
Histidine catabolism
Biological oxidations
Retinoic acid biosynthesis pathway
Glucose metabolism
Unwinding of DNA
Ethanol oxidation
Phase I
0
5
10
15
-log10(p-value)

B

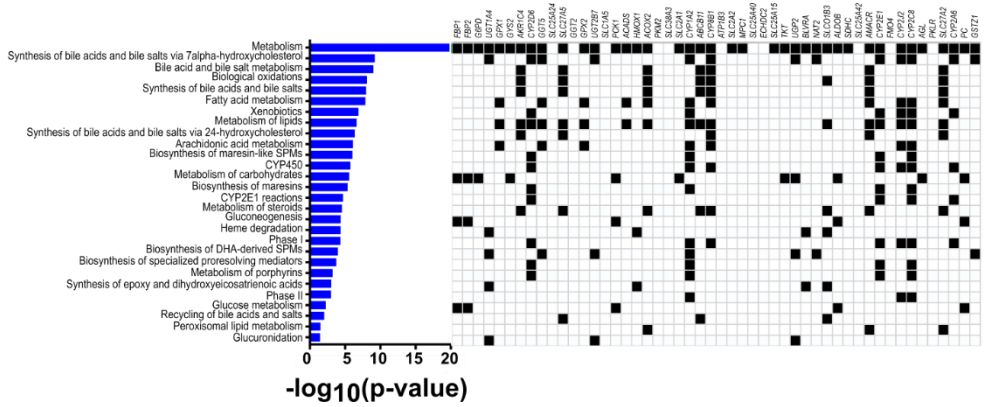
Metabolism
Synthesis of bile acids and bile salts via 7alpha-hydroxycholesterol
Bile acid and bile salt metabolism
Biological oxidations
Synthesis of bile acids and bile salts
Fatty acid metabolism
Xenobiotics
Metabolism of lipids
Synthesis of bile acids and bile salts via 24-hydroxycholesterol
Arachidonic acid metabolism
Biosynthesis of maresin-like SPMs
CYP450
Metabolism of carbohydrates
Biosynthesis of maresins
CYP2E1 reactions
Metabolism of steroids
Gluconeogenesis
Heme degradation
Phase I
Biosynthesis of DHA-derived SPMs
Biosynthesis of specialized proresolving mediators
Metabolism of porphyrins
Synthesis of epoxy and dihydroxyeicosatrienoic acids
Phase II
Glucose metabolism
Recycling of bile acids and salts
Peroxisomal lipid metabolism
Glucuronidation
0
5
10
15
20
-log10(p-value)

Appendix 5

List of 80 proteins related to transport, phase I and II metabolism, and bile acid metabolism analysed using data-independent acquisition (DIA) proteomics after treatment with cholestatic drugs. Proteins shown in bold were those detected by DIA proteomics.

Transporters	*Phase I CYP Enzymes*	*Glucuronidation Enzymes*	*Miscellaneous Proteins*	*Bile Acid Metabolism Enzymes*
BCRP	**CYP1A2**	**UGT1A1**	**AO**	**BAAT**
BSEP	**CYP2A6**	**UGT1A3**	**CES1**	**SLC27A5**
CNT1	**CYP2B6**	**UGT1A4**	**CES2**	CYP7A1
CNT3	**CYP2C8**	UGT1A5	**FMO3**	**CYP7B1**
ENT1	**CYP2C9**	**UGT1A6**	**FMO5**	**CYP8B1**
ENT2	**CYP2C19**	**UGT1A7**	**gamma GTP**	**CYP27A1**
ENT4	**CYP2D6**	UGT1A8	**ATP1A1-α**	
MATE1	**CYP2E1**	UGT1A10	**ATP1A1-β**	
MRP1	**CYP2J2**	**UGT2A3**	**ATP1A3-β**	
MRP2	**CYP3A4**	**UGT2B10**	**POR**	
MRP3	**CYP3A5**	**UGT2B15**	**SULT1A1**	
MRP4	CYP3A7	UGT2B17	**SULT1A3**	
MRP5	**CYP4F2**	**UGT2B4**	**SULT2A1**	
MRP6		**UGT2B7**		
MRP9				
NTCP				
OAT2				
OAT3				
OAT7				
OCT1				
OCT2				
OCT3				
OCTN1				
OST-α				
OST-β				
OATP1A2				
OATP2A1				
OATP1B1				
OATP1B3				

OATP2B1 OATP4C1 **P-gp** **MDR3**				

Appendix 6

Partial least squares-discriminant analysis (PLS-DA) component 1 lipids from the 'Fatty acids and glycerolipids' and 'Phospholipids' datasets with variable importance in projection (VIP) scores ≥ 1

Fatty acids and Glycerolipids		Phospholipids			
Lipid species	*VIP Scores*	*Lipid species*	*VIP Scores*	*Lipid species*	*VIP Scores*
TAG(62:7)	2.629	**PI(P-36:1)**	3.9483	**PG(38:4)**	1.1225
TAG(62:8)	2.4922	**PG(38:3)**	3.4739	**PE(36:2)**	1.111
TAG(42:2)	2.3816	**PC(P-32:4)**	3.2686	**PC(38:7)**	1.0892
TAG(62:12)	2.3815	**PS(32:1)**	3.2377	**PG(40:6)**	1.0845
TAG(42:3)	2.3773	**PG(P-36:5)**	2.9919	**PG(36:5)**	1.0584
TAG(44:4)	2.3448	**PG(36:4)**	2.6288	**PC(38:8)**	1.0548
TAG(62:6)	2.2704	**PG(36:3)**	2.628	**PE(34:1)**	1.0328
TAG(62:10)	2.209	**PC(40:1)**	2.4126	**PE(34:0)**	1.0219
TAG(42:1)	2.1208	**PE(34:2)**	2.2407	**PG(38:4)**	1.1225
TAG(44:3)	2.1163	**PC(P-28:0)**	2.128	**PE(36:2)**	1.111
DAG(42:2)	2.0435	**PG(P-36:6)**	2.0886	**PC(38:7)**	1.0892
DAG(44:2)	1.9586	**PG(P-34:4)**	2.0311	**PG(40:6)**	1.0845
TAG(60:10)	1.5873	**PG(38:6)**	1.9875	**PG(36:5)**	1.0584
DAG(34:2)	1.584	**PE(P-36:2)**	1.9026	**PC(38:8)**	1.0548
TAG(44:2)	1.5544	**PS(34:3)**	1.888	**PE(34:1)**	1.0328
TAG(62:5)	1.4821	**PG(40:8)**	1.8689	**PE(34:0)**	1.0219
TAG(60:8)	1.451	**LysoPC(20:0)**	1.7521		
TAG(60:9)	1.4231	**LysoPE(P-18:1)**	1.6807		
DAG(44:1)	1.4082	**LysoPC(24:0)**	1.6718		
TAG(46:4)	1.4026	**PS(40:4)**	1.6163		
DAG(52:2)	1.374	**PG(P-38:8)**	1.6111		
DAG(34:1)	1.3148	**PC(32:0)**	1.608		
MAG(20:0)	1.3147	**LysoPC(20:1)**	1.5568		
FA(24:0)	1.3124	**PE(36:3)**	1.5107		
DAG(36:2)	1.3086	**PG(38:5)**	1.5022		
MAG(18:0)	1.2959	**PI(30:0)**	1.5		
TAG(46:3)	1.2573	**PS(34:1)**	1.4982		

FA(26:0)	1.2105	**PE(34:3)**	1.4969		
TAG(48:3)	1.1937	**PG(36:2)**	1.4902		
MAG(26:4)	1.1871	**PG(34:2)**	1.4806		
TAG(60:7)	1.1858	**PC(P-44:7)**	1.4585		
TAG(44:1)	1.181	**PC(30:1)**	1.3955		
DAG(36:3)	1.1496	**PE(P-40:8)**	1.388		
TAG(58:7)	1.146	**PI(32:0)**	1.3631		
TAG(62:13)	1.1251	**PC(28:0)**	1.2955		
DAG(42:1)	1.0995	**PC(32:3)**	1.2753		
TAG(46:2)	1.0918	**PC(30:3)**	1.2602		
TAG(58:6)	1.0827	**PG(34:3)**	1.2437		
FA(22:0)	1.0747	**PI(34:2)**	1.242		
TAG(60:6)	1.069	**LysoPC(18:0)**	1.2321		
TAG(50:3)	1.0551	**PG(40:7)**	1.2281		
TAG(58:5)	1.0478	**PI(P-34:1)**	1.1812		
FA(20:0)	1.0367	**LysoPC(16:1)**	1.1686		
TAG(50:4)	1.0352	**PE(38:6)**	1.1541		
TAG(48:5)	1.0335	**PC(30:0)**	1.1531		
TAG(58:8)	1.0321	**PE(32:1)**	1.153		
TAG(48:4)	1.0162	**PS(38:6)**	1.1521		